

**FATIGUE CRACK INITIATION
IN CROSS-PLY CARBON FIBER LAMINATES**

A Thesis
Presented to
The Academic Faculty

by

Justin M. Ketterer

In Partial Fulfillment
of the Requirements for the Degree
of Master of Science in the
George W. Woodruff School of Mechanical Engineering

Georgia Institute of Technology
August 2009

**FATIGUE CRACK INITIATION
IN CROSS-PLY CARBON FIBER LAMINATES**

Approved by:

Dr. Steven Johnson, Advisor

School of ME, MSE

Georgia Institute of Technology

Dr. Richard Neu

School of ME

Georgia Institute of Technology

Dr. Jianmin Qu

School of ME

Georgia Institute of Technology

ACKNOWLEDGEMENTS

First, I must thank my advisor, Dr. Steve Johnson, for selecting me as the student for this research project. Second, I am grateful for his mentorship and teaching. I really admire his “respect for the data,” and I learned more useful skills in his classes (“Fatigue” and “Composite Mechanics”^{*}) than any other at Georgia Tech. When my research was not progressing well and I was growing frustrated, I have Dr. J. to thank for putting the heat on me to burn away my frustrated apathy. Without the motivation he gave me, the amount of work and learning I did at GT would have been severely undermined.

I would like to thank our project sponsors at the Boeing Company: Dr. Jonathan Gosse, and Stephen Christensen. Their funding allowed me to accomplish my goal for my graduate career: gain experience and understanding in the area of carbon fiber composite fatigue. Next, I would like to thank my committee members, Dr. Rick Neu and Dr. Jianmin Qu. Their presence on my committee was instrumental in allowing me to produce a clear summary of the knowledge I gained through my graduate research: a thesis which is not just a testament to what I learned, but which is a body of work whose quality befits the canon of *Mechanical Engineering Research at Georgia Tech*. Rick Brown’s assistance, and his unmatched depth of experience in experimentation, were indispensable to this research endeavor—thank-you, Rick.

I can’t thank my Mom and Dad enough. It is cliché to say “thanks for the support”—but I hope that they know how heartening it is to understand that I have

^{*} Joining the “List of Outstanding Graduate Courses at Georgia Tech” is ME 6101—“Engineering Design.” My learning at Georgia Tech—and my learning well into the future—has been profoundly influenced by Dr. Farrokh Mistree. His class rescued me from sloppy thinking in far more than just engineering design.

parents who are behind me with everything they have. Their exemplary parenting is the primary reason for why I have reached the point I have today. I thank my Dad for his respect for logical, reality-based analysis which, thankfully, he impressed on me. I also admire and am glad he taught me his respect for productive, hard work. I would like to thank my Mom for the long and tireless years which she spent raising my sister and I. The upbringing which my Mom gave me was a rare case in which both quality and quantity were omnipresent. Her personality traits, too, played a big role in my development as a thinker: her inquisitive, scientific, and practical nature are traits that I am glad to have acquired by her example. I have yet to find a way to repay her for the auspicious Christmas gift which she gave me one year—an Erector set which set me on the path to becoming a mechanical engineer. My sister is an irreplaceable friend to me who is always honest and supportive. I'm thankful for her wry wit, and for being a typical champion from the Chainmaker stable.

As much as he may regret it, I cannot thank my Dad enough for giving me a copy of Ayn Rand's novel, *Atlas Shrugged*. Reading that book set me on a learning path which has resulted in a far more passionate and engaged way of living for me. I attribute much of my success in recent years to the clarity of thought which stems from the reason-focused and reality-based philosophy of Objectivism. I am much indebted to Ayn Rand.

Finally, I would like to thank my friends Sarah Engelbrecht, Dan Rogers, and Rob Kupkovits. When I was not hanging out with them in Atlanta, we shared many good email conversations during grad school. I want to stay in contact with them for the rest of my life. Their presence in my graduate career gave me grounding, entertainment, and friendship. My life as a graduate student would have been far poorer without them.

TABLE OF CONTENTS

ACKNOWLEDGEMENTS	iii
LIST OF TABLES	vii
LIST OF FIGURES	ix
LIST OF SYMBOLS AND ABBREVIATIONS	xviii
LIST OF SYMBOLS AND ABBREVIATIONS	xviii
SUMMARY	1
CHAPTER I. INTRODUCTION	2
CHAPTER II. BACKGROUND	4
2.1 Fatigue Defined	4
2.2 Polymers	6
2.2.1 Microstructure Description	6
2.2.2 Load / Deformation Response	9
2.2.3 Fatigue Behavior and Characterization	17
2.3 Cross-Ply Carbon Fiber Laminates	32
2.3.1 Microstructure Description	32
2.3.2 Load / Deformation Response	33
2.3.3 Laminate Modeling	38
2.3.4 SIFT	47
2.3.5 Fatigue Behavior and Characterization	50
2.3.6 Predicting Cross-Ply Fatigue Response	58
CHAPTER III. MATERIALS, SPECIMENS, & EXPERIMENTAL METHOD	65
3.1 Specimen Preparation: Unidirectional and Cross-Ply Laminates	65
3.2 Test Equipment:	67
3.3 Testing Plan for Unidirectional and Cross-Ply Laminates	70
3.3.1 Overview	70
3.3.2 Unidirectional Static Tests	71
3.3.3 Unidirectional Fatigue Tests	71
3.3.4 Cross-Ply Static Tests	72
3.3.5 Cross-Ply Fatigue Test: 10 Hz, R = 0.1	72
3.3.6 Cross-Ply Fatigue Test: Effect of R-Ratio & Loading Frequency	73
3.3.7 Cross-Ply Fatigue Test: Effect of Edge Roughness	74
3.4 Damage Inspection Techniques for Unidirectional and Cross-Ply Laminates	76
3.4.1 Gold Leaf Surface	76
3.4.2 X-ray Inspection	78
3.4.3 Edge Replication	79
3.4.4 Painted Surface	83
3.4.5 Dye Penetrant Testing	84
3.4.6 Optical Microscope Analysis & Specimen Polishing	86
CHAPTER IV. EXPERIMENTAL RESULTS & DISCUSSION	89
4.1 Unidirectional Specimens: 90° Static Tests	89
4.2 Unidirectional Specimens: 10° Static Tests	91
4.3 Unidirectional Specimens: Fatigue Tests	93
4.4 Cross-Ply Specimen Testing	97
4.5 Cross-Ply Testing & Edge Replication	98

4.6 Cross-Ply Testing & Batch Discrepancies	102
4.7 Cross-Ply Static Tensile Testing	104
4.7.1 Moduli	104
4.7.2 Static Testing Crack Initiation	106
4.7.3 Static Tensile Testing Crack Development	110
4.7.4 Static Ultimate Failure-0 Degree Ply Rupture	117
4.8 Cross-Ply Specimens: Fatigue Testing	120
4.8.1 Fatigue Crack Initiation: 10 Hz R = 0.1, Batch A vs. Batch B	121
4.8.2 Fatigue Testing: Rate of Crack Development	124
4.8.3 Fatigue Testing: Effect of Loading Frequency & R-ratio	128
4.8.4 Fatigue Testing: Effect of Specimen Edge Roughness	131
4.8.5 Fatigue Testing: Effect of Loading History	133
CHAPTER V. CONCLUSIONS	135
5.1 Unidirectional Specimens	135
5.1.1 Unidirectional Test Results	135
5.1.2 Unidirectional Test Setup Conclusions	136
5.2 Cross-Ply Specimens	137
5.2.1 Cross-Ply Crack Inspection Method	137
5.2.2 Cross-Ply Batch Variability	137
5.2.3 Cross-Ply Modeling	138
5.2.4 Cross-Ply Fatigue Tests	139
5.3 Recommended Future Work	142
5.3.1 Future Work: Experimentaton	142
5.3.2 Future Work: Modeling	142
APPENDIX A: HEXCEL IM-7 CARBON FIBER PROPERTIES	145
APPENDIX B: CYTEC 977-3 TOUGHENED EPOXY PROPERTIES	146
APPENDIX C: UNIDIRECTIONAL SPECIMEN TEST RECORD	148
APPENDIX D: COMPUTATION OF 10 DEGREE STIFFNESS MATRIX	156
APPENDIX E: CROSS-PLY SPECIMEN TEST RECORD	158
APPENDIX F: EDGE REPLICATE ARCHIVE	166
REFERENCES	172

LIST OF TABLES

Table 1. Selected polymers which exhibit contrasting "Frequency Sensitivity Factors" (FSF) at room temperature (Hertzberg, et. al.) [], (Manson & Hertzberg) [].	27
Table 2. Crack growth rates of selected polymer for various waveforms (Hertzberg et. al.) [], (Skibo) [], (Manson, et. al.) [], (Harris & Ward, 1973) [].	28
Table 3. The effect of mean stress on fatigue crack propagation in selected polymers (Hertzberg & Manson) [2].	28
Table 4. Description of the unidirectional specimen starting materials. All fibers were IM-7, but epoxy matrix material varied. DOW's DEN 431 epoxy was used in five of the 10° specimens, while Huntsman's Tactix 123 epoxy formed the majority of these specimen's matrix material. "Practice" specimens were nine spare practice specimens which Boeing requested be used to develop the test setup which would not cause erroneous grip-related failures.	67
Table 5. The ϵ -N data for both the 90° and 10° specimens. Where "cycles to failure" is 1.00E6, failure did not occur—runout limit was reached.	94
Table 6. Comparisons of crack densities at two points in the static tests of the "practice" specimen from Group A (Practice tensile test specimen), and Specimen 20 from Group B. Lower crack density at the stress state of 41 ksi for Specimen 20b could be due to the absence of the degrading acetone, while a higher crack density at the C.D.S. for the same specimen could be explained by its lower σ_{ult22} , which was shown earlier experimentally, and which would cause higher cracking.	113
Table 7. The set of static ultimate strength tests performed on the cross-ply specimens, Specimen 20b was the only specimen from Batch B tested to ultimate strength—note its much lower ultimate strength value. Also worth noting is the consistency of the ultimate strain value across all the specimens. Though Specimen 6 reached a relatively remarkable ϵ_{ult} of 0.02003, the ultimate strain of IM-7 fibers (0.018), appears to govern ultimate failure of these specimens.	117
Table 8. Table describing which specimens from Group B were used for which of the R-ratio and test frequency investigations. (10 Hz, R = 0.1) was an average of the five specimens listed. Test result for "polished" specimens discussed in the following section.	128
Table 9. Table of crack initiation stress values for various test conditions. The value for the test condition of (10 Hz, R=0.1) is based on an average of five tests performed at those test conditions, all others based on single test performed for that condition. "Polished" specimens will be discussed in the following section.	130

Table 10. These are the notes which were recorded for each of the unidirectional specimen tests.	148
Table 11. Notes recorded for each of the cross-ply specimen tests.	158

LIST OF FIGURES

Figure 1. Examples of polymer chain molecular structure (Mallick) [6].	7
Figure 2. Amorphous (a) and semicrystalline (b) polymer chain arrangement (Mallick) [].	7
Figure 3. Thermoplastic (a) and thermosetting (b) polymer chain schematics (Mallick) [].	8
Figure 4. Stress-strain diagrams comparing the strain-to-failure of thermosetting epoxies to a thermoplastic: polysulfone (Mallick) [].	9
Figure 5. The load/deformation response of a typical polymer (F.R. Eirich, 1965) [].	10
Figure 6. Stress/strain response with increasing temperature or loading rate (Mallick) [].	12
Figure 7. Temperature dependant behavior of polymers (Mallick) [].	12
Figure 8. Creep and stress relaxation tests (Mallick) [].	13
Figure 9. Tensile strength of polystyrene as a function of molecular weight (Kumar & Gupta) [].	14
Figure 10. Emphasis of the various axes of alignment which polymer chains can take to the load axis. The chain group labeled 'A' will clearly bear most of the load (Hartwig, 1994) [].	14
Figure 11. Molecular schematic of "crazes" (left) and "shear bands" (right) (Hertzberg & Manson, 1976) [].	15
Figure 12. "Patch morphology revealing craze matter attached in segments on craze-matrix interface (Hertzberg, 1987) [12]."	16
Figure 13. "Hackles" on an amorphous polymer's fracture surface (Hertzberg, 1987) [12].	16
Figure 14. Example of polymer "thermal runaway" failure: stress-log cyclic life data for polytetrafluorethylene. 'x' denotes failure point (Riddell et. al., 1966) [].	20
Figure 15. Temperature increase resulting from uniaxial cycling at 5 Hz, load control, sine wave and zero mean stress in polyacetal. F = Fracture, U = Unbroken (Crawford et. al., 1975) [].	23

Figure 16. Stress-log cyclic life in polyacetal. Thermal failures denoted by 'T' (Crawford et. al., 1975) [].	23
Figure 17. Cyclic strain softening in polycarbonate (a), nylon 66 (b), and ABS (c). Tests at 298 degrees K (Beardmore & Rabinowitz) [].	24
Figure 18. Tensile cyclic and monotonic stress-strain curves for nylon 66 (a), polycarbonate (b), polypropylene (c), and ABS (d). Tests done at 298 degrees K (Beardmore & Rabinowitz) [18].	25
Figure 19. Contrasting effect of cyclic frequency on FCP rates in polycarbonate (a) and polystyrene (b) (Hertzberg, et. al.) [].	27
Figure 20. A plot of jump frequency against frequency sensitivity factor which might suggest a relation between the two (Hertzberg et. al., 1975) [20].	30
Figure 21. Effect of temperature on frequency sensitivity factor (FSF) relative to the beta transition temperature of various polymers (Hertzberg et. al., 1978) [].	30
Figure 22. Hysteretic heating induced temperature increase for nylon 66--temperature rise at thermocouple site along crack plane (Skibo, et. al., 1979) [].	31
Figure 23 A schematic of a cross-ply laminate with transverse cracks developing in the 90° plies (Berthelot et. al., 1996) [5].	35
Figure 24 The “layer specimen” employed by Lorenzo and Hahn (1986) [32]; when one graphite bundle failed, the stress concentration on the adjacent bundle increased to such a degree that catastrophic failure immediately occurred.	35
Figure 25. A stress-strain curve for a cross-ply laminate. Here, note the behavior in cycle 1. This shows the first three regimes mentioned above (Charewicz & Daniels) [29].	36
Figure 26. Stress-strain schematic illustrating separate behaviors of 0° and 90° plies, and their behavior when combined as a cross-ply laminate (Mallick) [6].	36
Figure 27. Transverse tensile loading of a 90° lamina, with <i>a single fiber</i> embedded in the matrix. Stress ratio at the top and bottom of the fiber, along the loading axis, are plotted. The radial tensile stress at the fiber/matrix interface is nearly 1.5 times the far-field stress (Mallick) [6].	41
Figure 28. Shear stress and tensile normal stress for two different fiber volume ratios: 55% (a) and 75% (b) (Mallick) [6].	42

Figure 29. Maximum principal stress as a function of fiber volume ratio and fiber to matrix modulus ratios. Note that V_f for this study is 0.60 and our peak stress concentration for this ideal square packing arrangement would be approximately two times the far-field stress (Adams & Doner) [39].	43
Figure 30. Illustration of matrix displacement field for a composite with $E_f \gg E_m$. []	44
Figure 31. Example of the plots which the Cox shear-lag model generates for shear and tensile stress in the fiber (Mallick) [6].	44
Figure 32. The “elementary cell” whose geometric variables are employed in the modified shear-lag analytical model (Berthelot et. al.) [5].	47
Figure 33 Micromechanical blocks with: (a) square (b) hexagonal and (c) diamond packing arrays (Tay, Tan, Tan, Gosse) [1].	48
Figure 34 Locations for extraction of amplification factors (Tay, Tan, Tan, Gosse) [1].	49
Figure 35 (a) Prescribed normal displacements, (b) prescribed shear deformations (Tay, Tan, Tan, Gosse) [1].	49
Figure 36. Evolution of damage in cross-ply laminates in fatigue loading. Note that the second damage mode which arises can be either longitudinal cracking or delamination. Which of these two forms occurs first is dependent on the layup and material properties (Rebiere et. al. 2002) [28].	50
Figure 37. Schematic of damage localization pattern (Jamison, 1986) [35].	51
Figure 38. Damage mechanisms in $[0/90_2]_s$ C.R.F.P.. These images illustrate the difference between high-stress (short life) loading which yields the localized longitudinal cracking visible in (A) while (B) displays the more distributed longitudinal cracking at low-stress fatigue loading (long life) (Charewicz & Daniel) [29].	52
Figure 39. Failure patterns of $[0/90_2]_s$ CFRP tested under static & fatigue loading conditions (Charewicz & Daniel) [29].	53
Figure 40. Stress-life (S-N) curves for unidirectional and cross-ply graphite/epoxy laminates (Charewicz & Daniel) [29].	55
Figure 41. Endurance limits for unidirectional composites with various epoxies. Epoxies which are more brittle exhibit higher endurance limits (Hartwig) [9].	56
Figure 42. Mode II fracture in unidirectional AS4/3501-6 CFRP (Arcan et. al.) [49].	57

- Figure 43. (A) Plane of principal stress for shear loading causes hackle formation in the matrix between fibers. (B) Direction of ‘hackle slant’ is dependant on whether microcracks coalesce at upper or lower boundary of fiber (Hibbs & Bradley) [50]. 57
- Figure 44 Mode I loading (left) shows clean failures at the fiber/matrix interface, and pure Mode II loading (right) shows shear hackles in the matrix (Hibbs & Bradley) [50].58
- Figure 45. A unidirectional 90° specimen in the 1000 lb mechanical grips of an MTS servo-hydraulic test machine. The brass tabs, epoxied to the specimen, are just visible above the lower grip. The extensometer is held in place with elastics in this image; springs were later determined to be a better approach. 68
- Figure 46. A cross-ply specimen in the mechanical 10,000 lb static / 5,000 lb fatigue grips. 69
- Figure 47. A cross-ply specimen in the 20,000 lb hydraulic wedge grips. The test-frame is encased in a lead-lined box for the purposes of X-raying specimens. 69
- Figure 48. A vise was used to hold the specimen during sanding; paper towels both caught water from the wet-sanding process and prevented the vise from damaging the specimen surface. 75
- Figure 49. The contrast in specimen surface roughness is visually evident with an optical light microscope. This contrasts the “before” and “after” sanding of two locations on the edges of Specimen 9b. 75
- Figure 50. The notch in the specimen and the gold leaf placed on the width are visible in this image. 77
- Figure 51. This is a view through the microscope of the notch put in the edge of one of the 10° unidirectional specimens. 77
- Figure 52. The optical microscope used to observe whether stable crack progress can be observed through the gold leaf surface. 78
- Figure 53a and Figure 53b. The specimen is in the grips in the lead-lined enclosure, to the left. To the right, the x-ray is rolled in front of the lead lined enclosure, properly positioned to perform a scan. In the image to the left, the grips are oriented 90° to where they were when the x-ray was taken. The specimen had to be oriented with the broad edge facing the x-ray for x-ray photos to effectively be taken; the Kodak film was supported behind the specimen with a metal clamp. 79
- Figure 54. A syringe is used to inject acetone between the replicate film and the specimen. An eraser is used to press the film against the specimen edge immediately after injecting the acetone []. 80

Figure 55. The replicate tape is butted against the masking tape shown; this ensures that the tape registers at the same location every time a replicate is taken. 81

Figure 56. A microscopic magnification of a typical edge replicate. Acetate “tendrils” are evident, where the acetate had flowed into the crack and then been pulled out by removing the replicate. The 0° plies are evident as darker bands on the “top” and “bottom” of the lighter colored 90° plies, internal to the cross-ply laminate image (Practice tensile test specimen, 1.5x Objective, 2.0x magnification. Taken at 25.8 ksi of stress when ultimate loading was 72.4 ksi). 82

Figure 57. A static test in which the remarkably regular spacing of chevron cracking was first noticed, which appear after the initial transverse crack. (This picture of the “Practice” tensile test specimen was taken at 1.5x Objective, 3.2x magnification. Taken at 25.8 ksi of stress; σ_{ULT} was 72.4 ksi). 82

Figure 58. The uniform spacing of cracks is evident in the painted edge of this specimen, this picture was taken at 43 ksi, where σ_{ULT} was 72 ksi. 83

Figure 59. A chevron crack, above a transverse crack in the 90° plies, is evident in this magnification of the specimen edge. Image was taken at 43 ksi, where σ_{ULT} was 72 ksi. 84

Figure 60a and Figure 60b. To the left, the specimen in the grips. To the right, the specimen and test frame is covered in the paper masking which prevents the aerosol from getting all over the test frame and focuses the penetrant and developer on the specimen edge. 85

Figure 61. When a crack occurs in the 90° plies of the cross-ply specimen, the dye which had wicked into the crack will be drawn to the surface by the white developer substance. It is readily visible to the naked eye and easily recorded with a digital camera. 86

Figure 62. A section with two cracks in it was removed from the rest of the composite test piece. Sharpie was used to mark the approximate locations of the two transverse cracks. 87

Figure 63. This is the diamond cut-off wheel which was used to section specimens. 87

Figure 64. This is the epoxy cylinder in which the two edges shown above in (Figure 62) were mounted for polishing. 87

Figure 65. The Struer’s polishing machine. 88

Figure 66. Magnified at 1000x. Scale at the base of the image is 50 μm in length. White “circles” in image are the tips of the fibers in the 90° ply, and the dark vertical line is the crack path. Features of these images will be discussed in the “Experimental Results” section. 88

Figure 67. The σ – ϵ curve to failure for a unidirectional 90° specimen. Note that there is negligible plasticity prior to rupture, which occurred at the peak load depicted. Similar linear-to-failure behavior was observed in the 10° specimens.	90
Figure 68. The σ – ϵ curve to failure for a 10° specimen (Group 4, Specimen 7)	92
Figure 69. The ϵ -N diagram for the 90° specimens which did not rupture due to poor test setup. Note that this is plotted as a percentage of ϵ_{ult} , which was defined as 0.0104 for this group.	93
Figure 70. The ϵ -N diagram for the 10° specimens which did not rupture due to poor test setup. Note that this is plotted as a percentage of ϵ_{ult} , which was defined as 0.0111 for Group 4, and 0.0102 for Group 2.	94
Figure 71. The two types of failures observed in fatigue loading the unidirectional 90° specimens. Top: Specimen 5 from Group 3 split in the middle then ruptured at the ends. Bottom: Specimen 2 from Group 3 simply split in the gauge section.	95
Figure 72. A magnified view of the transverse split from Specimen 5, Group 3.	95
Figure 73a and b. The left and right “quarter-circle” fracture surfaces of Specimen 5, Group 3.	96
Figure 74. 10° specimen fracture pattern. Both the static and fatigue tests fractured in this manner: at one location, along the axis of the fibers.	96
Figure 75. The three areas which were compared for crack densities. The lower area, circled and described in red, is where replicates were taken a couple dozen times.	99
Figure 76a & b. The edge replicates taken in the three areas described in Figure 75 are compared here. Notice that crack density is much higher in the area repeatedly exposed to acetone.	99
Figure 77. This picture compares an x-ray image to an optical picture of the specimen, to make the reader aware of what is being viewed in the x-ray. Any bright blue vertical lines are transverse cracks through the 90° plies. As mentioned in the figure label in the image, the masking tape label area typically had higher cracking. This is thought to be due to longer exposure to acetone—flowing between the label and the specimen surface, the acetone could not evaporate as quickly.	100
Figure 78. Comparison of an edge replicate to a magnified view of the x-ray in the same area. X-ray captures cracks with good fidelity, though “chevron cracks” appear more faintly than transverse cracks.	101

Figure 79. Here is solid proof that the acetate edge replication process causes earlier cracking than if it were not used. This shows four penetrant-enhanced x-rays of *four different specimens* from Batch A. The crack densities in the areas labeled “EDGE REPLICATE AREA” are consistently higher than in the bulk region which was not exposed to acetone, and are visible as the faint vertical lines off the edges in those areas. As peak load in fatigue testing increases, cracks appear in the area not exposed to acetone, but at lower densities. 101

Figure 80. This image compares the crack densities (for the same edge length) from two different specimens from Batch A, which had been cycled at the same peak load (18.3 ksi or 126 MPa average laminate stress). Specimen 18 had a lower crack density (cracks marked with green arrows), even though it had been exposed to dye penetrants, while the x-rayed region of Specimen 12 had not been exposed to chemicals at all. This confirms that the dye penetrant technique does not chemically attack the composite. 102

Figure 81. A histogram of the modulus values for the two batches of twenty cross-ply specimens. 105

Figure 82. σ - ϵ curve to failure for Sample 17 of Group A. In this test, the load was increased to 69.6 ksi, well beyond the point at which the characteristic damage state was reached, then unloaded, then loaded back to ultimate failure. This test shows parallels to Figure 25 and Figure 26, repeated below. 107

Figure 83. Interlaminar normal stress for a cross-ply laminate (y/b) = 1 corresponds to the edge of the laminate; a value of zero is the center of the laminate. Note that this reflects a $[90/0]_s$ layup (Pagano & Pipes) [54]. 110

Figure 84. These edge replicates taken during the static tensile testing performed on the first practice tensile test specimen. The ksi value to the right of each replicate corresponds to the (average) stress in the laminate at which the replicate was taken. σ_{ult} for this specimen was 72.3 ksi. Crack density is 21 inch^{-1} 111

Figure 85. This image shows the increasing number of cracks in Specimen 20 from Group B as it was being loaded to failure, as revealed by dye penetrant edge inspection. The peak stress at failure was 67.7 ksi. In contrast to Figure 84, which only inspected a 1.0” length for cracking, the length of inspected edge shown in this image is 4.25”. The peak crack density is similar—CCC cracks/inch. 112

Figure 86. Areas modeled by the shear-lag equations. The stress-field of σ_{xx}^{90} is highlighted in red; the interlaminar shear layer is highlighted in yellow. Crack spacing of “2l.” 113

Figure 87. σ_{xx}^{90} for 0.25 cracks/inch, 23.7 ksi (“first audible crack at 2200 lbs of loading”). 114

Figure 88. σ_{xx}^{90} for 18 cracks/inch at 40.9 ksi. 114

Figure 89. σ_{xx}^{90} for 26 cracks/inch at 61.3 ksi—reflects the C.D.S.	114
Figure 90. Interlaminar shear for 0.25 cracks/inch, 23.7 ksi (“first audible crack”).	115
Figure 91. Interlaminar shear for 18 cracks/inch at 40.9 ksi average laminate stress.	115
Figure 92. Interlaminar shear for 26 cracks/inch at 61.3 ksi average laminate stress (C.D.S.).	115
Figure 93. Here, the nature of the failure process is illustrated—the underlying crack in the 90° ply causes the 0° ply adjacent to it to split, at that location.	118
Figure 94. This image illustrates the “peeling” of delamination which can occur at rupture, as well as the fact that the rupture location of the fibers in the 0° plies need not occur on the same plane, at the same transverse crack location.	118
Figure 95. This image also illustrates that fracture of the 0° fibers can occur at locations far removed from where the bulk of the laminate fracture occurred.	119
Figure 96. Small longitudinal splits are also evident in the outer 0° plies after fracture.	119
Figure 97. σ_{ci} for cross-ply fatigue tests at 10 Hz, R = 0.1. The blue dots represent tests which reached run-out of 1M cycles without cracking. Only those fatigue specimens are included in which at least one test achieved run-out... For clarity, those tests where the specimen cracked in the first test are left out because it’s impossible to know what that specimen’s σ_{ci} value would be.	122
Figure 98. The same data as in Figure 97, but presented as strain data.	123
Figure 99. Edge replicates showing crack development in Specimen 9a—number of cycles at which each replicate was taken stated to the right of the replicate. Length of replicate is 1.0”.	124
Figure 100. Crack development in several specimens from Batch A.	125
Figure 101. One of the locations where a short delamination was observed in Specimen 12a—the specimen tested with the highest peak stresses performed in this study: 18.3 ksi, 10 Hz, R = 0.1. Taken at 1000x magnification and the scale at the base of the image is 50 μm .	126
Figure 102. Another location where delamination was observed in Specimen 12a. Taken at 1000x magnification and the scale at the base of the image is 50 μm .	127

Figure 103. Specimen 6b, no delaminations were evident at the 0° / 90° interface (for 10 Hz, R = 0.1 with a peak stress of 11.3 ksi). The “interlaminar matrix spots” were observed in all of the interlaminar boundaries of the polished specimens; it is unknown what causes these circles in the resin, but they were witnessed in both Batch A and Batch B. Image taken at 1000x, scale at image base is 50 μm. 127

Figure 104 a & b. Top shows the undamaged laminate of Specimen 7b, where no transverse cracks are evident in the white developer. Bottom: “first crack”—the dye from a transverse crack has stained the developer purple, marked with a small green arrow. 128

Figure 105. The effect of R-ratio and loading frequency on the appearance of “first crack.” Note that all of these data points—with the exception of 10 Hz, R = 0.1—are based on a single test performed at that specific test condition. In the case of (10 Hz, R = 0.1), the value is based on an average of five tests. Those five tests are shown here as red triangles, with the fitted curve for R = 0.1 intersecting the average value for these points. 130

Figure 106. A 500x image of the transverse crack in Specimen 6b shows many locations where the crack path preferentially splits along the fiber-matrix interface—i.e., where the stress is highest in the matrix. This, along with the data in Figure 105—which is suggestive of a “jump frequency”—show that the matrix material dominates fatigue cracking behavior in these plies. Therefore, fatigue behavior of the matrix material must be thoroughly understood if laminates built with them are to be understood. 131

Figure 107. The increase in the σ_{ci} value for the “polished” specimens. The polished data is plotted as green points; the icon shape mimics the R-ratio which the specimen was tested at—a green square for R = 0.5, and a green diamond for R = 0.1. The σ_{ci} value increased above the baseline in each of the three cases. The red dashed line is the crack initiation stress for unpolished static monotonic loading. 132

Figure 108. Specimen 1a edge replicate crack development. 166

Figure 109. Specimen 2a edge replicate crack development. 167

Figure 110. Specimen 7a edge replicate crack development. 168

Figure 111. Specimen 8a edge replicate crack development. 168

Figure 112. Specimen 11a edge replicate crack development. 169

Figure 113. Specimen 12a edge replicate crack development. 170

Figure 114. Specimen 13a edge replicate crack development. 171

LIST OF SYMBOLS AND ABBREVIATIONS

English

a	The “aspect ratio” of the elementary cell in shear-lag model of Lee & Daniel.
C	Material constant in Paris crack propagation law.
E_{11}	Lamina modulus in the fiber direction.
E_{22}	Transverse-to-fiber lamina modulus.
E_{33}	Out-of plane modulus of lamina.
$E_{11,LAM}$	Net laminate modulus in the load direction.
E_M	Matrix modulus.
E_F	Fiber modulus.
E_c	Energy dissipated per unit volume in polymer cyclic loading.
f	Frequency of loading in fatigue.
G	Shear modulus.
G'	Storage modulus.
G''	Loss modulus.
K	Stress concentration parameter
ΔK	Stress intensity range for Paris crack propagation law.
K_σ	Stress concentration parameter for Greszczuk model of σ_{ULT} of 90° plies.
l_f	Fiber length.
M	Polymer molecular weight.
[M]	Bending moments M_x , M_y , M_{xy} in macromechanical CLT equations.
m	Material constant exponent in Paris crack propagation law.
[N]	In-plane laminate stresses N_x , N_y , N_{xy} in macromechanical CLT equations.
p_f	Relevant fiber property, such as E_f , G_f , ν_f .
p_m	Relevant fiber property, such as E_m , G_m , ν_m .

r_f	Fiber radius.
$2R$	Center-to-center distance between two fibers.
V_f	Fiber volume fraction
V_M	Matrix volume fraction

Greek

α	Stacking parameter.
β	Cox model shear-lag parameter.
$\Delta\varepsilon$	Amplitude of strain in fatigue.
ε_{avg}	Mean strain in fatigue.
ε_{ci}	Strain at which cracks initiate and are first observed.
$\varepsilon_{\text{ULT},22}$	90° lamina ultimate tensile strain.
η	Shear-stress parameter in shear-lag model of Lee & Daniel
κ	Halpin-Tsai transverse modulus parameter.
σ_{avg}	Mean stress in fatigue.
σ_{ULT}	Ultimate strength of the material being considered.
σ_c	Average composite stress.
σ_f	Average fiber stress.
σ_m	Average matrix stress.
σ_{ci}	Stress (avg. laminate stress) at which cracks initiate and are first observed.
$\bar{\sigma}_{xx}^{90}$	Average longitudinal stress in 90° layer of cross-ply laminate.
$\bar{\sigma}_{xx}^0$	Average longitudinal stress in 0° layer of cross-ply laminate.

$\sigma_{xx}^{90}(x, z)$ Longitudinal stress in 90° plies in the Berthelot shear-lag model.

$\sigma_{xx}^0(x, z)$ Longitudinal stress in 0° plies in the Berthelot shear-lag model.

$\Delta\sigma$ Amplitude of varying stress in fatigue.

$\tau(x)$ Shear stress at $0^\circ / 90^\circ$ interface for shear-lag model of Lee & Daniel.

θ Lamina's fiber angle with respect to the load-axis.

ζ Halpin-Tsai equation variable which accounts for packing geometry.

Abbreviations

CLT Classical lamination theory.

CFRP Carbon fiber reinforced polymer.

ROM Rule of mixtures.

SIFT The "Strain-Invariant Failure Theory."

SUMMARY

The goal of this research was to investigate the tensile fatigue behavior of a carbon fiber / epoxy composite material. Specifically, the stress levels at which cracks initiated in static and fatigue loading in the 90° plies of a “quasi-cross ply layup” $[0/90_5]_S$ was investigated. For layups which contain them, cracks in composite laminates initiate and propagate from 90° plies (including the ubiquitous “quasi-isotropic layup” $0/\pm 45/90$). Thus, this work provides valuable insight into the fatigue behavior of the plies which originate fatigue damage. Unidirectional off-axis 90° and 10° specimens were also tested, but the bulk of testing was done on the cross-ply laminates. The project sponsors, Boeing, were in the process of extending a failure model to the case of fatigue. The body of work presented here provided empirical data for that effort.

Several different inspection techniques were used to investigate for cracking in the 90° plies, including: x-ray images, edge replicates, dye penetrants, and optical microscopy. Plots of the stress level at which crack initiation occurred will be presented, as well as images illustrating damage development in these layups. Comparisons are made to the experimental results of other investigations of this type of layup. Explorations of the effect of R-ratio (including $R = 0.1$ and 0.5), loading frequency (including 3, 10, and 30 Hz), and surface roughness (hand polished specimen edges to 1500 grit smoothness) on fatigue crack initiation were also performed. For the most damaging case (10 Hz, $R = 0.1$, no polishing), the crack initiation strain (0.00276) was one half of the strain at which cracks initiated in static monotonic loading (0.0054), and was 16% of the cross-ply specimen’s (0° fiber dominated) ϵ_{ULT} value of (0.018).

CHAPTER I. INTRODUCTION

Carbon fiber reinforced polymers (CFRP), are becoming more widespread in industries where strong, lightweight materials are required. Examples include sports equipment and aerospace applications. CFRP offers obvious benefits in the category of strength-to-weight ratio compared to metals. However, their relatively recent arrival as a widespread, cost-effective material—as well as their inhomogeneous, structural nature—presents unique and pressing challenges to the research community whose responsibility it is to study, describe, and predict the material's behavior, so that it can be used safely. This research endeavor is part of that effort and aims to investigate the onset of damage which first occurs in most laminates. This initial damage is also the origin of damage progression which can lead to ultimate failure. Obviously, safe use of CFRP requires that designers be aware of when the point of damage onset will occur when using this material.

This investigation focuses on static and fatigue crack initiation in the 90° plies of a quasi cross-ply specimen— $[0/90_5]_S$. For laminates which contain them, cracking will initiate in the 90° plies in both static and fatigue loading. If the loads are sufficient, stress concentrations cause damage to propagate into adjacent layers and ultimately, failure. Laminates which contain 90° plies are still quite common, such as the ubiquitous “quasi-isotropic” $[0 / \pm 45 / 90]_S$. Ideally and where it is feasible, designers wish to design below the threshold of crack initiation and thus must know this stress threshold for 90° plies. Matrix cracking also allows environmental attack, which can greatly reduce structural life.

There is a lot of CFRP fatigue work in the literature which describes tensile fatigue behavior at loads that result in ultimate failure (70% of static σ_{ULT} was a commonly observed peak stress in the background review of fatigue tests where $R = 0.1$). However,

not much work has been done to find the *lower* threshold of stress which *initiates* cracks in the 90° plies, much less determining what factors might affect this lower threshold value. Determining this lower threshold is the goal of this study. Also investigated is the effect of R-ratio, loading frequency, and edge roughness on crack initiation.

This research endeavor was initiated by project sponsors at Boeing's Phantom Works division—Jon Gosse and Stephen Christensen. They were in the process of developing a “Strain-Invariant Failure Theory” (SIFT)—a failure theory for composite laminates. They had had success in predicting cracking initiation and development for static loading, and wished to begin the process of extending the model to fatigue. In order to validate their model's predictions of crack onset in fatigue, the author was to perform a number of experimental tests to ensure that their model's predictions aligned with empirical observations.

The project sponsors originally elected to test unidirectional 90° and 10° specimens but after testing did not yield useful data, the focus switched to crack initiation in what shall be called the “cross-ply laminate”: [0 / 90₅]_s. Both unidirectional and cross-ply experimental results will be reported here, but the bulk of testing data consists of the cross-ply tests. In addition to presentation of the crack initiation data, analytical model predictions of the laminate behavior will also be presented for comparison (such as Classical Lamination Theory, and a shear-lag model which depicts axial stress in the 90° plies, and shear in the interlaminar region). The background section will discuss prior studies of cross-ply laminates, as well as polymer performance—a crucial, if not the central, factor affecting fatigue in 90° plies.

CHAPTER II. BACKGROUND

The background focuses on the subjects relevant to the experiments performed on fatigue crack initiation in the 90° plies of a quasi cross-ply laminate: $[0/90_5]_S$. Literature review of the performance of polymers—so critical to transverse lamina properties—will be performed, as well as prior studies involving cross-ply laminate experimentation and modeling. This project was initiated by project sponsors who wished to extend the strain invariant failure theory—“SIFT”—to the case of laminate fatigue. The results obtained here served as empirical evidence to support the development of their model. The SIFT theory is explained in detail in Reference [1] and is summarized in this paper in Section 2.3.4 (page 48).

2.1 Fatigue Defined

This research endeavor will mainly focus on characterization and prediction of fatigue in cross-ply composite laminates. In this investigation, fatigue is defined as: “*degradation of a material due to repetition of loads.*” The key element of fatigue is *cyclic* loading and resulting progressive damage. Hertzberg and Manson (1980) [2] summarize fatigue as being characterized by:

1. A periodically varying stress system having amplitude of $\Delta\sigma$.
2. A corresponding strain amplitude $\Delta\varepsilon$.
3. A mean stress level σ_{avg} .
4. A mean deformation ε_{avg} .
5. A frequency f .

6. A characteristic wave form (sinusoidal, square, etc.) for both the stress and strain.
7. Ambient and internal temperatures which are not necessarily identical.
8. A given specimen geometry, including notches.

A proper study of the mechanical behavior of composites necessarily involves an investigation of the characteristics of the *constituents* of the composite. The net mechanical behavior of a composite laminate is influenced by the properties of three different material regimes within the composite: the matrix, the interface, and the fiber. In addition to fiber orientation, material properties for each of these regimes will influence how the laminate responds to loading. This research endeavor focuses on studying cross-ply carbon fiber / epoxy laminates. Crack initiation in these plies has been observed to be dominated by matrix and interface cracking by the author, Reifsnider and Gao (1991) [3], Reifsnider (1977) [4], and Berthelot et. al. (1996) [5]. “It is believed that when the load is in the direction of the fiber, or nearly so, it is carried mainly by the fibers. Failure load is then determined by the fiber strength and the matrix and fiber elastic properties. For large values of θ (away from 0° , and approaching 90°), the fiber stress decreases and the matrix shear and transverse stress increase. The matrix then fails before the fibers by cracking in the fiber direction (Reifsnider & Gao) [3].” Due to the fact that polymer matrix behavior is quite influential in the CFRP behavior, an investigation of polymer mechanical behavior will precede the background study of cross-ply CFRP specifically. Thus, in the following sections of background investigation, the microstructure, load/deformation relationship, and typical fatigue behavior will be described for polymers, and the same features will be investigated for cross-ply laminates specifically.

Besides descriptions of empirically evident physical phenomena of cross-ply behavior in fatigue, mathematical models of this behavior will also be discussed. The power of engineering is in prediction via quantification, so a review of analytical composite modeling will be included for cross-ply layups.

2.2 Polymers

This investigation analyzes crack-onset behavior for the 90° plies in a quasi cross-ply laminate, [0/90₅]_S. This is essentially an analysis of the lamina's transverse-to-fiber behavior. For this type of loading, the behavior of the matrix becomes critical since the fibers are not in a favorable orientation to bear the load on their longitudinal axis. Accordingly, a review of polymer behavior is important in understanding the behavior of cross-ply laminate behavior—the 90° plies depend heavily on the polymer's characteristics.

2.2.1 Microstructure Description

A polymer is a long-chain molecule containing one or more repeating units of atoms, joined together by strong covalent bonds (Figure 1). A “polymeric material” is defined by P.K. Mallick as a material which is comprised of a large number of these chains, frozen in space in the solid state. The chains can be a randomly arranged (amorphous polymers, Figure 2a) or a mixture of random and orderly (semicrystalline polymers, Figure 2b) (1993) [6].

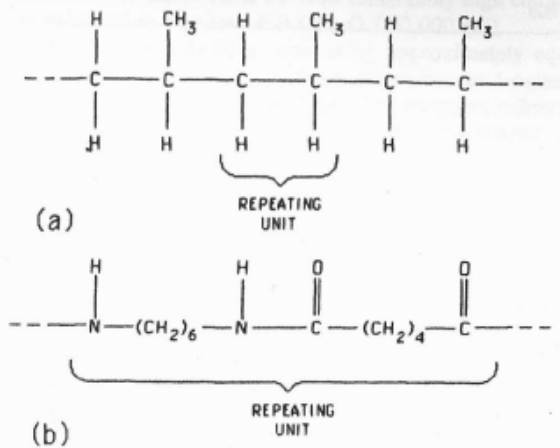


Figure 1. Examples of polymer chain molecular structure (Mallick) [6].

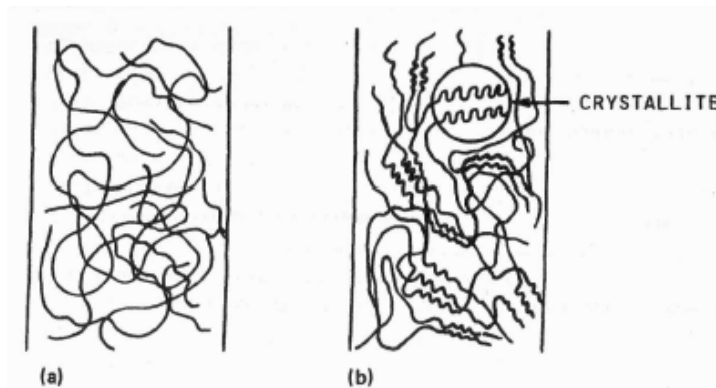


Figure 2. Amorphous (a) and semicrystalline (b) polymer chain arrangement (Mallick) [6].

Polymers can have varying degrees of “crosslinking”—defined as molecular chains which link separate polymer chains into a more connected molecular chain network. Polymers can have low crosslinking, where the molecular linearity is uninterrupted. In this state, polymer chains are held together only by weak secondary bonds (van der Waals and hydrogen bonds). Polymers that fit this description are “thermoplastics” and can be readily shaped and formed with the application of heat and pressure. A “thermoset” polymer on the other hand has a high degree of cross-linking between the polymer chains. Unless the degree of cross-linking is low, these polymers cannot be reshaped and will char and burn upon heating. Different schematics of these two broad categories of polymers are shown in Figure 3a and Figure 3b.

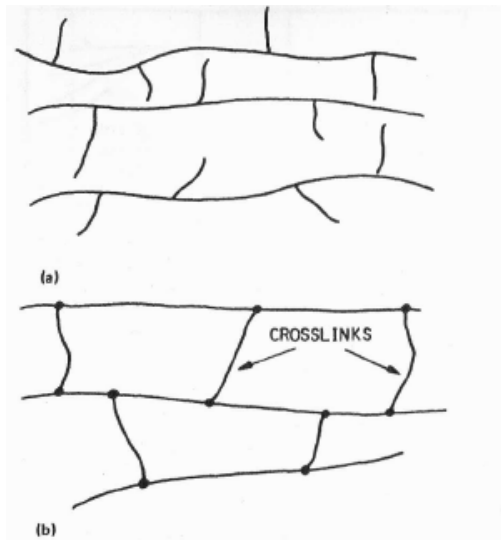


Figure 3. Thermoplastic (a) and thermosetting (b) polymer chain schematics (Mallick) [6].

Thermosetting polymers are commonly used as matrix materials for composites because they achieve good wet-out and exhibit less creep and stress relaxation. The trade-off is short shelf-life, a lengthy in-mold fabrication time, and low-strains-to-failure and impact strengths (compared to thermoplastics). Figure 4 illustrates how thermosetting polymer epoxies have lower strain-to-failures than a polysuflone thermoplastic.

Thermoplastic polymers have high impact strength and fracture resistance. This can be very helpful in retarding delamination, but is achieved at the cost of lowered matrix strength. They also have higher melt temperatures and viscosity (yielding poor wet-out), as well as relatively poor creep resistance and thermal stability (Mallick) [6].

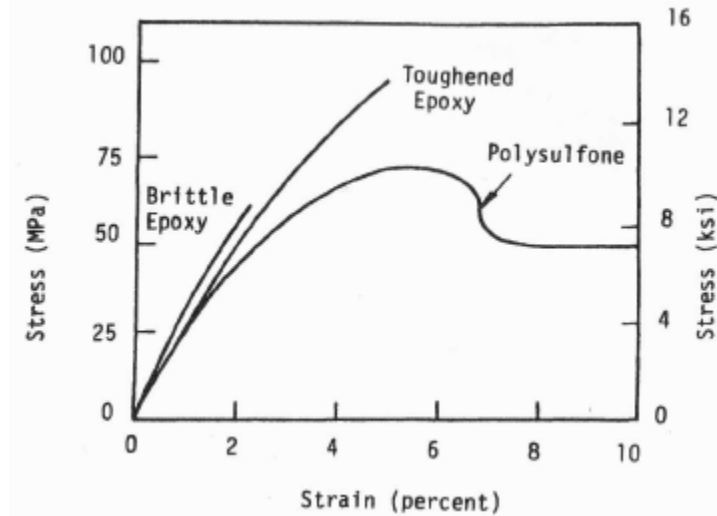


Figure 4. Stress-strain diagrams comparing the strain-to-failure of thermosetting epoxies to a thermoplastic: polysulfone (Mallick) [6].

2.2.2 Load / Deformation Response

When a polymer is loaded to failure, the load and deformation response can be described in several stages. They are:

1. Linear Elastic Regime: strain energy is essentially instantaneously recoverable; there is no significant delay in return to a stress and strain-free state.
2. Nonlinear Viscoelastic Regime: strain energy is recoverable, but this return to a stress-free and strain-free state requires a measurable amount of time.
3. Yield Point: defined as the point at which irreversible deformation occurs.
4. Necking: after the yield point, the nominal stress usually drops as extensive viscous and non-recoverable deformation occurs.
5. Failure: can occur in one of several ways.
 - a. If the polymer is significantly crystalline, a strain hardening process will occur as crystalline structures are reduced to molecular alignment of polymer chains along the loading axis.

- b. A ductile failure process can occur in which a linear molecular conformation is reached throughout the bulk of the material before failure occurs (and strain energy is non-recoverable for this form of failure).
- c. A rupture with partial elastic recovery can occur which is similar to the ductile failure process except that there is partial recovery from the peak strain state.

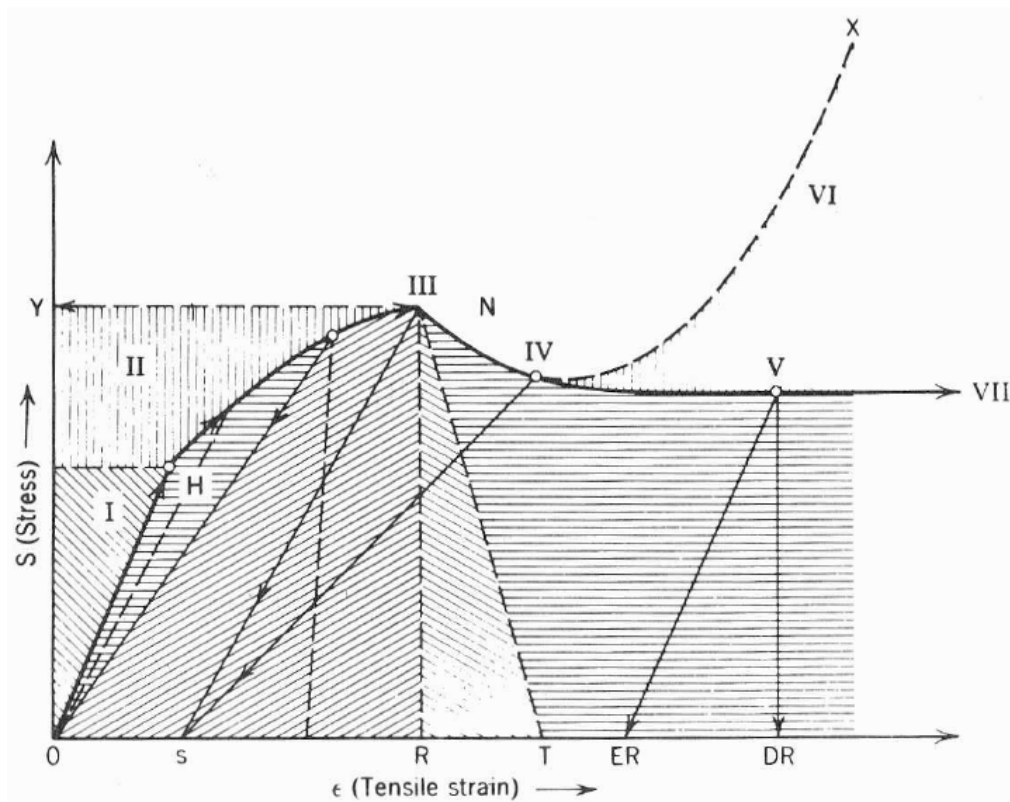


Figure 5. The load/deformation response of a typical polymer (F.R. Eirich, 1965) [7].

Figure 5 displays several different regimes of polymer behavior in tension:

- (I) Hookean elasticity; also linear viscoelasticity;
- (II) Nonlinear viscoelasticity;
- (III) Yield point;
- (Y) Yield stress;
- (H) Hysteresis of return curves;
- (N) Necking region;
- (IV) Beginning of strain hardening;

- (S) Set, permanent deformation; incipient failure;
- (R) Rupture;
- (T) Tearing;
- (V) Plastic flow;
- (ER) Partial elastic recovery, elastoviscous, orasticoelastic;
- (VI) Strain hardening and rupture;
- (DR) Ductile rupture;
- (VII) Ductile failure

A key aspect regarding polymeric solids is that their mechanical properties depend strongly on ambient temperatures, as well as loading rate. Temperature is not treated as a test variable in this investigation, but different loading frequencies are part of the analysis. In Figure 6, we see how increasing loading rate and increasing temperature affects a change in the stress/strain response of a polymeric solid. For a thermoplastic polymer, a glass transition temperature (T_g) exists. As the temperature of the polymer approaches this point, it rapidly changes from a hard, sometimes brittle material (glasslike) to a softer, leatherlike substance. Viscoelasticity (instantaneous elastic deformation followed by a slow viscous deformation) increases and as the temperature exceeds T_g , the material continues towards a completely melted state. Highly crosslinked thermoplastics do not exhibit this behavior, and will only char and burn when heated. Because of this, they are more thermally stable. Figure 7 illustrates this temperature dependant behavior (Mallick) [6].

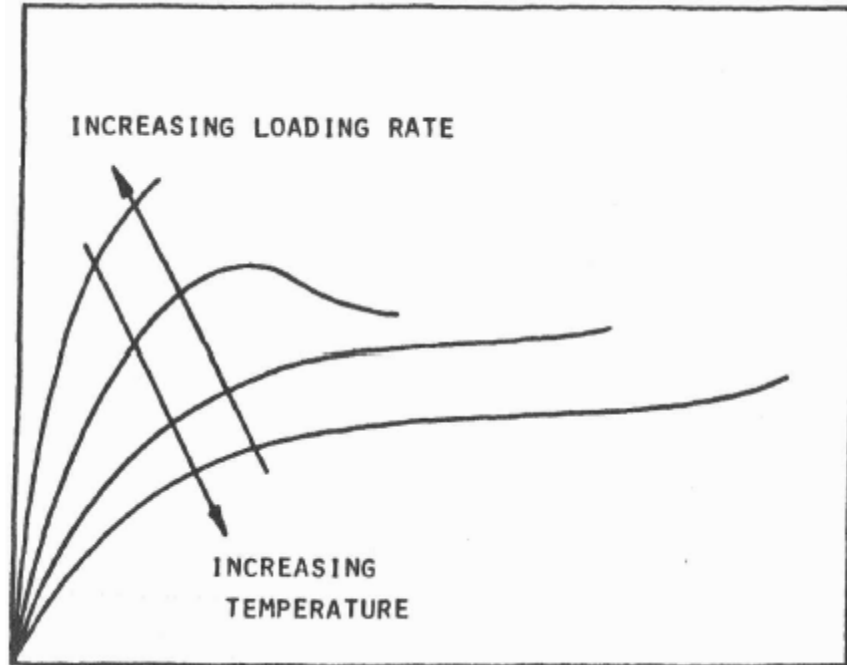


Figure 6. Stress/strain response with increasing temperature or loading rate (Mallick) [6].

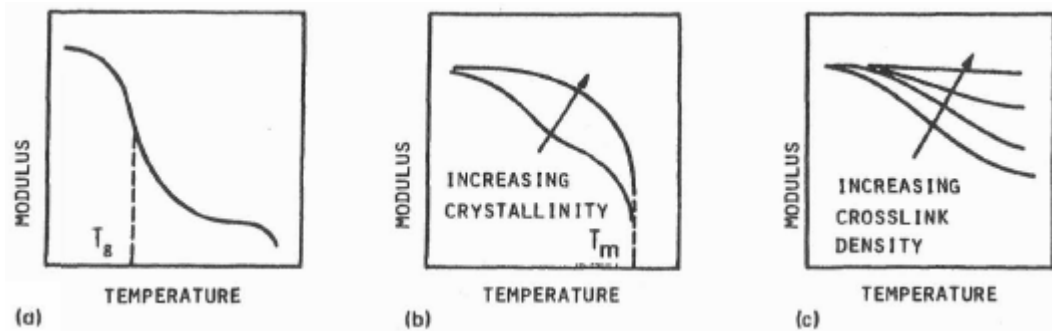


Figure 7. Temperature dependant behavior of polymers (Mallick) [6].

Viscoelasticity is best demonstrated in creep and stress relaxation tests. Some of these are shown in Figure 8. These tests show that there is a time dependant behavior when loading polymers—a direct result of molecular chain rearrangement; the time that it takes for these chains to rearrange themselves in response to a load (Mallick, 1993) [6], Hertzberg & Manson, 1980) [2].

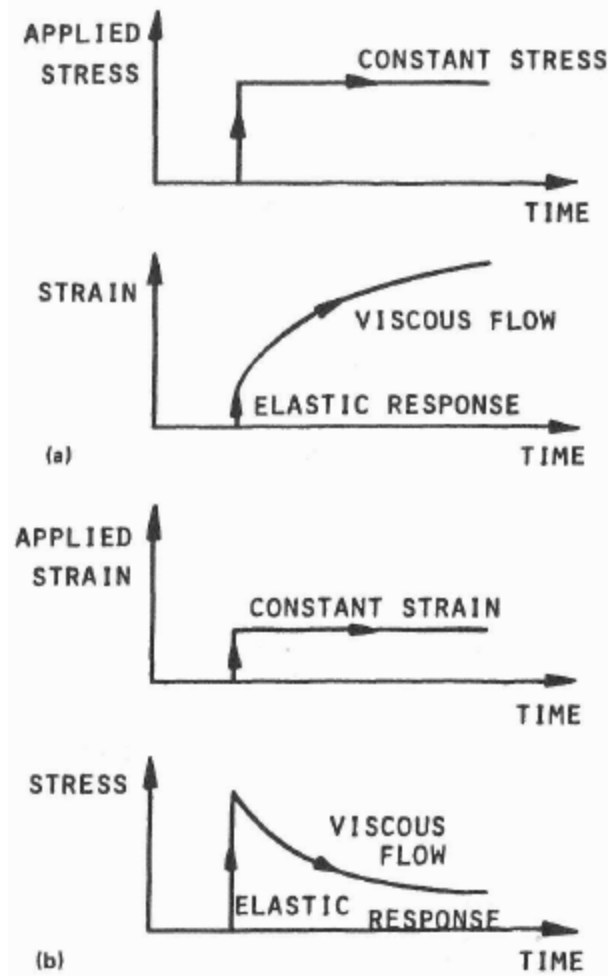


Figure 8. Creep and stress relaxation tests (Mallick) [6].

After temperature, the factor which most affects how polymers react to an applied load is molecular weight, M (Kumar & Gupta, 1998) [8]. This is defined as the mass of the molecule; for polymers this practically equates to a description of the average chain length of the polymer material being investigated—there is a stochastic distribution of chain lengths in any real polymeric material. Generally, tensile strength will increase as chain length increases, but this effect will plateau, as shown in Figure 9. Another method of increasing polymer strength is manufacturing the material to have oriented chains—presenting the primary chemical bond of the chain to the loading axis will favorably affect strength, as shown in Figure 10.

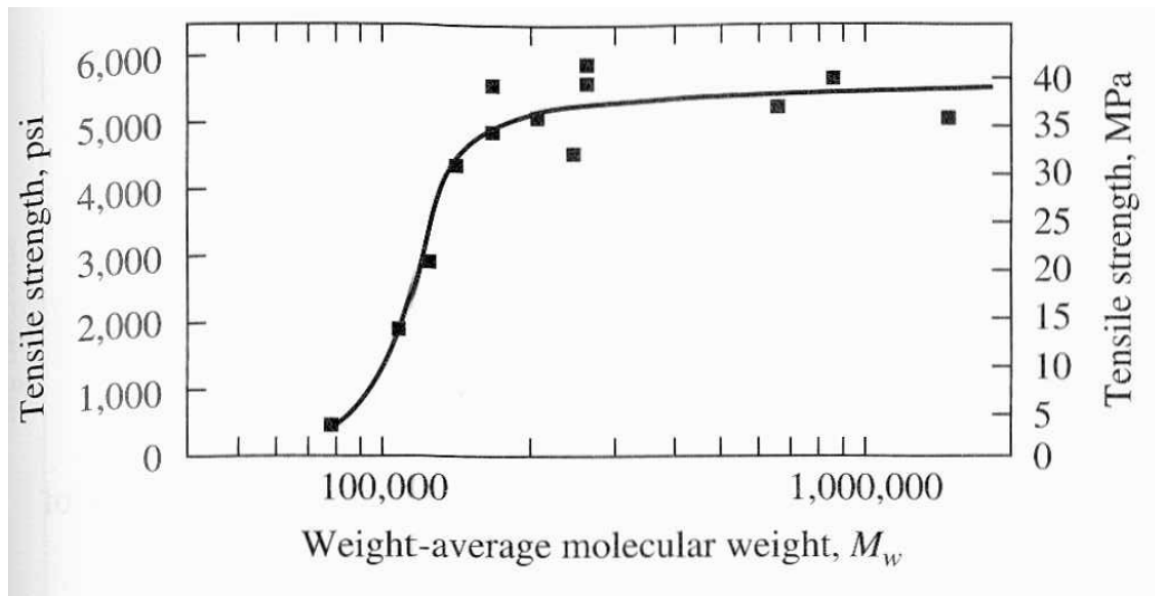


Figure 9. Tensile strength of polystyrene as a function of molecular weight (Kumar & Gupta) [8].

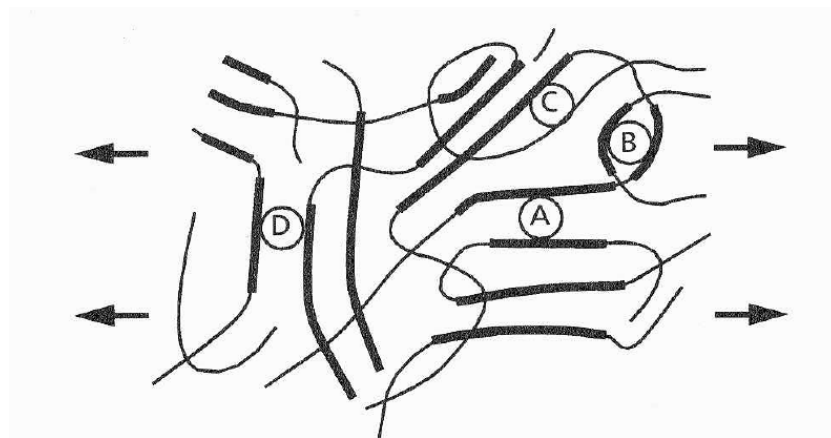


Figure 10. Emphasis of the various axes of alignment which polymer chains can take to the load axis. The chain group labeled 'A' will clearly bear most of the load (Hartwig, 1994) [9].

With respect to yielding, polymers exhibit two forms of macromechanical yielding states: “shear bands” and “crazes.” Both are thought to be the result of large-scale conformation changes in the polymer chains (Figure 11) [1]. Bands that are oriented perpendicular to the stress direction are crazes and result in polymer chains oriented along the stress axis. Crazes form mainly at the surface, but they can nucleate in the interior as well. They consist of a multitude of fine fibers ranging from 5 to 30 nm in diameter (Kumar & Gupta, 1998) [8]. Shear bands are evident on the surface of a polymer as lines

which run at a 38° to 45° angle to the load direction. The polymer will form shear bands before crazes if the shear component of force resolved onto a plane 45° to the loading direction exceeds the yield stress in tension. Crazing results in a reduction in the density of the material in that area (cavitation). Shear bands do not cause this (Kumar & Gupta) [8].

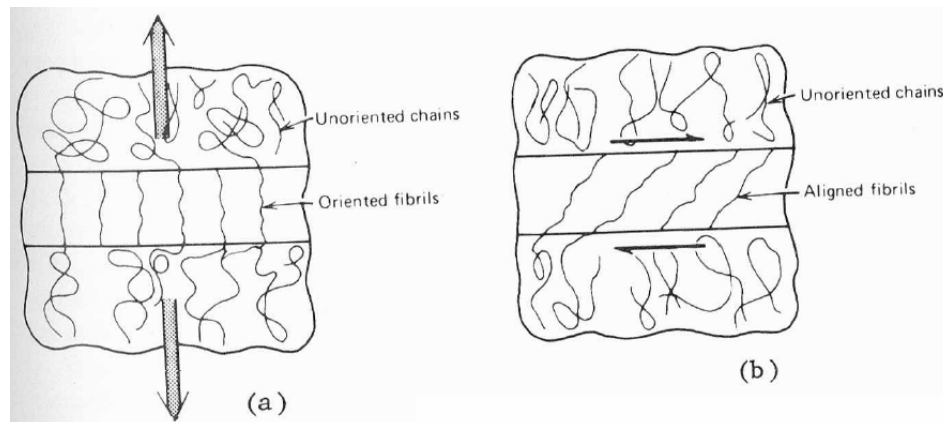


Figure 11. Molecular schematic of "crazes" (left) and "shear bands" (right) (Hertzberg & Manson, 1976) [10].

These features can serve as paths through which cracks can propagate. “Crazing ahead of fatigue cracks subjected to tensile loading is very common (Andrews, 1973) [11].” The rate of fracture will also affect the micromorphology of the fracture surface; “where the crack travels slowly through a preexisting craze, failure occurs at the midplane (midrib) of the craze where prior damage is more extensive (that is, higher void density). As crack speed increases, the crack path jumps back and forth from one craze-matrix interface to the another, leading to a “patch” fracture surface micromorphology (Figure 12) (Hertzberg, 1987) [12].” A more ordered fracture behavior—“hackle bands” (Figure 13)—consist of this “patch” fracturing behavior at the microscale level of the hackle bands themselves... The hackle bands too are the result of periodic buildup of bundles of crazes ahead of the crack front, and subsequent passage of the crack along one of the craze/matrix interfaces. It should be noted that hackle bands are a characteristic of an amorphous (acrystalline)

polymer, semicrystalline polymers exhibit a “plate-like” fast-fracture surface (Hertzberg, 1987) [12].

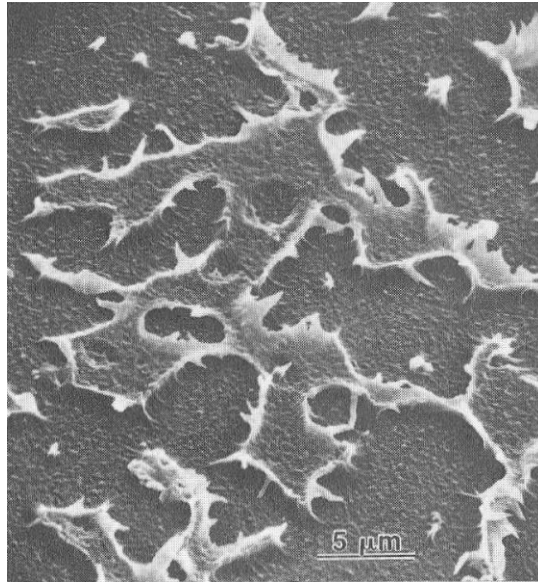


Figure 12. “Patch morphology revealing craze matter attached in segments on craze-matrix interface (Hertzberg, 1987) [12].”

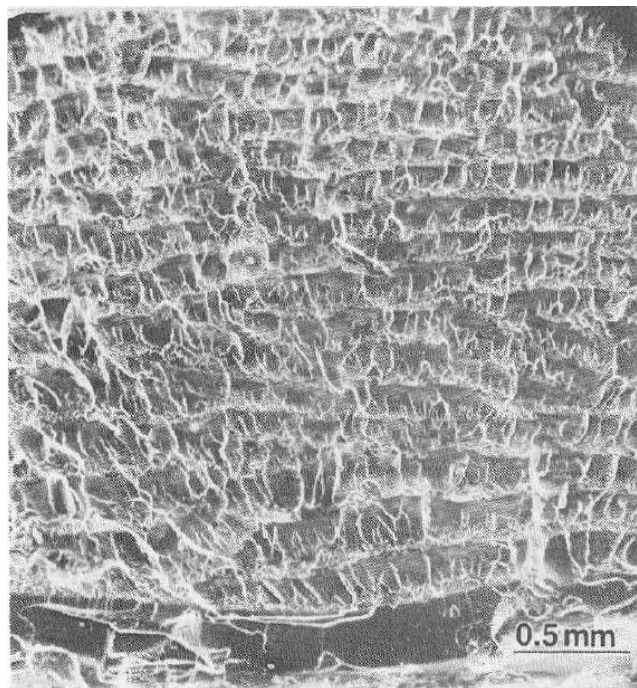


Figure 13. “Hackles” on an amorphous polymer’s fracture surface (Hertzberg, 1987) [12].

Where cracks propagate in polymers by the mechanism of craze fibril breakdown, studies have shown that crazing might be reduced by orienting polymer chains parallel to

the stress direction (Farrar & Kramer, 1981) [13] or by increasing the entanglement density of the polymer chains (Kramer, 1983) [14]. Increasing entanglement density can entirely suppress crazing and change the yield mode to one of shear band formation (Kumar & Gupta, 1998) [8]. It should be kept in mind that craze formation is a plastic deformation process and is therefore advantageous in dissipating energy; tradeoffs will result for ductility if crazes and shear bands are prevented from being allowed to develop in polymers.

Ductility of polymers has been theorized to be related to the “free volume”: the percentage volume not occupied by crystalline or amorphous polymer (Hertzberg & Manson) [2]. This hypothesis is not true in all cases but generally, when free volume is higher, ductility will be greater. Intuitively, a polymer structure with a lower density would enable molecules to rearrange themselves more easily upon loading, leading to higher ductility. Generally, ductility is also greater for those polymers which have bulky repeating units in the main chain, which is related to the free volume concept previously mentioned (Hertzberg & Manson) [2].

2.2.3 Fatigue Behavior and Characterization

Global stresses in fatigue loading that are kept relatively low with respect to the polymer’s fracture stress do not generally induce changes in the bulk properties of the material (Hertzberg & Manson) [2]. Different polymers have exhibited different behavior when net section plastic strains are introduced—softening has been observed in glassy

polymers for a constant strain range (appears to be due to crazing) while stiffening has been observed in PMMA and nylon 6 (Hertzberg & Manson) [2].

The molecular structure of the polymer of course heavily influences fatigue behavior. Generally, a polymer whose structure allows energy dissipation through rearrangement of the molecular structure during cyclic loading will be more fatigue resistant. This is witnessed in crystalline polymers, which actually have the highest fatigue resistance due to the crystalline structure's ability to unravel ordered chains, twinning, and molecular rotation (Hertzberg & Manson) [2]. Molecular weight, M , also has a profound effect on fatigue life. Generally, as molecular weight increases, fatigue life increases as well. It is hypothesized that a higher M leads to a polymer structure which is less able to disentangle itself at the fatigue crack tip; this consequently leads to a higher fatigue life (Hertzberg & Manson) [2]. Further, cross-linked polymers suffer from high crack growth rates for a given ΔK level (Hertzberg & Manson) [2]. The effect of cross-linking is to decrease the ability of plastic deformations to occur which could permit energy dissipation, causing earlier fracture.

With respect to polymer fracture in fatigue, how does the molecular structure relate to fracture energy? It would be wrong to assume that "polymer fracture" is wholly the result of the fracture and severing of the covalently bonded, carbon backbone of polymer chains. Covalent C-C bond rupture has been demonstrated to be correlated to fracture, but only constitutes a small portion of the amount of energy required to fracture polymers. "In an extensive series of elegant experiments by Zhurkov and Thomashevskii and by deVries, Williams et al., a close relationship between stress and bond breakage was confirmed and lifetimes predicted in terms of the rates of bond rupture. In fatigue it was found that the rate

of free-radical production in cyclic deformation was in phase with the load excursions (Hertzberg & Manson) [2].”

In crystalline and cross-linked polymers, restrictions of molecular movement results in a more tightly constrained molecular web, leading to transfer of large stresses to the chains in the vicinity of the crack. Thus, for polymer fracture energies which are on the order of 10^2 - 10^3 J/m², glassy polymer bond rupture only contributes 0.1 J/m². For crystalline polymers, the energy required to break polymer chains still consumes less than 10% of the total fracture energy. It should be noted that many bonds out of the plane of the crack are also broken—up to an order of magnitude more than in the plane of the crack itself (Hertzberg & Manson) [2].

Earlier, it was noted that in static monotonic tests both the rate at which a load is applied and specimen temperature influence the monotonic mechanical properties of most polymers. However, polymers in cyclic loading exhibit hysteretic heating effects—specimen temperature can actually increase if the peak load or loading frequency is sufficiently high while in cyclic testing. For sufficiently high loading and frequencies, “the temperature rise can be so great as to cause the sample to melt, thereby preventing it from carrying any load (Hertzberg & Manson) [2].” This behavior is a consequence of polymer molecular structure; “failure is presumed to occur by viscous flow though perhaps the occurrence of some bond breakage cannot be excluded (Hertzberg & Manson) [2].” An example of this, in which constant force ASTM Spec. D-671 specimens of polytetrafluorethylene were cycled to failure is shown in Figure 14 below. This image shows that samples loaded to failure exhibited hysteretic heating prior to failure, and intermittent rest periods in testing, which allow heat dissipation, have been shown to

significantly improve fatigue life. For fatigue failure of polymers due to hysteretic heating, surface area-to-volume ratio also plays a role (with respect to convection of heat off of the surface of the specimen).

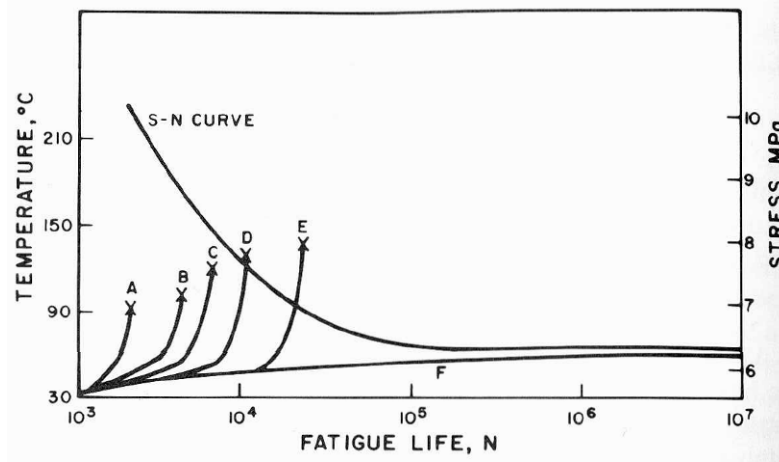


Figure 14. Example of polymer "thermal runaway" failure: stress-log cyclic life data for polytetrafluorethylene. 'x' denotes failure point (Riddell et. al., 1966) [15].

Sinusoidal loading of polymers and the energy dissipated through hysteretic heating are explained by the following analytical description (Kumar & Gupta) [8] of the out-of-phase reaction to cyclic loading. If a polymer is subjected to a sinusoidal strain ϵ of amplitude ϵ_0 and fixed frequency ω ,

$$\epsilon = \epsilon_0 \sin \omega t \quad (\text{Eq. 1})$$

then the stress response σ will be sinusoidal but will, in general, be out of phase by an angle δ and have a different amplitude σ_0 . Thus,

$$\sigma = \sigma_0 \sin(\omega t + \delta) \quad (\text{Eq. 2})$$

or

$$\sigma = (\sigma_0 \cos \delta) \sin \omega t + (\sigma_0 \sin \delta) \cos \omega t \quad (\text{Eq. 3})$$

On dividing the stress by the strain amplitude, one gets the modulus G as:

$$G = G'(\omega) \sin \omega t + G''(\omega) \cos \omega t$$

(Eq. 4)

where:

$$G' = \frac{\sigma_0 \cos \delta}{\varepsilon_0}, \quad G'' = \frac{\sigma_0 \sin \delta}{\varepsilon_0}$$

(Eq. 5, Eq. 6)

The term G' , called the storage modulus, is the in-phase component of the modulus and represents storage of strain energy. G'' , the loss modulus, is the out-of-phase component and is a measure of energy loss. The ratio of loss to storage modulus, G''/G' , is $\tan \delta$ and is an alternate measure of energy dissipation. For a perfectly elastic material, stress and strain are in phase and G' equals the elastic modulus whereas G'' is zero.

Further, E_c , the amount of energy dissipated per unit volume per cycle, can then be calculated as:

$$E_c = \int \sigma d\gamma = 2\sigma_0 \varepsilon_0 \int_0^\pi (\cos \delta \sin \omega t + \sin \delta \cos \omega t) \cos \omega t d(\omega t)$$

(Eq. 7)

$$E_c = \pi \sigma_0 \varepsilon_0 \sin \delta$$

(Eq. 8)

Because the strain amplitude is assumed to be small, ε_0 can be estimated using elasticity theory (Schultz, 1977) [16]. Thus,

$$E_c = \frac{\pi \sigma_0^2 \sin \delta}{E}$$

(Eq. 9)

Where E is the Young's modulus. The energy dissipated per unit time is given by

$$Q = \frac{\omega \sigma_0^2 \sin \delta}{2E}$$

(Eq. 10)

At steady state, all of this energy is lost to the atmosphere by convection from the surface of the sample. Thus, Newton's law of cooling:

$$Q = hA(T - T_0)$$

(Eq. 11)

where h is the heat transfer coefficient, A is the surface area per unit volume, T is the average steady-state temperature, and T_0 is the temperature of the surroundings.

Critically, it should be noted that “thermal runaway” fatigue failure is not what leads to fatigue failure of all polymers. A steady state temperature can be reached which is below T_g or T_m , and mechanical failure can then occur due to fracture development. Further, it is not thought that mechanical failure due to fracture crack extension is due to localized heating and thus thermal runaway failure at the crack tip;

“A comparison of fatigue markings produced by stable crack extension at different frequencies discredits the concept of stable crack advance by progressive crack tip melting. While hysteretic heat dissipation per cycle is undoubtedly very large within the crack tip plastic zone due to stress and strain amplification, it is believed that heat dissipation usually takes place from this small concentrated heat sink to the much cooler surrounding material and serves to preclude an uncontrolled temperature rise (Hertzberg & Manson) [2].”

It is suspected that this is what was occurring in this investigation. This analysis was investigating mechanical fatigue failure, and it's suspected that mechanical fracture was the cause of damage in these tests. To ensure this, a thermographic camera was used to observe whether there was any temperature rise in the specimen or near a crack in the specimen during testing at 10 Hz, a common test frequency in the investigation. Global temperature

rise above the surroundings was not observed. Figure 15 illustrates the leveling-off of temperature for sufficiently low stress levels in polymer fatigue testing.

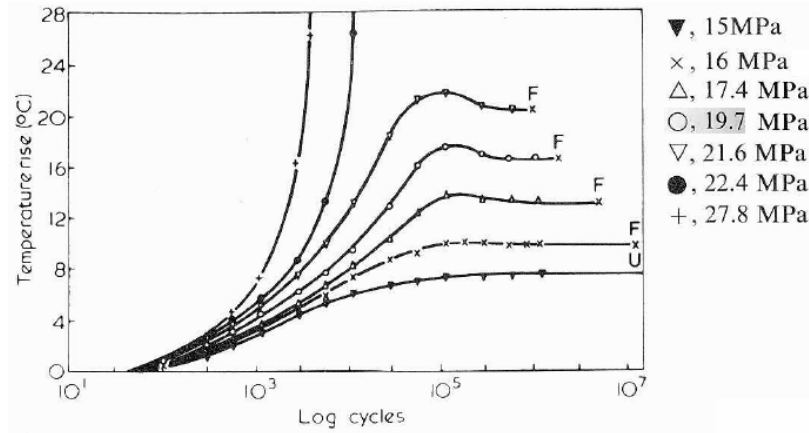


Figure 15. Temperature increase resulting from uniaxial cycling at 5 Hz, load control, sine wave and zero mean stress in polyacetal. F = Fracture, U = Unbroken (Crawford et. al., 1975) [17].

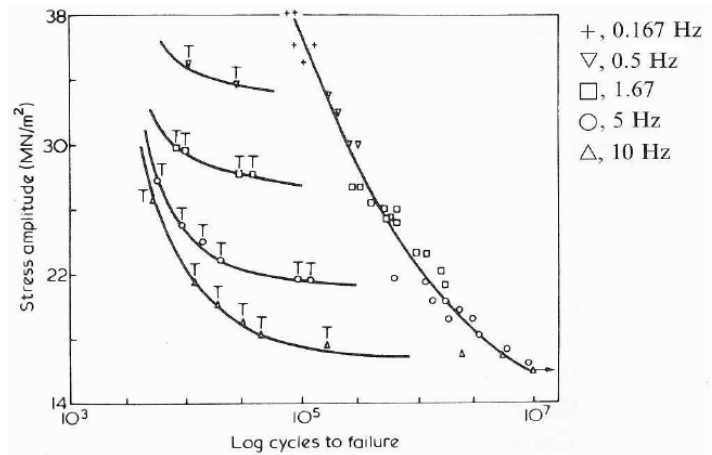


Figure 16. Stress-log cyclic life in polyacetal. Thermal failures denoted by 'T' (Crawford et. al., 1975) [17].

Thermal failure cannot occur for displacement or strain controlled testing. The initial displacement will cause heating, but this leads to a decreased modulus, leading to reduced stress which reduces heat generation and leads to a steady-state temperature. This is very important to note because the nature of the load state (constant load or constant deflection or strain) will affect how the polymer fails in fatigue. “For example, a polymer that exhibits considerable damping may possess a low fatigue limit under constant stress

due to premature thermal melting; without such uncontrolled heating as would exist in constant-deflection amplitude testing, this material might well exhibit a higher ranking relative to the other materials (Hertzberg & Manson) [2].”

Due to cyclic softening, a polymer does not necessarily follow the monotonic stress-strain curve when it is cyclically loaded. It’s important to remember that the “cyclically stabilized stress-strain response” may be quite different than the initial monotonic response. Figure 17 and Figure 18 illustrate that cyclic strain softening exists for different types of polymers.

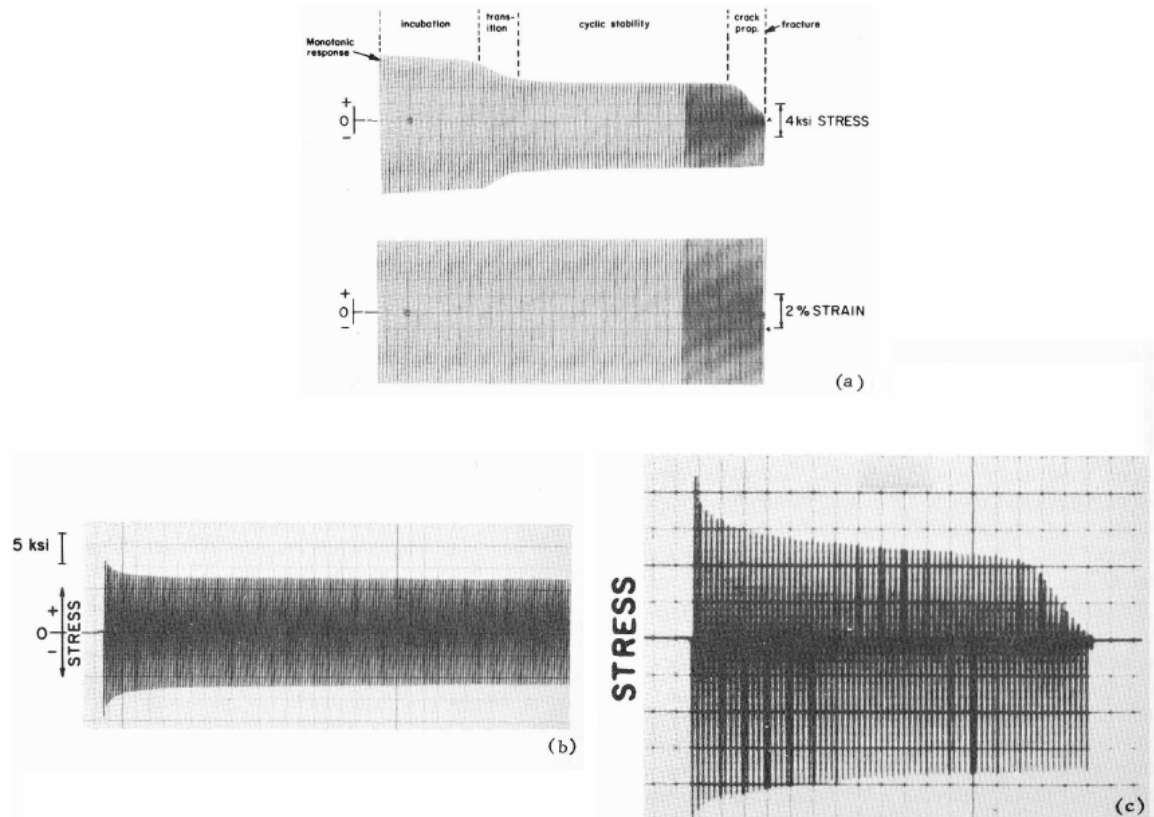


Figure 17. Cyclic strain softening in polycarbonate (a), nylon 66 (b), and ABS (c). Tests at 298 degrees K (Beardmore & Rabinowitz) [18].

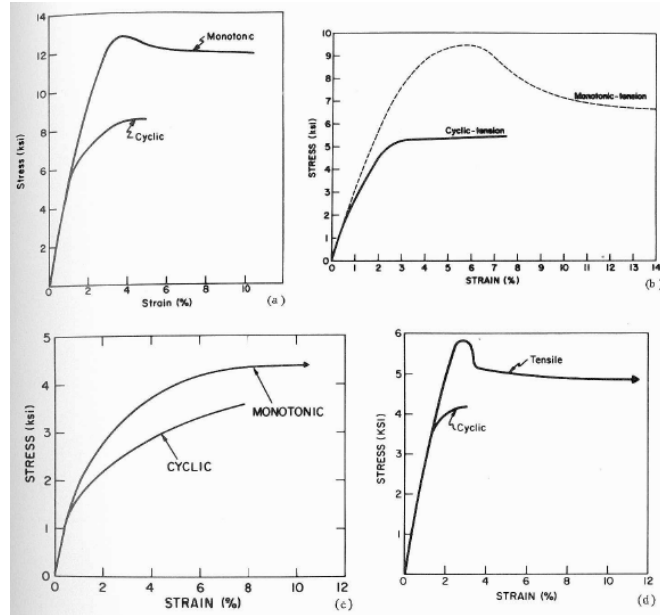


Figure 18. Tensile cyclic and monotonic stress-strain curves for nylon 66 (a), polycarbonate (b), polypropylene (c), and ABS (d). Tests done at 298 degrees K (Beardmore & Rabinowitz) [18].

Barring fatigue failure which can be attributed to thermal runaway, crack propagation in polymers can generally be related to the Paris crack propagation law, originally developed to describe metal fatigue crack propagation, which describes the crack growth rate (da) as crack advancement per cycle (dN):

$$\frac{da}{dN} = C(\Delta K)^m \quad (\text{Eq. 12})$$

Where C and m are material constants and ΔK is the stress intensity range ($K_{\max} - K_{\min}$). Nevertheless, “other polymeric solids have shown FCP plots which assume a sigmoidal shape; crack growth rates are sometimes found to decrease to vanishingly low values as ΔK approaches some limiting threshold value ΔK_{th} and increase to very high values as K_{\max} approaches K_c (Hertzberg, 1976) [10], (Manson & Hertzberg, 1973) [21].”

Loading frequency itself can influence the fatigue of polymers in several ways, but it should be noted that loading frequency effects are not uniform for all polymers—effects are

dependant on which polymer is being analyzed. With respect to fatigue crack growth rate, startling variation in crack growth rate is observed across different polymers when loading frequency is varied. “When prenotched samples were tested over a range of cyclic frequencies from 0.1 to 100 Hz, the associated fatigue crack propagation rates for several polymers... decreased with increasing frequency. Other polymers... showed no apparent sensitivity of fatigue crack propagation rate to test frequency (Hertzberg & Manson) [2].”

The contrasting behavior for two different polymers, polycarbonate and PVC, is shown in Figure 19. A table which shows polymers which exhibit negligible or significant effects on frequency sensitivity factor (defined as: the multiple by which the fatigue crack propagation rate changes per decade in change in test frequency) is shown in Table 1. It is known that frequency dependant crack propagation effects can frequently be attributed to environmental effects in metals (Bannantine, 1989) [19]. Environmental tests were performed which showed that PVC in an environment of N₂ and air and PMMA in environments of H₂O, air, and N₂ had no effects on crack propagation rates (Hertzberg & Manson) [2].

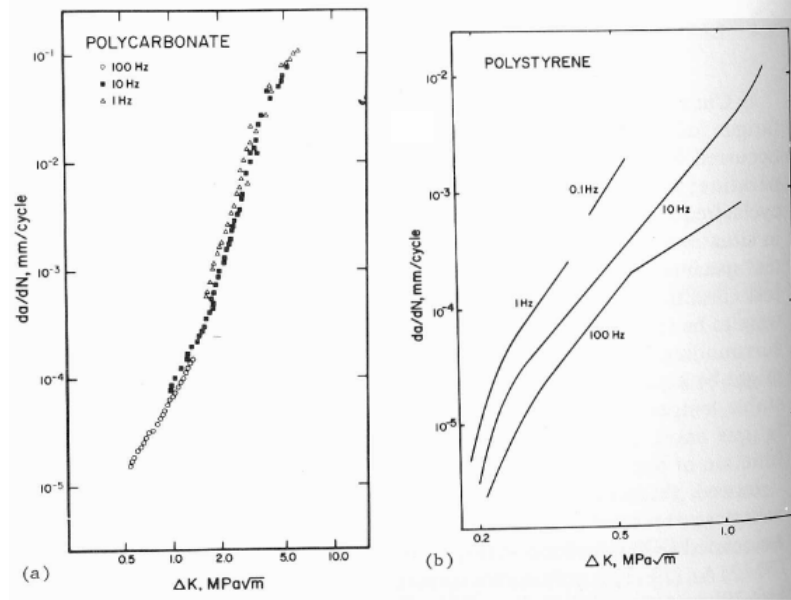


Figure 19. Contrasting effect of cyclic frequency on FCP rates in polycarbonate (a) and polystyrene (b) (Hertzberg, et. al.) [20].

Table 1. Selected polymers which exhibit contrasting "Frequency Sensitivity Factors" (FSF) at room temperature (Hertzberg, et. al.) [20] (Manson & Hertzberg) [21].

Material	FSF	Material	FSF
PMMA	2.5–3.3	PC	1
PS	2.3	PSF	1
PPO/HIPS	2	Nylon 66	1
PVC	1.8	PVDF	1
CLPS	<1.5		

The shape of the waveform itself also can have a dramatic effect on FCP rate. Table 2 illustrates this. Similar to frequency effects, there is no uniform response to waveform shape for all polymers. Some polymers exhibit FCP rates which improve for a certain waveform, while in other polymers this same waveform exhibits a strongly deleterious effect. When the R-ratio is varied, the response of a polymer varies for different kinds of polymers. For a fixed ΔK level, metal alloys typically have an increasing crack growth rate when R is increased. This is true of some polymers as well. Others however, as shown in Table 3 below, actually have their crack growth attenuated when the mean stress is increased.

Table 2. Crack growth rates of selected polymer for various waveforms (Hertzberg et. al.) [20], (Skibo) [22], (Manson, et. al.) [23], (Harris & Ward, 1973) [24].





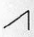
Material	$\Delta K(\text{MPa} \cdot \text{m}^{1/2})$	$(da/dN) \times 10^4 (\text{mm/cycle})$				
						
PVC ⁵⁵	0.72	1.17	1.41	1.02	1.08	0.8
PS ⁵⁵	0.77	—	21.6	17.8	14.5	13.9
PMMA ³⁴	0.83	—	19.2	7.8	8.2	7.8
Epoxy(A/E = 1.6) ⁵⁵	0.70	2.26	2.20	—	2.3	—
PC ⁵⁶	1-3	No Change		—	—	—
Vinyl Urethane ⁵⁷	1.25	—	17	—	100	—

Table 3. The effect of mean stress on fatigue crack propagation in selected polymers (Hertzberg & Manson) [2].

Material	Condition	Change in da/dN as R^a increases from 0.1 to 0.5
PMMA	Commercial sheet High M_w	Increase
PMMA	High M_w ; cast	Increase
PVC	Molded; M_w —96,000	Increase
PVC	Molded; M_w —141,000	Increase
PVC	Molded; M_w —220,000	Increase
Epoxy	Amine/epoxy—1.8/1	Increase
Epoxy	Commercial grade	Increase
PVDF	Extruded	Increase
Nylon 66	Extruded	Increase
HI-N66	Extruded	Increase
Polystyrene	Extruded	Increase
PVC	Commercial sheet extruded	Decrease
PC	Commercial sheet extruded	Decrease
ABS	Commercial sheet extruded	Decrease
PSF	Commercial sheet extruded	Decrease
PPO/HIPS	Commercial sheet extruded	Decrease
LDPE	Commercial sheet	Decrease

^a R = minimum load/maximum load.

One interesting feature of polymers which suggests a principle of polymer fatigue behavior, true for most polymer types, is the relation of frequency sensitivity to the “jump frequency.” The jump frequency is “the frequency of movement of main chain segments

responsible for generating the principal transition— β peak—at a common test temperature (Hertzberg et. al., 1975) [20] (Skibo, 1977) [22].” Notice that the polymers with lower jump frequencies in Figure 20 are also those which have a higher frequency sensitivity factor in Table 1 (page 27). This is because the “frequency sensitivity factors” in Table 1 were recorded at feasible testing frequencies of between 0.1 and 100 Hz. Those polymers which have jump frequencies which are, relatively, higher in Figure 20 will not exhibit frequency sensitivity when testing frequencies are well below their jump frequency. Jump frequencies can be lowered by temperature—theoretically, a lower test temperature will either attenuate or amplify frequency sensitivity depending on whether the temperature shift brings the jump frequency into the range of the testing frequency. This has been empirically shown to occur in tests of PMMA. At temperatures well below ambient, its jump frequency is significantly lowered and it behaved as predicted: its frequency sensitivity lessened as temperature was lowered and disappeared at 150° K (Hertzberg & Manson) [2]. Figure 21 shows that the difference between the test temperature, T , and the jump frequency temperature—the beta transition temperature T_{β} --determines the degree of frequency sensitivity for several different polymers. It should be remembered that the plastic zone ahead of a polymer crack will experience a temperature rise and influence the effective jump frequency which is actually controlling progressive cracking (Figure 22).

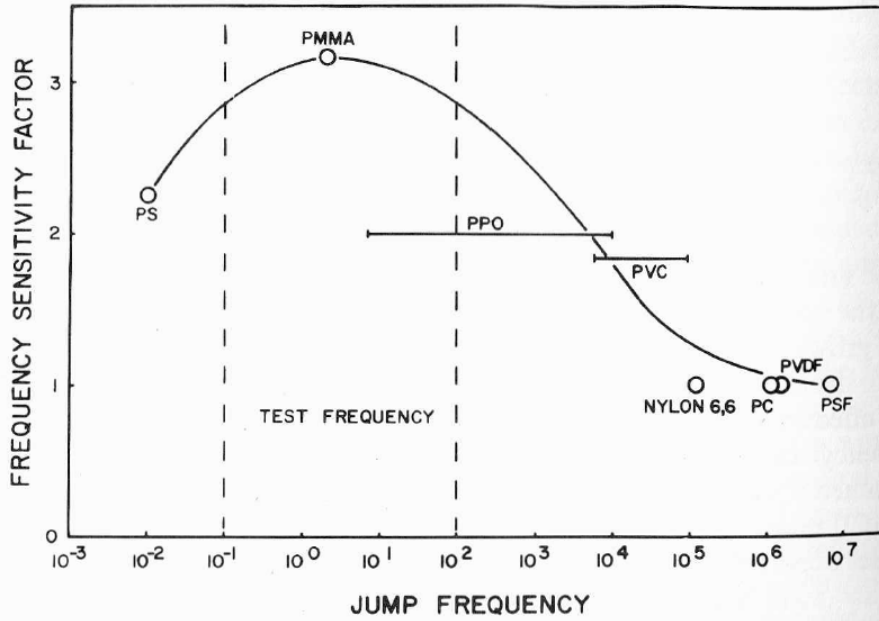


Figure 20. A plot of jump frequency against frequency sensitivity factor which might suggest a relation between the two (Hertzberg et. al., 1975) [20].

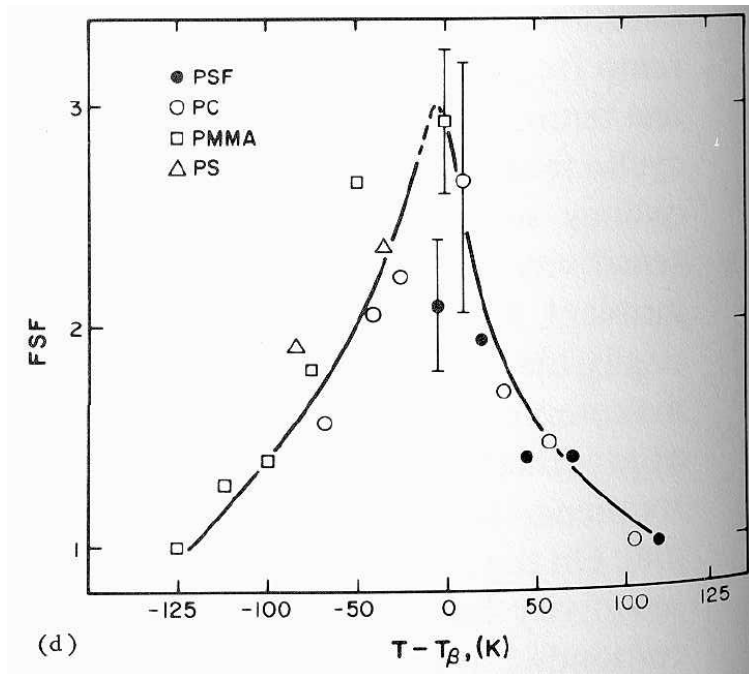
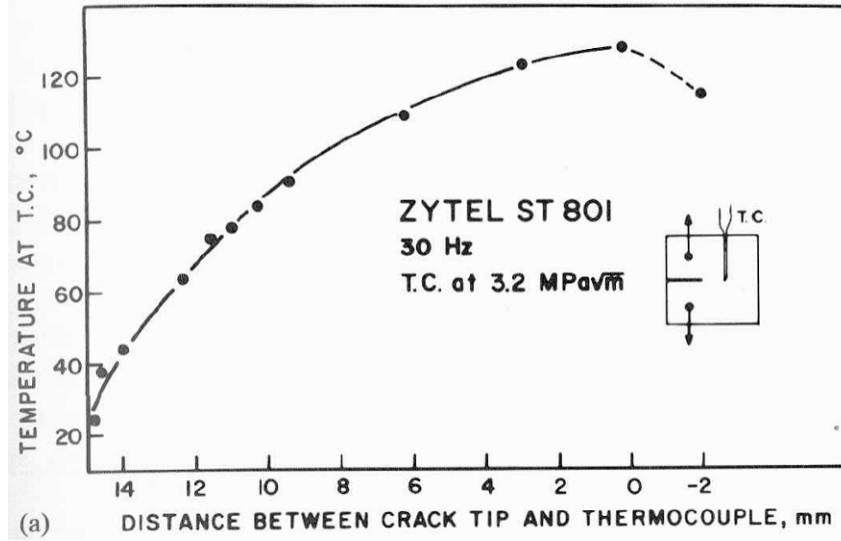


Figure 21. Effect of temperature on frequency sensitivity factor (FSF) relative to the beta transition temperature of various polymers (Hertzberg et. al., 1978) [25].



(a) Figure 22. Hysteretic heating induced temperature increase for nylon 66--temperature rise at thermocouple site along crack plane (Skibo, et. al., 1979) [26].

2.3 Cross-Ply Carbon Fiber Laminates

Because this study investigates the static and fatigue crack initiation of a $[0/90_5]_S$ laminate, this portion of the background will be devoted to a review of general laminate theory as well as research studies which specifically studied cross-ply laminates.

2.3.1 Microstructure Description

Composites consist of at least two materials which are bonded together in some manner to share the bearing of a load. The materials retain a distinct boundary and distinct physical and chemical properties are maintained. The reinforcement material is typically a fiber (Mallick, 1993) [6]. One way of building composite structures is employing cloth woven from these fibers, but high performance applications typically rely on layups of multiple unidirectional laminas stacked on top of each other. Composites consist of essentially three constituents.

1. Matrix. This material keeps the fiber reinforcement oriented in its intended direction, acts as a load transferring medium between fibers, and protects the fibers from environmental damage.
2. Reinforcement. Typically have a high modulus and high strength relative to the matrix—particularly for the CFRP investigated in this study.
3. Interface. The bond between the reinforcing phase and the matrix surrounding it. This region is typically quite critical to the fracture behavior of the composite; cracking typically propagates along the interface due to stress concentrations there.

Cross-ply carbon fiber laminates, the subject of this research, are comprised of only two ply orientations: 0° and 90° . The stacking sequence can be of any order, but is typically

symmetric about the layup's midline with a 0° ply sandwiching or being sandwiched by several 90° plies.

There is value to be gained from studying crack initiation in 90° plies. Quasi-isotropic laminates are still heavily used in those industries which employ CFRP (Panel, 2007) [27], and these laminates contain 90° plies. Cracks will first initiate in 90° plies in both monotonic or fatigue testing of CFRP (Mallick, 1993) [6], (Rebiere, 2002) [28], (Charewicz, 1986) [29]. Cracks then propagate from the 90° plies into adjacent plies. Thus, cracking in the 90° plies is the origin of material degradation and failure in laminates which contain them. To prevent or mitigate degradation in CFRP laminates, crack initiation in 90° plies must be studied. This is the motivation for this study, as well as this portion of the background research investigation.

Unidirectional laminas, and those used to build up the laminates in this study, have a typical "fiber volume fraction" of 60% (Tay, et. al.) [1], (Jones, 1999) [30]. For this study, individual laminas are approximately $1.88\text{E-}04$ m thick ($7.4\text{E-}03$ inch) (Gosse, Christensen, Yu, 2007) [31], and the fibers in these laminas are Hexcel IM-7, with a diameter of $5.2\text{E-}06$ m ($2.03\text{E-}04$ inch) [APPENDIX A, Hexcel IM-7 Fiber Material Properties]. Thus, the thickness of the lamina is approximately 36 fiber diameters.

2.3.2 Load / Deformation Response

For static loading, the load-to-failure curve of a cross-ply laminate exhibits four distinct stages of material response (Mallick [6], and Charewicz & Daniel[29]) to load:

1. Elastic Response: a given cross-ply laminate will have no residual strain upon unloading, if the peak static load applied is below a certain threshold value—determined by the constituents and the stacking sequence.

2. 90° Ply Rupture: transverse splits in the 90° plies begin to appear, as in Figure 23.
3. Characteristic Damage State: a maximum crack density in the 90° plies is reached (Reifsnider) [4]. This maximum crack density can be modeled with a “shear-lag” analysis (Berthelot et. al.) [5]. The 0° plies are now exposed to bearing the maximum tensile loading at all locations where the 90° plies have cracked. Jamison note that this is a laminate property and dependant on local stress (suggesting an analysis of this form) in some way—i.e. C.D.S. is only dependant on properties of the plies, their thickness, and the stacking sequence, but is a property which is independent of load history or load magnitude [35]. The C.D.S. can be reached through sufficiently high quasi-static loading or via a sufficient amount of fatigue loading.
4. Rupture: the unidirectional 0° plies fail, causing specimen rupture. When a load is reached which induces a sufficient number of local fiber failures (at the transverse crack tip’s interface with the 0° laminas), a catastrophic propagation of cracking through all 0° fibers of the lamina occurs. In a study by Charewicz & Daniel (1986) [29], they noted that, “random fiber breakage leads to matrix cracking in the load-carrying plies, for example, 0° plies, in the loading direction which can be distributed or localized. The criterion for ultimate failure is the maximum strain in the 0° plies. When the local strain reaches the ultimate strain for the ply, with the appropriate statistical distribution, failure occurs.” A study by Lorenzo and Hahn (1986) [32] employed the unique specimens shown in Figure 24 below. Their study showed that there was little or no ductile matrix crack growth after a single fiber failure in static loading (and the same behavior was noted in fatigue)—the matrix

crack which stems from a single fiber failure cut the adjacent bundles immediately. In a unidirectional lamina, close spacing of 0° fibers would likely allow more load-sharing than the specimens employed by Lorenzo & Hahn, and thus a single fiber failure will not cause catastrophic failure of the whole 0° ply.

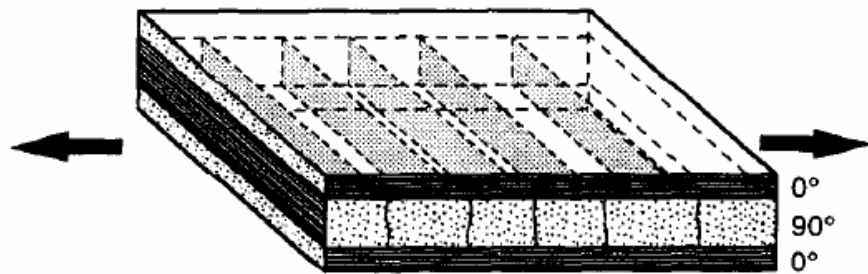


Figure 23 A schematic of a cross-ply laminate with transverse cracks developing in the 90° plies (Berthelot et. al., 1996) [5].

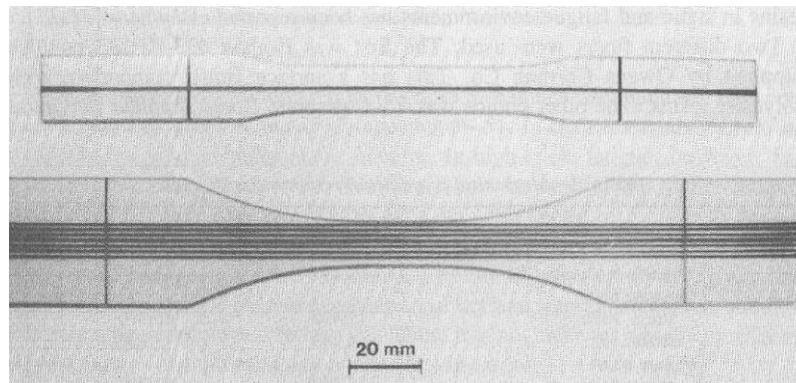


Figure 24 The “layer specimen” employed by Lorenzo and Hahn (1986) [32]; when one graphite bundle failed, the stress concentration on the adjacent bundle increased to such a degree that catastrophic failure immediately occurred.

Thus, matrix stress concentrations play a pivotal role in failure of composite laminates. Lagace & Nolet (1986) [33] performed residual strength studies on honeycomb core laminates with through-thickness holes loaded in fatigue. They showed that delaminations can serve to redistribute stress in the laminate and alleviate stress concentrations on the major load-bearing plies. This ‘stress redistribution’ can even cause a slight *increase* in the residual strength of delaminated specimens, as compared to uncycled

specimens. Delamination is observed in fatigue loading of composite laminates but not in static monotonic tests; this was shown in a study of quasi-isotropic laminates by Carlsson, Eidefeldt, & Mohlin (1986) [34], and in the cross-ply studies of Jamison (1986) [35], and the Charewicz & Daniels [29] study, illustrated in the radiography images of Figure 38. The static behavior of a cross-ply laminate is shown in Figure 25 and Figure 26 below. The static monotonic test results which were obtained in the current study were similar, and can be seen in Figure 82.

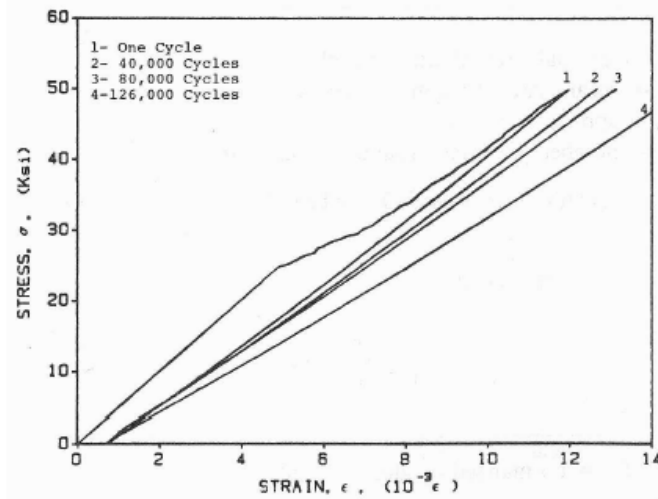


Figure 25. A stress-strain curve for a cross-ply laminate. Here, note the behavior in cycle 1. This shows the first three regimes mentioned above (Charewicz & Daniels) [29].

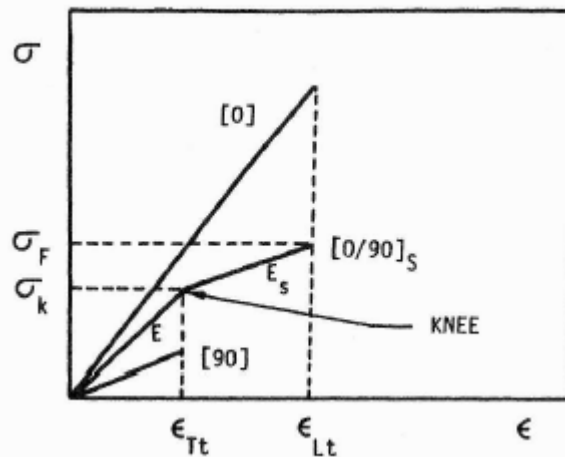


Figure 26. Stress-strain schematic illustrating separate behaviors of 0° and 90° plies, and their behavior when combined as a cross-ply laminate (Mallick) [6].

It was stated earlier that damage development in CFRP is a progressive event. Cracks initiate in 90° plies and then propagate via stress concentrations on the adjacent plies at the lamina interface. For a sufficient load, these stress concentrations will cause failure of the primary load-bearing plies, causing ultimate failure / rupture of the laminate. The motivation for this study was to study crack *initiation* in the 90° plies, which originate damage. There are several reasons to study the behavior of 90° plies embedded in cross-ply laminates, as opposed to unidirectional 90° laminates:

1. It is thought that cracks which initiate in the 90° plies of cross-ply laminates propagate immediately in quasi-static testing, and the observations in this study and the conclusions of other authors (Jamison, 1986) [35], suggest that the same is true in fatigue testing. However, in tensile testing of *unidirectional* 90° laminates, this property of “immediate crack propagation” renders the study of progressive damage development in monotonic loading impossible: the first crack destroys the specimen. A cross-ply specimen prevents this immediate specimen rupture, and enables the study of progressive damage development in the 90° laminas. This is even more important for the study of fatigue.
2. Failure of 90° unidirectional laminates also appears to be, statistically, an event with a wide range of scatter in σ_{ult} . Before the formal testing of cross-ply laminates for this study, static and fatigue testing of unidirectional 90° and unidirectional 10° laminates was performed. For both of these unidirectional laminates, a large amount of statistical scatter for the same strain conditions was observed, and this behavior was also reported by Plumtree & Shi for 10° unidirectional laminates (Plumtree &

Shi, 2002) [36]. The results of the current study suggest that specimen edge smoothness influences crack initiation in fatigue. As in the fatigue of metals then, it appears to be the presence of a “favorable flaw”—a statistical phenomenon—which initiates the cracking in cross-ply.

3. With respect to real-world application of fibrous composite structures, there are few design situations which will necessitate strictly 90° plies (Mallick) [6], without any adjacent on-axis plies restraining them. 90° laminate behavior, independent of adjacent load-bearing plies, would be a purely academic study. A caveat to this could exist: if unidirectional ply behavior as a function of fiber orientation would be useful *if* that behavior could be translated into a laminate analysis. However, typical composites are multidirectional laminates and the damage which develops in these laminates is propagating *from* the cracks which initiated in the 90° plies (Jamison) [35]. Therefore, static and fatigue behavior independent of adjacent plies does not add much value with respect to predictive modeling of real composite structures.

2.3.3 Laminate Modeling

Several simple analytical models can be used to calculate three values of interest for the cross-ply laminate with a fair amount of accuracy:

1. The distribution of loading between the 0° and 90° plies, via the Rule of Mixtures (ROM) and the Halpin-Tsai equations.
2. The σ_{ult} value for the cross-ply laminate in monotonic loading, through a simple ultimate stress calculation applied to the 0° ply cross-sectional area.

3. The gross laminate modulus can also be predicted with fair accuracy using Classical Lamination Theory (CLT) and the Rule-of-Mixtures (ROM).

First, the modulus of the 90° plies can be calculated. Though the fibers are incapable of bearing load along their longitudinal axis, they do contribute to stiffening these plies, and serve as hard asperities within the matrix (Mallick) [6]. Thus the modulus cannot simply be assumed to be equivalent to the matrix modulus. For this reason, Halpin and Tsai (1976) [37] developed equations which account for fiber packing geometry via fitting parameters. E_{22} , the transverse modulus, can be calculated as:

$$\frac{E_{22}}{E_M} = \frac{1 + \zeta \kappa V_f}{1 - \kappa V_f}$$

(Eq. 13)

Where

$$\kappa = \frac{(p_f / p_m) - 1}{(p_f / p_m) + \zeta}$$

(Eq. 14)

E_M is the matrix modulus, V_f the fiber volume fraction. ζ is a measure of reinforcement geometry, packing geometry, and loading conditions. When computing E_{22} , it takes on a value of 2. ‘ p_f ’ is the fiber property of interest (E_f , G_f , ν_f , etc.), while ‘ p_m ’ is the same property for the matrix. An alternative prediction for E_{22} can be obtained from the “inverse rule of mixtures”:

$$E_{22} = \frac{E_f E_m}{V_m E_f + V_f E_m}$$

Eq. 15

and this calculation compared favorably with experiments performed in this study.

The σ_{ULT} value for a cross-ply laminate can also be calculated via ROM, once the E_{22} value has been computed using the Halpin-Tsai equations. First, the net modulus of the 0° plies has to be computed, E_{11} . This is calculated using the rule of mixtures as well:

$$E_{11} = E_f V_f + E_m V_m$$

(Eq. 16)

Where E_f is the fiber modulus, V_f the volume ratio of fibers (60% for this study), and subscripts ‘m’ denote the same properties for the matrix. Then, the net laminate modulus, $E_{11,Lam}$, can be computed using the laminate volumetric ratios of the 0° plies (V_{0° , with modulus of E_{11}) and 90° plies (V_{90° , with the modulus of E_{22} computed with Halpin-Tsai) as:

$$E_{11,Lam} = E_{11} V_{0^\circ} + E_{22} V_{90^\circ}$$

(Eq. 17)

Finally, the σ_{ULT} value for a cross-ply laminate can also be calculated with fair accuracy (within 10-15% of experimental values, except when edge delamination dominates the failure process, (Reifsnider & Jamison, 1982) [38] using a simple analytical model. Referring to Figure 23 will help in visualizing this analysis. In the laminate cross sections where transverse cracks have already split the 90° plies, the load is being borne solely by the outer 0° plies. The ultimate load is thus dependant on the ultimate strength and cross-sectional area of those 0° plies. Ultimate load in this study was predicted with fair accuracy in this study, using this method.

Having performed some simple calculations to predict the macromechanical cross-ply laminate behavior, it is worthwhile to discuss analytical solutions which predict micromechanical stress behavior in the 90° plies. These models investigate the stress-field in the neighborhood of the fiber/matrix interface and model the fiber and matrix as discrete

entities. The first and simplest analysis is shown in Figure 27 (Mallick) [6]. The plot displays the fact that tensile stress at the top and bottom of the fiber are nearly 1.5 times the far-field stress.

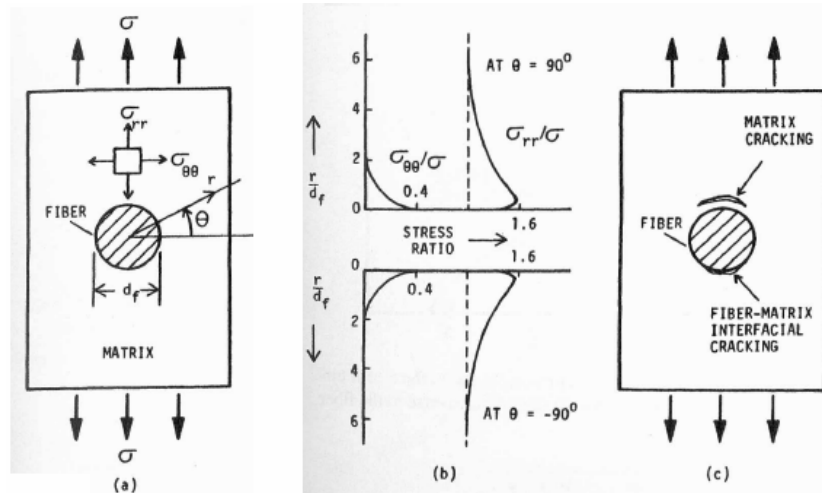


Figure 27. Transverse tensile loading of a 90° lamina, with a single fiber embedded in the matrix. Stress ratio at the top and bottom of the fiber, along the loading axis, are plotted. The radial tensile stress at the fiber/matrix interface is nearly 1.5 times the far-field stress (Mallick) [6].

Though a model of one fiber embedded in a matrix material is a good starting point for determining matrix crack initiation behavior, any real composite lamina looks nothing like Figure 27. Fibers in real unidirectional laminas are packed closely together, and matrix stress concentrations around fibers interact with each other to magnify stresses well beyond the single fiber stress concentration of 1.5. Mallick [6] and Adams and Doner (1967) [39] modeled circular fibers arranged in a square array. Their model was a finite difference method which varied fiber volume fractions by varying interfiber spacing. Logically, the peak principal stress will be at $\theta = 90^\circ$ and -90° , along the length of the fiber loading, refer to Figure 28 and Figure 29. The Halpin-Tsai equations show that transverse modulus increases with increasing fiber packing density, but this incremental gain in modulus can be outweighed by these stress concentrations which cause earlier failure (far better to design for strength by relying on 0° laminas, when designing with laminates). A simple equation

offered by Greszczuk (1966) [40], predicts the ultimate tensile strength of 90° plies through the use of K, the familiar stress concentration parameter:

$$\sigma_{90^\circ,ULT} = \frac{\sigma_{M,ULT}}{K_\sigma}$$

(Eq. 18)

Where

$$K_\sigma = \frac{1 - V_f [1 - (E_m / E_f)]}{1 - \sqrt{(4V_f / \pi) [1 - (E_m / E_f)]}}$$

(Eq. 19)

This equation too assumes a square array of fibers, but still achieves good results when compared to the finite difference model for V_f less than ~60%.

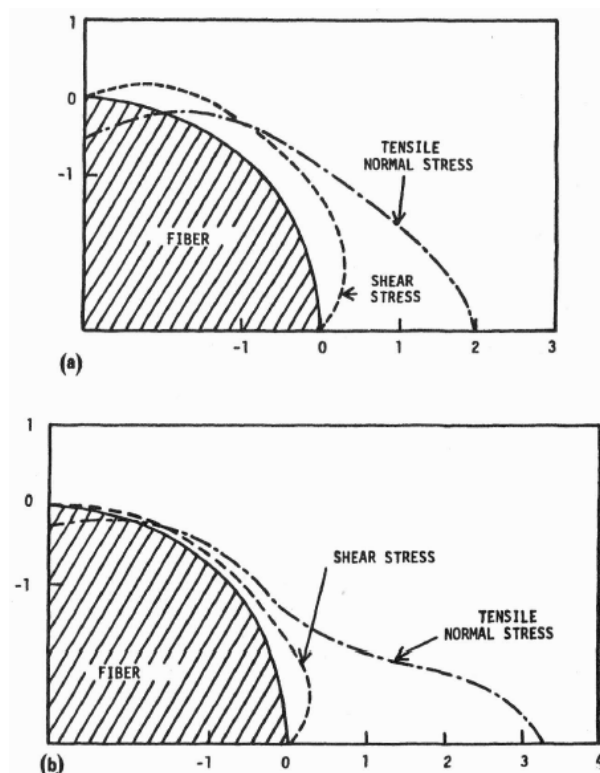


Figure 28. Shear stress and tensile normal stress for two different fiber volume ratios: 55% (a) and 75% (b) (Mallick) [6].

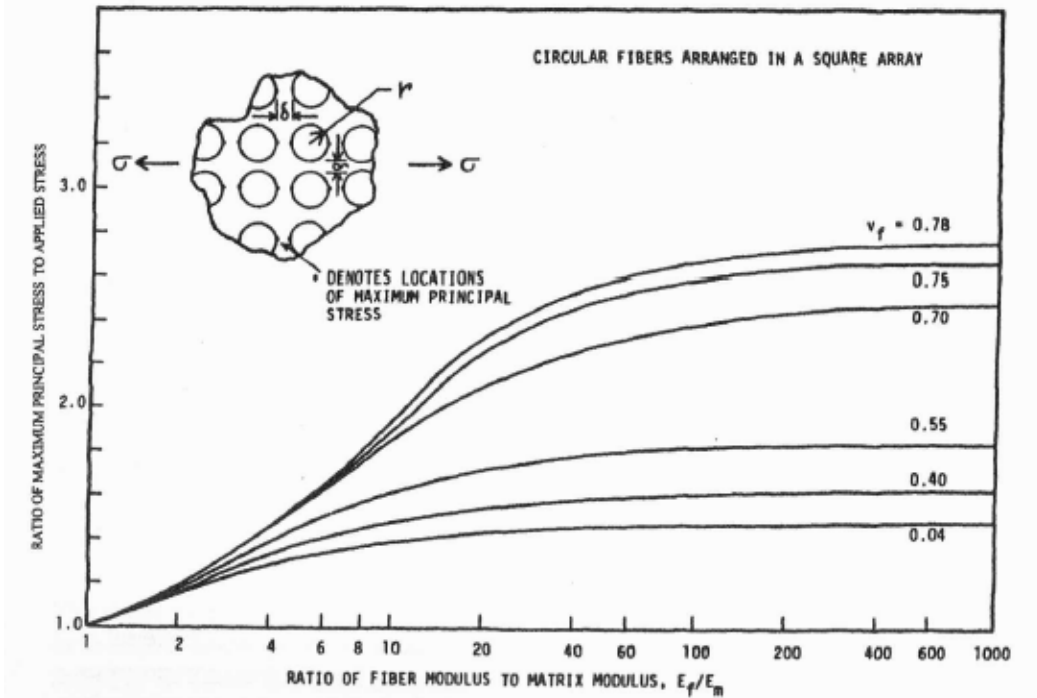


Figure 29. Maximum principal stress as a function of fiber volume ratio and fiber to matrix modulus ratios. Note that V_f for this study is 0.60 and our peak stress concentration for this ideal square packing arrangement would be approximately two times the far-field stress (Adams & Doner) [39].

For static loading, analytical and FEA models have been used to describe the stress and strain field in the neighborhood of a crack for cross-ply laminates. The concept of “shear-lag” in particular has relevancy to the case of cross-ply: the progressive transfer of tensile load into the compliant 90° plies, from the 0° plies, with increasing distance from a transverse crack in the 90° plies. The shear-lag model was originally developed by Cox (1952) [41], and was an analytical model which explained how tensile stress developed in a discontinuous fiber. It models shear stress transfer from the matrix material, applied at the ends of the fiber, visualized in Figure 30. This model stated average axial fiber stress, σ_f , as a function of x , the position along the length of the fiber (Figure 31), in the following way:

$$\sigma_f = E_f \varepsilon_1 \left[1 - \frac{\cosh \beta(l_f/2 - x)}{\cosh \beta l_f/2} \right] \quad \text{for } 0 \leq x \leq \frac{l_f}{2}$$

(Eq. 20)

where:

$$\beta = \sqrt{\frac{2G_m}{E_f r_f^2 \ln(R/r_f)}} \quad (\text{Eq. 21})$$

In the equation for β , “2R” is the center-to-center distance from a fiber to its nearest neighbor.

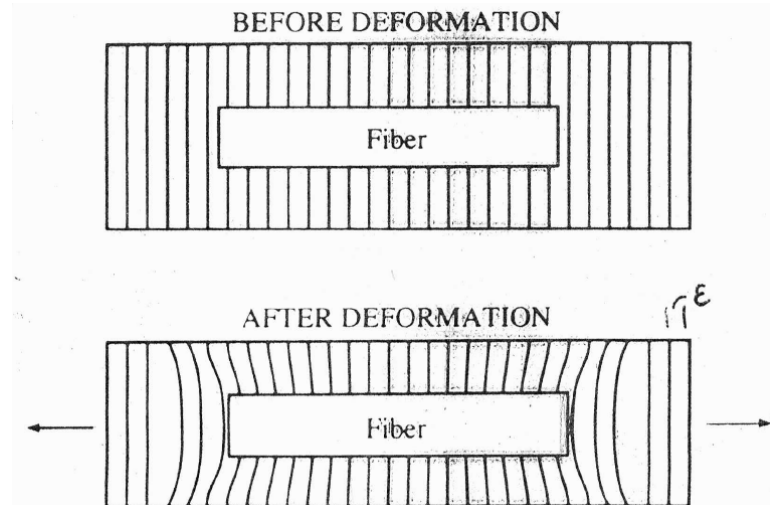


Figure 30. Illustration of matrix displacement field for a composite with $E_f \gg E_m$. [42]

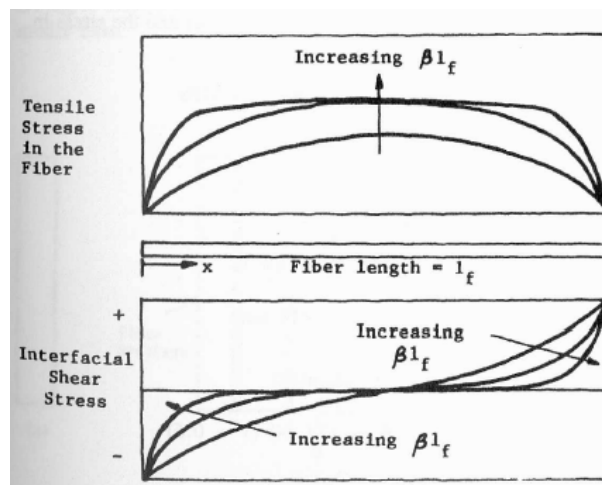


Figure 31. Example of the plots which the Cox shear-lag model generates for shear and tensile stress in the fiber (Mallick) [6].

This model has been extended to the case of interlaminar load transfer in cross-ply laminates, where shear load progressively applies a tensile load in the 90° plies from the

neighboring, unruptured 0° ply(s), starting from an already-present transverse crack in the 90° plies. This modified shear-lag analysis, which incorporated an interlaminar shear-layer concept, was formulated first by Fukunaga et. al. (1984) [43]. By employing the “elementary cell” geometry illustrated in Figure 32, selecting appropriate boundary conditions and governing equations (parabolic variation of longitudinal displacement), Lee and Daniel (1990) [44] developed the “complete parabolic shear-lag analysis.” With this formulation, the calculation of average longitudinal stresses in the 0° layer is:

$$\bar{\sigma}_{xx}^{90}(x) = \sigma_c \frac{E_{90}}{E_x^0} \left(1 - \frac{\cosh \eta a(x/l)}{\cosh \eta a} \right)$$

(Eq. 22)

Average longitudinal stress in the 90° layer:

$$\bar{\sigma}_{xx}^0(x) = \sigma_c \frac{E_0}{E_x^0} \left(1 + \frac{t_{90}}{t_0} \frac{E_{90}}{E_0} \frac{\cosh \eta a(x/l)}{\cosh \eta a} \right)$$

(Eq. 23)

And shear stress at the 0°/90° interface:

$$\tau(x) = \sigma_c \frac{E_{90}}{E_x^0} \eta \frac{\sinh \eta a(x/l)}{\cosh \eta a}$$

(Eq. 24)

Where:

$$a = \frac{l}{t_{90}} \text{ (called the “aspect ratio” of the elementary cell, Figure 32.)}$$

(Eq. 25)

and,

$$\eta^2 = \frac{3G(t_0 + t_{90})E_x^0}{t_0 E_0 E_{90}}$$

(Eq. 26)

and,

$$G = \frac{G_{xz}^{90}}{1 + \frac{t_0 G_{xz}^{90}}{t_{90} G_{xz}^0}}$$

(Eq. 27)

By incorporating an average displacement term within the displacement relationships, Berthelot et. al. [5] extended the model of Lee and Daniel; this enabled calculation of longitudinal stress in the 0° plies as a function of location (x, z):

$$\sigma_{xx}^0(x, z) = \bar{\sigma}_{xx}^0(x) - \sigma_c \frac{E_0 E_{90}}{2G_{xz}^0 E_x^0} \frac{t_{90}}{t_0} \eta^2 \times \left[\left(\frac{z}{t_{90}} \right)^2 - 2(1 + \alpha) \frac{z}{t_{90}} + \frac{2}{3} \alpha^2 + 2\alpha + 1 \right] \times \frac{\cosh \eta a(x/l)}{\cosh \eta a}$$

(Eq. 28)

Where α is called the “stacking parameter”:

$$\alpha = \frac{t_0}{t_{90}}$$

(Eq. 29)

And similarly, the longitudinal stresses for the 90° layer can be computed as:

$$\sigma_{xx}^{90}(x, z) = \bar{\sigma}_{xx}^{90}(x) + \sigma_c \frac{E_{90}^2}{2G_{xz}^{90} E_x^0} \eta^2 \times \left[\left(\frac{z}{t_{90}} \right)^2 - \frac{1}{3} \right] \times \frac{\cosh \eta a(x/l)}{\cosh \eta a}$$

(Eq. 30)

A shear-lag model was also relied on by Caslini, Zanotti, and O’Brien (1987) [45] to calculate the critical strain energy release (G_c) rate for the onset of 90° ply matrix cracking in a $[0_m / 90_n]_s$ laminate with critical nominal strain ϵ_c :

$$G_c = \frac{(n + m) E_2 E_0}{m E_1 \lambda} \epsilon_c^2$$

(Eq. 31)

where:

$$\lambda = \sqrt{\frac{3}{h^2} \cdot \frac{G_{12}}{E_1} \cdot \frac{E_0}{E_2} \cdot \frac{(n+m)}{n^2 m}}$$

(Eq. 32)

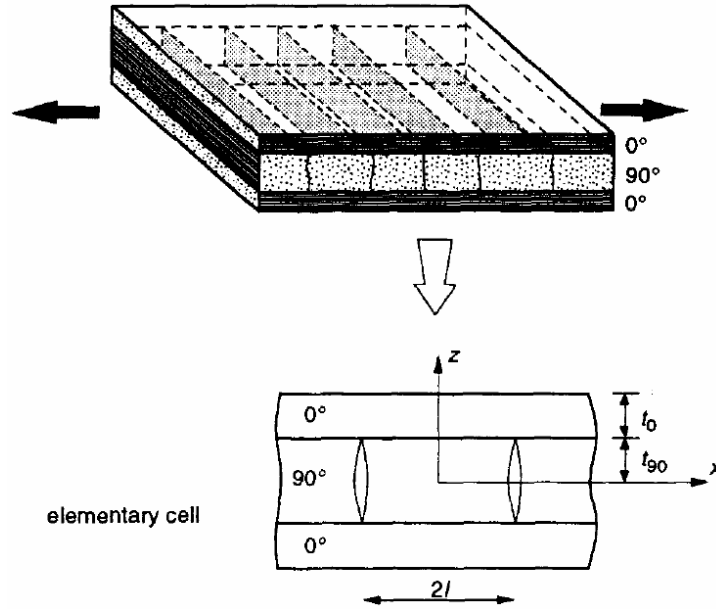


Figure 32. The “elementary cell” whose geometric variables are employed in the modified shear-lag analytical model (Berthelot et. al.) [5].

2.3.4 SIFT

SIFT, a laminate failure model being developed by this project’s sponsors, is a “physics-based” failure theory, in that it relies on the intrinsic material properties, geometry, and strain state of the composite fiber-matrix system to determine whether composite failure will occur. It is currently proven as a static failure theory, but is being extended to the case of fatigue. The method involves the computation of the strain invariants for the applied strain state, which are then “amplified” by factors obtained from micromechanical F.E.M. block models of the system (Figure 33 and Figure 34). The F.E. block model is subjected to various normal and shear deformation modes (Figure 35). Then, the maximum strain

invariant amplification factor is selected from the points in the F.E. block model which was subjected to the same strain field. As explained by Tay, Tan, Tan, and Gosse in (2005) [1], there are three strain invariants needed to determine whether failure will occur: J_1 is the dilatational strain invariant ($\epsilon_x + \epsilon_y + \epsilon_z$); J_2 is the deviatoric strain invariant, related to constant volume von-mises/equivalent strain ($1/3*\epsilon_{VM}^2$); and the third invariant is an effective property determined from testing of coupons: ϵ_{vm}^f . When either of these three strain invariants reaches their respective critical values, failure is predicted to occur. In this investigation, the Boeing sponsors wished to see experimental fatigue failures which their model was predicting.

Jon Gosse at Boeing originally proposed the testing of unidirectional off-axis 10° specimens and unidirectional 90° specimens. 90° specimen testing would furnish material behavior in fatigue for a dilatational strain case, while 10° specimens would suggest fatigue performance for deviatoric strain. After performing a batch of tests with these types of specimens, it was determined that cross-ply specimens would give better data with respect to characterizing crack initiation in 90° plies. The experimental tests of the cross-ply specimens formed the bulk of this study.

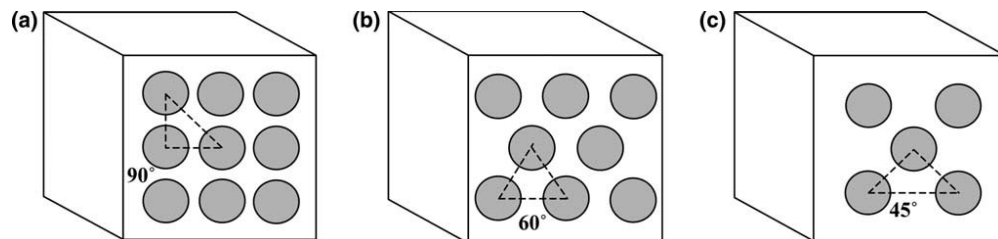


Figure 33 Micromechanical blocks with: (a) square (b) hexagonal and (c) diamond packing arrays (Tay, Tan, Tan, Gosse) [1].

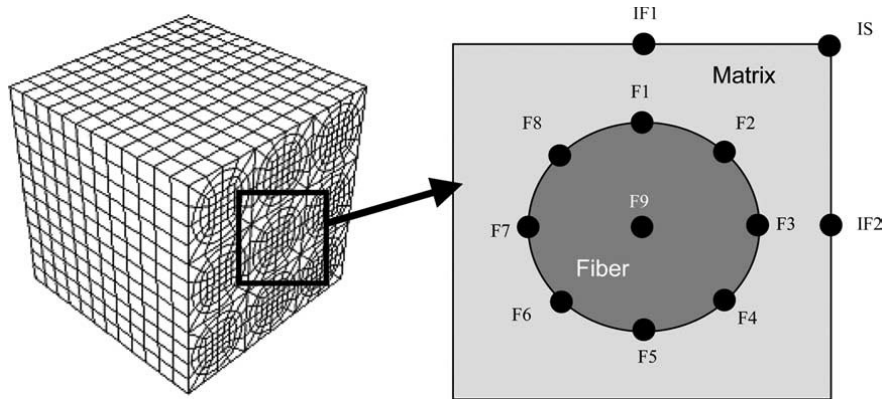


Figure 34 Locations for extraction of amplification factors (Tay, Tan, Tan, Gosse) [1].

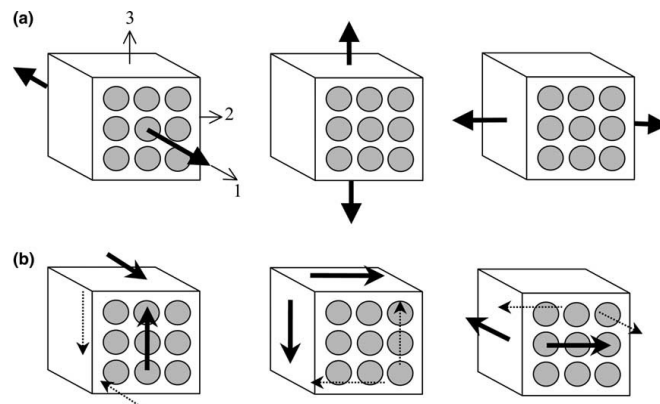


Figure 35 (a) Prescribed normal displacements, (b) prescribed shear deformations (Tay, Tan, Tan, Gosse) [1].

2.3.5 Fatigue Behavior and Characterization

It was noted in the prior section that there are four stages of material response for the cross-ply monotonic testing case: elastic recovery, 90° ply rupture, characteristic damage state, final laminate rupture. The case of fatigue is much more complex with respect to damage development. It was observed by Wang & Crossman (1980) [46], and Xu (1994) [47] that thick cross-ply laminates experience significant delamination. However, Charewicz & Daniel, Jamison, and Highsmith & Reifsnider have observed transverse cracking followed by longitudinal splitting, and only then do small delaminations appear where transverse and longitudinal plies intersect, [29], [35], [48]. The Poisson's mismatch between the 0° and 90° plies causes tensile σ_{yy} stresses in the adjacent 0° ply and, magnified at the tip of the transverse crack, initiate the longitudinal splitting (Jamison, 1986) [35]. The alternative paths in damage development are captured in Figure 36. Based on these studies, it can be concluded that damage progression is dependant on laminate thickness, stacking sequence, and starting materials (Jamison, 1986) [35].

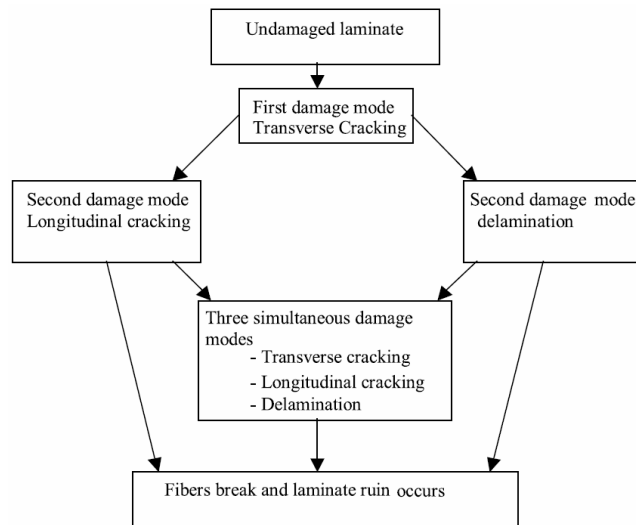


Figure 36. Evolution of damage in cross-ply laminates in fatigue loading. Note that the second damage mode which arises can be either longitudinal cracking or delamination. Which of these two forms occurs first is dependent on the layup and material properties (Rebiere et. al. 2002) [28].

The transverse cracking, longitudinal cracking, and the delaminations which form at the intersection of these two types of cracks are illustrated schematically in Figure 37, and typical radiographs of cross-ply laminates subjected to fatigue at $R = 0.1$ at 10 Hz are shown in Figure 38. Note in Figure 39 that, as peak stresses become lower, the failure mode becomes more like a static failure—a transverse rupture—while at lower peak stresses, the failure mode is one of distributed ruptures in the 0° laminas, giving the failed specimen a “fan-like” appearance.

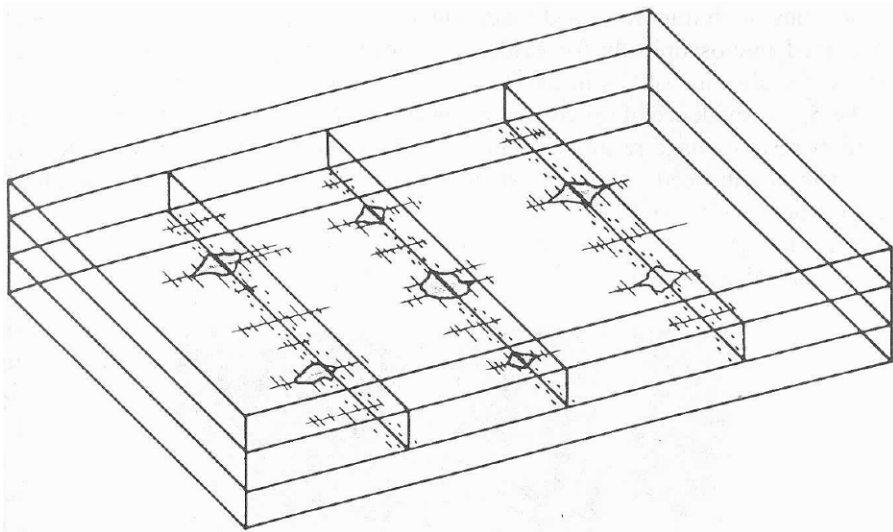


Figure 37. Schematic of damage localization pattern (Jamison, 1986) [35].

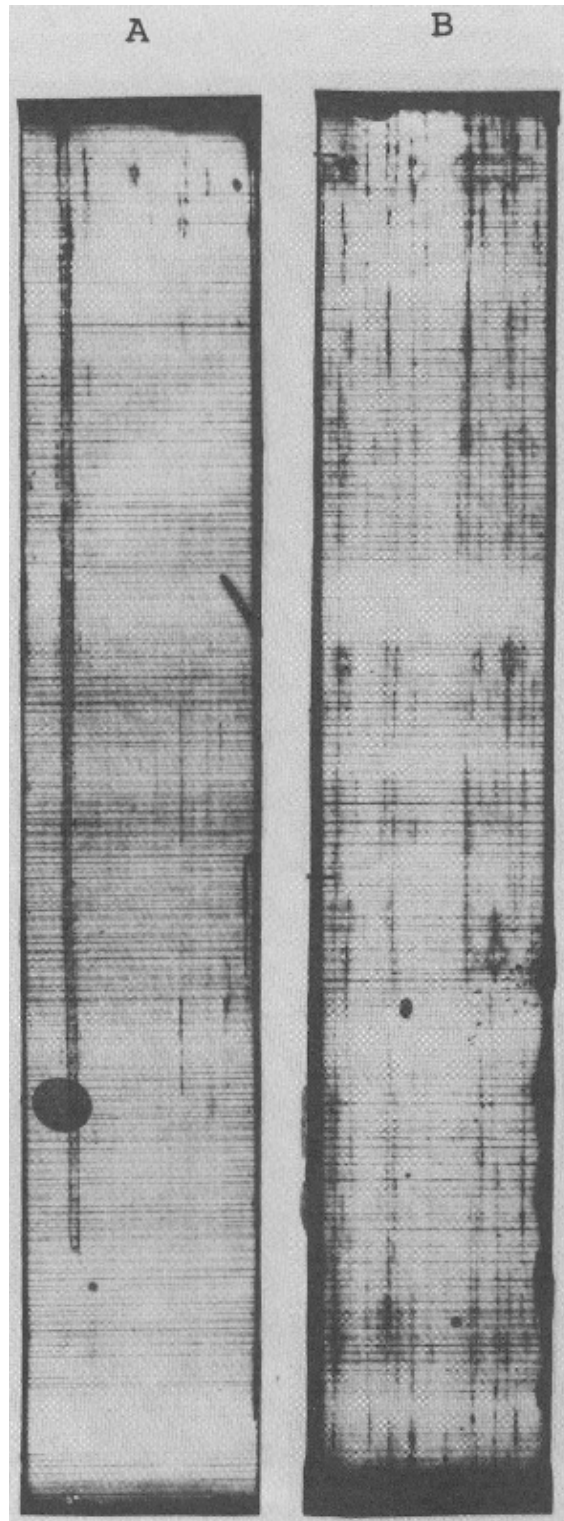
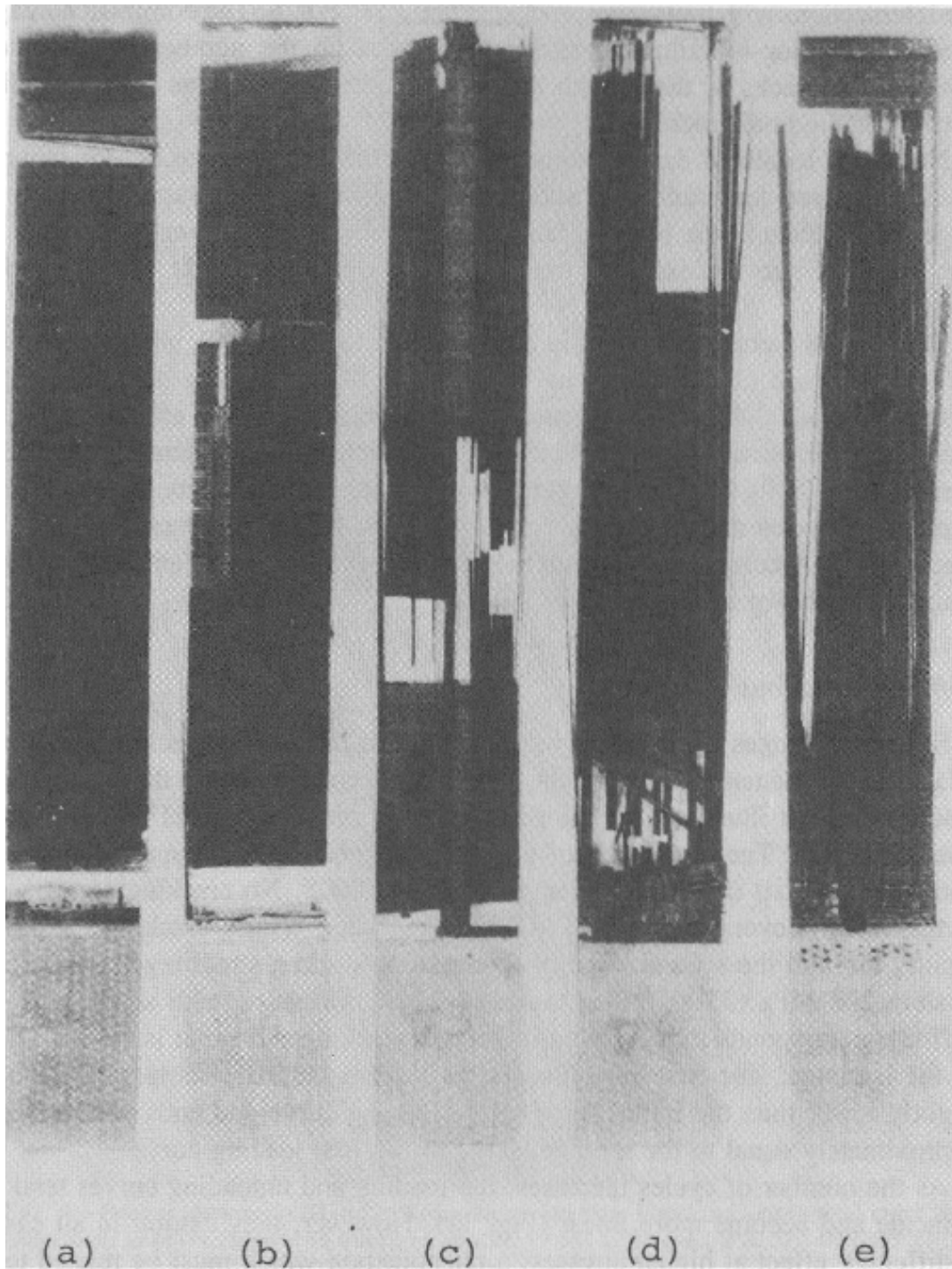


Figure 38. Damage mechanisms in $[0/90]_2$ C.R.F.P.. These images illustrate the difference between high-stress (short life) loading which yields the localized longitudinal cracking visible in (A) while (B) displays the more distributed longitudinal cracking at low-stress fatigue loading (long life) (Charewicz & Daniel) [29].



(a) static test, $\sigma_u = 616 \text{ MPa}$ (89 ksi);
 (b) fatigue test, $R = 0.1$, $\sigma_{max} = 606 \text{ MPa}$ (88 ksi), $N = 370$ cycles;
 (c) fatigue test, $R = 0.1$, $\sigma_{max} = 548 \text{ MPa}$ (79 ksi), $N = 2140$ cycles;
 (d) fatigue test, $R = 0.1$, $\sigma_{max} = 531 \text{ MPa}$ (77 ksi), $N = 12\,357$;
 (e) fatigue test, $R = 0.1$, $\sigma_{max} = 495 \text{ MPa}$ (72 ksi), $N = 349\,529$.

Figure 39. Failure patterns of $[0/90_2]_s$ CFRP tested under static & fatigue loading conditions (Charewicz & Daniel) [29].

The purpose of this study was to investigate crack *initiation* in fatigue. Thus, the load levels applied to the specimens in this study did not develop damage beyond transverse cracking damage. The damage progression described in the flowchart of Figure 36 and illustrated in Figure 37, Figure 38, and Figure 39 display the damage process which leads up to laminate ruin—typical of much higher loads than were used in this study. Whereas this study was employing peak tensile loads of ~15% of σ_{ult} to initiate fatigue cracks at R = 0.1 and 10 Hz, the aforementioned authors and images illustrate tensile fatigue tests performed at 70% or 80% of σ_{ult} at R = 0.1 and 10 Hz.

Run-out values for cross-ply laminates (to one million cycles) vary according to the stacking sequence and the number of adjacent 90° plies. This was demonstrated in an interesting study by Charewicz & Daniel [29] and is shown in Figure 40. This figure demonstrates that, with increasing numbers of adjacent 90° plies, the layup becomes less sensitive to fatigue. Typical run-out values for cross-ply laminates to one-million cycles vary between approximately 50% - 80% of σ_{ULT} accordingly.

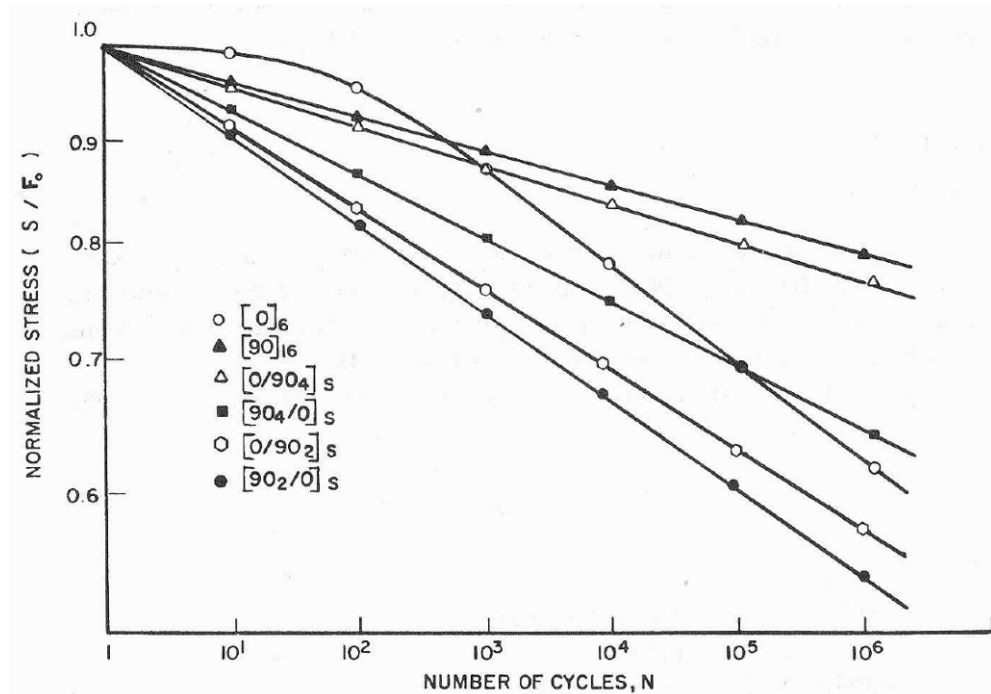


Figure 40. Stress-life (S-N) curves for unidirectional and cross-ply graphite/epoxy laminates (Charewicz & Daniel) [29].

Carbon fibers exhibit negligible plastic deformation prior to rupture and are generally thought to not experience fatigue failure—fiber failure in laminates in fatigue testing is due to increased stresses from development of damage in the matrix (Jamison, 1986) [35]. Therefore, matrix material selection has a very large impact on laminate fatigue performance. For a given layup and fiber, a more brittle polymer matrix will allow a higher endurance limit. This is because brittle epoxies can dissipate more energy and decrease stress concentrations via a higher number of cracks in the material [9]. This is demonstrated in Figure 41 for unidirectional carbon fiber composites. As described earlier and shown in (Figure 13), pure polymers, when subjected to fatigue loading, frequently exhibit shear-band “hackles” at the microscopic scale. These same hackle features are frequently witnessed—Arcan et. al. (1987) [49], Hibbs & Bradley (1987) [50]—in composite fracture studies where the composite laminate is subjected to Mode II loading (Figure 42). As the

percentage of Mode II loading is increased, particularly for more brittle epoxies (between 0.07 and 0.32 kJ/m² for G_{Ic}—the epoxy used in the current study was 0.217 kJ/m²), “the number of hackles as well as their orientation or angle with respect to the ply plane increase as the percentage of shear loading is increased... In the tougher epoxy system (G_{Ic} = 0.73 kJ/m²), yielding and ductile fracture occurs which prevents hackle formation, even at high levels of Mode II loading. Since no change in failure mechanism takes place as loading conditions change from Mode I to Mode II, a less substantial change in delamination fracture toughness occurs (Hibbs & Bradley) [50].” Intuitively, the shearing stress-state ahead of the crack would suggest this would happen, and this is shown in (Figure 43). In Mode I delamination tests (which are analogous to the loading of the 90° plies within a cross-ply laminate), failure is observed to occur at the fiber-matrix interface (Figure 44). This is supported by the author’s own observations in this study. Due to the stress concentrations in the matrix around the fibers and the potentially weak adhesion between the fiber and matrix, the interfacial zone can be prone to serving as ‘the path of least resistance’ for crack development.

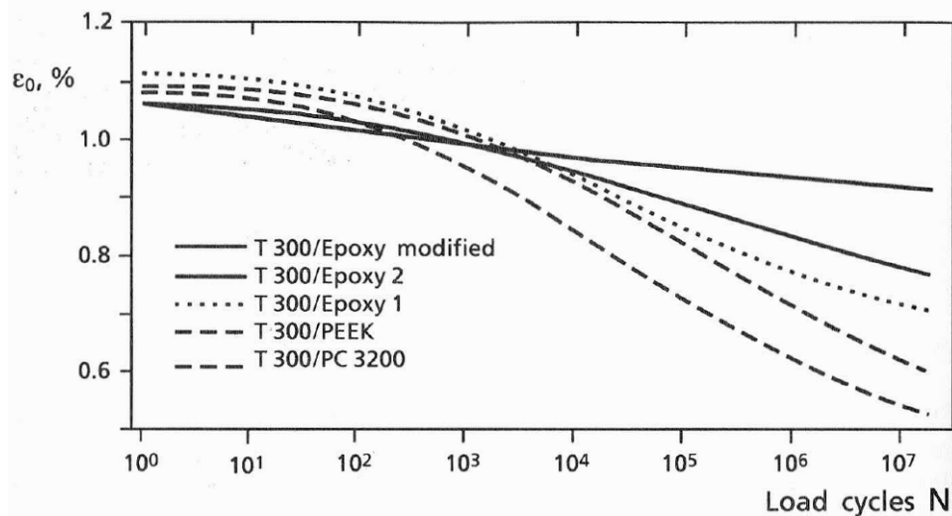


Figure 41. Endurance limits for unidirectional composites with various epoxies. Epoxies which are more brittle exhibit higher endurance limits (Hartwig) [9].

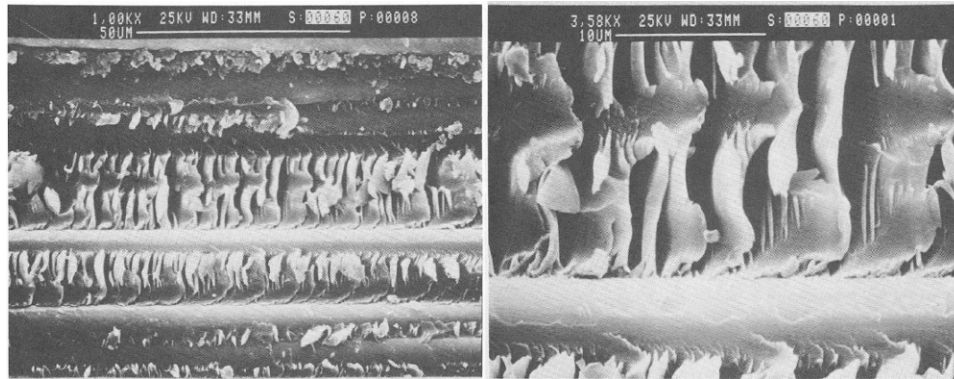


Figure 42. Mode II fracture in unidirectional AS4/3501-6 CFRP (Arcan et. al.) [49].

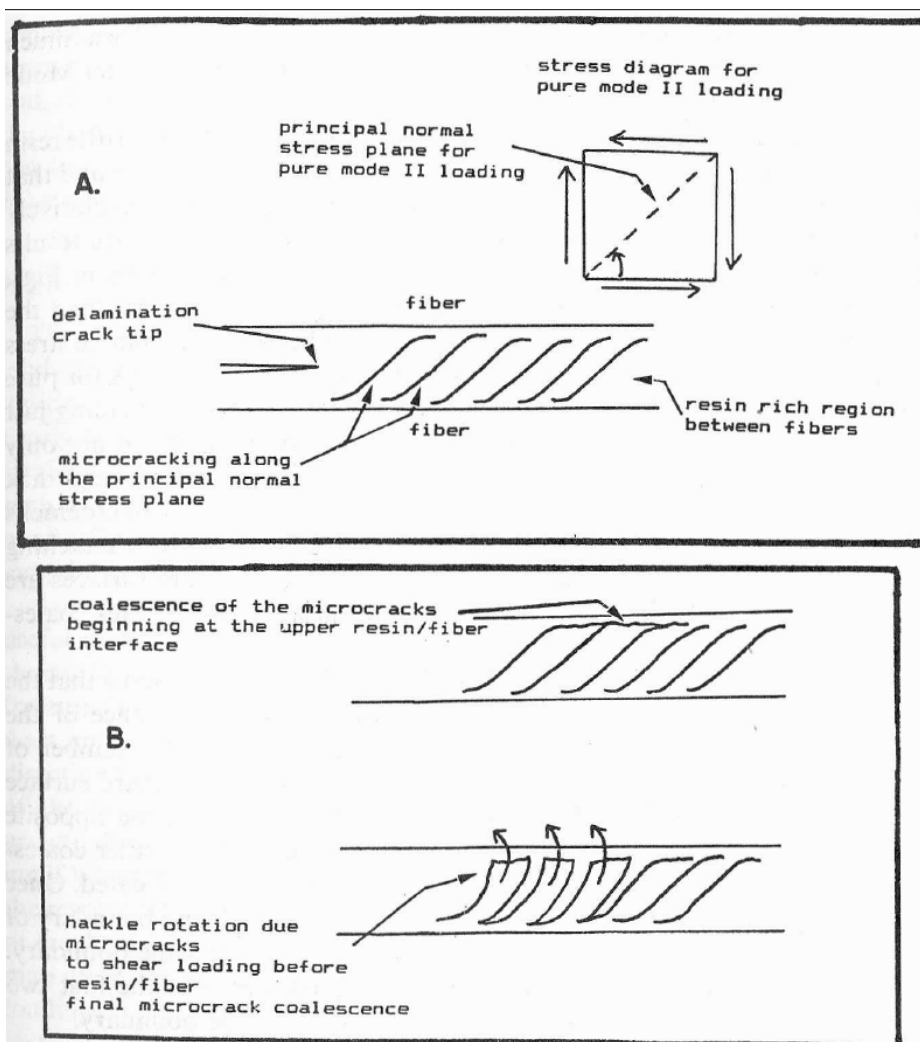


Figure 43. (A) Plane of principal stress for shear loading causes hackle formation in the matrix between fibers. (B) Direction of 'hackle slant' is dependant on whether microcracks coalesce at upper or lower boundary of fiber (Hibbs & Bradley) [50].

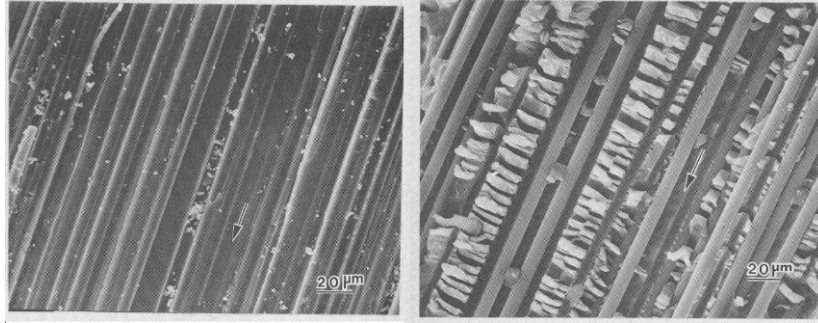


Figure 44 Mode I loading (left) shows clean failures at the fiber/matrix interface, and pure Mode II loading (right) shows shear hackles in the matrix (Hibbs & Bradley) [50].

2.3.6 Predicting Cross-Ply Fatigue Response

Modeling and prediction techniques for fatigue in cross-ply laminates will now be explored. Thus far in this section on fatigue behavior and characterization, empirical *observations* of behavior in fatigue tests have been shown. Experimentation is indispensable to understanding the response of material to fatigue loading. However, ending a research investigation with only experimental observations, and delimiting conclusions to the very specific experimental case investigated does not add much value. Experimental investigations of course should serve the advancement of the discipline and purpose of engineering: *predicting* physical behavior. Thus, experimentation serves as

1. *The source of information for conclusions* which can be used to **create** predictive models and,
2. *The standard by which predictive models can be **validated**.*

For this investigation, our purpose should serve the ends of predicting fatigue behavior in other CFRP laminate fatigue scenarios. Several analytical modeling techniques proposed by other authors will be reviewed here.

Early research which developed analytical models for prediction of fatigue failure in composites began by addressing the simplest layups possible. Models became more

complex as the problem of fatigue in composites became better understood. Early predictive models focused on unidirectional laminates, were based on simple failure criteria equations, and employed quite a bit of empirical fitting as inputs to these equations. For example, Hashin and Rotem [51], employed a two-part criteria which predicted fatigue failure as a function of R-ratio, number of cycles N, and the frequency f. This is, essentially, a macromechanical model and does not explicitly identify the two-component, structural nature of the composite laminate. Where (11) is the fiber direction, (22) is transverse to and in the plane of the lamina and (33) is out of the lamina plane, the two-part failure criteria is:

$$\sigma_{11} = \sigma_{11}^u$$

(Eq. 33)

and

$$\left(\frac{\sigma_{22}}{\sigma_{22}^u} \right)^2 + \left(\frac{\sigma_{12}}{\sigma_{12}^u} \right)^2 = 1$$

(Eq. 34)

When either of these criteria are met, a fatigue failure will occur. σ_{11}^u , σ_{22}^u , and σ_{12}^u should be determined through experimentally testing unidirectional specimens as a function of R-ratio, number of cycles, and loading frequency. Note that the definition of “failure” in these equations is determined in the experiments which determine the three function variables—“failure” can be defined as crack initiation or ultimate laminate failure. The first failure criteria bears a resemblance to the maximum principal stress theory for failure of brittle materials in uniaxial tension [52]:

$$|\sigma_1| = \sigma_u$$

(Eq. 35)

While the second criterion is similar to the maximum distortion energy criteria for ductile materials in plane stress (here, σ_1, σ_2 are principal stresses) (Ugural & Fenster, 2003) [52]:

$$\left(\frac{\sigma_1}{\sigma_{yp}}\right)^2 - \left(\frac{\sigma_1}{\sigma_{yp}}\right)\left(\frac{\sigma_2}{\sigma_{yp}}\right) + \left(\frac{\sigma_2}{\sigma_{yp}}\right)^2 = 1$$

(Eq. 36)

Given the nature of the material structure of a unidirectional layup, the similarities between these sets of equations make sense: carbon fibers themselves are thought to behave as a brittle material with negligible fatigue life (and could be represented by a max. principal stress failure theory) while the matrix of CFRP and GFRP is typically a more ductile epoxy material (and could be represented by the max. distortional energy criteria). This relation between the composite's material structure and its material behavior did not go unnoticed by other authors.

Aboudi (1989) [53] and Reifsnider & Gao (1991) [3] further developed this model by explicitly recognizing that failure in a unidirectional laminate along the fiber direction (“for θ less than 2° ”) is due to the fatigue properties of the *fiber*, while failure for “large values of θ ” is determined by the transverse and shear stress properties of the matrix. This also suggests a two-part failure criteria, similar to that of Hashin and Rotem, but which now explicitly acknowledges the importance of fatigue failure properties of the fibers (X^f), unreinforced matrix fatigue properties (X^m), and matrix shear properties in fatigue (S^m):

$$\langle \sigma_{11}^f \rangle = X^f$$

(Eq. 37)

and

$$\left(\frac{\langle \sigma_{22}^m \rangle}{X^m}\right)^2 + \left(\frac{\langle \sigma_{12}^m \rangle}{S^m}\right)^2 = 1$$

(Eq. 38)

Again, just like the Hashin and Rotem equations: failure occurs when one of these conditions is met and, likewise, the three ‘fatigue function’ inputs are defined through experimentation, this time in tests of neat fiber and matrix specimens.

It might be tempting to assume that, for a multi-directional laminate, these two fatigue criterion could simply be applied for all of the differently oriented laminas in the laminate, and whichever lamina “lasts the longest” for the loading conditions of the test, will be that which causes final rupture. But this would be a gross oversimplification. Fatigue in multidirectional laminates is a progressive event: cracks which initiate in one ply induce stress concentrations in neighboring plies, which themselves crack or delaminate, and so on until laminate rupture occurs. However, it is interesting to consider that these fatigue criteria models could be used as a “jumping off point” for a fatigue analysis which better represents the fact that fatigue is a progressive event, which creates stress concentrations within the structure:

1. For a virgin laminate, “first crack” could potentially be predicted for a 90° lamina by relying on the “first-ply failure” fatigue criteria already specified.
2. After the first crack forms in one ply, the iso-strain assumption common to composite laminate analysis is no longer applicable. The “fatigue functions” of the laminas adjacent to the crack will now be affected by the altered stress-field and stress concentrations (For example, SIFT acknowledges and models fracture damage development as a progressive event, Tay, Tan, Tan, Gosse) [1].
3. Micromechanical modeling (F.E.M.) or analytical fracture mechanics could be employed to determine the subsequent damage development—delamination, matrix cracking, or fiber fracture. For example, (Caslini, Zanotti, and O’Brien) [45].

It was noted in the second point above that “the iso-strain assumption of composite laminate analysis is no longer applicable after the first crack forms.” This is true, particularly in the neighborhood of the crack after it has formed. But it’s a fairly generous assumption to make even before a large through-the-lamina-thickness flaw can be observed... Flaws in the lamina and inter-fiber stress concentrations in the matrix greatly increase stresses above classical lamination theory stress levels. For the purposes of a quick calculation, the iso-strain assumption of classical lamination theory is useful, but necessarily ignores several features which shouldn’t be ignored in a more thorough analysis:

1. All real materials have flaws. For composites, flaws can stem from several sources: matrix micro-cracking from residual thermal stresses, voids in the matrix, imperfect adhesion at the interface, flaws in the fibers, delaminations, or stress concentrations from the laminate finishing process—finish cutting of the edges of a laminate will likely not be a mirror-smooth edge, and drilling holes for fasteners increases stress concentrations and can delaminate the drilled area (Mallick) [6]. If these facts are to be accounted for, then classical lamination theory would need to be augmented by techniques from fracture mechanics.
2. The “stiffening” of the polymer matrix must be accounted for if the laminate is exposed to sufficiently high strain-rates (Hertzberg & Manson) [2]. CLT has to acknowledge the behavior of the polymer properties *at the test frequency*—and temperature.

3. Poisson mismatch effects between, due to the varying fiber angles between plies. This can cause out-of-plane tensile or compressive forces, driving delamination (Pagano & Pipes) [54].
4. Residual thermal stresses must also be accounted for (Jones) [30].

And, as noted in the earlier background section on polymers, if the strain rate and polymer type is favorable, then thermal failure of the polymer can occur. In this study, a thermographic camera was used to observe if the specimen exhibited any temperature rise during 10 Hz cyclic loading at $R = 0.1$. There was no observable increase in temperature throughout the specimen, or in the neighborhood of an already-existent crack. However, heat dissipation from such a small volume around the crack to the surroundings and the limits of the equipment's ability to observe the crack at high magnification prevent any conclusions about the role of matrix thermal failure's role in laminate cracking. Charewicz & Daniel [29], also investigated cross-ply laminate fatigue at the same frequency and R-ratio and noticed a mere 2°C temperature rise in the laminate.

So, there are likely five sources which can serve to amplify stress above what might be predicted by CLT and/or cause failure in the matrix during fatigue loading:

1. Stress concentrations around the fibers—related to fiber spacing (Mallick) [6].
2. Physical flaws in the matrix: voids, imperfect bonding, etc, (Mallick) [6].
3. Residual thermal stresses from fabrication (Jones) [30].
4. The “stiffening” of polymers at higher strain-rates (Hertzberg & Manson) [2].
5. The potential for matrix thermal degradation or failure (Hertzberg & Manson) [2].

The first two, if the geometry of the flaw and/or fiber size and spacing are known, can be calculated through fracture mechanics techniques. The latter two can be determined through extensive experimental characterization of the matrix polymer.

CHAPTER III. MATERIALS, SPECIMENS, & EXPERIMENTAL METHOD

This chapter will present the procedure used to perform the experimentation in this study. A description of how the specimens were prepared, and a statement of the specimen's constituent materials is included. Following that, a description of the test equipment and the testing procedure will be described. Finally, descriptions of the damage inspection techniques used in this study are listed.

3.1 Specimen Preparation: Unidirectional and Cross-Ply Laminates

Jon Gosse, one of the project sponsors at Boeing, originally proposed the testing of unidirectional off-axis 10° specimens and unidirectional 90° specimens. 90° specimen testing would furnish material behavior in fatigue for a dilatational strain case, while 10° specimens would suggest fatigue performance in a deviatoric stress-state. The 10° unidirectional specimens were created with a length such that there would be fibers in the gauge length which could not bear the load grip-to-grip (i.e., the gauge section contained fibers whose ends terminated outside of the grips on the specimen edge and, obviously, the 90° specimen's fibers couldn't bear the load grip-to-grip either.). These specimens (and later, the cross-ply specimens) were prepared in the following way (Gosse, Christensen, Yu, 2007) [55]:

“The majority of the un-notched test coupons utilized for the determination of the effective critical matrix strain invariants were extracted from a unidirectional lamina panel configuration consisting of pre-impregnated 30.48 cm wide tape (nominal resin content of 32% by weight) manufactured by Cytec Engineered Materials Inc[®] (IM7/977-3) . The IM7/977-3 unidirectional tape was hand laid-up, bagged, and autoclave consolidated per industry standard practices. In order to ensure smooth test specimen surfaces,

a 0.127 cm thick sheet of aluminum was placed on the bag, or non-tooled side, of the lamina. In addition, a release agent (coated sheet of mylar) was placed between the aluminum sheet and the tool surface to further enhance the lamina surface smoothness. The thickness of the lamina panel (approximately 0.508 cm thick) results in a coupon that is less prone to damage due to inadvertent handling and pre-test preparation than thinner configurations. Each coupon was carefully excised from the cured unidirectional lamina panel. All machining utilized a precision controlled high-speed pneumatic water-cooled diamond saw. The use of the water-cooled diamond saw for coupon preparation ensured that an edge finish of no greater than a RMS (root mean square) 16 was obtained.”

APPENDIX A contains the material properties for IM-7 carbon fibers (Hexcel) (56).

APPENDIX B contains material properties for 977-3 Cytec epoxy (57). The unidirectional fiber specimens were 10.0” x 0.755” x ~0.235” thick, at 30 plies (with the exception of a “practice” group of specimens which were ~0.187” thick at 24 plies). The cross-ply laminates were 10” x 1.0” x ~0.093” thick, at 12 plies. The epoxy matrix used for the cross-ply specimens was the same for all 40 cross-ply specimens and was the 977-3 toughened epoxy mentioned above. However, the matrix materials of the unidirectional specimens varied. DOW chemical’s DEN 431 epoxy and Hunstman’s Tactix 123 epoxy were used in these specimens. While the material properties for these three types of epoxy varied, strain-life properties in fatigue were observed to be the same for one pair of specimens, even for the sparse data collected, i.e.: the 977-3 and Tactix 123 epoxy in the 90 degree specimens had a similar fatigue life, and so did the DEN 431 and Tactix 123 epoxies in the 10 degree specimens. Much more extensive testing would be needed to confirm this observation of similar behavior in unidirectional specimens, as scatter is rampant in unidirectional fatigue testing, and a limited number of unidirectional fatigue tests were able to be performed in this test. The matrix materials employed in each of the groups of unidirectional specimens are shown in Table 4.

Table 4. Description of the unidirectional specimen starting materials. All fibers were IM-7, but epoxy matrix material varied. DOW's DEN 431 epoxy was used in five of the 10⁰ specimens, while Huntsman's Tactix 123 epoxy formed the majority of these specimen's matrix material. "Practice" specimens were nine spare practice specimens which Boeing requested be used to develop the test setup which would not cause erroneous grip-related failures.

Group #	Matl Composition	Orientation	# of Specimens	Best Fracture ϵ
1 - Practice	IM-7/977-3	90	9	0.0103
2	IM-7/DEN-431-33DDS	10	5	0.0102
3	IM-7/Tactix 123(a bisA epoxy)-33DDS	90	6	0.0104
4	IM-7/Tactix 123-33DDS	10	7	0.0111
5	IM-7/Tactix 123-33DDS	90	7	0.0104

3.2 Test Equipment:

Two MTS brand servo-hydraulic testing machines were used for all of the tests. One machine was controlled by Testware SX software coupled with a TestStar II controller. The other machine was controlled by TestStar IIs Station Manager software coupled with a TestStar IIs controller. The machine controlled by the TestStar II software was a 20,000 lb machine, Instron Model 1331. On this machine, 1,000 pound (blue grips in Figure 45) and 10,000 lb static / 5,000 lb fatigue mechanical grips (dark grips in Figure 46) were used in testing, both of which had toothed grip faces. A 1.0" span MTS clip gauge extensometer ($\pm 15\%$ max strain range, S/N 0349824) was used to monitor the strain in ultimate tensile and fatigue testing on this machine. The machine which was controlled by the TestStar IIs control software was also a 20,000 lb tensile testing machine, Instron Satec Uniframe Model CAT TC-25. This machine had MTS 647 hydraulic wedge grips (20,000 pound grips shown in Figure 47). A grip pressure of 1200 lbs was calculated to be appropriate for the cross-ply specimens tested in this machine. The wedge grips used in this machine had "surfalloy" faces. This second machine was only used in the latter portion of the study when cross-ply specimens were being tested (these tests were performed in load control and

thus an extensometer was not required in these tests beyond measuring the specimen's modulus). The tensile testing machines were calibrated and certified according to their maintenance schedules by an MTS technician. Additionally, an aluminum bar of known cross-section was occasionally monotonically tested with the extensometer attached to ensure that both the load cell and the extensometer were functioning correctly. The test results from these "proof tests" were compared to and found to be in agreement with the typical modulus of aluminum.



Figure 45. A unidirectional 90° specimen in the 1000 lb mechanical grips of an MTS servo-hydraulic test machine. The brass tabs, epoxied to the specimen, are just visible above the lower grip. The extensometer is held in place with elastics in this image; springs were later determined to be a better approach.



Figure 46. A cross-ply specimen in the mechanical 10,000 lb static / 5,000 lb fatigue grips.



Figure 47. A cross-ply specimen in the 20,000 lb hydraulic wedge grips. The test-frame is encased in a lead-lined box for the purposes of X-raying specimens.

3.3 Testing Plan for Unidirectional and Cross-Ply Laminates

3.3.1 Overview

The main goal for testing both the unidirectional and cross-ply specimens was to define fatigue run-out values as a percentage of static ultimate stress and strain. The Boeing sponsors wished to determine the stress and strain levels which initiate the “first crack” in fatigue. Therefore, both static tests and fatigue tests were performed with the unidirectional and cross-ply specimens.

Additionally, an exploration of the effect of loading frequency, R-ratio, and specimen edge roughness on crack initiation was performed. With few exceptions, only a single specimen could be tested for each of these various test scenarios. Thus, the investigation cannot be regarded as a statistically exhaustive study. However, it can suggest general trends, particularly in cases where scatter is unlikely to explain large differences between test results: where wide discrepancies exist between the stress-state at crack initiation. The results may help to suggest which of the variables is most influential in initiating cracks in this material system and layup, and which variables may be worth investigating in the future. The results of this exploration may also suggest the importance of polymer behavior in the fatigue of the cross-ply: if the behavior observed across these various laminate tests is similar to that of epoxy in fatigue, then it is likely that the properties of the matrix are, in effect, governing the crack initiation behavior of the cross-ply. If this is true, then characterizing and understanding the matrix behavior may be of more value to understanding laminate behavior than jumping to an investigation of the laminate itself.

3.3.2 Unidirectional Static Tests

Unidirectional specimen static tests were performed in stroke control, with a cross-head displacement rate of 0.01 in./min with the clip extensometer attached. One static ultimate test was performed for each of the 90° and 10° specimens—a number of static tests did not have to be performed because the “best static strain values” had been given to the author by the sponsors for both these specimens (Table 4, page 67). However, the author wished to see how the specimens sent for testing compared to these “best strain” values.

3.3.3 Unidirectional Fatigue Tests

The fatigue tests of the unidirectional specimens were performed at 10 Hz, $R = 0.1$, in strain control. For the unidirectional specimens, strain control was used in fatigue testing because strain is the pertinent variable with respect to the SIFT model. An important point to note about the test procedure (for both the unidirectional and cross-ply fatigue tests) is that if a specimen was tested to 1 million cycles and no cracks were evident, then the same specimen would be tested again at an increased peak load, with the same R-ratio and loading frequency. This increasing of the peak load with the same specimen was repeated, until failure occurred in the case of the unidirectional specimens (or until a crack appeared in the case of the cross-ply). Of course, this testing procedure relies heavily on the assumption that cracks immediately propagate in the 90° plies of the cross-ply specimens... It is assumed that there is no stable crack growth at lower peak loads than the test in which the crack was first noticed. Observations presented in the “Experimental Results & Discussion” support the validity of this assumption.

3.3.4 Cross-Ply Static Tests

After it was found that unidirectional specimens were not yielding very useful data due to large statistical scatter, the project sponsors decided that cross-ply laminates could, perhaps, provide more useful data. Static tests of the cross-ply specimens were performed in stroke control, with a cross-head displacement rate of 0.01 in./min with the clip extensometer attached. Four of these tests were performed on Batch A specimens, and one was performed on Batch B. Results are presented in Table 7, on page 117.

Two batches of twenty cross-ply specimens were provided by the sponsors and, unfortunately, it was noticed late in the testing of the first batch of twenty specimens (“Batch A”) that the technique used to investigate for specimen cracking—the acetate film edge replication technique—was chemically degrading the specimen. It was causing cracks to initiate earlier than they would have, if the acetate film replication process had not been used. The edge replication technique will be described in the section on “Damage Inspection Techniques.” The experimental evidence which demonstrates that this technique was causing early cracking is described in the “Experimental Results & Discussion” section.

3.3.5 Cross-Ply Fatigue Test: 10 Hz, R = 0.1

To get an idea of the scatter in fatigue for the cross-ply specimens, several Batch A specimens and 7 specimens from Batch B were tested at 10 Hz, R = 0.1. Unfortunately, much of the data on crack initiation from Batch A was gathered with edge replication, which proved to chemically attack the specimens—crack initiation data from this batch must be observed with that knowledge in mind. Several cross-ply laminates were also

tested at 10 Hz, $R = 0.1$ at stress levels which were known to be well above the “first crack” stress level; this permitted the author to compare the speed at which the “characteristic damage state” was reached, as a function of peak load in fatigue testing.

The sponsors, in addition to agreeing to testing cross-ply specimens for the latter half of the study, also agreed that load control would maintain the same stress and strain range as controlling in strain would. Running in load control for the fatigue tests of the cross-ply specimens also removed the problems inherent to machine control based on a cantilevered clip extensometer.

3.3.6 Cross-Ply Fatigue Test: Effect of R-Ratio & Loading Frequency

In testing some of the specimens from Batch B, the test variables were expanded—the loading frequency and R-ratio were varied. The fatigue test matrix for this second set of twenty cross-ply laminates is shown in Table 8 (p. 128). Several tests were performed at 3 Hz, and several were performed at 30 Hz. With respect to R-ratio, a few of the cross-ply laminates were tested at $R = 0.5$, in addition to the laminates tested at $R = 0.1$.

After a couple dozen tests of the cross-ply laminates (encompassing Batch A’s specimens and those from Batch B which were tested at 10 Hz, $R = 0.1$), it was evident that cracks typically initiate within the first 200k cycles. Running to 1 million cycles, in addition to consuming a lot of testing time, contained little more value in determining crack initiation than simply running the first 200k cycles. Thus, for the 3.0 Hz and 30 Hz testing just described, tests were run to 200k cycles instead of 1 million before a new load level was tested. Also, this second batch of twenty cross-ply specimens (“Batch B”) was

inspected for cracking using dye penetrant inspection, which was proven to be a benign NDI method.

3.3.7 Cross-Ply Fatigue Test: Effect of Edge Roughness

Several specimens were polished to a much finer edge finish by a staged, progressively finer hand-sanding process using “GatorGrit” brand wet sanding paper. The grits used were 320 grit → 400 grit → 600 grit → 1500 grit. The sanding setup is shown in Figure 48. The contrast in roughness between the “as received, diamond cut-off wheel surface finish” and “after sanding finish” is shown in Figure 49. Approximately five minutes was spent sanding each side of these specimens, for each of the grits listed above. It is acknowledged that this is a fairly crude method to test the effect of “surface roughness”—an in-depth study would require more reliable polishing machinery and a measure of the decrease in surface roughness as an RMS value. However, the investigation here may suggest that this is a factor worth investigating in the future. The reduction in specimen area due to the sanding, though minimal, was taken into account in computations of stress for these specimens.



Figure 48. A vise was used to hold the specimen during sanding; paper towels both caught water from the wet-sanding process and prevented the vise from damaging the specimen surface.

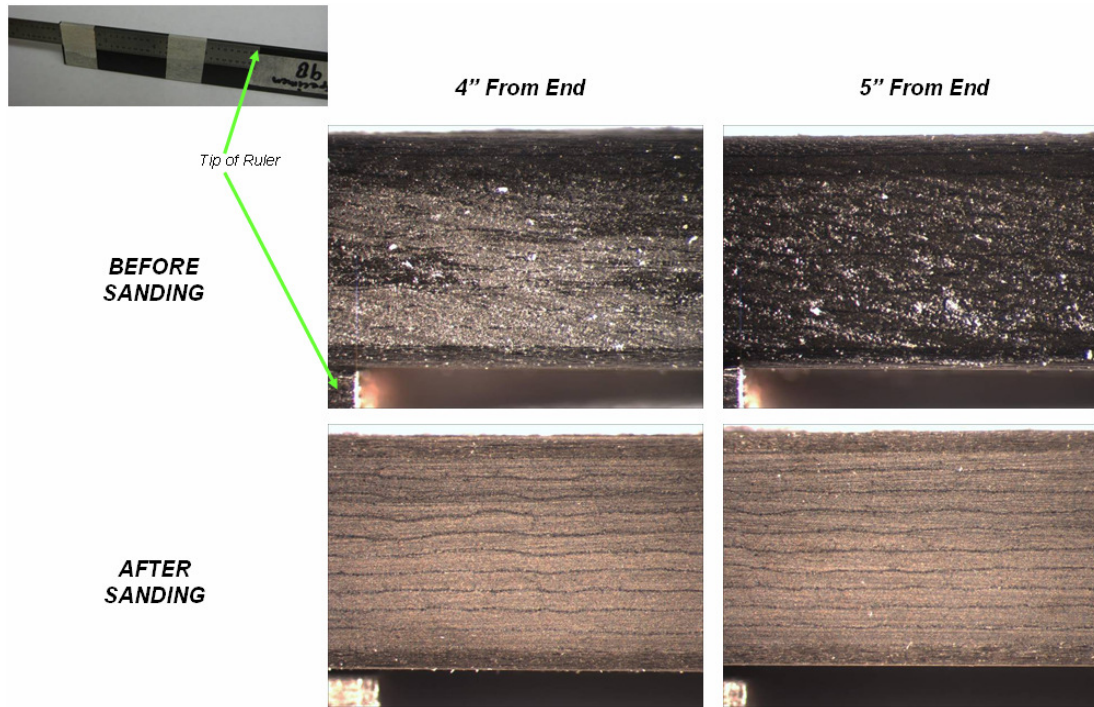


Figure 49. The contrast in specimen surface roughness is visually evident with an optical light microscope. This contrasts the “before” and “after” sanding of two locations on the edges of Specimen 9b.

3.4 Damage Inspection Techniques for Unidirectional and Cross-Ply Laminates

3.4.1 Gold Leaf Surface

As mentioned by Jamison in the background [35], cracks are thought to propagate immediately in tests where no 0° plies exist to restrain crack development in unidirectional specimens. In these tests, the matrix bears the load in a manner which causes Mode I or Mode II fracture along the fiber direction. In the assumption about immediate crack propagation, which testing has borne out, it is the presence of plies with a different fiber orientation which can prevent sudden and catastrophic laminate failure and permit the study of cumulative damage development. Nevertheless, this study undertook a brief study to investigate whether stable crack propagation could be observed in the unidirectional 90° and 0° specimens.

To test this assumption about immediate crack propagation, several investigations were performed, one of which was implemented in the unidirectional testing, while another was implemented during tests of the cross-ply specimens. The test of a unidirectional specimen involved notching the edge of a 10° specimen with a razor blade along the fiber direction (Figure 50). Thin gold leaf was placed on the width of the specimen; 3M Super 77 spray adhesive was used to adhere the gold leaf to the specimen. An optical microscope was used to observe the area through which the crack would propagate (Figure 51 and Figure 52). The intent was to witness the crack's progress as a fracture in the gold leaf surface. Starting at a low load-level, the peak load level was slowly increased at $R = 0.1$. No observable stable crack growth was witnessed in the edge and the specimen's immediate rupture supports the hypothesis of 'effectively' immediate crack propagation in unidirectional off-axis laminates—i.e., very small irregularities in the surface require

extremely short growth times to reach this material's K_{IC} . In-depth microscopic studies, where crack depth is more carefully controlled than it was here, would be required in order to characterize what is likely a very short crack growth time for this material.

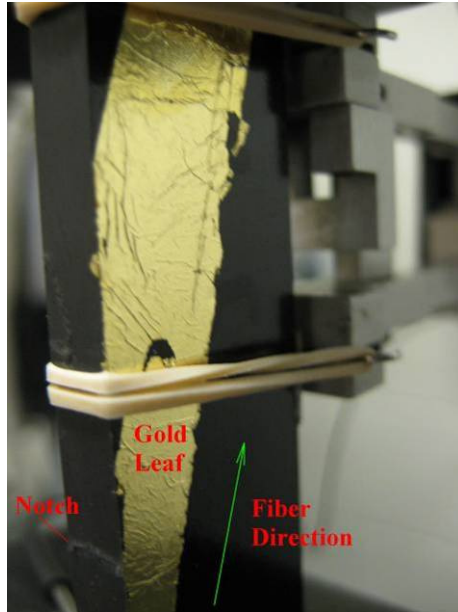


Figure 50. The notch in the specimen and the gold leaf placed on the width are visible in this image.

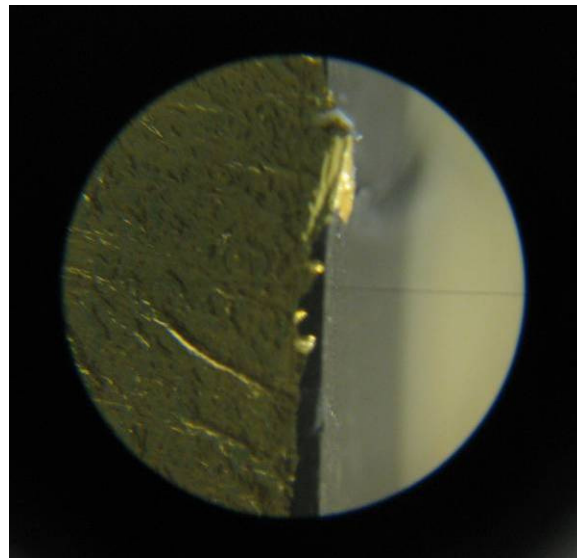


Figure 51. This is a view through the microscope of the notch put in the edge of one of the 10° unidirectional specimens.



Figure 52. The optical microscope used to observe whether stable crack progress can be observed through the gold leaf surface.

3.4.2 X-ray Inspection

Penetrant enhanced radiography is a commonly used technique to investigate crack development in composite laminates. This technique involves applying a zinc iodide solution to the edge of the specimen, which easily wicks into any cracks in the specimen. The solution in this study consisted of 60g zinc iodide, 8mL water, 10mL isopropyl alcohol, and 6mL of Kodak PhotoFlow solution. The specimen is then x-rayed with a piece of Polaroid 55 P/N sheet film behind it. In this investigation, the x-ray was set to a voltage of 52kV, 3mA amperage, and 73 seconds of exposure time.

The zinc iodide within the cracks interferes with the x-ray beam and leaves clear lines on the film after it is developed, and this indicates where cracks are located in the specimen. The x-ray system was maneuvered on a forklift in front of the lead-lined box containing the specimen, which is held in the grips of the tensile machine (Figure 53). The

x-ray had a 0.5 mm focal spot size, a self-rectifying thermionic X-ray tube with 0.76 mm thick beryllium window, and a 30 degree beam divergence. Though x-ray inspection was not used frequently in this study, it was used to show that edge replication was causing earlier damage than if that technique had not been used. Exposed x-ray film was developed according to Kodak's specifications and the film was scanned to make a digital copy of the image.



Figure 53a and Figure 53b. The specimen is in the grips in the lead-lined enclosure, to the left. To the right, the x-ray is rolled in front of the lead lined enclosure, properly positioned to perform a scan. In the image to the left, the grips are oriented 90° to where they were when the x-ray was taken. The specimen had to be oriented with the broad edge facing the x-ray for x-ray photos to effectively be taken; the Kodak film was supported behind the specimen with a metal clamp.

3.4.3 Edge Replication

Edge replication is a method which can detect cracks on the surface of a specimen. In this method, a piece of acetate film is pressed against the flat edge of the specimen to be investigated. Acetone is drawn in between the specimen surface and the film by capillary action from a syringe, which softens the film. The softened film is pressed firmly against the surface with a compliant object—such as an eraser—and the softened film conforms to the surface shape. After a few moments, the acetone will evaporate; the acetate film will have regained its firm state and the eraser can be removed. The replicate can then be peeled

off the specimen, creating a “negative” of the surface. This negative can easily be viewed with an optical microscope.

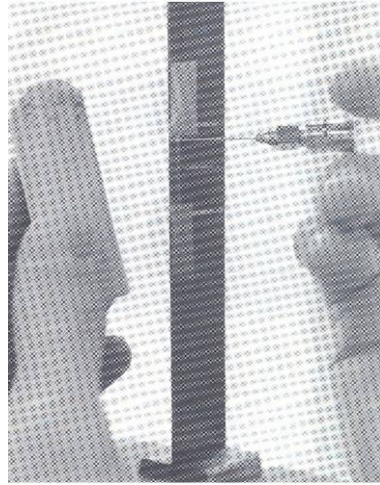


Figure 54. A syringe is used to inject acetone between the replicate film and the specimen. An eraser is used to press the film against the specimen edge immediately after injecting the acetone [58].

The acetate film used in this study was 0.005” thick replicating tape made by Ernest F. Fullam, Inc. (this was their “Thick Replicating Tape,” Product no. 11340). Masking tape is placed on the specimen to several layers of thickness, and the acetate film is “butted up against” the masking tape to ensure that the same area on the edge of the specimen is “replicated” every time a replication is taken (Figure 55). In this study, a 1.0” length of the specimen edge was replicated—this was the width of the replicating tape, and a wider inspection area would have made performing the replication process difficult. A small piece of scotch tape holds the piece of acetate film in place against the scotch tape. Very little acetone is required and if too much is applied then the acetate film will dissolve completely.

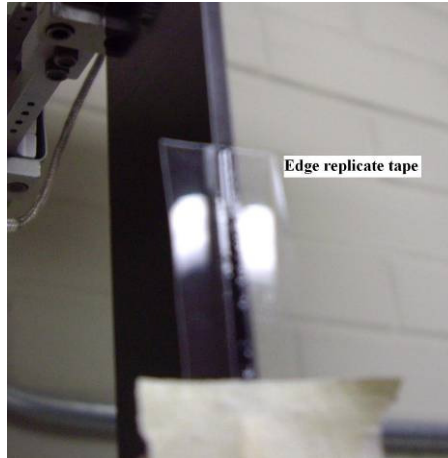


Figure 55. The replicate tape is butted against the masking tape shown; this ensures that the tape registers at the same location every time a replicate is taken.

Examples of edge replicates are shown in Figure 56 and Figure 57; these edge replicates were taken from the initial “Practice” ultimate tensile strength test specimen from Batch A. In Figure 56, the 0° plies and 90° plies are labeled, and the “tendrils” of acetate are visible. The tendrils are due to softened acetate which had flowed into the crack, solidified, and then adhered to the replicate as it was removed from the specimen edge. Figure 57 illustrates the “characteristic spacing” which was repeatedly observed in many of the cross-ply fatigue tests that employed high loads and developed more than just the single “first crack.” The microscopic investigation of the edge replicates was carried out with a Leica MZ6 microscope equipped with a Qimaging Micropublisher 3.3 RTV CCD which was connected to a PC equipped with Image-Pro Express software.

It will be demonstrated in the “Experimental Results” section that edge replication is NOT a good technique to use for damage inspection of composites—it was found to cause cracking much earlier than if the inspection technique had not been used. It is suspected that the acetone degraded the polymer, which led to earlier cracking in the 1.0” area inspected repeatedly with replicates. Edge replication cannot be assumed to be a “Non-destructive Inspection Technique” where polymer matrix composites are concerned.

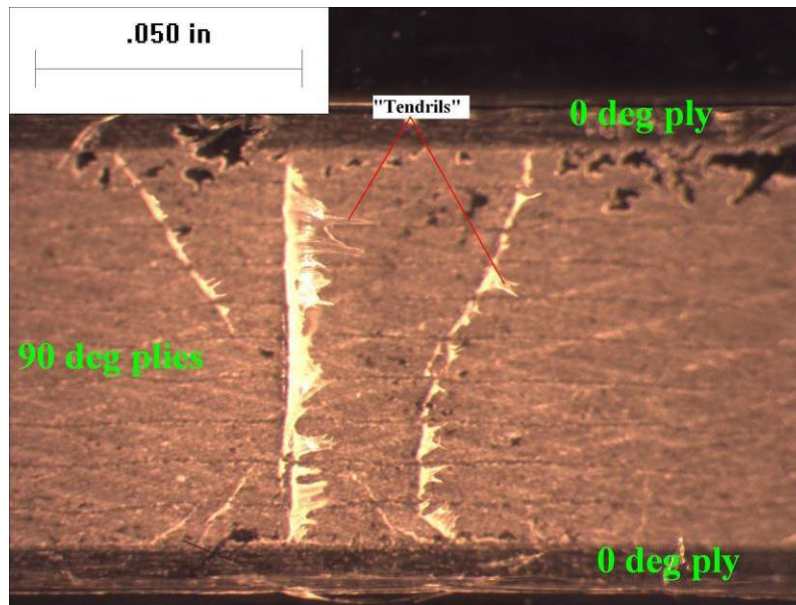


Figure 56. A microscopic magnification of a typical edge replicate. Acetate “tendrils” are evident, where the acetate had flowed into the crack and then been pulled out by removing the replicate. The 0° plies are evident as darker bands on the “top” and “bottom” of the lighter colored 90° plies, internal to the cross-ply laminate image (Practice tensile test specimen, 1.5x Objective, 2.0x magnification. Taken at 25.8 ksi of stress when ultimate loading was 72.4 ksi).

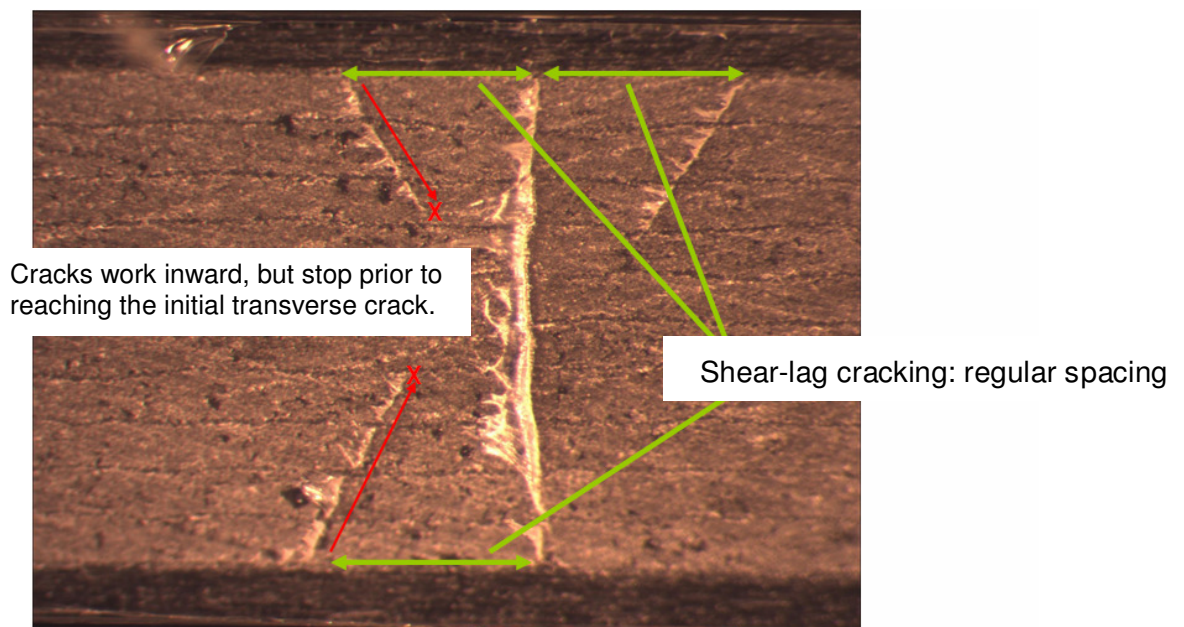


Figure 57. A static test in which the remarkably regular spacing of chevron cracking was first noticed, which appear after the initial transverse crack. (This picture of the “Practice” tensile test specimen was taken at 1.5x Objective, 3.2x magnification. Taken at 25.8 ksi of stress; σ_{ULT} was 72.4 ksi).

3.4.4 Painted Surface

Without some kind of visual enhancement, it is difficult to discern cracks optically in the specimen edge: the carbon fiber, the darkly pigmented epoxy, and the crack itself are black in color. Prior to employing dye penetrants, two static tensile tests of cross-ply laminates were performed in which the edges had been painted. By painting the edge, it was hoped that specimen cracking would be revealed through the lighter coat of paint. “Colorplace” brand white spray paint was applied to the edges of two specimens, 14a and 16a, and allowed to dry. Cracks were visible in the edge (Figure 58), and the “chevron pattern” of cracking was also witnessed (Figure 59). This method was abandoned due to potential unreliability: spray paint is difficult to apply in a uniform thickness and it was not easy to assess whether the cracks in the specimen would propagate through the spray-paint coating. Dye penetrants were recognized to be a superior method of detecting cracks.

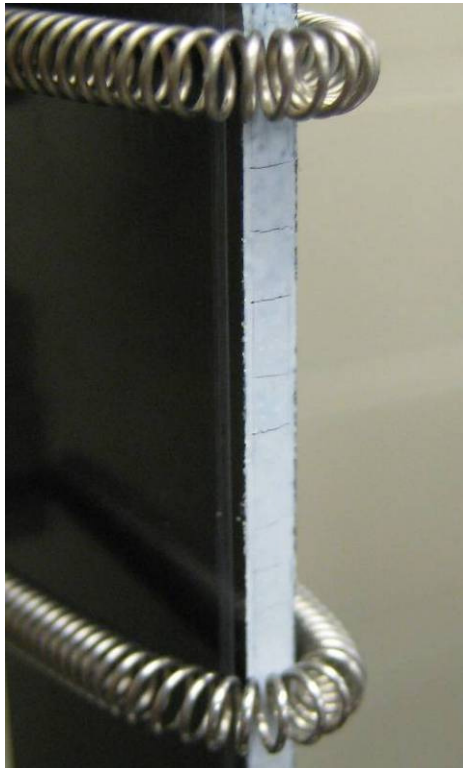


Figure 58. The uniform spacing of cracks is evident in the painted edge of this specimen, this picture was taken at 43 ksi, where σ_{ULT} was 72 ksi.



Figure 59. A chevron crack, above a transverse crack in the 90° plies, is evident in this magnification of the specimen edge. Image was taken at 43 ksi, where σ_{ULT} was 72 ksi.

3.4.5 Dye Penetrant Testing

All of the “first crack” inspections performed on the second batch of 20 cross-ply specimens relied on dye penetrants. Dye penetrant is a NDI technique in which fluid dye is sprayed onto the surface to be inspected for cracks. The dye wicks into any cracks and the crack is revealed by “developing” the dye after the surface is wiped clean. The dye penetrant was purchased from Sherwin, Inc. It was a three step process which employed three different aerosol chemical applications:

1. *Sherwin DP-40 Dye Penetrant:* The specimen, in the machine and loaded to one-half the peak load value of the current fatigue test, is sprayed with DP-40 dye penetrant. To prevent the surroundings from being covered in dye penetrant residue, paper masks can be made to expose only the edge of the specimen to the aerosol sprays (Figure 60). The length of specimen edge exposed to penetrant and inspected for cracking in this study was 4.25.” About one minute is allowed for the dye to penetrate any cracks which exist on the edge of the specimen.

2. *Sherwin DR-60 Cleaner-Remover*: the paper masks are removed and the excess dye penetrant is wiped off the specimen edge with a paper towel. DR-60 Cleaner is sprayed onto a clean portion of paper towel and the edge of the specimen is wiped down. The cleaner removes any dye which a simple clean paper towel cannot remove.
3. *Sherwin D-100 Developer*: once the specimen surface is clean, the paper mask is put back onto the test frame and D-100 developer is sprayed on the specimen edge. This aerosol dries to a whitish substance which draws any dye present in the cracks out to the surface. The cracks appear as bright purple lines in the developer on the specimen edge (Figure 61).



Figure 60a and Figure 60b. To the left, the specimen in the grips. To the right, the specimen and test frame is covered in the paper masking which prevents the aerosol from getting all over the test frame and focuses the penetrant and developer on the specimen edge.



Figure 61. When a crack occurs in the 90° plies of the cross-ply specimen, the dye which had wicked into the crack will be drawn to the surface by the white developer substance. It is readily visible to the naked eye and easily recorded with a digital camera.

3.4.6 Optical Microscope Analysis & Specimen Polishing

One of the composite specimens (Specimen 6b) was sectioned, mechanically polished, and inspected under an optical microscope. The Leica optical microscope, mentioned earlier, had been sufficient for investigating features of the edge replicates. However, for a more detailed optical study of the specimen edge, the cracked portions within Specimen 6b were removed (Figure 62) with a diamond cut-off wheel (Figure 63), mounted in an epoxy cylinder per Struer's instructions (Figure 64), and wet-polished (with water) using a Struer's polishing machine (Figure 65). The polishing process in terms of sanding paper grits, length of sanding, and normal pressure for sanding was:

1. P360, 5 minutes, 30 N pressure – sand non-specimen end to make it planar
2. P360, 5 minutes, 30 N pressure – new sheet, polishing end with specimen in it.
3. P800, 8 minutes, 25 N
4. P1200, 8 minutes, 25 N

5. P2400, 8 minutes, 20 N
6. P4000, 8 minutes, 20 N



Figure 62. A section with two cracks in it was removed from the rest of the composite test piece. Sharpie was used to mark the approximate locations of the two transverse cracks.



Figure 63. This is the diamond cut-off wheel which was used to section specimens.

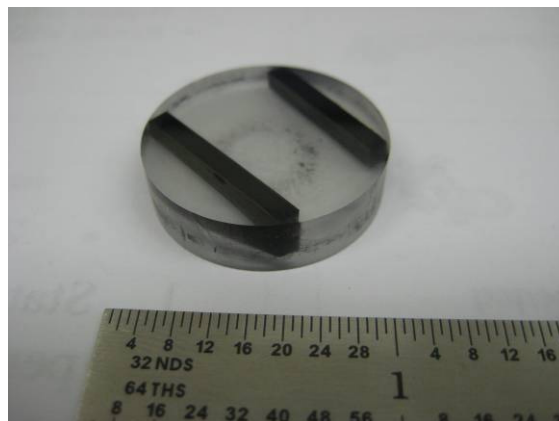


Figure 64. This is the epoxy cylinder in which the two edges shown above in (Figure 62) were mounted for polishing.



Figure 65. The Struer's polishing machine.

With the aid of a 1000x optical microscope, laminate features and cracking were easily visible on the edges of the specimen, including individual carbon fibers. Below, Figure 66 demonstrates how clearly features are visible in a polished specimen at high magnification.

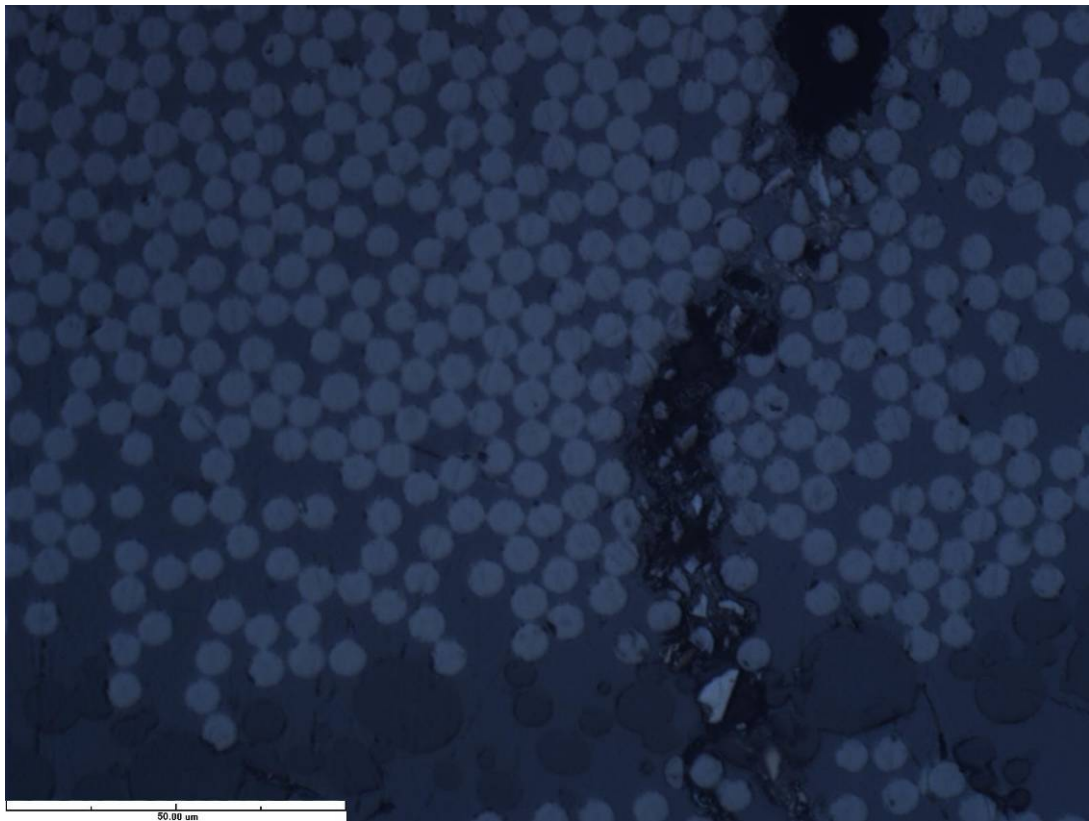


Figure 66. Magnified at 1000x. Scale at the base of the image is 50 μm in length. White “circles” in image are the tips of the fibers in the 90° ply, and the dark vertical line is the crack path. Features of these images will be discussed in the “Experimental Results” section.

CHAPTER IV. EXPERIMENTAL RESULTS & DISCUSSION

4.1 Unidirectional Specimens: 90° Static Tests

Before the unidirectional specimens were tested in fatigue, the 90° and 10° specimens were tested statically to determine the modulus and the stress-strain curve which led to the ultimate strength and strain. APPENDIX C contains a full table describing all of the tests performed on the unidirectional specimens, with short summaries of the test results for each specimen. For the geometry of these specimens (which was described in the “Experimental Method” section), the theoretical modulus can be predicted in the following manner: E_{22} is calculated using (Eq. 15):

$$E_{22} = \frac{E_f E_m}{V_m E_f + V_f E_m} = 1420 \text{ksi}$$

The values used in this computation are stated in APPENDIX A and APPENDIX B, the manufacturer’s material property specifications for the fiber and matrix, respectively. Fiber volume fraction, V_f , is 0.62 for this layup. Compare the predicted value of 1420 ksi (9.75 GPa) to the experimentally measured value of $E_{22} = 1100$ ksi (7.58 GPa, obtained from Sample #3 of the batch of 90° ‘Practice Specimens,’ Figure 67). The experimental value is in closer agreement with the manufacturer’s “typical properties of 977-3 composite laminates” listed in APPENDIX B, stated as $E_{22} = 1210$ ksi (8.34 GPa). Reasons for the experimental modulus being less than the predicted value include the transverse properties of the fibers potentially being less than their longitudinal values, or a model which is overly generous in its assumptions—which is somewhat true of the inverse rule of mixtures model (alternating fiber and matrix assumption).

Regarding the calculation of σ_{ult} and ϵ_{ult} for 90° plies, (Eq. 18) and (Eq. 19) can be used for prediction:

$$K_\sigma = \frac{1 - V_f [1 - (E_m / E_f)]}{1 - \sqrt{(4V_f / \pi) [1 - (E_m / E_f)]}} = 3.14$$

Thus:

$$\sigma_{90^\circ,ULT} = \frac{\sigma_{M,ULT}}{K_\sigma} = 6.69 \text{ksi} (46.1 \text{MPa})$$

Experimentally, $\sigma_{ult} = 8.36$ ksi (58 MPa) and $\epsilon_{ult} = 0.0076$. The epoxy manufacturer Cytec's claimed "typical properties of 977-3 laminates" values are $\sigma_{ult} = 9.3$ ksi (64 MPa) and $\epsilon_{ult} = 0.0077$; the claimed values overshoot the σ_{ult} value obtained here, but are in almost exact agreement for this study's experimental ϵ_{ult} . A typical fracture pattern is shown in Figure 72 (page 95).

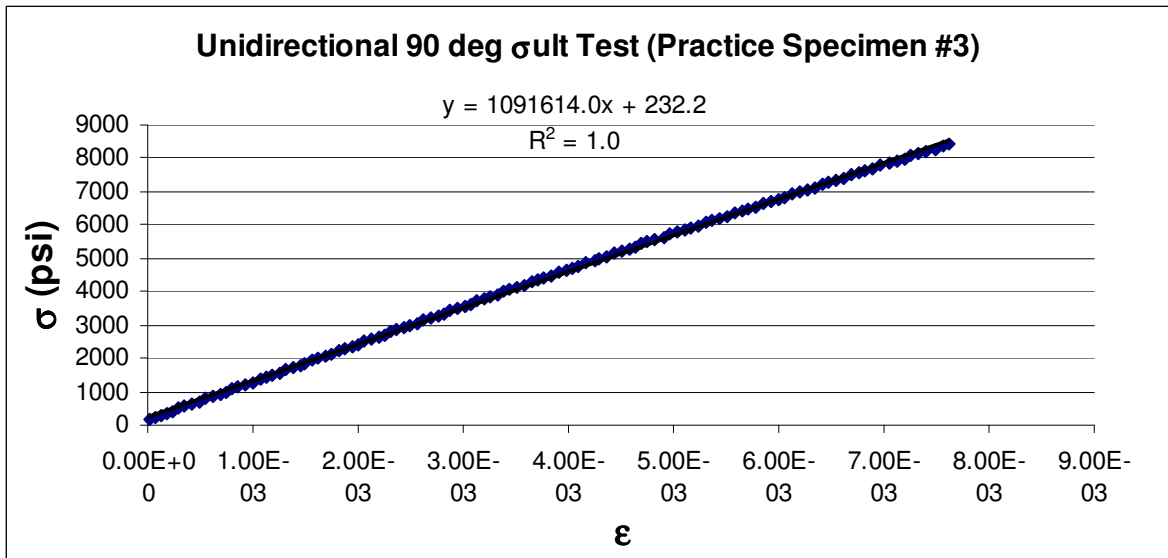


Figure 67. The σ - ϵ curve to failure for a unidirectional 90° specimen. Note that there is negligible plasticity prior to rupture, which occurred at the peak load depicted. Similar linear-to-failure behavior was observed in the 10° specimens.

The author's intent was to perform a number of static ultimate strength tests to get an idea of experimental scatter in this value but as testing progressed, the focus of

experimentation switched to the pressing issue of discovering a test setup which would not cause erroneous failures in fatigue. Additionally, a number of 10° and 90° static ultimate tests had been performed before this study by the project sponsors and the best ϵ_{ult} values had been supplied to the author (Table 4). For both the 90° and 10° specimens, fatigue testing to find the right test setup consumed all but one of the specimens—a single ultimate strength static test was attempted for each type of specimen.

4.2 Unidirectional Specimens: 10° Static Tests

The 10° specimens, by the fact that they are off-axis, induce a shearing stress-state in the matrix; shear-extension coupling. Because of this, the modulus measured on the loading axis by the extensometer is but one part of a thorough description of an off-axis ply's response to loading. A “full characterization” describes the material in terms of the transformed reduced stiffnesses. APPENDIX D contains the calculations which translate E_{11} , E_{22} , G_{12} , and ν_{12} into the transformed reduced stiffness matrix for a 10° specimen—in terms of M_{si} :

$$\begin{bmatrix} \sigma_x \\ \sigma_y \\ \tau_{xy} \end{bmatrix} = [\bar{Q}] \begin{bmatrix} \epsilon_x \\ \epsilon_y \\ \gamma_{xy} \end{bmatrix} = \begin{bmatrix} \bar{Q}_{11} & \bar{Q}_{12} & \bar{Q}_{16} \\ \bar{Q}_{12} & \bar{Q}_{22} & \bar{Q}_{26} \\ \bar{Q}_{16} & \bar{Q}_{26} & \bar{Q}_{66} \end{bmatrix} \begin{bmatrix} \epsilon_x \\ \epsilon_y \\ \gamma_{xy} \end{bmatrix} = \begin{bmatrix} 22.2 & 0.937 & 3.67 \\ 0.937 & 1.12 & 0.034 \\ 3.67 & 0.034 & 1.04 \end{bmatrix} \begin{bmatrix} \epsilon_x \\ \epsilon_y \\ \gamma_{xy} \end{bmatrix}$$

Eq. 39

Where a sufficient number of the stress and strain variables in this relationship are known (i.e., by load cell monitoring on the tensile test frame, and strain gauge measurement of specimen deformation), the theoretical values for any remaining unknowns can be computed.

Material strength is a property which does not transform like stiffness does, and analytical predictions for off-axis lamina strength are not as commonly available as the more straightforward “fiber-axis” and “transverse-to-fiber” loading states. As stated by Jones: “The continuing search to determine the shear modulus and shear strength consists of a collection of tests... Each test has faults... to some extent, there is no universal agreement on the best way to measure shear properties [30].” Tensile test specimens (as opposed to torsional tube tests) are especially subject to the problems of edge effects if the specimen length-to-width ratio is not sufficient. Also, the batch of 10° specimens used in this study was fabricated poorly; one end of the specimen had a taper to its thickness. This required cutting off 1.5” – 2.0” of the 10.0” length, shortening the gauge length, and increasing the likelihood of edge effects. An ultimate strength test was attempted, and is depicted in Figure 68, but failure was not reached due to test setup issues. The “ 10° ultimate ϵ static tensile test values” used to normalize the fatigue data (Table 4 page 67, 0.0102 for Group 2, 0.0111 for Group 4) were the values supplied by our sponsors, who had successfully performed static tests with these specimens previously.

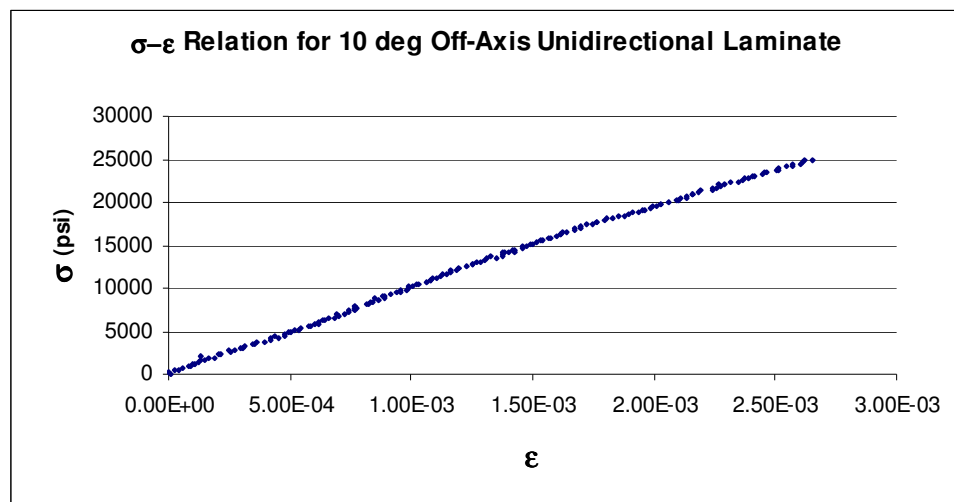


Figure 68. The σ - ϵ curve to failure for a 10° specimen (Group 4, Specimen 7)

4.3 Unidirectional Specimens: Fatigue Tests

For both the 90° and 10° specimens, many of the specimens were spent in trying to discover a test setup which would not cause erroneous failures. A record of the tests performed, with short summaries of each, is in APPENDIX C. The few data points which were able to be attained in fatigue testing demonstrated a high amount of scatter. Scatter for unidirectional fatigue testing was also reported by Reifsnider and Gao [3]. The ϵ -N curves for the 90° specimens are shown in Figure 69. The same data for the 10° specimens is shown in Figure 70 and the data for both fiber orientations which constitutes these plots is in Table 5. No in-depth optical or SEM investigation of the fracture surfaces was performed as time was spent on discovering a functional test setup. Scatter is particularly prevalent in the 90° data in Figure 69. The 10° data in Figure 70 is better, in terms of following a typical ϵ -N curve, but it is sparse in data points.

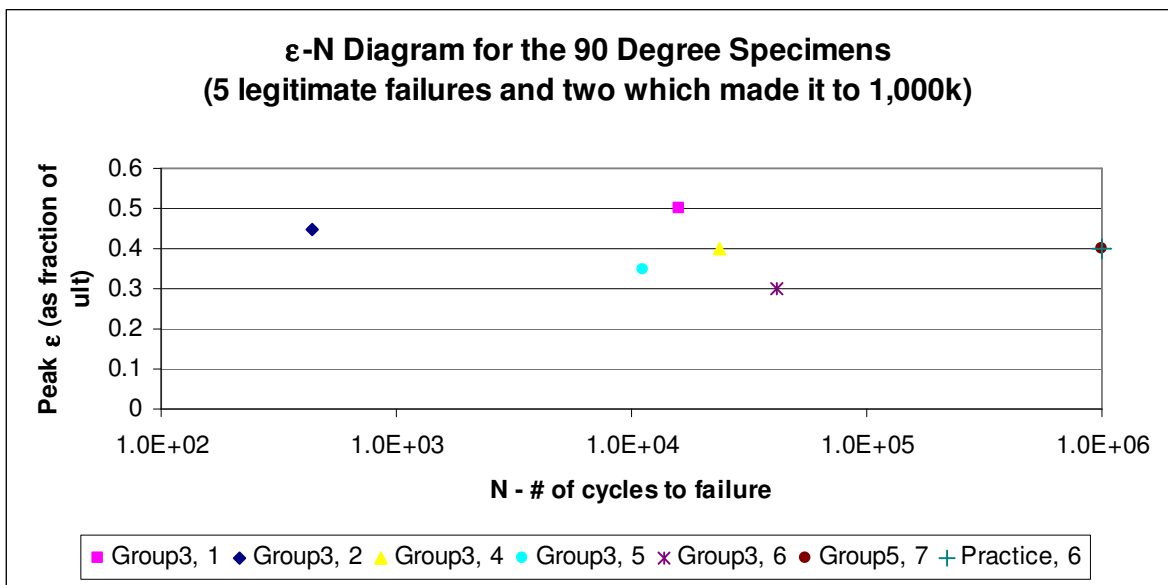


Figure 69. The ϵ -N diagram for the 90° specimens which did not rupture due to poor test setup. Note that this is plotted as a percentage of ϵ_{ult} , which was defined as 0.0104 for this group.

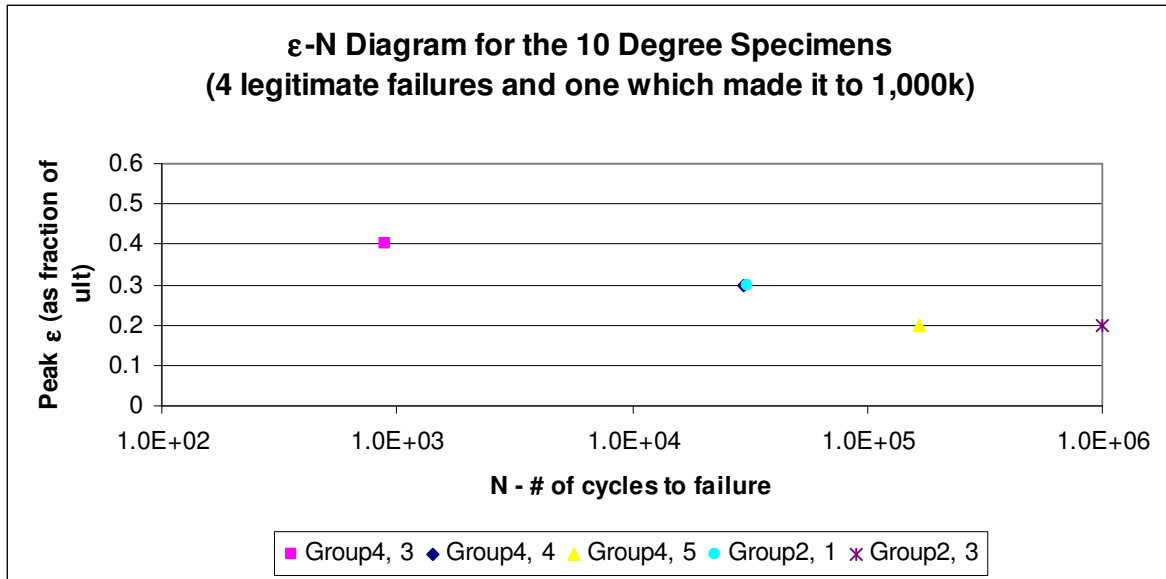


Figure 70. The ϵ -N diagram for the 10° specimens which did not rupture due to poor test setup. Note that this is plotted as a percentage of ϵ_{ult} , which was defined as 0.0111 for Group 4, and 0.0102 for Group 2.

Table 5. The ϵ -N data for both the 90° and 10° specimens. Where “cycles to failure” is $1.00E6$, failure did not occur—runout limit was reached.

90 degree specimens		
Group/#	Cycles to failure	ϵ (% ult)
Group3, 1	15884	0.5
Group3, 2	435	0.45
Group3, 4	23733	0.4
Group3, 5	11154	0.35
Group3, 6	41618	0.3
Group5, 7	1.00E+06	0.4
Practice, 6	1.00E+06	0.4
10 degree specimens		
Group/#	Cycles to failure	ϵ (% ult)
Group4, 3	893	0.4
Group4, 4	30100	0.3
Group4, 5	166508	0.2
Group2, 1	30799	0.3
Group2, 3	1.00E+06	0.2

When legitimate failures occurred in the 90° specimens in fatigue, two forms of specimen failure were observed. Both forms exhibit the feature of a rupture plane which is transverse to the specimen axis within the gauge section between the grips, though not

always within the 1.0” extensometer area. Such a rupture is exhibited in Figure 71 and Figure 72. However, some specimens, such as Specimen 5 from Group 3 (shown in Figure 71 and Figure 73a and b), exhibited non-planar fractures near the brass-tabbed ends which, in cross-section, resemble a quarter-circle. It is suspected that specimens such as this failed first by rupture at the transverse plane location. The machine control at that point in the test was in a state which brought the separated pieces back together, causing them to buckle outwards and rupture on quarter-circle surfaces as shown here. Without exception, the 10° specimens fractured in fatigue as shown in Figure 74, along the fiber direction.

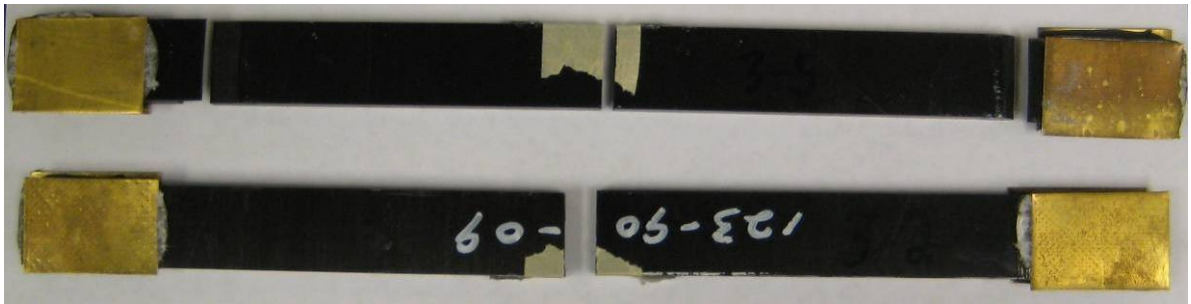


Figure 71. The two types of failures observed in fatigue loading the unidirectional 90° specimens. Top: Specimen 5 from Group 3 split in the middle then ruptured at the ends. Bottom: Specimen 2 from Group 3 simply split in the gauge section.

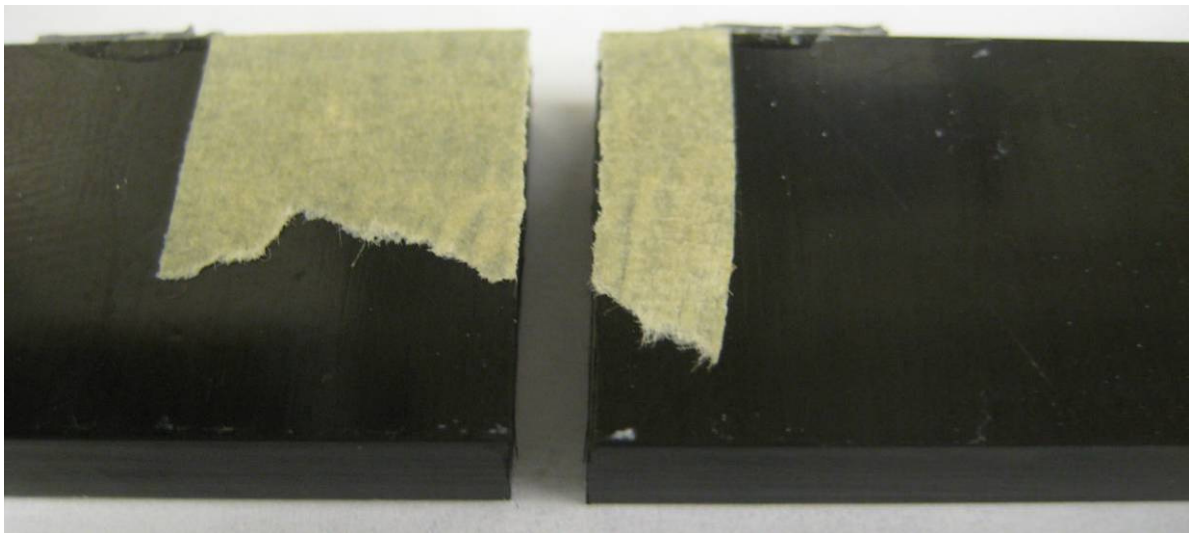


Figure 72. A magnified view of the transverse split from Specimen 5, Group 3.

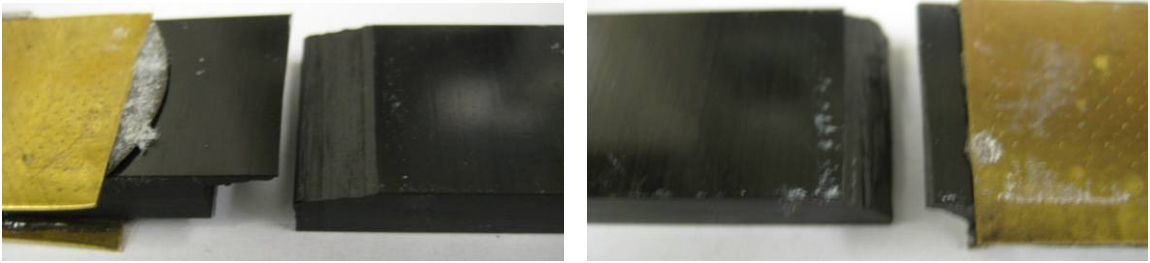


Figure 73a and b. The left and right “quarter-circle” fracture surfaces of Specimen 5, Group 3.



Figure 74. 10° specimen fracture pattern. Both the static and fatigue tests fractured in this manner: at one location, along the axis of the fibers.

4.4 Cross-Ply Specimen Testing

After the project sponsors agreed that results from the unidirectional specimens were not delivering promising or very useful data, the study switched to the investigation of crack initiation in 90° plies as observed in a cross-ply laminate: $[0/90_5]_s$. As described earlier, there were two batches of twenty cross-ply specimens. An extended tabular record of all the cross-ply testing performed is in APPENDIX E, but a brief summary of the tests performed on each of the cross-ply batches would be:

1. Batch “A”: consumed by several ultimate strength static tensile tests, and many fatigue crack initiation tests which relied on acetate film edge replication (all of these tests were performed at 10 Hz, $R = 0.1$). Several of the fatigue tests were devoted to an investigation of *rate* of crack development in fatigue, by cycling at loads which were known to be well above the crack initiation stress value.

Unfortunately, the acetate edge replication technique was found to degrade the material—it caused earlier cracking than if it had not been used. Thus, all the data on crack initiation from this batch must be studied with this fact in mind.

2. Batch “B”: all specimens devoted to crack initiation studies with the dye penetrant technique (with the exception of a single ultimate static tensile test for this group). Samples from the latter half of this specimen batch were devoted to investigating how R-ratio, loading frequency, specimen edge finish, and loading history affected crack initiation in the 90° plies.

4.5 Cross-Ply Testing & Edge Replication

Edge replication was thought to be a method which falls into the category of “N.D.I.” but has proven itself not to, for this material. Prior to noticing the negative effects, it was observed in background reading that several authors had used this technique on CFRP including Reifsnider & Jamison (1982) [38], Jamison (1986) [35], and Bartley-Cho (1998) [59], and it was also listed as a commonly employed testing procedure for crack detection in laminates in a Society for Experimental Mechanics manual (1989) [58].

However, late in the literature review, and after the author had discovered the deleterious effect, this passage was found in a paper by Skibo, Hertzberg, and Manson (1976) [60], “It should be noted that the use of cleaning solvents may be suitable for metal alloys, but are unsuitable for use with most plastics and their composites since these organic fluids either dissolve or severely attack the polymer structure. Furthermore, the mechanical action of stripping replica tapes (water soluble polyacrylic acid in this instance) from a polymer fracture introduces undesirable artifacts.” For this reason, crack inspection starting late in the first batch, and throughout all of the second batch, relied on dye penetrants and optical observation for cracking.

The issue was discovered after replicates were taken in two areas which had *not* been exposed repeatedly to the acetate film / acetone softening process several dozen times during fatigue testing to record crack development. The two areas in which this comparison was performed on two different specimens (Specimen 1 and 2 from Batch A) are shown in Figure 75. The crack density discrepancy between the area repeatedly exposed to acetone, and the two areas which had not been exposed to acetone at all is shown in Figure 76a & b.

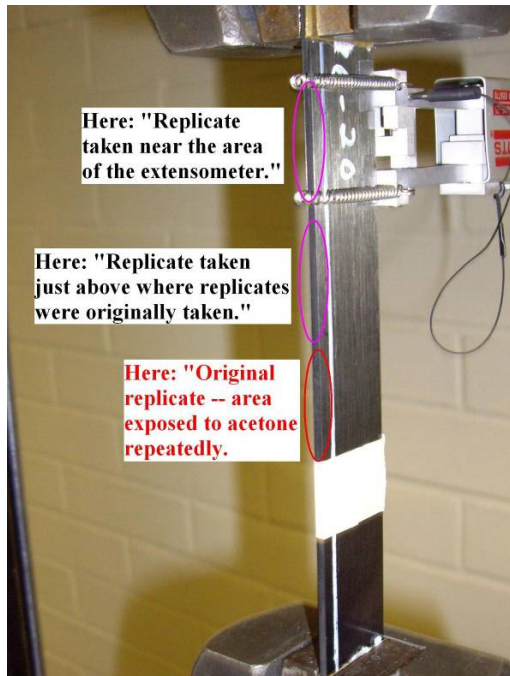
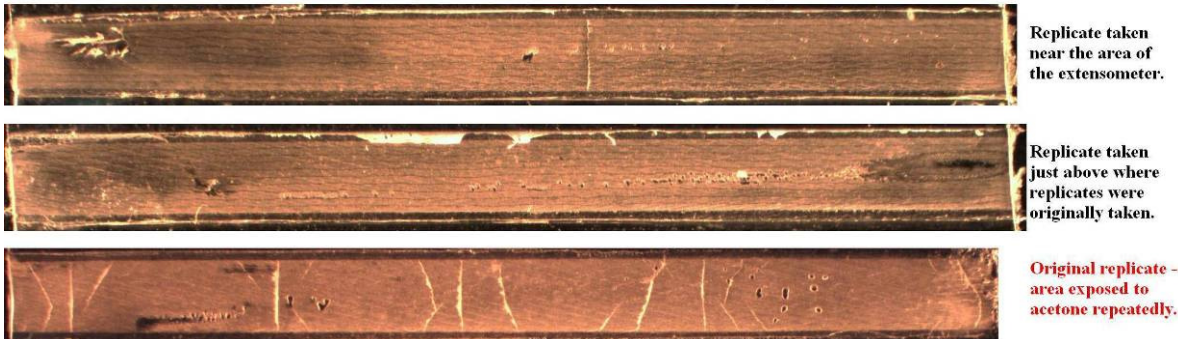


Figure 75. The three areas which were compared for crack densities. The lower area, circled and described in red, is where replicates were taken a couple dozen times.

Fatigue specimen 1 : $R = 0.1$, equiv $\epsilon_{\text{peak}} = 0.00276$,
 Strain control, $\sigma_{\text{peak}} = 13.4$ ksi



Fatigue specimen 2 : $R = 0.1$, equiv $\epsilon_{\text{peak}} = 0.004$,
 Load control, $\sigma_{\text{peak}} = 17.4$ ksi

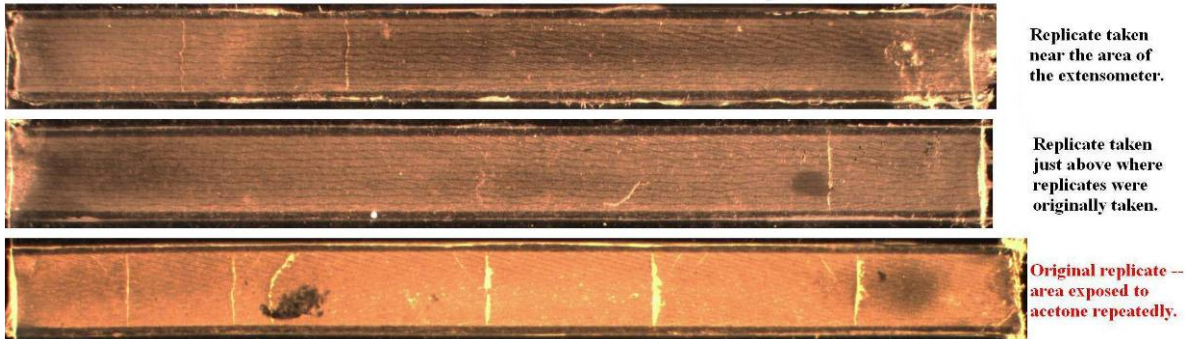


Figure 76a & b. The edge replicates taken in the three areas described in Figure 75 are compared here. Notice that crack density is much higher in the area repeatedly exposed to acetone.

The fact that acetone causes earlier cracking was further reinforced when penetrant enhanced x-rays were taken of specimens which had been subjected to different peak loads. Figure 77 compares an optical image of a specimen and its x-ray, illustrating the features which are visible in the x-ray. Figure 78 compares an x-ray to an edge replicate, showing that the x-ray is capable of revealing the cracks which are clearly evident in the edge replicate. Figure 79 shows clearly via x-ray that cracks appeared in the area where the edge replicate was taken, in higher numbers, than the rest of the length of the specimen.

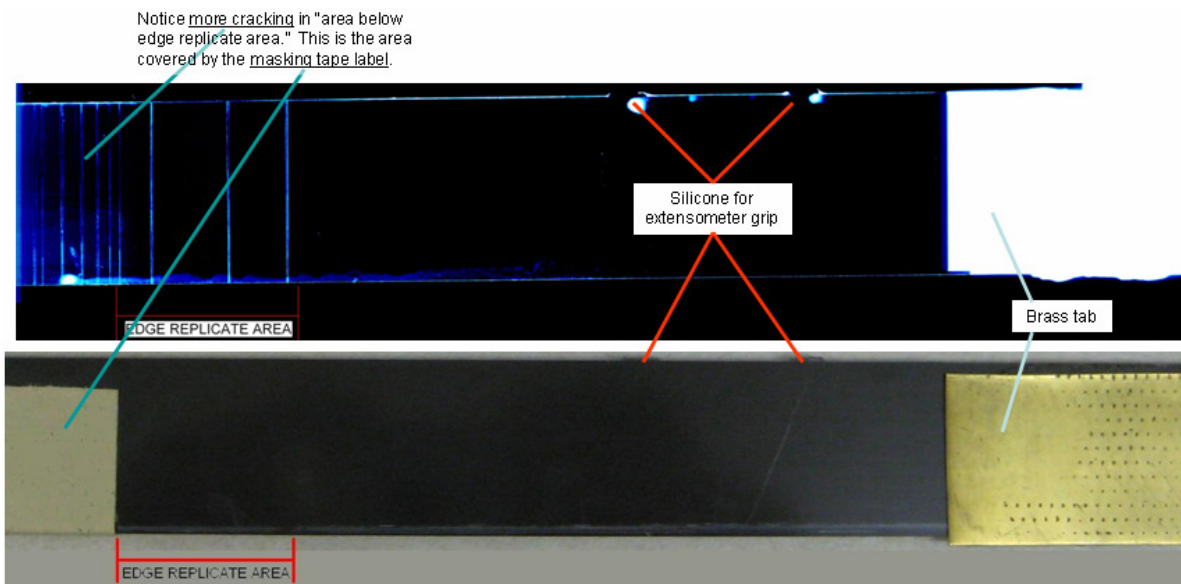


Figure 77. This picture compares an x-ray image to an optical picture of the specimen, to make the reader aware of what is being viewed in the x-ray. Any bright blue vertical lines are transverse cracks through the 90° plies. As mentioned in the figure label in the image, the masking tape label area typically had higher cracking. This is thought to be due to longer exposure to acetone—flowing between the label and the specimen surface, the acetone could not evaporate as quickly.

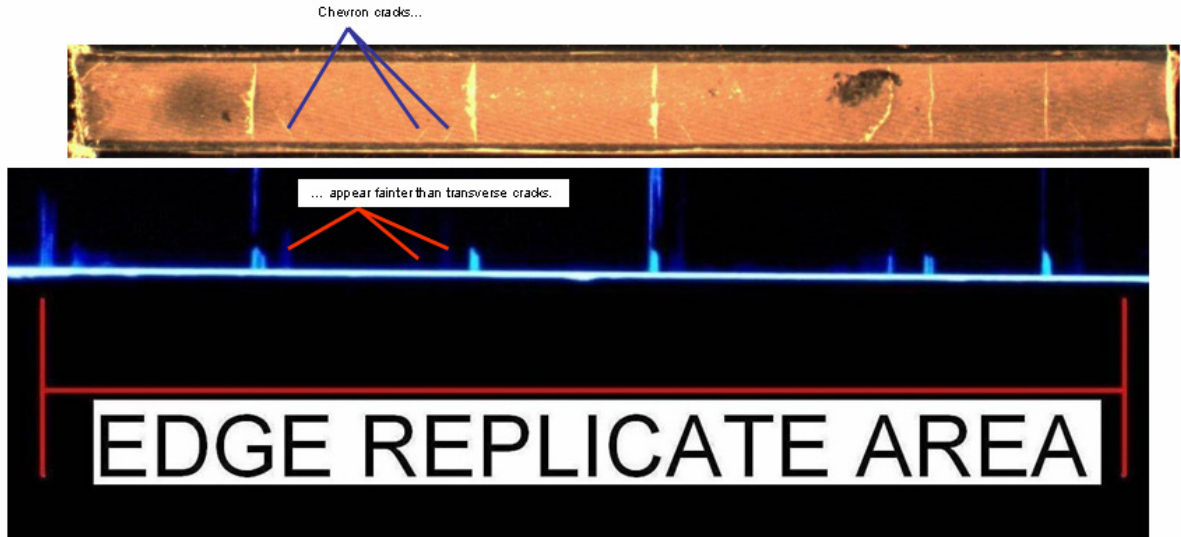


Figure 78. Comparison of an edge replicate to a magnified view of the x-ray in the same area. X-ray captures cracks with good fidelity, though “chevron cracks” appear more faintly than transverse cracks.

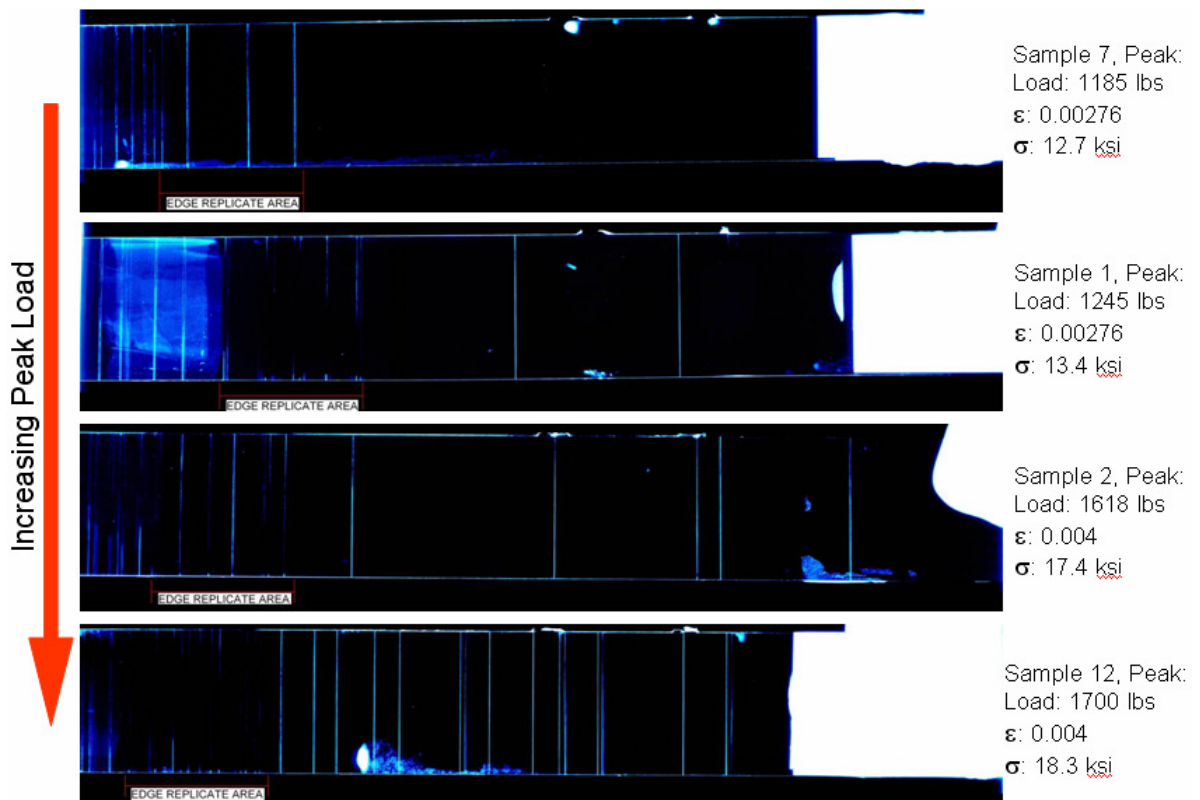


Figure 79. Here is solid proof that the acetate edge replication process causes earlier cracking than if it were not used. This shows four penetrant-enhanced x-rays of *four different specimens* from Batch A. The crack densities in the areas labeled “EDGE REPLICATE AREA” are consistently higher than in the bulk region which was not exposed to acetone, and are visible as the faint vertical lines off the edges in those areas. As peak load in fatigue testing increases, cracks appear in the area not exposed to acetone, but at lower densities.

To ensure that dye penetrants were not chemically attacking the composite, the crack densities from two specimens from the first batch (Specimens 12a and 18a) were compared, after they were subjected to the same fatigue test conditions. One was not subjected to chemical exposure (Specimen 12a) while one was inspected with dye penetrants (Specimen 18a). This ensured that dye penetrant inspection was not chemically attacking the specimens. This comparison is shown in Figure 80.

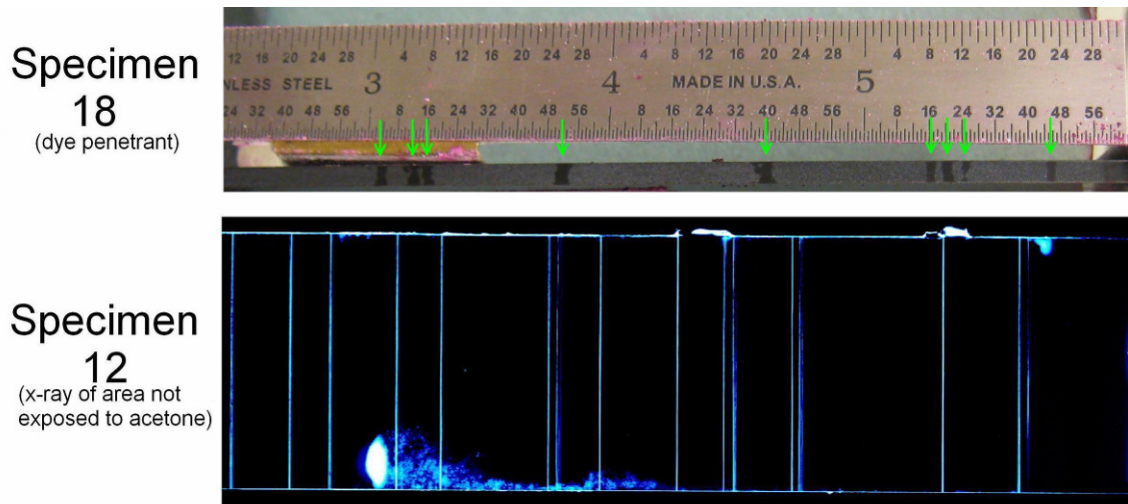


Figure 80. This image compares the crack densities (for the same edge length) from two different specimens from Batch A, which had been cycled at the same peak load (18.3 ksi or 126 MPa average laminate stress). Specimen 18 had a lower crack density (cracks marked with green arrows), even though it had been exposed to dye penetrants, while the x-rayed region of Specimen 12 had not been exposed to chemicals at all. This confirms that the dye penetrant technique does not chemically attack the composite.

4.6 Cross-Ply Testing & Batch Discrepancies

Apart from issues stemming from the damage inspection technique, there appears to be differences in material properties between the two batches of twenty specimens—differences in performance were observed between the groups. This list, whose items will

be described in more detail in the subsequent sections, summarizes the differences observed between the two batches:

1. *Modulus*: Batch A had a higher average modulus than Batch B.
2. *Ultimate strength*: four static ultimate tests were performed on Batch A, and they all outperformed Batch B's single ultimate strength test.
3. *Fatigue Crack Initiation*: Tests have shown that edge replication causes chemical attack, while dye penetrants were benign. Even so, Batch A initiated cracks at higher stresses than Batch B, though Batch A was the set of specimens exposed to acetone.

Why then is the second batch underperforming the first, when the second was not exposed to acetone? Likely explanations include variations in the constituent materials or preparation procedure between the two batches. However, our sponsors believe that both batches which they sent for testing were fabricated from the same material, and were careful to prepare the specimens to the specifications described in the section on "Specimen Preparation." Short of the sponsors discovering an error in the fabrication process, or doing a chemical analysis to determine differences between the batches, one way to possibly determine which of the batches may have been prepared improperly is to calculate the theoretical performance values (modulus, crack initiation stress levels, etc.). Whichever batch best matches the theoretical value may be the batch which was unaffected, or prepared from the correct materials. This will be commented on below as static and fatigue test results are presented along with their theoretical performance calculations.

4.7 Cross-Ply Static Tensile Testing

4.7.1 Moduli

With the cross-ply specimens, a low-load static test was performed on each sample before any subsequent testing was executed. This allowed a record of the modulus for all the specimens to be kept. Where cracking typically initiated in these specimens in static monotonic testing at 33% of the ultimate strength, these “low-load” tests were typically only run up to about 15% of the ultimate strength. The intent was to prevent damage by recording the modulus well within the region of elastic recovery for these specimens.

These modulus tests, in addition to showing that the specimen moduli varied widely in general, contributed to demonstrating performance differences between the two batches of specimens. In Figure 81 below, the specimen moduli are plotted in a histogram, grouped by whether they are in Batch A or B. Two things are evident here. First: that the average modulus clusters around two separate values for the two different batches (4.5 Msi for batch A, 4.23 Msi for batch B). Second, even within the same batch, the modulus value can vary across a range which is 20% of the average modulus value.

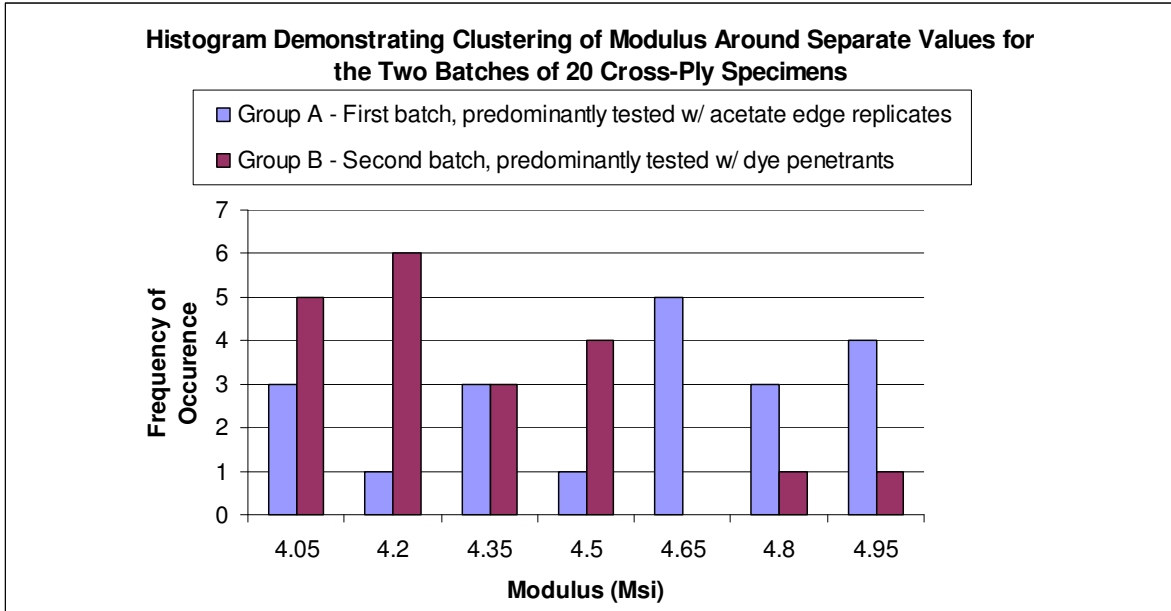


Figure 81. A histogram of the modulus values for the two batches of twenty cross-ply specimens.

Rule-of-mixtures can be used to predict the modulus based on the (claimed) constituent properties listed in APPENDIX A and APPENDIX B. ROM (Eq. 16) can then be used to calculate the modulus of the 0° plies:

$$E_{11} = E_f V_f + E_m V_m = 25 \text{Msi} (172.0 \text{GPa})$$

The theoretical and experimental modulus, E_{22} , of the 90° plies was determined in the section on unidirectional specimen tests. The theoretical transverse modulus E_{22} for IM-7/977-3 composite is 1420 ksi (9.75 GPa) and was observed to be 1100 ksi (7.58 GPa) in experimentation. Using the experimentally measured E_{22} modulus, the ROM can again be applied to calculate the net section modulus of the cross ply laminate (Eq. 17):

$$E_{11, Lam} = E_{11} V_{0^\circ} + E_{22} V_{90^\circ} = 5.08 \text{Msi} (35.0 \text{GPa})$$

Compared to the average modulus of 4.50 Msi for batch A and 4.23 Msi for batch B, it appears that batch A is in better agreement with the theoretical modulus. It may be the case

that batch B's properties were affected by some unknown factor, causing them to be reduced from the theoretical modulus performance.

4.7.2 Static Testing Crack Initiation

In static tensile testing of cross-ply laminates, crack initiation begins in the 90° plies when $\epsilon_{ULT,22}$ is reached. Experimentally, in the unidirectional 90° study, this value was found to be 0.0076 strain (at 8.36 ksi or 58 MPa), and the epoxy manufacturer claims “typical properties of 977-3 laminates” values are $\epsilon_{ULT,22} = 0.0077$ (at $\sigma_{ULT,22} = 9.3$ ksi or 64 MPa). In the static tensile tests, for both Batches A and B, cracking in the 90° specimens could be heard as audible snapping and was first heard to occur at (and was shortly thereafter observed to be present with dye penetrants or edge replication) at a common average laminate stress of 23.7 ksi (163 MPa). Jamison [35] first observed cracking in quasi-static testing at 30% of σ_{ult} —quite close to the first cracking observed at 32% σ_{ult} observed here.

This average overall laminate stress translates to a ϵ of 0.0052 for batch A's Specimen 17 (Figure 82), and a ϵ of 0.0061 for Specimen 20 of batch B (...remember—varying moduli between batches will cause different strains for same stress level). This underperforms the original unidirectional test and the manufacturer's ϵ_{ULT} claims. It is noted that the point at which there is a sufficient number of cracks to degrade the modulus *as recorded by the extensometer*—i.e., the point at which the σ - ϵ data noticeably “peels off” of the initial linear elastic loading curve—is closer to, but still less than, the original

observations of $\epsilon_{ULT,22} = 0.0077$. This value is approximately 0.0062 ϵ for Group A Specimen 17 and approximately 0.0072 ϵ for Group B Specimen 20.

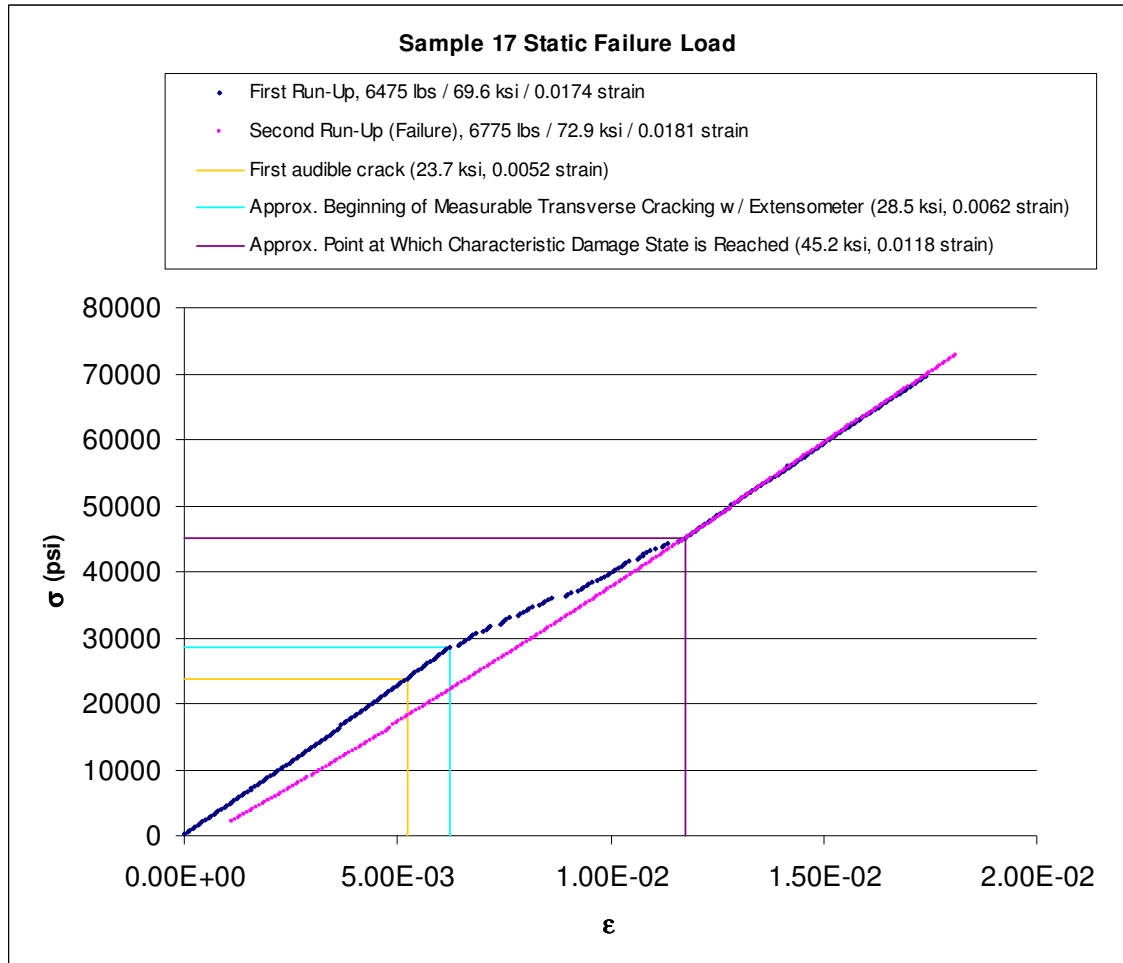


Figure 82. σ - ϵ curve to failure for Sample 17 of Group A. In this test, the load was increased to 69.6 ksi, well beyond the point at which the characteristic damage state was reached, then unloaded, then loaded back to ultimate failure. This test shows parallels to Figure 25 and Figure 26, repeated below.

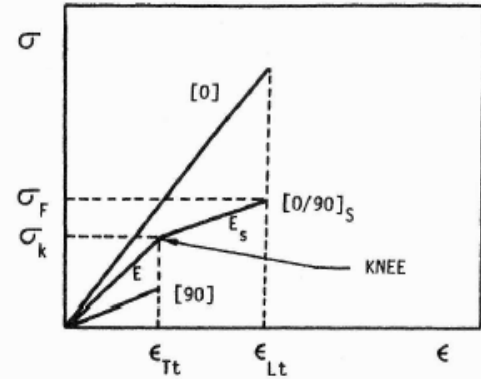
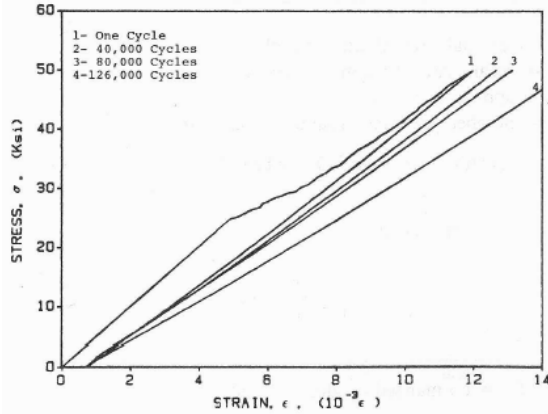


Figure 25 to the left [29] and Figure 26 to the right (Mallick, repeated from earlier) [6] closely mimic the cross-ply behavior observed in this study's static tests. Figure 25 shows a stress-strain curve for a cross-ply laminate. The behavior in cycle 1 is very similar to that illustrated in Figure 82. The stress-strain schematic illustrating separate behaviors of 0° and 90° plies to the right is an idealized version of these experimental results.

The question of “why is there a drop in $\epsilon_{ULT,22}$ for the 90° plies in a cross-ply laminate, as compared to a unidirectional 90° laminate?” might be answered by investigating the opposing Poisson effects of the neighboring 90° and 0° layers. This effect could cause earlier failure than in a laminate consisting strictly of 90° plies. Below are the classical lamination theory matrices which describe the macromechanical load and deformation response for a laminated orthotropic material. In addition to the transformed reduced stiffness calculations of APPENDIX D, the laminate in-plane load and moment (per unit width of the laminate) are N and M respectively, A is the extension stiffness matrix, B the bending-extension matrix, D the bending stiffness, and ϵ and κ are the middle-surface strains and curvatures, respectively:

$$\begin{bmatrix} N_x \\ N_y \\ N_{xy} \end{bmatrix} = \begin{bmatrix} A_{11} & A_{12} & A_{16} \\ A_{12} & A_{22} & A_{26} \\ A_{16} & A_{26} & A_{66} \end{bmatrix} \begin{bmatrix} \epsilon_x^o \\ \epsilon_y^o \\ \gamma_{xy}^o \end{bmatrix} + \begin{bmatrix} B_{11} & B_{12} & B_{16} \\ B_{12} & B_{22} & B_{26} \\ B_{16} & B_{26} & B_{66} \end{bmatrix} \begin{bmatrix} \kappa_x^o \\ \kappa_y^o \\ \kappa_{xy}^o \end{bmatrix} \quad (\text{Eq. 40})$$

$$\begin{bmatrix} M_x \\ M_y \\ M_{xy} \end{bmatrix} = \begin{bmatrix} B_{11} & B_{12} & B_{16} \\ B_{12} & B_{22} & B_{26} \\ B_{16} & B_{26} & B_{66} \end{bmatrix} \begin{bmatrix} \epsilon_x^o \\ \epsilon_y^o \\ \gamma_{xy}^o \end{bmatrix} + \begin{bmatrix} D_{11} & D_{12} & D_{16} \\ D_{12} & D_{22} & D_{26} \\ D_{16} & D_{26} & D_{66} \end{bmatrix} \begin{bmatrix} \kappa_x^o \\ \kappa_y^o \\ \kappa_{xy}^o \end{bmatrix} \quad (\text{Eq. 41})$$

Where (from APPENDIX D):

$$A_{ij} = \sum_{k=1}^N (\bar{Q}_{ij})_k (z_k - z_{k-1})$$

$$B_{ij} = \frac{1}{2} \sum_{k=1}^N (\bar{Q}_{ij})_k (z_k^2 - z_{k-1}^2)$$

$$D_{ij} = \frac{1}{3} \sum_{k=1}^N (\bar{Q}_{ij})_k (z_k^3 - z_{k-1}^3)$$

For this laminate, B (the bending-extension stiffness) is zero. For this loading case, κ (the mid-plane curvature) is also zero. This then reduces this layup's predicted stress-state to:

$$\begin{bmatrix} N_x \\ N_y \\ N_{xy} \end{bmatrix} = \begin{bmatrix} 7.22 & 1.06 & -2.48 \\ 1.06 & 19.1 & -2.48 \\ -2.48 & -2.48 & .351 \end{bmatrix} \begin{bmatrix} \epsilon_x^o \\ \epsilon_y^o \\ \gamma_{xy}^o \end{bmatrix} (\times 10^5)$$

Future work could include strain-gage verification of ϵ_y^o prediction of this stress-state. This induces a compressive stress in the fiber direction of the 90° plies, which was not present in the unidirectional 90° specimens, and which could be part of the stress-state which causes earlier cracking. Pagano and Pipes (1971) [54] also theorize a distribution of normal tensile stresses which develop at the edges of cross-ply laminates (of $[90/0]_s$ layup, but a similar principle applies here) whose presence counteracts the interlaminar shearing stress between adjacent 90° and 0° plies (Figure 83)—this can also contribute to the stress-state which reduces the crack initiation performance of 90° plies in a cross-ply, as compared to its unidirectional counterpart.

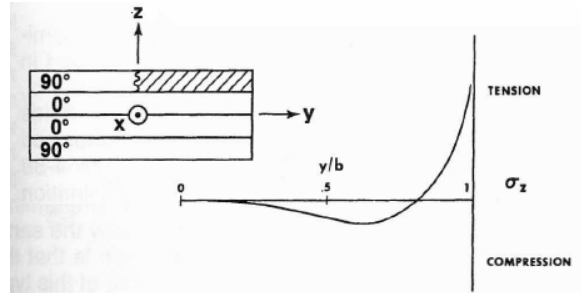


Figure 83. Interlaminar normal stress for a cross-ply laminate ($y/b = 1$) corresponds to the edge of the laminate; a value of zero is the center of the laminate. Note that this reflects a $[90/0]_2$ layup (Pagano & Pipes) [54].

4.7.3 Static Tensile Testing Crack Development

Another interesting point to observe about the σ - ϵ curve-to-failure in Figure 82 is the modulus before cracking has begun (elastic recovery regime), and after the characteristic damage state has fully developed (slope of the line formed by the pink data points in Figure 82). Due to the fact that the 90° plies effectively carry very little load after the C.D.S. has been achieved, the load is effectively carried only by the 0° plies. Indeed, if the post-C.D.S. load uptake per increase in strain is divided by the cross-sectional area of just the 0° plies, a modulus of 25.2 MPa is calculated—where a theoretical E_{11} modulus of 25 MPa was predicted earlier. This empirically demonstrates that the 90° plies have been cracked to such an extent that the shear-lag effect is incapable of imparting significant load to the fractured 90° material, and thus the 0° plies are all that is effectively contributing to the laminate’s modulus after the C.D.S. is reached.

As loading increases in a static tensile test in which a single crack has developed, further cracking in the 90° plies occurs and the crack density increases up to the “characteristic damage state”—at which point, the maximum number of cracks which can possibly develop will be present. The crack inspection techniques of edge replication and dye penetrants were used to monitor this development of damage. In Batch A, the first

“Practice” tensile test specimen was incrementally inspected with edge replicates at 200 lb (2.15 ksi) intervals as it was loaded to failure (Figure 84); the first crack observed was at 23.7 ksi. After edge replication was recognized to cause early cracking in the 90° plies, another specimen (Specimen 17) was loaded to failure without any in-test inspection—the first audible crack heard in this test was at 23.7 ksi as well. Figure 85 shows crack development as recorded by dye penetrants on a 4.25” edge section of Specimen 20 from Group B.

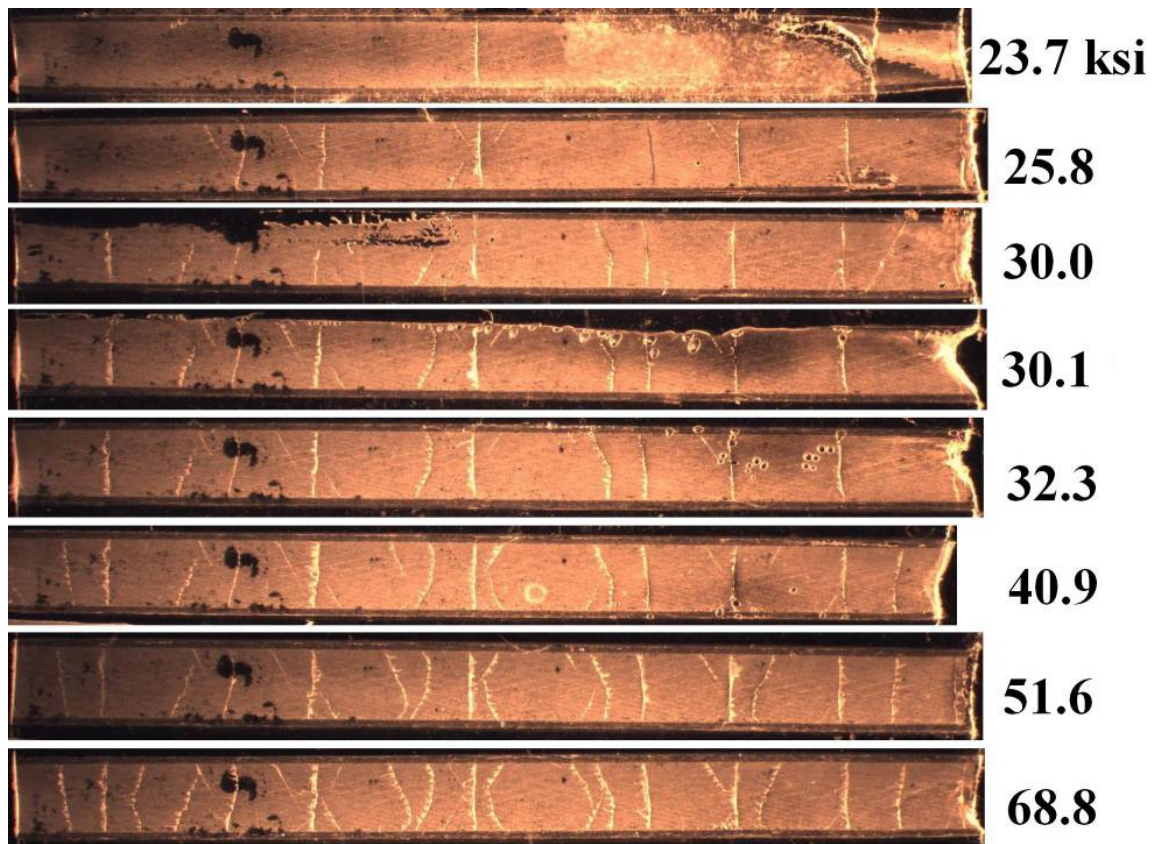


Figure 84. These edge replicates taken during the static tensile testing performed on the first practice tensile test specimen. The ksi value to the right of each replicate corresponds to the (average) stress in the laminate at which the replicate was taken. σ_{ult} for this specimen was 72.3 ksi. Crack density is 21 inch^{-1}

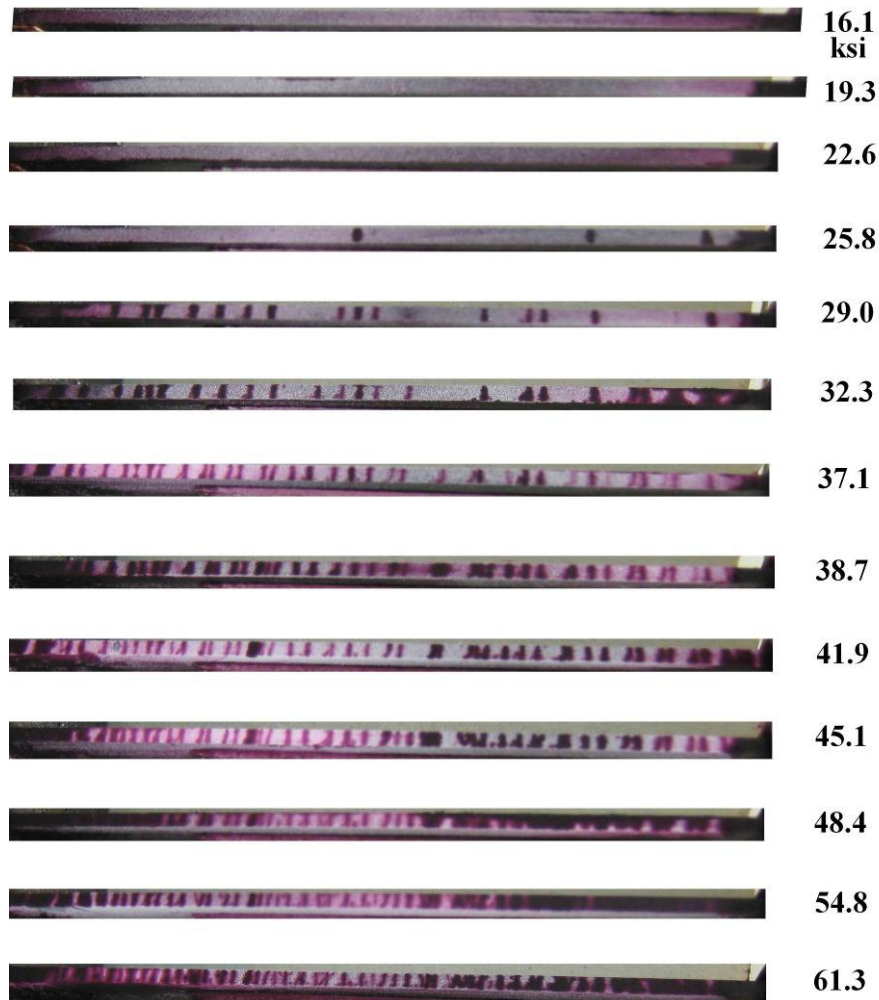


Figure 85. This image shows the increasing number of cracks in Specimen 20 from Group B as it was being loaded to failure, as revealed by dye penetrant edge inspection. The peak stress at failure was 67.7 ksi. In contrast to Figure 84, which only inspected a 1.0” length for cracking, the length of inspected edge shown in this image is 4.25”. The peak crack density is similar—CCC cracks/inch.

Comparisons of crack densities are made in a quantitative manner in Table 6 as follows: visible transverse cracks are counted as a single instance of cracking, as are visible laminate midline pairs or single instances of chevron cracking (the latter being a one-sided crack at 45°—not mirrored across the laminate centerline). This is a somewhat arbitrary way to count crack densities, but if applied consistently across different specimens, still provides some measure of how much “damage” has occurred in the laminate. In Table 6, note that crack density for the specimen from Batch B is *lower* at ~41 ksi, while being

higher once the characteristic damage state is reached. Acetone from edge replication may have caused earlier cracking for the Group A specimen at 41 ksi, while a lower σ_{ult22} value may have caused the higher ultimate crack density for Group B.

Table 6. Comparisons of crack densities at two points in the static tests of the “practice” specimen from Group A (Practice tensile test specimen), and Specimen 20 from Group B. Lower crack density at the stress state of 41 ksi for Specimen 20b could be due to the absence of the degrading acetone, while a higher crack density at the C.D.S. for the same specimen could be explained by its lower σ_{ult22} , which was shown earlier experimentally, and which would cause higher cracking.

Inspection Point	"Cracks / Inch"	
	"Practice" Group A	#20 Group B
~41 ksi stress	21	18
C.D.S.	23	26

As explained in (Eq. 22) through (Eq. 31), researchers Lee and Daniel [44] and Berthelot et. al. [5] have applied the concept of shear-lag to the case of stress transfer into the 90° plies of a cross-ply laminate with a transverse crack present. With this method, the load-axis stress-field (σ_{xx}^{90}) as a function of transverse crack spacing and laminate thickness can be plotted with an excel table containing an array of locations within the 90° plies. Similarly, interlaminar shear can be plotted along the 0°/90° interface (refer to Figure 86). As a comparison for the σ_{xx}^{90} stress-field prediction: a relatively low crack spacing of 4/inch (Figure 87), 18/inch (Figure 88, observed at 41 ksi in Specimen 20b), and the maximum crack density reached for this specimen: 26/inch (Figure 89). The plots for interlaminar shear stress for the same crack densities are shown in Figure 90, Figure 91, and Figure 92 respectively.

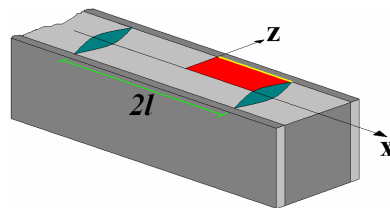


Figure 86. Areas modeled by the shear-lag equations. The stress-field of σ_{xx}^{90} is highlighted in red; the interlaminar shear layer is highlighted in yellow. Crack spacing of “2l.”

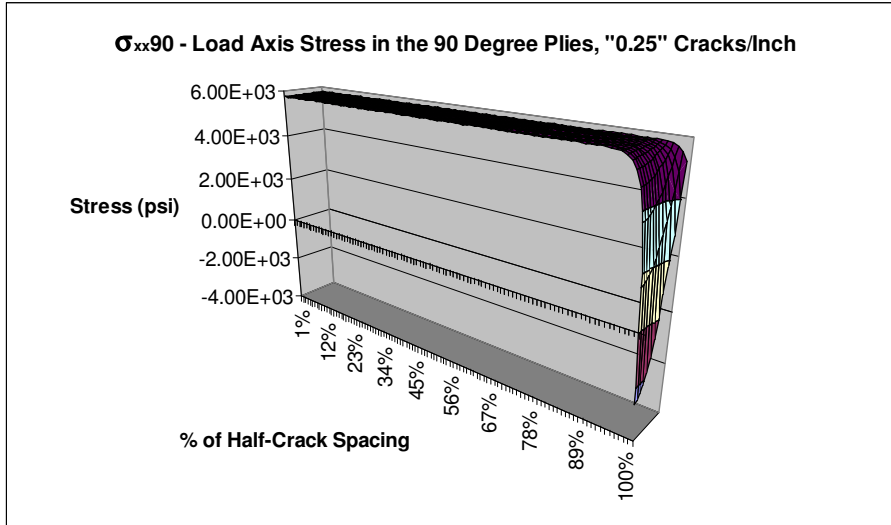


Figure 87. σ_{xx}^{90} for 0.25 cracks/inch, 23.7 ksi (“first audible crack at 2200 lbs of loading”).

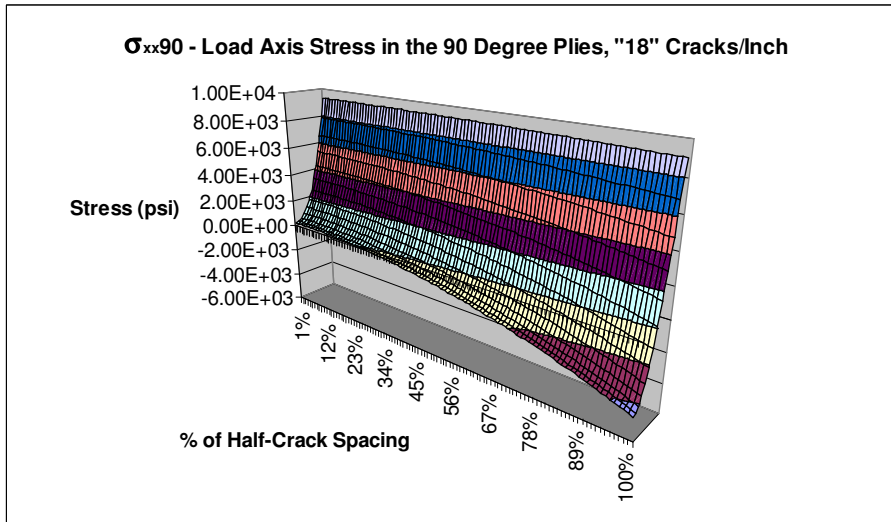


Figure 88. σ_{xx}^{90} for 18 cracks/inch at 40.9 ksi.

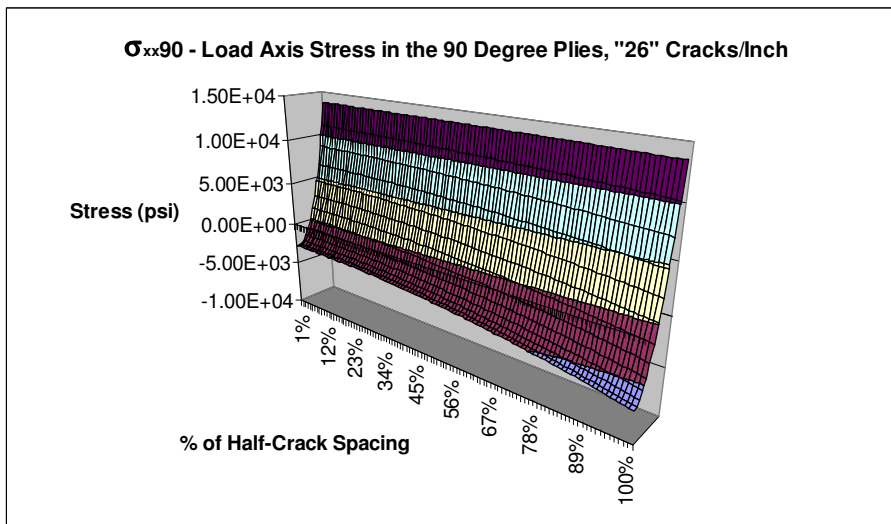


Figure 89. σ_{xx}^{90} for 26 cracks/inch at 61.3 ksi—reflects the C.D.S.

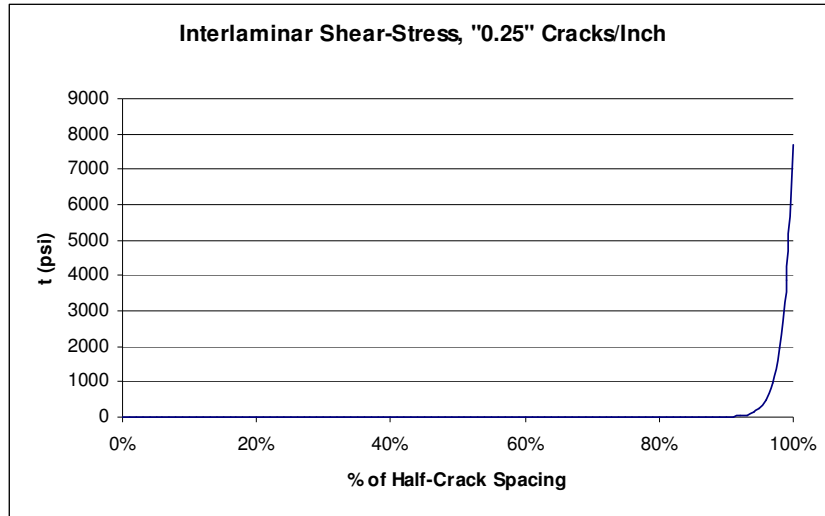


Figure 90. Interlaminar shear for 0.25 cracks/inch, 23.7 ksi (“first audible crack”).

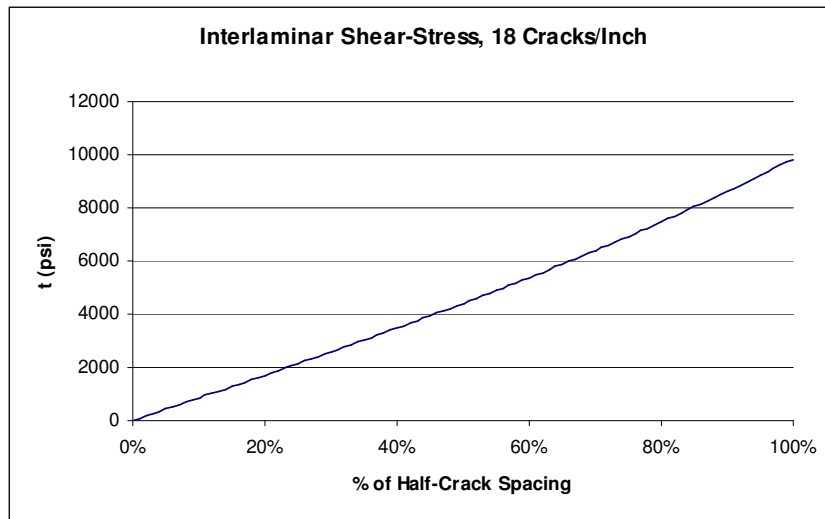


Figure 91. Interlaminar shear for 18 cracks/inch at 40.9 ksi average laminate stress.

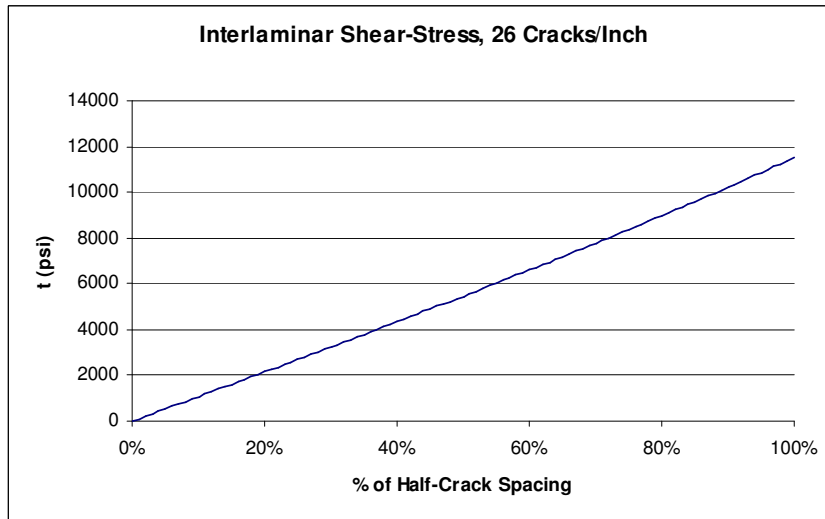


Figure 92. Interlaminar shear for 26 cracks/inch at 61.3 ksi average laminate stress (C.D.S.).

Some points to note about these stress predictions:

1. For these plots, the edge length over which the plot is modeled obviously changes (it models the “half-crack length”). This model proves to display the characteristics of shear-lag stress behavior—at 4 cracks/inch, a much larger inter-crack spacing causes stress to reach uniformity across the width of the 90° plies in a *smaller percentage of the half-crack spacing*. Similarly, for shorter crack spacing, the shear and the σ_{xx}^{90} tensile force is unable to transfer a tensile force to the center of the laminate (which is the origin of the large dip in σ_{xx}^{90} along the laminate centerline).
2. Cytec’s claimed 0° interlaminar shear strength is 18.5 ksi (APPENDIX B). While the interlaminar shear calculated here is not between two 0° plies, the maximum predicted interlaminar shear is 11.5 ksi (at 26 cracks/inch, well below the 18.5 ksi value). In addition to the fact that delamination was not observed in static testing here, these calculations bolster the idea that, in ultimate tensile strength testing, delamination is not critical or even present to affect performance.
3. This model provides some insight into fatigue behavior as well. Specimen 12a—exposed to the highest peak cyclic stresses in this study (~25% σ_{ULT}) exhibited small delaminations at the 0/90 interface (refer to Figure 101 and Figure 102, page 126 for images of this). This specimen, at its maximum crack density, had a calculated peak interlaminar shear of 4.8 ksi. It is also known that for sufficiently high peak stresses, longitudinal cracking in the 0° plies and larger delaminations than those observed here will occur. For example, Jamison [35] observed these features in fatigue at 10 Hz, R = 0.1 when peak stresses were 70% σ_{ULT} . Specimen 12a’s interlaminar shear stress level of 4.8 ksi may be close to the delamination initiation stress-state.
4. The σ_{xx}^{90} stress-field suggests why the chevron cracks grow, but terminate before reaching the already-present transverse crack—as the crack grows towards the centerline, the driving force for the crack, partly a function of σ_{xx}^{90} , tapers off.
5. An interesting feature of this model is that crack density can be maintained while average laminate stress is increased. In this way, the 90° ply stress leading to increased crack density can be calculated, in a stepwise manner.
6. The model for σ_{xx}^{90} displays a compressive axial force near the laminate centerline near the crack—this is an artifact of the hyperbolic functions which the model employs, but is a deviation from the actual axial stress behavior in the laminate—which must be stress free at the crack boundary.
7. As the number of 90° plies in the model is decreased, both the maximum values of σ_{xx}^{90} and interlaminar shear *decrease*. The laminates in this study, with ten adjacent 90° plies, will provide *conservative* predictions of behavior in cross-ply with fewer adjacent 90° plies.
8. The model, above approximately 66% of the average laminate σ_{ult} value, displays σ values along the 0° / 90° boundary which are beyond the σ_{22ULT} value (8.36 ksi measured experimentally). Plasticity in the resin rich interlaminar boundary may be occurring, preventing delamination development in static monotonic loading.

4.7.4 Static Ultimate Failure-0 Degree Ply Rupture

Another instance where Batch A outperformed Batch B was σ_{ult} . This is demonstrated in Table 7, below. Note the relative uniformity of ϵ_{ult} —with the exception of Specimen 6 from Group A, all of the ultimate ϵ values were very close to the IM-7 fiber manufacturer’s claim of a ϵ_{ult} value of 0.018. A calculation of ultimate load with this ϵ_{ult} value, based on the modulus and cross-sectional area of the two 0° plies, predicts an ultimate load of 6500 lbs; Specimen 20b failed at 6300 lbs. Figure 93 - Figure 96 suggest how the laminate behaves at ultimate failure—rupture occurs where transverse cracks in the 90° plies apply a stress concentration on the 0° plies. Occasionally, the 0° fibers fail at different transverse crack locations, causing the rupture surface to be non-planar.

Delamination and some longitudinal 0° cracking are observed.

Table 7. The set of static ultimate strength tests performed on the cross-ply specimens, Specimen 20b was the only specimen from Batch B tested to ultimate strength—note its much lower ultimate strength value. Also worth noting is the consistency of the ultimate strain value across all the specimens. Though Specimen 6 reached a relatively remarkable ϵ_{ult} of 0.02003, the ultimate strain of IM-7 fibers (0.018), appears to govern ultimate failure of these specimens.

Specimen	E (Msi)	E(GPa)	Peak σ (ksi)	ϵ peak	Description
Test Specimen	4.82	33.2	72.3	0.0182	Ran to failure. This was on the screw drive machine and was intended to get ultimate load and strain values. Inaccuracy of measurements on this machine warranted another ult load/strain test later.
Specimen 4	4.53	31.2	74.7	N.A. See Description	Recorded ult load but strain gage voltage ranges were set improperly: did not get final strain reading.
Specimen 6	4.11	28.3	76.1	0.02003	No crack investigation--had to do this to get ultimate strain value.
Specimen 17	4.67	32.2	72.8	0.01811	Did this test to make sure that acetone hadn't influenced peak load value from previous tests.
Sample 20b	4.05	27.9	67.7	0.0188	Ruptured at 6300 lbs, 0.0188 strain. First audible snap at 23.7 ksi. Cracks at next observation--25.8 ksi.

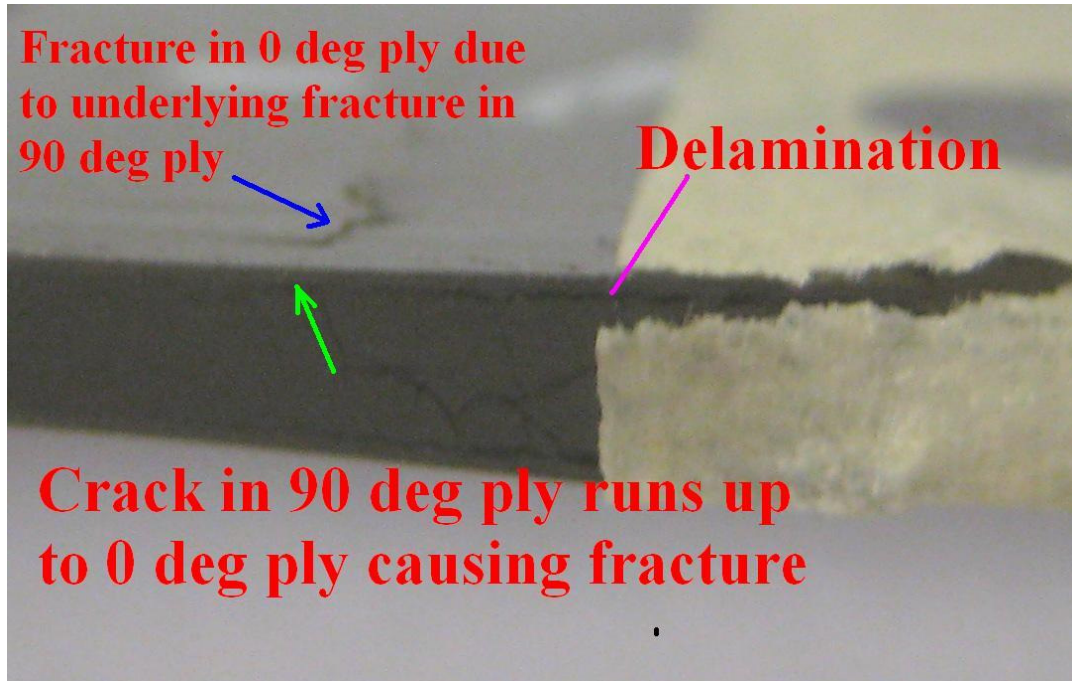


Figure 93. Here, the nature of the failure process is illustrated—the underlying crack in the 90° ply causes the 0° ply adjacent to it to split, at that location.

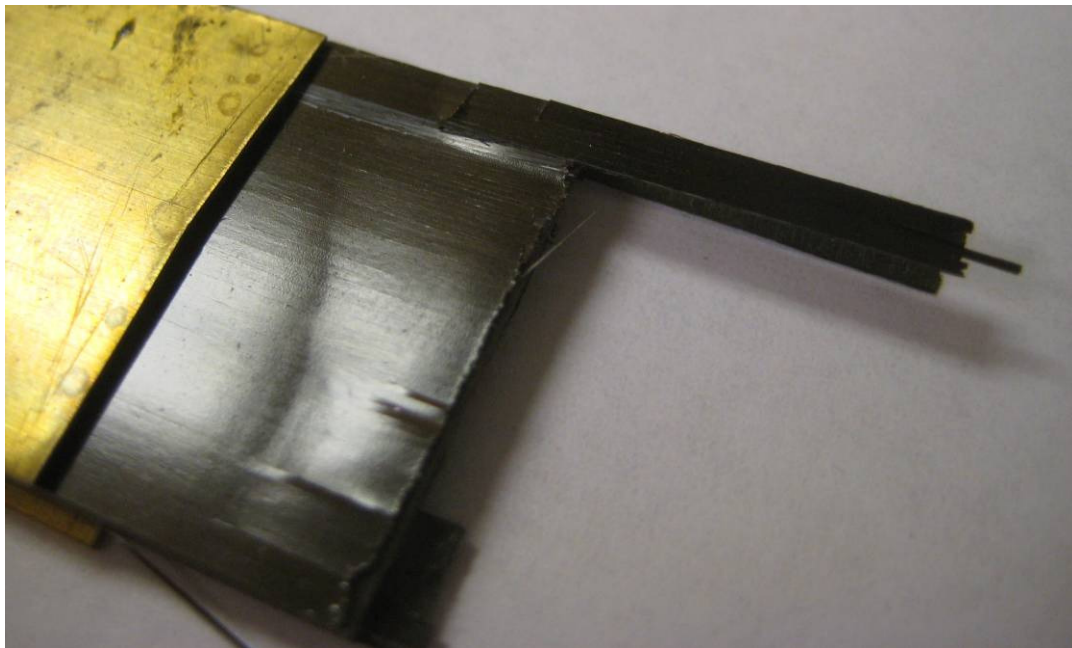


Figure 94. This image illustrates the “peeling” of delamination which can occur at rupture, as well as the fact that the rupture location of the fibers in the 0° plies need not occur on the same plane, at the same transverse crack location.

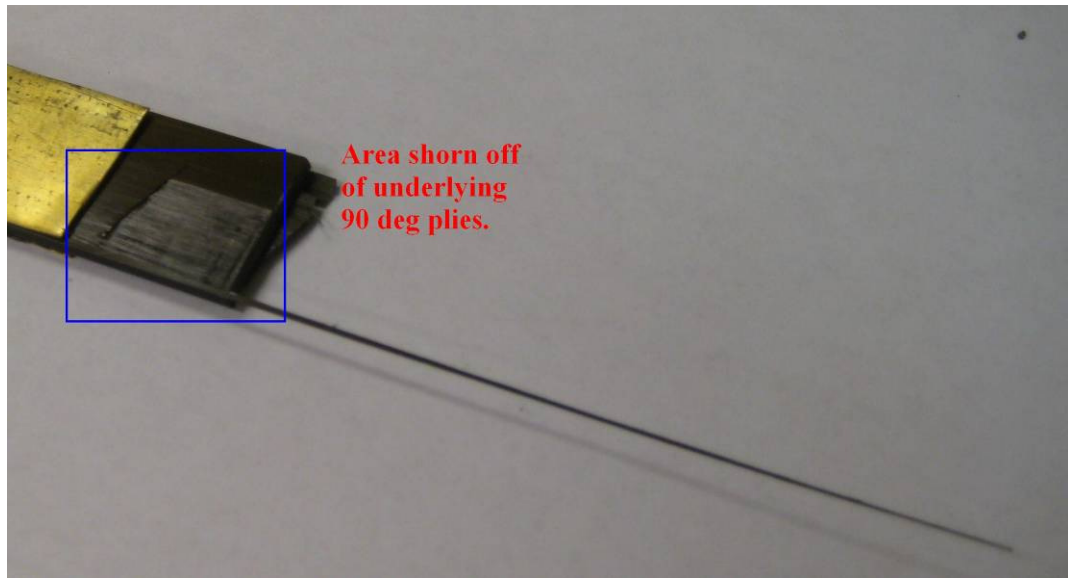


Figure 95. This image also illustrates that fracture of the 0° fibers can occur at locations far removed from where the bulk of the laminate fracture occurred.

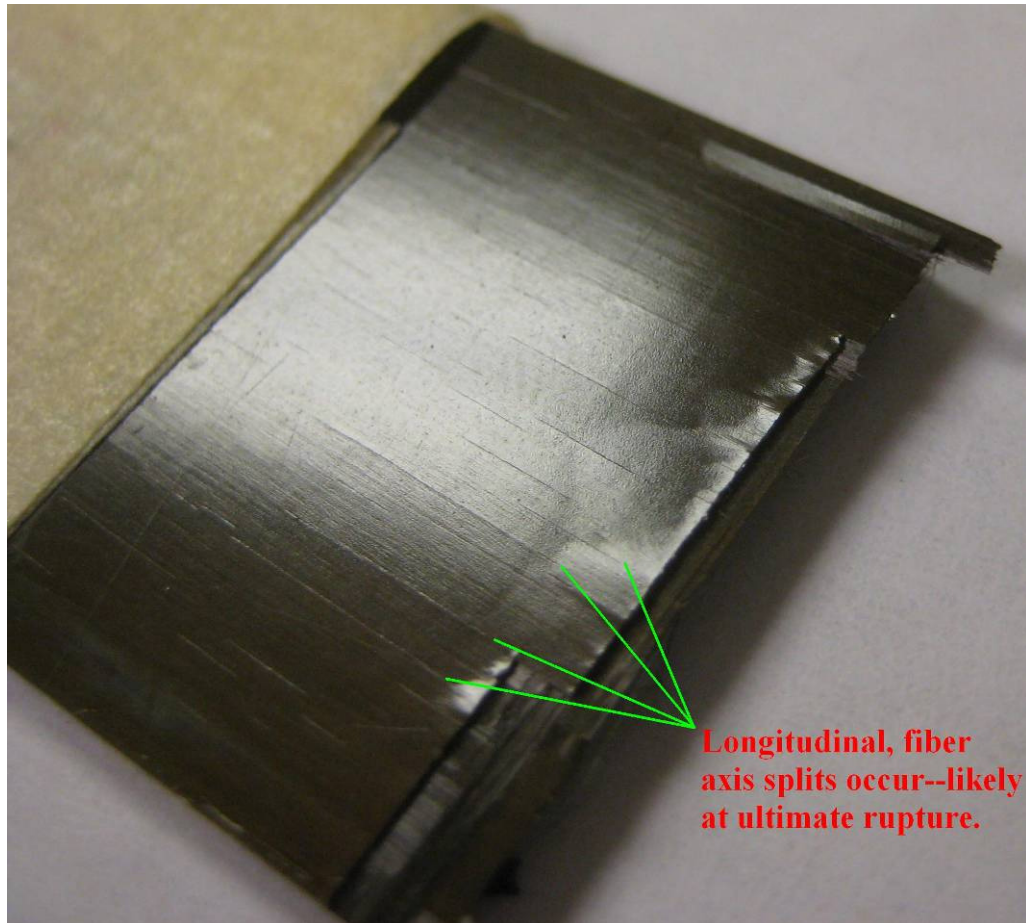


Figure 96. Small longitudinal splits are also evident in the outer 0° plies after fracture.

4.8 Cross-Ply Specimens: Fatigue Testing

Cross-ply fatigue testing formed the bulk of the experimentation in this study. For both Batch A and B, the average laminate stress level which would initiate cracks (σ_{ci}) for the “baseline case” of 10 Hz, $R = 0.1$ was determined experimentally. Additionally, several other types of tests were performed between the two batches:

- **First Batch:**
 - *Rate of Crack Development:* several specimens were cycled at loads well above the crack initiation stress level, rate of crack development was recorded with edge replicates (thus: “conservative” in their presentation of crack development—acetone exposure seems to cause earlier cracking).
- **Second Batch:** several tests studied how crack initiation was affected by:
 - *Effect of R-Ratio:* besides $R = 0.1$, a few tests were run at $R = 0.5$.
 - *Effect of Loading Frequency:* several tests were run at 3 Hz and 30 Hz
 - *Effect of Edge Roughness:* hand-sanded specimen edges prior to testing.
 - *Effect of Load-Frequency History:* cycled at 7 Hz for several increasing load levels, then at 3 Hz—will this lower the crack initiation stress at 3 Hz?

A tabular record containing the test setup and short test result summaries for each of the fatigue tests is contained in (APPENDIX E). An important assumption in these tests is that if cracks were not observed for a certain peak load and R-ratio out to 1M cycles, then the specimen was assumed to have no damage imparted to it in that test—and the peak load was then increased for that specimen, and testing was continued. Later in the study, after it was observed that damage, if it were to occur, would likely show up in the first 200k cycles (and most likely in the first 50k), the “run-out” test length was shortened to 200k cycles.

For the second batch of specimens on which these “exploration of effects” tests were performed, a summary of σ_{ci} for all of the various investigations (R-ratio, loading frequency, etc.) is listed in Table 9 (page 130). An important point to note is that conclusions from these tests are based on a single specimen tested in each of the variations

in R-ratio, loading frequency, and edge quality. The exception to this is the test of “10 Hz, R=0.1, No Polish”—whose value is an average of five samples. A number of samples were tested for this test case in order to get an idea of scatter. Generally, the following conclusions can be made about these tests:

1. 10 Hz was “the worst frequency” in that 3 and 30 Hz tests had a higher σ_{ci} .
2. Edge sanding always increased σ_{ci} values—sometimes dramatically.
3. Compared to R = 0.5, R = 0.1 had a lower peak stress at crack initiation (σ_{ci}). R = 0.1 is likely more damaging because it has a higher stress range.

The data supporting these conclusions is contained in the following sections.

4.8.1 Fatigue Crack Initiation: 10 Hz R = 0.1, Batch A vs. Batch B

All of the fatigue crack initiation studies from Batch A, and quite a few from Batch B, were performed at 10 Hz, R = 0.1. As mentioned previously, when cracks were not observed in a test that had been cycled to the run-out value, the specimen was “reused” and fatigue tested again at a slightly higher load. This process was repeated until a crack was detected via edge replication for most of the specimens in Batch A, and with dye penetrants for all of Group B’s tests. This data is presented in terms of σ_{ci} in Figure 97 and in terms of ϵ_{ci} in Figure 98 below. Several things are observed:

1. Consider the group of specimens formed by 2b, 4b, 5b, 6b, and 7b: they were all tested up to first crack with the same load-increase interval, and are therefore comparable. For these specimens, it is evident that crack initiation clusters more closely around an average peak *stress* value (σ_{ci}), as opposed to an average peak strain value (ϵ_{ci}). The standard deviation as a percentage of the average value for the group is 4% for σ_{ci} , and 9% for ϵ_{ci} . Thus, even though strains for the same load varied widely due to moduli discrepancies between the specimens, the laminate stress may provide a better prediction of crack initiation.
2. For the group of specimens formed by 2b and 4b-7b, the average laminate stress σ_{ci} value was 11.4 ksi, at an average ϵ_{ci} of 0.00271 (with an experimentally measured E_{22} of 1.10 Msi, this strain value translates to a stress of 2.98 ksi in the 90° plies). The epoxy manufacturer claims “typical properties of 977-3 laminates” values are $\epsilon_{ULT,22} = 0.0077$ (at $\sigma_{ULT,22} = 9.3$ ksi or 64 MPa). This significant decrease in the

stress capable of being sustained by 90° plies in this laminate is at least partly explained by the increased strain rate of these tests (10 Hz).

- Group A’s fatigue tests were not subjected to the same steadily increasing incremental peak load values as Group B’s specimens were. This was largely due to testing inexperience at the time that these tests were performed—the early tests were an attempt at trying to home in on the “ballpark” σ_{ci} value. However, even accounting for the coarse load-increase increments of Group A, and knowing that all of Group A’s specimen’s were exposed to acetone (except 19a), Group A still showed a higher σ_{ci} value than Group B. In particular, note Specimen 2a, 8a, and 10a, which all had at least one run-out test which occurred well above the average σ_{ci} value of 11.4 ksi for Group B.

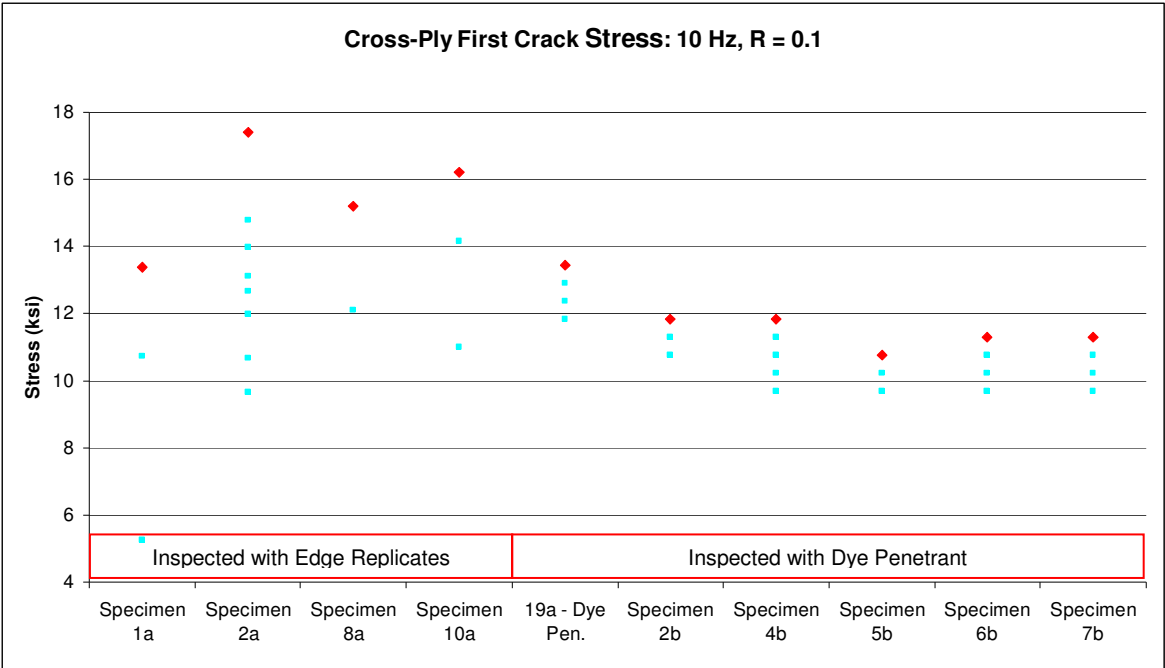


Figure 97. σ_{ci} for cross-ply fatigue tests at 10 Hz, R = 0.1. The blue dots represent tests which reached run-out of 1M cycles without cracking. Only those fatigue specimens are included in which at least one test achieved run-out... For clarity, those tests where the specimen cracked in the first test are left out because it’s impossible to know what that specimen’s σ_{ci} value would be.

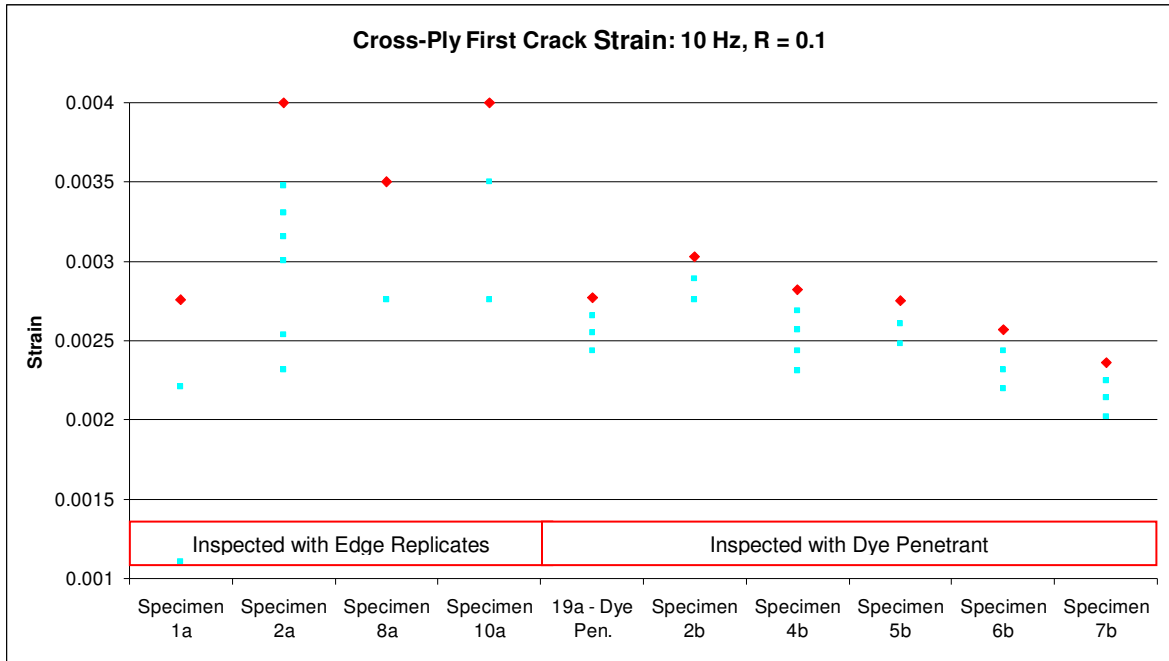


Figure 98. The same data as in Figure 97, but presented as strain data.

There was some overlap in the crack inspection techniques between the two groups. Two of the specimens from Group A were inspected in fatigue with dye penetrants, not edge replication (only one of which is shown in Figure 97 and Figure 98—Specimen 19a). The first, Specimen 18a, was used to investigate whether the dye penetrants caused earlier cracking, like edge replication had. It was shown in Figure 80 that the dye penetrant in fact did not cause earlier damage... Specimen 18a was exposed to the same peak stress level as Specimen 12a and the edge area of Specimen 12a which had *not* been exposed to acetone was inspected for crack density and compared to 18a. Crack density was actually *lower* for Specimen 18a, even though it had been exposed to dye penetrants. Specimen 19a was also tested in fatigue in the usual manner (incrementally increasing peak load at 10 Hz, R = 0.1 until cracking appeared) but used dye penetrants. Interestingly, this specimen’s σ_{ci} value also significantly exceeded any of the σ_{ci} values for the same test conditions in Batch B—again showing that Batch A generally outperformed Batch B.

4.8.2 Fatigue Testing: Rate of Crack Development

In testing Batch A, several specimens were tested at stress levels which were well above what was likely the σ_{ci} for that group. This was done to see if any meaningful relationship between peak stress and rate of crack development could be observed (at 10 Hz, $R = 0.1$). To determine “rate of crack development,” tests were periodically stopped on their way to 1M cycles, and an edge replicate was taken to determine that cycle interval’s crack density (counted using the method mentioned in the “Cross-Ply Static Tensile Testing: Crack Development” section). An example of the damage development recorded via edge replication is shown in Figure 99. The full archive of images these images, displaying crack density development are included in (APPENDIX F).

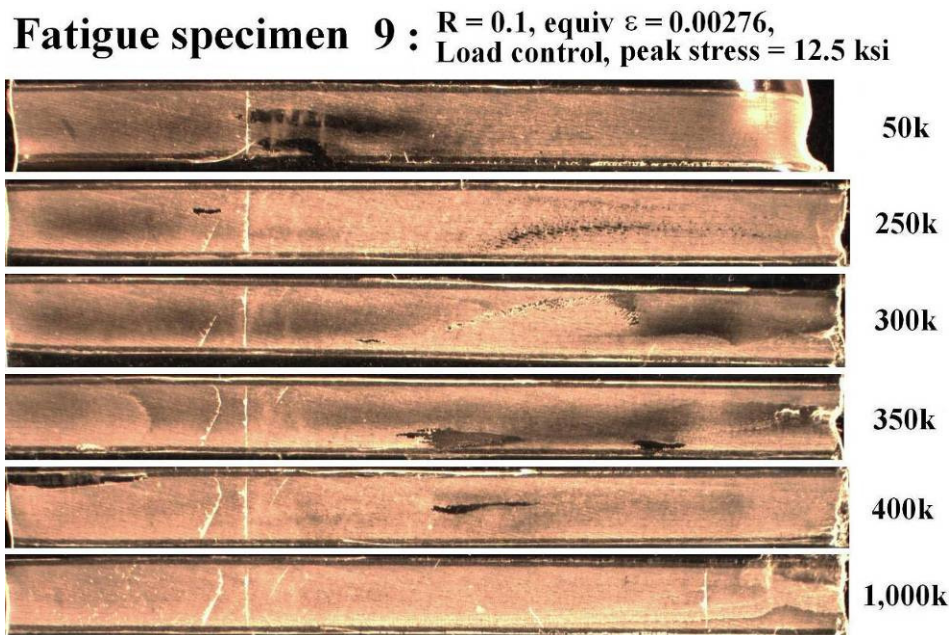


Figure 99. Edge replicates showing crack development in Specimen 9a—number of cycles at which each replicate was taken stated to the right of the replicate. Length of replicate is 1.0”.

Relevant crack development data for this investigation is shown in Figure 100.

Possibly due to the variable of acetone attack, it does not appear that there is a strong, direct

relationship between peak stress and rate of crack development. Notice that Specimen 11a was cycled at a peak stress of 17.9 ksi, but had a *lower* rate of crack development than Specimen 1a, at a peak stress of 13.4 ksi! This data does support the notion that if damage is going to appear, it will do so in the first 200k cycles. It also suggests that a characteristic damage state is achieved for a certain peak load level, and that this C.D.S. is achieved faster, for a higher peak load. Also, for the lower loading cases of 7a and 9a at 12.7 ksi and 12.5 ksi respectively, an additional crack occurred between 400k and 1M cycles; this raises the question of: “Is 1M cycles an appropriate run-out value—when is stability in damage development reached?”

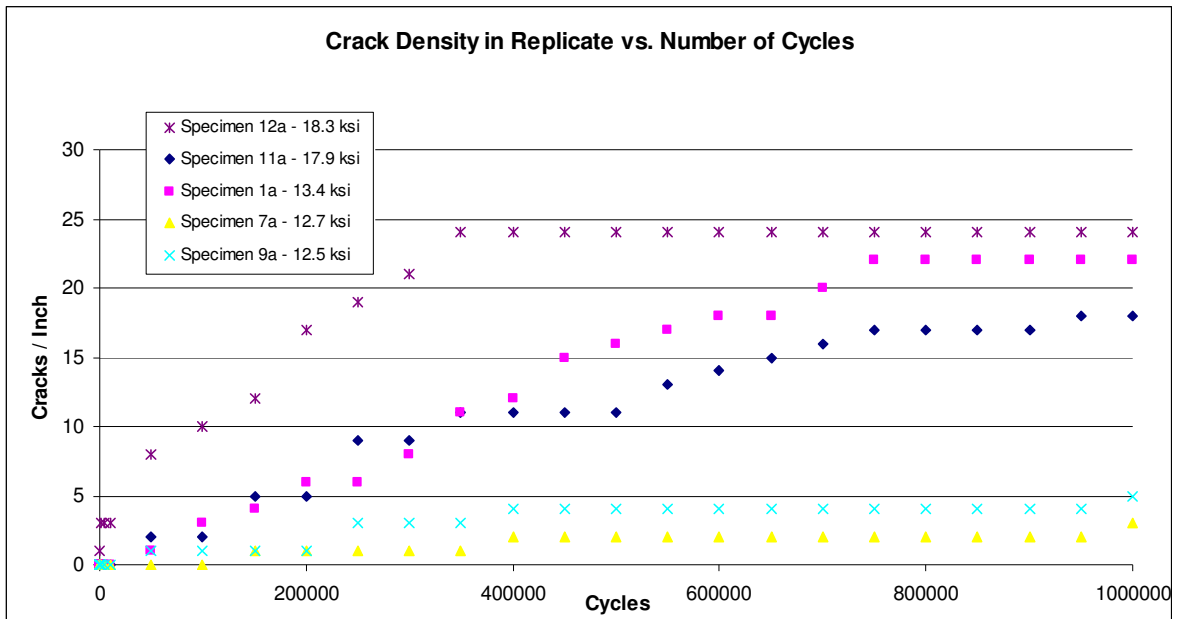


Figure 100. Crack development in several specimens from Batch A.

It’s worth noting that, even at the highest stresses at which the cross-plyies were exposed to in the tests of Figure 100, only microscopic delamination was observed. Specimen 12a, the specimen exposed to the highest peak load at 18.3 ksi only showed short

delaminations at the 0/90 interface for 10 Hz, R = 0.1 (two of which are shown in Figure 101 and Figure 102). Specimen 6a on the other hand (10 Hz, R = 0.1, 11.3 ksi peak stress), showed no delaminations (Figure 103). Thus, the threshold for delamination initiation may lie between 11.3 and 18.3 ksi. Reifsnider and Jamison [38] *did* witness large delaminations at much higher peak stresses for a similar case: laminates of $[0/90_2]_s$, at $0.70 \sigma_{Ult}$, R = 0.1, 10 Hz (this loading also resulted in laminate failure as separation into two pieces, at 10^5 cycles). Much lower peak stresses were used here—a maximum of approximately $0.25 \sigma_{Ult}$ for the most heavily loaded case of Specimen 12a.



Figure 101. One of the locations where a short delamination was observed in Specimen 12a—the specimen tested with the highest peak stresses performed in this study: 18.3 ksi, 10 Hz, R = 0.1. Taken at 1000x magnification and the scale at the base of the image is 50 μm .



Figure 102. Another location where delamination was observed in Specimen 12a. Taken at 1000x magnification and the scale at the base of the image is 50 μm .

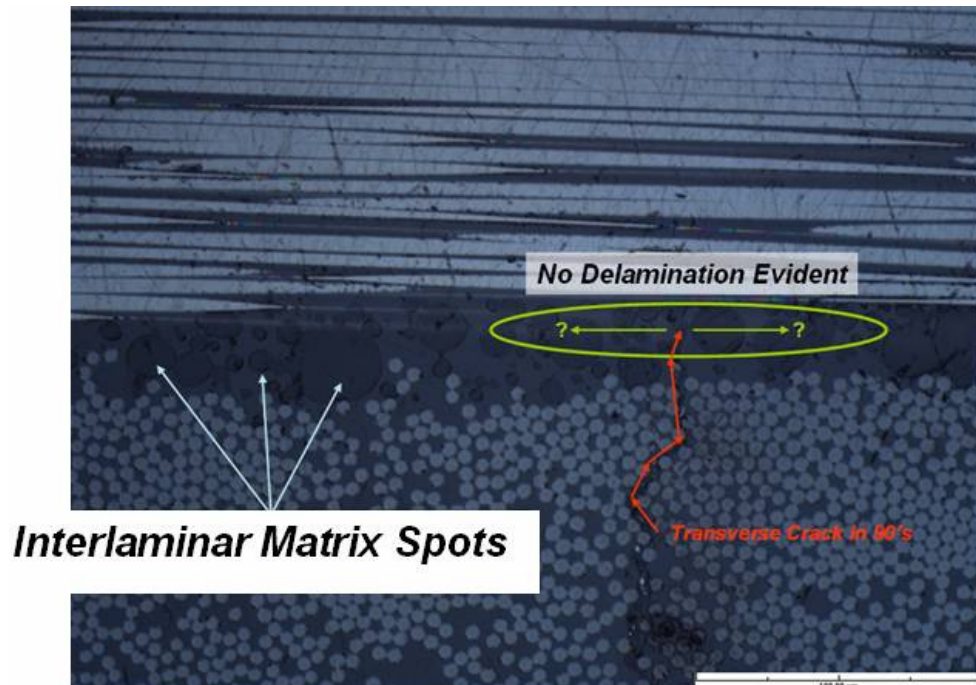


Figure 103. Specimen 6b, no delaminations were evident at the $0^\circ / 90^\circ$ interface (for 10 Hz, $R = 0.1$ with a peak stress of 11.3 ksi). The “interlaminar matrix spots” were observed in all of the interlaminar boundaries of the polished specimens; it is unknown what causes these circles in the resin, but they were witnessed in both Batch A and Batch B. Image taken at 1000x, scale at image base is 50 μm .

4.8.3 Fatigue Testing: Effect of Loading Frequency & R-ratio

An investigation was performed to determine the effect of R-ratio and loading frequency on σ_{ci} for fatigue. All of these tests were performed on specimens from Batch B (Table 8) and for these tests a run-out value of 200k cycles was selected—it was observed that cracking, if it will appear, almost always appears in the first 200k cycles. APPENDIX E contains short descriptions of the tests performed on each of the specimens in this study. Examples of the dye penetrant “before crack” and “after crack” investigation are shown in Figure 104a & Figure 104b. Since stress levels were not well above the σ_{ci} level, damage progression images were not created for these tests since they would not illustrate anything useful—the author was just searching for the first crack, as shown in Figure 104b.

Table 8. Table describing which specimens from Group B were used for which of the R-ratio and test frequency investigations. (10 Hz, R = 0.1) was an average of the five specimens listed. Test result for “polished” specimens discussed in the following section.

R-ratio	Polished (Y/N)	Loading Frequency (Hz)		
		3.0	10.0	30.0
R = 0.1	Y		9b	
	N	11b	2b, 4b-7b	17b
R = 0.5	Y	10b		15b
	N	12b	13b	16b

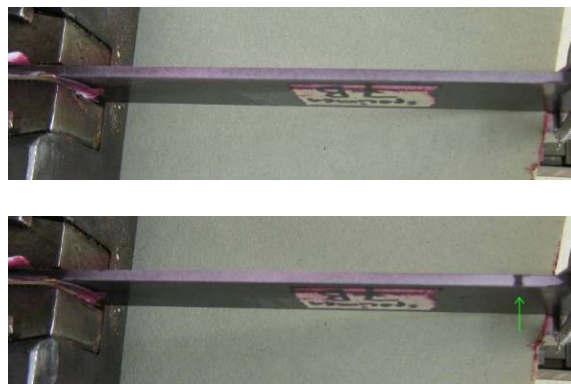


Figure 104 a & b. Top shows the undamaged laminate of Specimen 7b, where no transverse cracks are evident in the white developer. Bottom: “first crack”—the dye from a transverse crack has stained the developer purple, marked with a small green arrow.

Due to the constraints of time and a limited number of specimens, only one specimen could be tested for each of the cases formed by a test matrix of $R = 0.1$ and 0.5 , and frequencies of 3, 10, and 30 Hz (test results shown in Table 9). Plotting the results of Table 9 in Figure 105, several interesting points are observed:

1. 10 Hz appears to be the “most damaging” in terms of lowering σ_{ci} . This could relate to a point mentioned in the background—perhaps the “jump frequency” of this epoxy is near 10 Hz (refer to figure Figure 20, page 30. i.e., the frequency at which this polymer structure is optimally excited for fracture is near 10 Hz).
2. Of the frequencies tested, 30 Hz—the highest frequency tested—was the *least* damaging, i.e. it had the highest σ_{ci} values. This is an interesting observation, considering that polymers are generally thought to behave in a more brittle manner as strain-rate is increased. This may tie back in with the point made in (1): that it is actually the jump frequency which governs fracture of polymers across a spectrum of loading frequencies, not the general rule of “increasing strain rate = increased likelihood of fracture.” This also suggests that it is matrix performance which dominates crack behavior—this is reinforced by Figure 106 which illustrates that the crack path is following the fiber/matrix boundary in splitting through the epoxy.
3. Also apparent—though only based on the evidence of two data points—is that crack initiation behavior at high frequencies could be more uniformly dependant on the peak stress, as opposed to the stress amplitude. The σ_{ci} value was the same for $R = 0.1$ and $R = 0.5$ at 30 Hz. Since only two R-ratios were able to be tested here, it is acknowledged that it is riskier to extrapolate conclusions about relationships between fatigue and stress peak, mean, and amplitude.
4. As a follow-on to point (1) and (3), the data also might suggest that, the farther the loading frequency is from the “jump frequency,” crack initiation behavior depends less on stress amplitude, and more on the test’s peak load value.

Table 9. Table of crack initiation stress values for various test conditions. The value for the test condition of (10 Hz, R=0.1) is based on an average of five tests performed at those test conditions, all others based on single test performed for that condition. “Polished” specimens will be discussed in the following section.

		Loading Frequency (Hz)		
		3.0	10.0	30.0
R-ratio	Polished (Y/N)	Crack Initiation Stress (ksi)		
R = 0.1	Y		12.9	
	N	15.1	11.4	18.3
R = 0.5	Y	18.5		26.1
	N	16.1	14.0	18.3

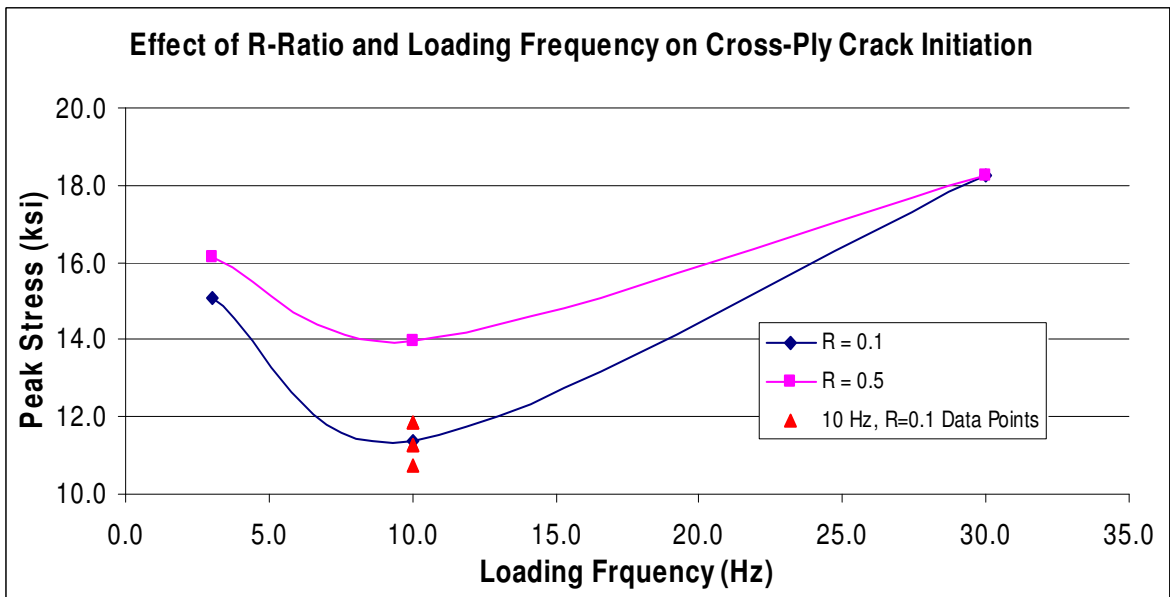


Figure 105. The effect of R-ratio and loading frequency on the appearance of “first crack.” Note that all of these data points—with the exception of 10 Hz, R = 0.1—are based on a single test performed at that specific test condition. In the case of (10 Hz, R = 0.1), the value is based on an average of five tests. Those five tests are shown here as red triangles, with the fitted curve for R = 0.1 intersecting the average value for these points.

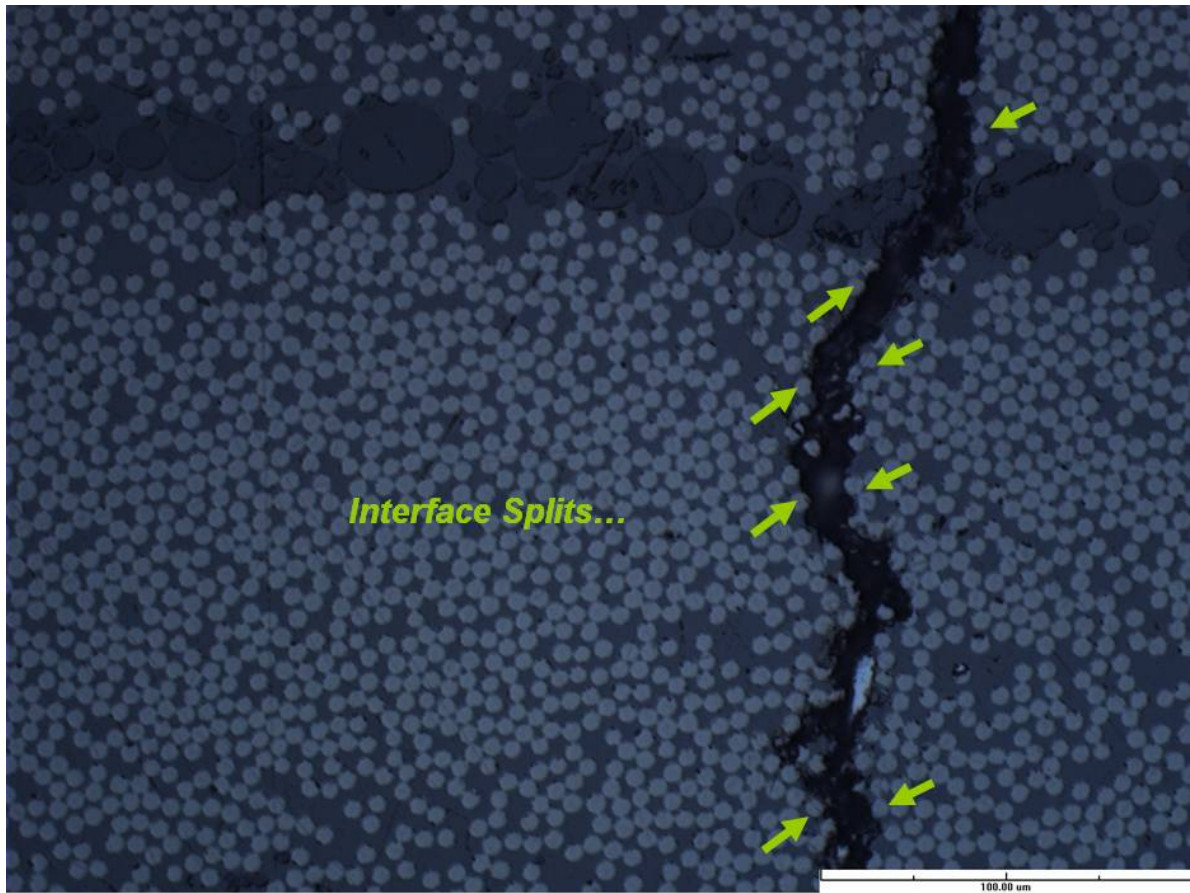


Figure 106. A 500x image of the transverse crack in Specimen 6b shows many locations where the crack path preferentially splits along the fiber-matrix interface—i.e., where the stress is highest in the matrix. This, along with the data in Figure 105—which is suggestive of a “jump frequency”—show that the matrix material dominates fatigue cracking behavior in these plies. Therefore, fatigue behavior of the matrix material must be thoroughly understood if laminates built with them are to be understood.

4.8.4 Fatigue Testing: Effect of Specimen Edge Roughness

An investigation of the effect of edge roughness on crack initiation was also performed. The edges of Specimens 9b, 10b, and 15b (as shown in Table 8) were hand-sanded with progressively finer wet sanding papers with the procedure described in the “Testing Plan” section and Figure 48 and Figure 49 (page 75). The σ_{ci} values for these polished specimens are included in Table 9 and are plotted in Figure 107. Conclusions which can be made include:

1. Without exception, the σ_{ci} value increased over the tests of the as-received specimens. In addition to Poisson mismatch tensile effects at laminate edges, these results are another strong argument for the idea that fatigue crack analysis and prediction should focus on analysis of the edge. Flaws in the bulk of the laminate are far less relevant to fatigue cracking than edge quality and stress-field behavior at that location.
2. There were moderate improvements in σ_{ci} values at 3 Hz, R = 0.5 and at 10 Hz, R = 0.1 (15% and 13% over the baseline, respectively) but there was an outstanding increase in the R = 0.5, 30 Hz test—an increase of 43% over the baseline! This is even more remarkable because this crack initiation stress—in *fatigue*—was above even the *static* value for crack initiation of this batch—23.7 ksi for the static test and 26.1 ksi for this fatigue test!
3. Since a relatively crude hand-polishing technique was used for this study, it may be worth investigating edge finish quality in future work. A more consistent polishing technique and testing several specimens for measurement of scatter would provide valuable insight... It's possible that the 30 Hz specimen received a better polishing in this study, and that similar improvements could be seen at 3 and 10 Hz.
4. There were moderate improvements for σ_{ci} at 3 and 10 Hz, and a large improvement at 30 Hz. With respect to design, a cost-benefit analysis would have to be performed by manufacturers to determine if the gain in preventing crack development for their application would be worth the costs associated with polishing and maintaining laminate edge surface quality.

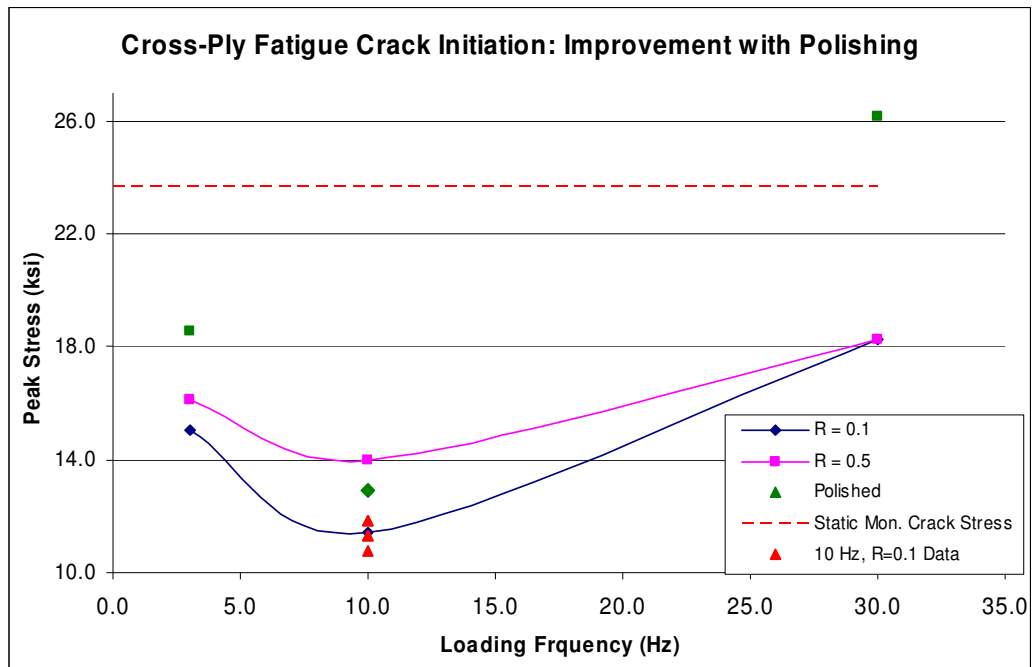


Figure 107. The increase in the σ_{ci} value for the “polished” specimens. The polished data is plotted as green points; the icon shape mimics the R-ratio which the specimen was tested at—a green square for R = 0.5, and a green diamond for R = 0.1. The σ_{ci} value increased above the baseline in each of the three cases. The red dashed line is the crack initiation stress for unpolished static monotonic loading.

4.8.5 Fatigue Testing: Effect of Loading History

A key assumption in fatigue testing was that specimens could be “reused” after cycling to the run-out value for a certain load level if it exhibited no cracking. In other words, no damage had developed during that test, and no material changes occurred in the test which would affect its performance in a new test, at a higher load level. The 90° plies are essentially regarded as brittle in behavior. Several pairs of tests from Batch B specimens helped to confirm that this assumption is reasonable.

First: the example consisting of Specimens 14b and 16b. Specimen 14b was being cycled at 30 Hz, R = 0.5, trying to determine the σ_{ci} value for this set of test conditions. At one point during the testing of this specimen, while starting up a test, an instance of “operator error” occurred on the part of the author—the specimen was compressed, buckled, and crushed in the grips. This was after this specimen had been tested to 200k cycles at 14 different increments between 5.4 ksi and 17.2 ksi. Making the assumption of “no prior damage,” a new specimen (16b) was then cycled at at 17.2 ksi—and again, no cracks appeared. However, in the very next test—at 18.3 ksi peak stress—a crack appeared. Now, if Specimen 14b was exposed to *fourteen* tests and no cracks were evident, but another specimen fractured at a stress just above the maximum stress of those fourteen tests, after only *two* tests to 200k cycles, it would appear that cracking damage is developed at the peak load level and little, if any, prior to that.

Another set of tests also suggest that the “no damage in previous tests” hypothesis is reasonable. Before realizing that the test matrix had to be scaled back from one which was

too ambitious given the time available (which would have also included $R = 0.7$ and a frequency of 7 Hz), one specimen—Specimen 8b—had been cycled at 7 Hz a number of times to 200k cycles (six test increments between 9.7 and 12.4 ksi). Due to time limitations, the test frequency of 7 Hz was abandoned, and this specimen was dropped down to 3 Hz, $R = 0.1$ at 9.7 ksi—at which point it immediately cracked! This was unexpected, as it was thought that a much higher σ_{ci} value might be observed for 3 Hz, $R = 0.1$. Subsequently a test (Specimen 11b) was run at *only* 3.0 Hz, $R = 0.1$ (with no cycling at 7 Hz) and a σ_{ci} of 15.1 ksi was achieved. This was unnerving—was it possible that testing at 7 Hz had induced some kind of damage or material change in Specimen 8b—which then caused it to fracture at a much lower stress when tested at 3 Hz? If so, then the assumption of “no damage from previous tests” would be rendered suspect!

To duplicate the case of Specimen 8b, another specimen (18b) was run through the same battery of cycling at 7 Hz which 8b had been exposed to, and then cycled at 3 Hz. Specimen 18b reached a peak σ_{ci} of 16.1 ksi. In addition to the σ_{ci} value of 15.1 ksi for Specimen 11b (which had been exposed *only* to 3 Hz loading), it's suspected that Specimen 8b may have just had some kind of significant defect which significantly depreciated its σ_{ci} value from the “typical performance”—typical performance being that observed in 11b and 18b—somewhere between 15.1 and 16.1 ksi for σ_{ci} .

An interesting point to note about the 7 Hz tests performed on Specimens 8b and 18b: they both survived through 12.4 ksi at 7 Hz, $R = 0.1$. Since the σ_{ci} value for 10 Hz, $R = 0.1$ was 11.4 ksi, this suggests that the “jump frequency” is either close to or somewhere between 10 and 30 Hz.

CHAPTER V. CONCLUSIONS

This chapter will summarize the major facts and lessons learned in this study. The major points learned will be divided up between several major subheadings: Unidirectional Specimens, Cross-Ply Specimens, and the Future Work which this investigation suggests would be worth studying farther.

5.1 Unidirectional Specimens

5.1.1 Unidirectional Test Results

Cross-ply laminate testing was preceded by the testing of unidirectional 90° and 10° specimens. In testing these specimens, it quickly became evident that unidirectional specimens are extremely sensitive to flaws and test-setup variation in general. Regarding static ultimate tests of the unidirectional specimens:

- In static testing of a *single* unidirectional 90° specimen, the peak strain and load were 0.0076 and 8.4 ksi, respectively (the best strain observed in a *multi*-specimen study by the sponsors was 0.0104—suggesting wide scatter in static test results too).
- Test setup issues prevented an ultimate strength test of the 10° specimens, but the best strain for these specimens found previously by the sponsors was 0.0111.

The unidirectional fatigue test results could be summarized as:

- High amount of scatter in the ϵ -N data for the 90° specimens (Figure 69, page 93).
- The 10° specimens ϵ -N results are more suggestive of typical σ -N curve behavior. However, this is based on a small number of data points (Figure 70—page 94)
- Conclusive curves regarding ϵ -N behavior could not be obtained for the 10° and 90° unidirectional specimens.
- The wide variability observed in these specimens with unidirectional off-axis fibers (which cannot bear load from one grip to the other) and by other authors renders this type of testing questionably useful. It is the author's conclusion that experimental

fatigue testing of off-axis unidirectional specimens is not useful, besides for identifying that composite material variability leads to wide scatter for this material.

- Crack progression or crack density studies involving unidirectional off-axis specimens are prevented by the nature of these laminates. Cracks in this material are thought to have very short growth lengths before rupture.

5.1.2 Unidirectional Test Setup Conclusions

The majority of the unidirectional specimens received from Boeing were used in trying to find a test setup which would not cause erroneous setup failures for these extremely sensitive specimens. Many different forms of gripping and specimen tabbing had to be tried before a setup was found which would not result in grip failures of the unidirectional specimens. For posterity—who may wish to save themselves a drawn-out process of test setup experimentation before experimentation proper can begin—some of the setups which were tried but found not to work were:

- Minimizing stress concentrations from grip faces—especially if they are “toothed” grips—is imperative. Tabs must be used, even with surfalloy grips.
- Bonding brass tabs to the specimen with 3M Super 77 adhesive did not work. This spray adhesive is not strong enough to bear large loads in shear.
- Placing emory cloth between the grip face and the specimen seemed to cause failure; it seemed to abrade the surface which induced grip failure.
- Specimen flatness is critical for unidirectional specimens; uneven loads due to non-parallel surfaces give false data and early failures.
- Perfect alignment of the grips is necessary; any amount of bending will cause earlier failure—particularly in 90° unidirectional testing.
- Lateral pressure at the extensometer knife edges must be mitigated to prevent failure in these locations.

The final experimental setup which mitigated issues stemming from specimen sensitivity was the following (also shown in Figure 45, Figure 46, and Figure 47):

- Brass tabs epoxied to the specimen with JB-Kwik two-party epoxy. For the cross-ply specimens, it was found that grit cloth, placed between the specimen and the grips, can work well in place of brass tabs (not affected by it, as the unidirectional

specimens had been). This saved time since the JB-Kwik would occasionally peel off of the specimen.

- Extensometer held to specimen edge with springs.
- Extensometer knife edges held in place on specimen edge—and prevented from cutting into the specimen—by silicone caulk. This provides a tacky surface for the knife edges to “bite into,” but which also is resilient enough to the knife edge pressure to prevent the knife edges from harming the specimen edge surface.

5.2 Cross-Ply Specimens

5.2.1 Cross-Ply Crack Inspection Method

The first lesson learned in cross-ply experimentation was that the crack detection technique must be matched with the material being tested, in order to prevent spurious “environmental effects” from affecting test results:

- Acetate film edge replication should not be used on epoxy-matrix composites unless testing has shown that the epoxy is resistant to degradation by acetone. Figure 79 (page 101) demonstrated conclusively that cracking initiates earlier when this technique is used.
- Dye penetrants were shown to not chemically attack the composite in Figure 80 (page 102), and this technique was used in subsequent tests.
- Techniques which work for metal experimentation may not necessarily be applied directly to composites.

5.2.2 Cross-Ply Batch Variability

Variability between the two batches of specimens was observed for several different factors in testing. Batch A, even though it was exposed to acetone, generally demonstrated superior performance in both static and fatigue tests, in the following criteria:

- Batch A demonstrated a higher average modulus: 4.5 Msi for batch A, 4.23 Msi for batch B (Figure 81, page 105).
- Higher ultimate strength: 74 ksi average for batch A, 67.7 ksi for batch B (Table 7, page 117).
 - However both batches shared a common ϵ_{ULT} of 0.018.

- Also, even with the variability in moduli, the first crack in static tensile testing typically appeared at the common stress value of ~23.7 ksi.
- For fatigue testing at 10 Hz, R = 0.1, Batch A demonstrated a higher average stress value at which cracks initiated (Figure 97, page 122). For example, Specimen 19a $\sigma_{ci} = 13.4$ ksi, while the average of the specimens from Batch A was $\sigma_{ci} = 11.4$ ksi.
 - Note that these σ_{ci} values in fatigue are ~50% of the σ_{ci} value in static loading, and are ~16% of the σ_{ULT} .

The origin of the variability between the batches is unknown—perhaps Batch B was prepared improperly or made of different constituent materials. The specimens were prepared by the sponsors and sent to the author for testing. To their knowledge, their lab technicians used the same materials and a carefully specified preparation procedure for both batches. This situation illustrates how critical process control is in characterizing and working with composites.

5.2.3 Cross-Ply Modeling

Various theories were used to predict the behavior and stress-state of the cross-ply specimens:

- Prediction of modulus with the rule-of-mixtures overestimated the net laminate modulus by a little over 10%—it predicted 5.08 Msi where the average modulus was 4.5 Msi for Batch A and 4.23 Msi for Batch B.
- Crack onset in static loading for the 90° laminas in the cross-ply was below the manufacturer’s claimed $\epsilon_{ULT,22}$ (0.0077).
 - In an experiment with a *unidirectional* 90° specimen, ϵ_{ULT} was in good agreement with the manufacturer’s claim at 0.0076 (at 8.36 ksi or 58 MPa).
 - However both Batch A and B, in static testing, initially cracked at a common average laminate stress of 23.7 ksi (163 MPa). This was a ϵ of 0.0052 for Specimen 17a (Figure 82), and a ϵ of 0.0061 for Specimen 20b.
 - The reduction in $\epsilon_{ULT,22}$ between these cases is likely explained by the edge effects which are present in the cross-ply, but which are not present in unidirectional specimens.
- Description of the 90° lamina stress-state for a certain crack-density and load was facilitated by the analytical shear-lag model of Lee and Daniel [44] and Berthelot et. al. [5] (Eq. 30).

- Cytec’s claimed 0° interlaminar shear strength is 18.5 ksi (APPENDIX B). This model’s predicted interlaminar shear was well below this, and bolstered the idea that, in ultimate tensile strength testing, delamination is not critical or even present to affect performance.
- The σ_{xx}^{90} stress-field predicted by this model suggests why the chevron cracks grow, but stop before reaching the transverse crack—the driving force for this crack, partly a function of σ_{xx}^{90} , tapers off towards the centerline.
- The model, above approximately 66% of the average laminate σ_{ult} value, displays σ values along the $0^\circ / 90^\circ$ boundary which are unfeasibly high (beyond the experimentally measured σ_{22ULT} value of 8.36 ksi). Plasticity in the resin rich interlaminar boundary may be occurring, which prevents delamination from occurring. Small delaminations were observed in fatigue however, for a test at 10 Hz, $R = 0.1$, with a peak stress of $\sim 0.25\sigma_{ULT}$.
- As the number of 90° plies in the model is decreased, both the maximum values of σ_{xx}^{90} and interlaminar shear *decrease*. The laminates in this study, with ten adjacent 90° plies, will provide *conservative* predictions of behavior in cross-ply with fewer adjacent 90° plies.
- Ultimate failure occurred at the ϵ_{ULT} of the fibers-0.018 according to the manufacturer’s specifications.
 - Only the 0° plies are bearing load at this point. Calculation of the ultimate load can be performed with the ϵ_{ULT} value, based on the cross-sectional area of the 0° plies—ultimate load is predicted as 6500 lbs, where Specimen 20b failed at 6300 lbs.

As the number of 90° plies in the model is decreased, both the maximum values of σ_{xx}^{90} and interlaminar shear *decrease*. The laminates in this study, with ten adjacent 90° plies, will provide *conservative* predictions of behavior in cross-ply with fewer adjacent 90° plies.

5.2.4 Cross-Ply Fatigue Tests

The main result of the fatigue tests from Batch A, in fatigue testing at $R = 0.1$, 10 Hz, was an exploration of the rate of crack development as a function of peak stress:

- A generally direct relationship between peak stress and rate of crack development was observed (Figure 100, page 125).
- However, this data was not entirely consistent: some tests with lower peak stresses developed cracks at a faster rate than tests with higher peak stresses.

- The variability in this data may be explained by the fact that this data was collected with the edge replication technique—which subjects this data to the variable of chemical attack.
- Specimen 12a, exposed to the highest peak stress (18.3 ksi at 10 Hz, R = 0.1) had small delaminations at the 0/90 interface (in an area *not* exposed to acetone). However, at a stress of 11.3 ksi (the typical crack initiation stress for 10 Hz, R = 0.1 for Batch B) Specimen 6b did *not* exhibit delaminations. Thus, the stress at which delamination initiates probably lies somewhere within this stress range, and transverse cracking is the initiation point for the development of delaminations.

The results of Batch B provided more useful conclusions. A group of five specimens from Batch B (2b and 4b-7b) were tested at 10 Hz, R = 0.1, to get an idea of the scatter present in fatigue crack initiation.

- Average laminate stress at crack initiation, σ_{ci} , for this group was 11.4 ksi.
- The average ϵ_{ci} value for this group was 0.00271.
 - *This directly relates to the dilatational critical fatigue strain invariant which our sponsors were seeking* (acknowledging the possibility that the stress-state is altered from pure tension at the edge, due to edge effects).
 - This strain value translates to a stress of 2.98 ksi in the 90° plies for the experimentally measured E_{22} of 1.10 Msi.
- Crack initiation values clustered more closely about the average σ_{ci} , not average ϵ_{ci} .
 - The σ_{ci} and ϵ_{ci} values for the 90° plies in these cross-ply laminates is much lower than that observed in the static test of a unidirectional 90° specimen (where peak strain and load was 0.0076 and 8.4 ksi).
 - Discrepancies are likely attributable to the increased strain rate in fatigue (10 Hz was shown to be “the most damaging” frequency” for these specimens) and the presence of Poisson mismatch edge effects.

Other specimens in Batch B were devoted to exploring the effects of R-ratio and loading frequency (Figure 105, page 130), and specimen edge roughness (Figure 107, page 132). Only one specimen was able to be tested for each of the cases in the test matrix formed by these variables, but fairly consistent and interesting results were obtained.

- A 10 Hz loading frequency was found to lower the σ_{ci} value the most, with 3 Hz being the next most damaging. Interestingly, the 30 Hz case was least damaging.
 - It’s hypothesized that the “jump frequency” of this epoxy is near 10 Hz, causing a lower σ_{ci} near this loading frequency.

- $R = 0.1$ has a higher stress range and was found to be more damaging than $R = 0.5$, in terms of the peak stress at crack initiation. The exception to this was at 30 Hz where equal σ_{ci} values were found for both R-ratios.
- In all three of the cases where a specimen's edge was polished with sandpaper up to 1500 grit, the σ_{ci} value increased—polishing improves specimen survival!
- Where static ultimate strength tests were performed, edges were not polished. However, in the case of the 30 Hz polished specimen, the σ_{ci} value in *fatigue* was actually *above* the stress level at which the first crack appeared in the static tests. This may suggest a “leveling off” of crack initiation at higher cyclic frequencies, where peak load might govern crack initiation less than mean stress.

5.3 Recommended Future Work

5.3.1 Future Work: Experimentation

There are several interesting jump-off points for experimental research which could build directly on the work done here:

- Easiest, and possibly most interesting: expand the number of R-ratios and testing frequencies which the cross-ply laminates are exposed to. This would “fill out” the fitted lines in Figure 105 (page 130).
 - There could be a lower minima for σ_{ci} , between 10 and 30 Hz, than that observed here, at 10 Hz. The suspected “jump frequency” for this epoxy could actually lie somewhere in this untested range of frequencies.
- A more consistent polishing method could be used to discover what benefits exist in quantified and carefully controlled levels of surface roughness.
- Longitudinal and transverse strain gage measurements, to verify the accuracy of application of CLT, could be included in future experimentation.
- Future work might include searching for a chemical analysis which would be able to detect constituent material differences between the two batches.
 - Currently, it is unknown if there is a test capable of measuring the chemical differences between different fiber and epoxy manufacturers, or improper preparation procedures.

5.3.2 Future Work: Modeling

Composites are decidedly *structures*, not materials. It is the author’s opinion that the field of composite laminate research currently seems to focus mostly on the study of net laminate behavior, as opposed to the characterization of the three main constituent regions *within* the composite structure:

- Matrix
- Fiber
- Interface.

Current testing mostly follows the path of: “test numerous specimens of a *layup* which might offer benefits, relative to the layups which have already been thoroughly studied.”

- This approach studies the behavior of *structures*—not the constituents which comprise that structure (fiber, matrix, interface).
 - A notable exception is the SIFT model, which employs constituent-level amplification factors derived from micromechanical models containing discrete boundaries for fiber and matrix.
- Experimentally investigating and understanding the micromechanical behavior of the fiber, matrix, and interface *separately*—as the ‘materials’ which comprise the composite *structure*—could go a long way in being able to predict the onset of damage in the structure.
- Understanding properties such as K_{IC} , strain energy release rate, and strain-rate hardening (or softening) as a function of loading frequency, for *each of these material regimes* and combined with micromechanical models, could yield a model with a strong ability to predict damage development—for any layup structure!
- Work done here suggests that an accurate model to predict fatigue crack initiation behavior requires a thorough understanding of the state of the *edge* of the composite:
 - Surface roughness (which could provide information for fracture mechanics; stress concentration factors based on surface roughness measurement).
 - Environmental effects; will the environment degrade the material?
 - Effect of strain-rate on the matrix (knowledge of its jump frequency?).
 - Theoretical layup-dependant stress-state at the specimen *edge*. This includes Poisson effects and residual thermal stresses.
- Where global loading is known, CLT can predict laminate strains, but these other factors must be accounted for since they serve to “knockdown” the σ_{ci} value from the static case at the specimen edge.
- An accurate analytical prediction of crack initiation in the 90° plies, though not achieved here, could potentially be performed through a combination of several theories.
 - First, the transformed reduced stiffness values can be used to calculate the force-strain-curvature and moment-strain-curvature equations of CLT, (Eq. 40) and (Eq. 41).
 - The output of these relationships (achieved with a strain gage measurement of ϵ_x and ϵ_y) could be used in the application of the theory of “Poisson mismatch stresses” by Pagano and Pipes [54] at the edge.
 - The CLT stresses, with the Poisson mismatch stresses, and knowledge of thermal residual stresses could yield a decent approximation of the stress-state at the laminate edge.
 - Then, an appropriate failure theory could be applied for each of the constituents, such as the maximum distortion energy criteria (Eq. 36) combined with the σ_{ULT22} equation (Eq. 18) of Greszczuk [40].

As an example application for this more in-depth, constituent analysis: the assumption of an *effectively* immediate crack propagation in this study may have been sufficient for the macromechanical investigation performed here. But the true behavior at the constituent level is much more likely to be: an extremely short stable crack growth period through the matrix or the interface (stemming from an edge roughness stress concentration), leading up to a very low K_{IC} value causing rupture. Knowledge of the failure properties of the fiber, matrix, and interface—coupled with a measurement of edge roughness—could go a long way in describing this short crack-growth behavior, as well as serving to suggest crack mitigation tactics. The author suspects that resistance to the approach of “full characterization of constituent materials” is most likely due to its perceived cost: fully characterizing three materials may cost more in the short-run, when compared to just testing the current laminate of interest. However, with the potential ability to predict the behavior of any layup once its constituents are fully understood, the long-term benefits are attractive.

APPENDIX A: HEXCEL IM-7 CARBON FIBER PROPERTIES

Hexcel's technical data sheet for the carbon fiber used in this study (56):



HexTow™ IM7 (HS-CP-5000) carbon fiber is a continuous, high performance, intermediate modulus, PAN based fiber available in 6,000 (6K) and 12,000 (12K) filament count tows. The fiber has been surface treated and can be sized to improve its interlaminar shear properties, handling characteristics, and structural properties. HexTow™ IM7 (HS-CP-5000) fiber has shear properties equivalent to those of standard AS type fibers. It is suggested for use in prepregging and filament winding.

The unique properties of HexTow™ IM7 (HS-CP-5000) fiber, such as higher tensile strength and modulus, as well as good shear strength, allow structural designers to achieve both higher safety margins for both stiffness and strength critical applications.

Typical Fiber Properties	U.S. Units	SI Units
Tensile strength 6K	795,000 psi	5,480 MPa
12K	808,000 psi	5,570 MPa
Tensile modulus Chord 6000-1000	40.0 x 10 ⁶ psi	276 GPa
Ultimate elongation ^(a) 6K	1.8%	1.8%
12K	1.9%	1.9%
Carbon content	94.0%	94.0%
Density	0.0643 lb/in ³	1.78 g/cm ³

(a) Calculated from tow test data.

Typical Epoxy Composite Properties* (at Room Temperature)	U.S. Units	SI Units
Tensile strength	400,000 psi	2,760 MPa
Tensile modulus	24.5 x 10 ⁶ psi	168 GPa
Flexural strength	240,000 psi	1,655 MPa
Flexural modulus	21.5 x 10 ⁶ psi	148 GPa
Short-beam shear strength	18,500 psi	128 MPa
Fiber volume	62%	62%

* 12K

Yarn/Tow Characteristics	U.S. Units	SI Units
Filament diameter	0.203 mil	5.2 microns
Filament shape	Round	Round
Twist	None	None
Tow cross-sectional area 6K	1.94 x 10 ⁴ in ²	0.13 mm ²
12K	3.89 x 10 ⁴ in ²	0.25 mm ²
Approximate yield 6K	6,674 ft/lb	4.48 m/g
12K	3,337 ft/lb	2.24 m/g
Weight/Length 6K	12.5 x 10 ⁻⁶ b/in	0.223 g/m
12K	25.0 x 10 ⁻⁶ b/in	0.446 g/m

© Copyright Hexcel Corporation

™ HexTow bgo are registered trademarks of Hexcel Corporation, Stamford, Connecticut.

® Hexcel and the Hexcel bgo are registered trademarks of Hexcel Corporation, Stamford, Connecticut.



APPENDIX B: CYTEC 977-3 TOUGHENED EPOXY PROPERTIES

First relevant page from Cytec's technical data sheet for the epoxy used in this study (57):

CYCOM[®] 977-3 Toughened Epoxy Resin		Page 2 of 5
TECHNICAL DATASHEET		
Cured⁽¹⁾ neat resin properties		
	RT	250°F/Wet ⁽²⁾ (121°C/Wet) ⁽²⁾
Compressive Yield Strength, ksi	27.0 ± 0.3	
Compressive Yield Strength, MPa	186 ± 2.1	
Flexural Strength, ksi	21.0 ± 4.4	10.14 ± 0.4
Flexural Modulus, Msi	0.55 ± 0.01	0.354 ± 0.3
Flexural Strength, MPa	144.7 ± 30.3	69.6 ± 2.8
Flexural Modulus, GPa	3.79 ± 0.07	2.41 ± 2.1
K _{1c} ⁽⁴⁾ MPa · m ^{1/2}	0.90 ± 0.08	
G _{1c} ⁽⁴⁾ J/m ² 217 ± 24		
RDS DMA Tg, °C (tested @ 5°C/min)		
G'		178, 218
G''		189, 226
Tan Delta		190, 240


⁽¹⁾Cured at 355°F (180°C) for 6 hours.

⁽²⁾Wet = 7-day water immersion at 160°F (71°C)

⁽³⁾Flexural testing performed using a 3-point loading fixture and a 16:1 S/D ratio

⁽⁴⁾K_{1c} and G_{1c} tested using 3-point bending mode.

This information is provided for informational purposes only and without legal responsibility.
User is expected to perform adequate verification and testing to ensure that material meets required specifications.



Cytec
ENGINEERED MATERIALS
CREATING A HORIZONTAL ADVANTAGE

Second relevant page from Cytec's technical data sheet for the epoxy used in this study (57):

CYCOM® 977-3 Toughened Epoxy Resin

Page 3 of 5

Typical properties of 977-3 composite laminates

**INTERMEDIATE MODULUS (40 Msi/276 GPa CLASS)
CARBON FIBER REINFORCED UNIDIRECTIONAL TAPE**

Typical CEM Product Codes

Hy-E 1377-3T; Hy-E 5377-3A; Hy-E 1577-3E

Mechanical Properties	-75°F	RT	220°F		250°F		270°F		300°F	
			Dry	Wet	Dry	Wet	Dry	Wet	Dry	Wet
0° Tensile Properties										
Strength, ksi	353	364								
Modulus, Msi	22.9	23.5								
Strain, %	1.52	1.46								
90° Tensile Properties										
Strength, ksi		9.3								
Modulus, Msi		1.21								
Strain, %		0.77								
0° Compressive Properties										
Strength, ksi		244		221 ¹		195 ¹		180 ¹		160 ¹
Modulus, Msi		22.3	21.4	21.2 ¹	20.4	21.2 ¹	20.2	22.6 ¹	21.5	21.7 ¹
Open Hole Compression										
Strength, ksi (25/50/25 orientation)		46.7		37.0 ²		35.0 ²				
0° Interlaminar Shear Properties										
Strength, ksi		18.5	13.6	12.9 ¹	13.3	11.4 ¹	12.4	10.1 ¹	11.4	9.0 ¹
In-Plane Shear Properties (+45)										
Modulus, Msi		0.72		0.61 ²		0.58 ²		0.50 ²		0.34 ²
Weight Gain = 0.9%										
0° Flexural Properties										
Strength, ksi		256	246	173 ¹	221	162 ¹	218	140 ¹	206	125 ¹
Modulus, Msi		21.7	22.2	20.1 ¹	20.8	21.2 ¹	21.0	19.6	21.0	18.9
90° Flexural Properties										
Strength, ksi		19.0								
Modulus, Msi		1.19								
Edge Delamination Strength, ksi										
Onset		37								
Ultimate		92								
Compression After Impact, ksi (25/50/25 orientation 270 in-lb impact level)										
		28								
Interlaminar Fracture Toughness										
G _{IC} (DCB), in-lb/in		1.8								
G _{IC} (ENF), in-lb/in		3.3								

NOTES: All panels cured for 6 hours at 355°F, 85 psi
¹Wet = 1 week immersion in 160°F water
²Wet = 2 week immersion in 160°F water
³Wet = 150°F/85% RH to equilibrium (approximately 1.1% weight gain)

The data listed has been obtained from carefully controlled samples considered to be representative of the product described. Because the properties of this product can be significantly affected by the fabrication and testing techniques employed and since Cytec Engineered Materials does not control the conditions under which its products are tested and used, Cytec Engineered Materials cannot guarantee that the properties listed will be obtained with other processes and equipment.



The information is provided for informational purposes only and without legal responsibility.
 User is expected to perform adequate verification and testing to ensure that material meets required specifications.

APPENDIX C: UNIDIRECTIONAL SPECIMEN TEST RECORD

Table 10. These are the notes which were recorded for each of the unidirectional specimen tests.

Specimen	E (Msi)	E (GPa)	Control Mode	Stress Peak (psi)	ϵ peak	Cycles	Description
Prac. A	4.82	33.2	Displ.	7.23E+04	0.0182	Load to failure	Static test. Ran to failure. Detailed in "Update 2-29-08" powerpoint. This was on the screw drive machine and was intended to get ultimate load and strain values. Inaccuracy of measurements on this machine warranted another ult load/strain test later.
1a	4.93	34	Strain	5.24E+03	0.001104	50k	Fatigue test. No cracks
			Strain	1.07E+04	0.002208	50k	Fatigue test. No cracks
			Strain	1.34E+04	0.00276	1000k	Fatigue Test. Cracks at 50k, and proceeded taking edge replicates to 1,000k cycles. The replicates were shown in the "Update 3-14-08" powerpoint.
2a	4.35	30	Strain	9.66E+03	0.002318	1000k	Fatigue tests: still no cracks observed at 1375 peak load!! Relatively high peak strain/loads relative to crack onset for other specimens!
			Strain	1.07E+04	0.002539	1000k	
			Strain	1.20E+04	0.0030048	1000k	
			Strain	1.27E+04	0.003155	1000k	
			Strain	1.31E+04	0.003305	1000k	
			Strain	1.40E+04	0.003305	1000k	
			Load	1.48E+04	~0.00348	1000k	
Load	1.74E+04	~.004	1000k	Fatigue Test: crack at 50k			
3a	4.05	27.9	Displ.	N.A. See "Description"	N.A. See "Description"	1	Static test, tabs slipped at ~5000 lbs; did not get ult strain or load.
4a	4.53	31.2	Displ.	7.47E+04	N.A. See "Description"	1	Static Test. Broke, recorded ult load but strain gage voltage ranges were set improperly: did not get final strain reading.

5a	4.05	27.9	Displ.	N.A. See "Description"	N.A. See "Description"	1	Static test. Tabs slipped; epoxied tabs may have not been cured fully.
6a	4.11	28.3	Displ.	7.61E+04	0.02003	Load to failure	True ult static test values.
7a	4.64	32	Displ.	1.48E+04	0.0031	1	Static test to 3000 micro strain test for Jon to verify modulus.
			Load	1.27E+04	~0.00276	1000k	Fatigue test. First crack appeared at 150k. Second crack at 400k. Third at 1000k. Curious: continue, to find runout?
8a	4.34	29.9	Load	1.21E+04	~0.00276	1000k	Fatigue test. No cracks
				1.52E+04	~0.0035	1000k	Fatigue test. First crack noted at 150k cycles
9a	4.54	31.3	Load	1.25E+04	~0.00276	1000k	Fatigue test. Crack at 50k. Then at 250. Then at 400k. Then at 1,000k.
10a	4.05	27.9	Load	1.10E+04	~0.00276	1000k	Fatigue test. No cracks at .00276. For this and subsequent tests, employed log approach when gathering replicates for first 50k cycles (1,5,10,50,100,500,1000 ...).
				1.42E+04	~0.0035	1000k	Fatigue test. No cracks...
				1.62E+04	~0.004	503k	Fatigue test. First crack observed at 491k, around 6-25-08. This was when acetone was found to degrade composite, did not finish out to 1,000k cycles.
11a	4.3	29.6	Load	1.79E+04	~0.004	1000k	Fatigue test. First crack at 50k. Possible crack saturation at 950k. More cycling needed to validate this.
12a	4.7	32.4	Load	1.83E+04	~0.004	1000k	Fatigue test. Crack first observed at 500 cycles, crack density max reached at 400 k cycles.
13a	4.62	31.8	Load	1.60E+04	~0.0035	1000k	Fatigue test. Crack first observed at 50k cycles.

14a	4.72	32.5	Displ.	6.32E+04	0.0148	1	Static test. Put spray paint on edge and watched through microscope for cracks. Took some pictures. First crack was visible in the paint at 3,000 lbs after looking at 2,000 and 2,500 lbs. Tabs slipped at 5875 lbs.
15a	4.39	30.3	Load	1.40E+04	~0.0032	560	Fatigue test. Ran tests to see what "effective modulus" was for various loading frequencies. 1, 5, 10, and 13 Hz (140 cycles each). Stiffening appears with increasing loading rate. All these tests were R = 0.1 and 1300 lb peak, load control.
			Load	1.40E+04	~0.0032	400	Fatigue test. Ran a test to 400 cycles at 1 cycle per minute, R = 0.1 and 1300 lb peak, load control. Attempting to see strain accumulation - - was not evident.
			Load	1.86E+04	~0.0042	400	Fatigue test. 400 cycles again, this time to 1730 lb peak load. Attempting to see strain accumulation - - was not evident
			Load	1.40E+04	~0.0032	145	Fatigue test. Put a strain gage on the specimen and ran to see whether the hysteresis loops observed previously were just artifacts of extensometer dynamics. Strain gage and extensometer data tracked each other well.

16a	4.54	31.3	Displacement	3.98E+04	~0.0094	1	Static test. Attempted to better find the "first crack" value with spray painted edge. Was more successful at narrowing down the first crack appearance to a value of 2900 lbs for first visible. 2600 lbs first audible. Lock collar rings came loose at ~3700 lbs, didn't finish test to failure.
17a	4.67	32.2	Displ.	7.28E+04	0.01811	1	Static Ultimate Strength. Load peak was 6775 lbs. Did this to make sure that acetone hadn't influenced peak load value from previous tests.
18a	4.87	33.6	Load	1.83E+04	~0.00375	1000k	Fatigue test. First fatigue test which employed dye penetrant. Purpose: load peak of 1700 lbs is same as Specimen 12a--crack density of dye penetrant should be same as x-ray image of Specimen 12, if dye penetrant isn't degrading composite. Test result: crack density appears to be LESS for this specimen--> dye penetrant does not degrade composite.
19a	4.84	33.4	Load	1.18E+04	~0.00244	1000k	Fatigue test. No cracks
				1.24E+04	~0.00255	1000k	Fatigue test. No cracks
				1.29E+04	~0.00266	1000k	Fatigue test. No cracks
				1.34E+04	~0.00277	1000k	Fatigue test. Crack appeared between 150 and 200k.
				1.40E+04	~0.00288	1000k	Fatigue test. Continued cycling. No more cracks
				1.45E+04	~0.00299	1000k	Fatigue test. No new cracks
				1.51E+04	~0.00310	1000k	Fatigue test. No more cracks at 200k cycles, but cracks appeared at 1,000k.
1b	4.13	28.5	Load	1.18E+04	~0.00286	1000k	Fatigue test. Crack at 200k cycles.
2b	3.90	26.9	Load	1.08E+04	~0.00276	1000k	Fatigue test. No cracks

				1.13E+04	~0.00289	1000k	Fatigue test. No cracks
				1.18E+04	~0.00303	1000k	Fatigue test. Cracked between 200k and 1,000k cycles.
3b	4.83	33.3	Load	1.08E+04	~0.00223	1000k	Fatigue test. Cracked between 0 and 50k cycles.
4b	4.19	28.9	Load	9.68E+03	~0.00231	1000k	Fatigue test. No cracks
				1.02E+04	~0.00244	1000k	Fatigue test. No cracks
				1.08E+04	~0.00257	1000k	Fatigue test. No cracks
				1.13E+04	~0.00269	1000k	Fatigue test. No cracks
				1.18E+04	~0.00282	1000k	Fatigue test. Cracked between 200k and 1,000k
5b	3.91	27.0	Load	9.68E+03	~0.00248	1000k	Fatigue test. No cracks
				1.02E+04	~0.00261	1000k	Fatigue test. No cracks
				1.08E+04	~0.00275	1000k	Fatigue test. Crack <i>might</i> have appeared at 200k, but definitely at 300k..
6b	4.40	30.3	Load	9.68E+03	~0.00220	1000k	Fatigue test. No cracks
				1.02E+04	~0.00232	1000k	Fatigue test. No cracks
				1.08E+04	~0.00244	1000k	Fatigue test. No cracks
				1.13E+04	~0.00257	1000k	Fatigue test. Cracked between 50k and 100k cycles. Sectioned & polished for optical microscope.
7b	4.78	33.0	Load	9.68E+03	~0.00202	1000k	Fatigue test. No cracks
				1.02E+04	~0.00214	1000k	Fatigue test. No cracks
				1.08E+04	~0.00225	1000k	Fatigue test. No cracks
				1.13E+04	~0.00236	1000k	Fatigue test. Crack between 50k and 100k.
8b (7Hz, 3Hz, R=0.1)	4.00	27.6	Load	7.53E+03 , 13 Hz	~0.00188	14k	Fatigue test. No cracks
				9.68E+03 , 7 Hz	~0.00242	1000k	Fatigue test. No cracks
				1.02E+04 , 7 Hz	~0.00255	1000k	Fatigue test. No cracks
				1.08E+04 , 7 Hz	~0.00269	1000k	Fatigue test. No cracks
				1.13E+04 , 7 Hz	~0.00282	1000k	Fatigue test. No cracks
				1.18E+04 , 7 Hz	~0.00296	1000k	Fatigue test. No cracks
				1.24E+04 , 7 Hz	~0.00309	200k	Fatigue test. No cracks
				9.68E+03 , 3 Hz	~0.00229	1000k	Fatigue test. Crack between 0 and 50k.
9b	4.22	29.1	Load	9.68E+03	~0.00229	1000k	Fatigue test. No cracks

(10 Hz R=0.1) (Polished)				1.02E+04	~0.00242	1000k	Fatigue test. No cracks
				1.08E+04	~0.00255	1000k	Fatigue test. No cracks
				1.13E+04	~0.00268	1000k	Fatigue test. No cracks
				1.18E+04	~0.00280	1000k	Fatigue test. No cracks
				1.24E+04	~0.00293	1000k	Fatigue test. No cracks
				1.29E+04	~0.00306	1000k	Fatigue test. Crack between 0 and 50k
10b (3Hz, R=0.5) (Polished)	4.15	28.6	Load	1.51E+04	~0.00363	200k	Fatigue test. No cracks
				1.61E+04	~0.00389	200k	Fatigue test. No cracks
				1.72E+04	~0.00415	200k	Fatigue test. No cracks
				1.83E+04	~0.00441	200k	Fatigue test. Crack observed near the lower grip between 0 and 50k.
				1.94E+04	~0.00466	200k	Fatigue test. No new crack
				2.04E+04	~0.00492	200k	Fatigue test. No new crack
11b (3Hz, R = 0.1)	4.40	30.3	Load	7.53E+03	~0.00171	50k	Fatigue test. No cracks
				7.53E+03	~0.00171	200k	Fatigue test. No cracks
				8.60E+03	~0.00196	200k	Fatigue test. No cracks
				9.68E+03	~0.00220	200k	Fatigue test. No cracks
				1.02E+04	~0.00232	200k	Fatigue test. No cracks
				1.08E+04	~0.00244	200k	Fatigue test. No cracks
				1.13E+04	~0.00257	200k	Fatigue test. No cracks
				1.18E+04	~0.00269	200k	Fatigue test. No cracks
				1.29E+04	~0.00293	200k	Fatigue test. No cracks
				1.40E+04	~0.00318	200k	Fatigue test. No cracks
				1.51E+04	~0.00342	200k	Fatigue test. Crack between 50k and 100k.
12b (3Hz, R=0.5)	4.00	27.6	Load	6.45E+03	~0.00161	1000k	Fatigue test. No cracks
				7.53E+03	~0.00188	1000k	Fatigue test. No cracks
				8.60E+03	~0.00215	1000k	Fatigue test. No cracks
				9.68E+03	~0.00242	1000k	Fatigue test. No cracks
				1.08E+04	~0.00269	900k?	Fatigue test. No cracks...
				1.18E+04	~0.00296	1000k	Fatigue test. No cracks
				1.29E+04	~0.00323	1000k	Fatigue test. No cracks
				1.40E+04	~0.00349	1000k	Fatigue test. No cracks
				1.51E+04	~0.00376	200k	Fatigue test. No cracks
				1.61E+04	~0.00403	200k	Fatigue test. Crack between 50k and 100k
13b (10Hz, R=0.5)	4.10	28.3	Load	8.60E+03	~0.00184	1k	Tuning
				9.68E+03	~0.00236	200k	Fatigue test. No cracks
				1.02E+04	~0.00249	200k	Fatigue test. No cracks
				1.08E+04	~0.00262	200k	Fatigue test. No cracks
				1.13E+04	~0.00275	200k	Fatigue test. No cracks
				1.18E+04	~0.00288	200k	Fatigue test. No cracks
				1.29E+04	~0.00315	200k	Fatigue test. No cracks

				1.40E+04	~0.00341	200k	Fatigue test. Crack between 100 & 200k
14b (30H z, R=0. 5)	4.39	30.3	Load	5.38E+03	~0.00122	200k	Fatigue test. No cracks
				6.45E+03	~0.00147	200k	Fatigue test. No cracks
				7.53E+03	~0.00171	200k	Fatigue test. No cracks
				8.60E+03	~0.00196	200k	Fatigue test. No cracks
				9.68E+03	~0.00220	200k	Fatigue test. No cracks
				1.08E+04	~0.00245	200k	Fatigue test. No cracks
				1.13E+04	~0.00257	200k	Fatigue test. No cracks
				1.18E+04	~0.00269	200k	Fatigue test. No cracks
				1.24E+04	~0.00282	200k	Fatigue test. No cracks
				1.29E+04	~0.00294	200k	Fatigue test. No cracks
				1.40E+04	~0.00318	200k	Fatigue test. No cracks
				1.51E+04	~0.00343	200k	Fatigue test. No cracks
				1.61E+04	~0.00367	200k	Fatigue test. No cracks
				1.72E+04	~0.00392		Fatigue test. No cracks
				~0.00392	200k	Fatigue test. 1600 lbs performed again because I buckled the specimen in the grips (-500 lbs!). No cracks appeared for 200 k cycles @ 1600 lbs after this event. Next morning, specimen crushed due to improper control of machine.	
				1.72E+04			
15b (30H z, R=0. 5) (Poli shed)	4.24	29.2	Load	1.72E+04	~0.00406	200k	Fatigue test. No cracks
				1.83E+04	~0.00431	200k	Fatigue test. No cracks
				1.94E+04	~0.00456	200k	Fatigue test. No cracks
				2.04E+04	~0.00482	200k	Fatigue test. No cracks
				2.15E+04	~0.00507	200k	Fatigue test. No cracks
				2.26E+04	~0.00533	200k	Fatigue test. No cracks
				2.37E+04	~0.00558	200k	Fatigue test. No cracks
				2.47E+04	~0.00583	200k	Fatigue test. No cracks
2.58E+04	~0.00609	200k	Fatigue test. Crack between 0 and 200k.				
16b (30H z, R=0. 5)	4.11	28.3	Load	1.72E+04	~0.00419	200k	Fatigue test. No cracks
				1.83E+04	~0.00445	200k	Fatigue test. Crack between 100k and 200k
17b (30H z, R=0. 1)	4.20	29.0	Load	9.68E+03	~0.00230	200k	Fatigue test. No cracks
				1.08E+04	~0.00256	200k	Fatigue test. No cracks
				1.18E+04	~0.00282	200k	Fatigue test. No cracks
				1.29E+04	~0.00307	200k	Fatigue test. No cracks
				1.40E+04	~0.00333	200k	Fatigue test. No cracks
				1.51E+04	~0.00358	200k	Fatigue test. No cracks
				1.61E+04	~0.00384	200k	Fatigue test. No cracks
1.72E+04	~0.00410	200k	Fatigue test. No cracks				

				1.83E+04	~0.00435	200k	Fatigue test. Cracked in 3 spots between 0 and 200k.
18b (7Hz, 3Hz R=0. 1)	4.46	30.7	Load	9.68E+03		200k	Fatigue test. No cracks
				1.02E+04		200k	Fatigue test. No cracks
				1.08E+04		200k	Fatigue test. No cracks
				1.13E+04		200k	Fatigue test. No cracks
				1.18E+04		200k	Fatigue test. No cracks
				1.24E+04		200k	Fatigue test. No cracks
				7.53E+03		200k	Fatigue test. No cracks
				8.60E+03		200k	Fatigue test. No cracks
				9.68E+03		200k	Fatigue test. No cracks
				1.08E+04		200k	Fatigue test. No cracks
				1.18E+04		200k	Fatigue test. No cracks
				1.29E+04		200k	Fatigue test. No cracks
				1.40E+04		200k	Fatigue test. No cracks
				1.51E+04		200k	
				1.61E+04			
19b	4.21	29.0		9.68E+03		1	Static test. Got the modulus to complete modulus record for all 20 specimens in Batch B--no fatigue test performed on this specimen.
20b (Static Ult)	4.05	27.9	Displ.	6.77E+04	~0.0188		Static test. Ruptured at 6300 lbs, 0.0188 strain. First audible snap at 2200 lbs, and next observation at 2400 lbs had cracks.

APPENDIX D: COMPUTATION OF 10 DEGREE STIFFNESS MATRIX

G_{12} and ν_{12} are assumed to be “typical” of CFRP material, and assume the values attributed to the material in Jones [30]; $G_{12} = 2.6$ GPa and $\nu_{12} = 0.25$. With $E_{11} = 23.5$ Msi, and $E_{22} = 1.1$ Msi from experimentation. Then ν_{21} can be computed as:

$$\nu_{21} = \frac{E_2 \nu_{12}}{E_1} = 0.017$$

Eq. 42

Then the reduced stiffnesses are:

$$Q_{11} = \frac{E_1}{1 - \nu_{12} \nu_{21}}$$

Eq. 43

$$Q_{22} = \frac{E_2}{1 - \nu_{12} \nu_{21}}$$

Eq. 44

$$Q_{12} = \frac{\nu_{21} E_1}{1 - \nu_{12} \nu_{21}}$$

Eq. 45

$$Q_{66} = G_{12}$$

Eq. 46

Then the transformed reduced stiffnesses are:

$$\bar{Q}_{11} = Q_{11} \cos^4 \theta + 2(Q_{12} + 2Q_{66}) \sin^2 \theta \cos^2 \theta + Q_{22} \sin^4 \theta = 22.2 \text{ Msi}$$

Eq. 47

$$\bar{Q}_{12} = (Q_{11} + Q_{22} - 4Q_{66}) \sin^2 \theta \cos^2 \theta + Q_{12} (\sin^4 \theta + \cos^4 \theta) = 0.937 \text{ Msi}$$

Eq. 48

$$\bar{Q}_{22} = Q_{11} \sin^4 \theta + 2(Q_{12} + 2Q_{66}) \sin^2 \theta \cos^2 \theta + Q_{22} \cos^4 \theta = 1.12 \text{ Msi}$$

Eq. 49

$$\bar{Q}_{16} = (Q_{11} - Q_{12} - 2Q_{66}) \sin \theta \cos^3 \theta + (Q_{12} - Q_{22} + 2Q_{66}) (\sin^3 \theta + \cos \theta) = 3.67 \text{ Msi}$$

Eq. 50

$$\bar{Q}_{26} = (Q_{11} - Q_{12} - 2Q_{66})\sin^3 \theta \cos \theta + (Q_{12} - Q_{22} + 2Q_{66})(\sin \theta + \cos^3 \theta) = 0.034 \text{ Msi}$$

Eq. 51

$$\bar{Q}_{66} = (Q_{11} + Q_{22} - 2Q_{12} - 2Q_{66})\sin^2 \theta \cos^2 \theta + Q_{66}(\sin^4 \theta + \cos^4 \theta) = 1.04 \text{ Msi}$$

Eq. 52

Thus, the transformed reduced stiffness matrix (Eq. 39) is, in numerical units of Msi:

$$\begin{bmatrix} \sigma_x \\ \sigma_y \\ \tau_{xy} \end{bmatrix} = [\bar{Q}] \begin{bmatrix} \epsilon_x \\ \epsilon_y \\ \gamma_{xy} \end{bmatrix} = \begin{bmatrix} \bar{Q}_{11} & \bar{Q}_{12} & \bar{Q}_{16} \\ \bar{Q}_{12} & \bar{Q}_{22} & \bar{Q}_{26} \\ \bar{Q}_{16} & \bar{Q}_{26} & \bar{Q}_{66} \end{bmatrix} \begin{bmatrix} \epsilon_x \\ \epsilon_y \\ \gamma_{xy} \end{bmatrix} = \begin{bmatrix} 22.2 & 0.937 & 3.67 \\ 0.937 & 1.12 & 0.034 \\ 3.67 & 0.034 & 1.04 \end{bmatrix} \begin{bmatrix} \epsilon_x \\ \epsilon_y \\ \gamma_{xy} \end{bmatrix}$$

APPENDIX E: CROSS-PLY SPECIMEN TEST RECORD

Table 11. Notes recorded for each of the cross-ply specimen tests.

Specimen	E (Msi)	E (GPa)	Control Mode	Stress Peak (psi)	ϵ peak	Cycles	Description
Prac. A	4.82	33.2	Displ.	7.23E+04	0.0182	Load to failure	Static test. Ran to failure. Detailed in "Update 2-29-08" powerpoint. This was on the screw drive machine and was intended to get ultimate load and strain values. Inaccuracy of measurements on this machine warranted another ult load/strain test later.
1a	4.93	34	Strain	5.24E+03	0.001104	50k	Fatigue test. No cracks
			Strain	1.07E+04	0.002208	50k	Fatigue test. No cracks
			Strain	1.34E+04	0.00276	1000k	Fatigue Test. Cracks at 50k, and proceeded taking edge replicates to 1,000k cycles. The replicates were shown in the "Update 3-14-08" powerpoint.
2a	4.35	30	Strain	9.66E+03	0.002318	1000k	Fatigue tests: still no cracks observed at 1375 peak load!! Relatively high peak strain/loads relative to crack onset for other specimens!
			Strain	1.07E+04	0.002539	1000k	
			Strain	1.20E+04	0.0030048	1000k	
			Strain	1.27E+04	0.003155	1000k	
			Strain	1.31E+04	0.003305	1000k	
			Strain	1.40E+04	0.003305	1000k	
			Load	1.48E+04	~0.00348	1000k	
Load	1.74E+04	~.004	1000k	Fatigue Test: crack at 50k			
3a	4.05	27.9	Displ.	N.A. See "Description"	N.A. See "Description"	1	Static test, tabs slipped at ~5000 lbs; did not get ult strain or load.
4a	4.53	31.2	Displ.	7.47E+04	N.A. See "Description"	1	Static Test. Broke, recorded ult load but strain gage voltage ranges were set improperly: did not get final strain reading.
5a	4.05	27.9	Displ.	N.A. See "Description"	N.A. See "Description"	1	Static test. Tabs slipped; epoxied tabs may have not been cured fully.
6a	4.11	28.3	Displ.	7.61E+04	0.02003	Load to failure	True ult static test values.

7a	4.64	32	Displ.	1.48E+04	0.0031	1	Static test to 3000 micro strain test for Jon to verify modulus.
			Load	1.27E+04	~0.00276	1000k	Fatigue test. First crack appeared at 150k. Second crack at 400k. Third at 1000k. Curious: continue, to find runout?
8a	4.34	29.9	Load	1.21E+04	~0.00276	1000k	Fatigue test. No cracks
				1.52E+04	~0.0035	1000k	Fatigue test. First crack noted at 150k cycles
9a	4.54	31.3	Load	1.25E+04	~0.00276	1000k	Fatigue test. Crack at 50k. Then at 250. Then at 400k. Then at 1,000k.
10a	4.05	27.9	Load	1.10E+04	~0.00276	1000k	Fatigue test. No cracks at .00276. For this and subsequent tests, employed log approach when gathering replicates for first 50k cycles (1,5,10,50,100,500,1000...).
				1.42E+04	~0.0035	1000k	Fatigue test. No cracks...
				1.62E+04	~0.004	503k	Fatigue test. First crack observed at 491k, around 6-25-08. This was when acetone was found to degrade composite, did not finish out to 1,000k cycles.
11a	4.3	29.6	Load	1.79E+04	~0.004	1000k	Fatigue test. First crack at 50k. Possible crack saturation at 950k. More cycling needed to validate this.
12a	4.7	32.4	Load	1.83E+04	~0.004	1000k	Fatigue test. Crack first observed at 500 cycles, crack density max reached at 400 k cycles.
13a	4.62	31.8	Load	1.60E+04	~0.0035	1000k	Fatigue test. Crack first observed at. 50k cycles.
14a	4.72	32.5	Displ.	6.32E+04	0.0148	1	Static test. Put spray paint on edge and watched through microscope for cracks. Took some pictures. First crack was visible in the paint at 3,000 lbs after looking at 2,000 and 2,500 lbs. Tabs slipped at 5875 lbs.

15a	4.39	30.3	Load	1.40E+04	~0.0032	560	Fatigue test. Ran tests to see what "effective modulus" was for various loading frequencies. 1, 5, 10, and 13 Hz (140 cycles each). Stiffening appears with increasing loading rate. All these tests were R = 0.1 and 1300 lb peak, load control.
			Load	1.40E+04	~0.0032	400	Fatigue test. Ran a test to 400 cycles at 1 cycle per minute, R = 0.1 and 1300 lb peak, load control. Attempting to see strain accumulation -- was not evident.
			Load	1.86E+04	~0.0042	400	Fatigue test. 400 cycles again, this time to 1730 lb peak load. Attempting to see strain accumulation -- was not evident
			Load	1.40E+04	~0.0032	145	Fatigue test. Put a strain gage on the specimen and ran to see whether the hysteresis loops observed previously were just artifacts of extensometer dynamics. Strain gage and extensometer data tracked each other well.
16a	4.54	31.3	Displacement	3.98E+04	~0.0094	1	Static test. Attempted to better find the "first crack" value with spray painted edge. Was more successful at narrowing down the first crack appearance to a value of 2900 lbs for first visible. 2600 lbs first audible. Lock collar rings came loose at ~3700 lbs, didn't finish test to failure.
17a	4.67	32.2	Displ.	7.28E+04	0.01811	1	Static Ultimate Strength. Load peak was 6775 lbs. Did this to make sure that acetone hadn't influenced peak load value from previous tests.

18a	4.87	33.6	Load	1.83E+04	~0.00375	1000k	Fatigue test. First fatigue test which employed dye penetrant. Purpose: load peak of 1700 lbs is same as Specimen 12a--crack density of dye penetrant should be same as x-ray image of Specimen 12, if dye penetrant isn't degrading composite. Test result: crack density appears to be LESS for this specimen--> dye penetrant does not degrade composite.
19a	4.84	33.4	Load	1.18E+04	~0.00244	1000k	Fatigue test. No cracks
				1.24E+04	~0.00255	1000k	Fatigue test. No cracks
				1.29E+04	~0.00266	1000k	Fatigue test. No cracks
				1.34E+04	~0.00277	1000k	Fatigue test. Crack appeared between 150 and 200k.
				1.40E+04	~0.00288	1000k	Fatigue test. Continued cycling. No more cracks
				1.45E+04	~0.00299	1000k	Fatigue test. No new cracks
				1.51E+04	~0.00310	1000k	Fatigue test. No more cracks at 200k cycles, but cracks appeared at 1,000k.
1b	4.13	28.5	Load	1.18E+04	~0.00286	1000k	Fatigue test. Crack at 200k cycles.
2b	3.90	26.9	Load	1.08E+04	~0.00276	1000k	Fatigue test. No cracks
				1.13E+04	~0.00289	1000k	Fatigue test. No cracks
				1.18E+04	~0.00303	1000k	Fatigue test. Cracked between 200k and 1,000k cycles.
3b	4.83	33.3	Load	1.08E+04	~0.00223	1000k	Fatigue test. Cracked between 0 and 50k cycles.
4b	4.19	28.9	Load	9.68E+03	~0.00231	1000k	Fatigue test. No cracks
				1.02E+04	~0.00244	1000k	Fatigue test. No cracks
				1.08E+04	~0.00257	1000k	Fatigue test. No cracks
				1.13E+04	~0.00269	1000k	Fatigue test. No cracks
				1.18E+04	~0.00282	1000k	Fatigue test. Cracked between 200k and 1,000k
5b	3.91	27.0	Load	9.68E+03	~0.00248	1000k	Fatigue test. No cracks
				1.02E+04	~0.00261	1000k	Fatigue test. No cracks
				1.08E+04	~0.00275	1000k	Fatigue test. Crack <i>might</i> have appeared at 200k, but definitely at 300k..
6b	4.40	30.3	Load	9.68E+03	~0.00220	1000k	Fatigue test. No cracks

				1.02E+04	~0.00232	1000k	Fatigue test. No cracks
				1.08E+04	~0.00244	1000k	Fatigue test. No cracks
				1.13E+04	~0.00257	1000k	Fatigue test. Cracked between 50k and 100k cycles. Sectioned & polished for optical microscope.
7b	4.78	33.0	Load	9.68E+03	~0.00202	1000k	Fatigue test. No cracks
				1.02E+04	~0.00214	1000k	Fatigue test. No cracks
				1.08E+04	~0.00225	1000k	Fatigue test. No cracks
				1.13E+04	~0.00236	1000k	Fatigue test. Crack between 50k and 100k.
8b (7Hz, 3Hz, R=0.1)	4.00	27.6	Load	7.53E+03 , 13 Hz	~0.00188	14k	Fatigue test. No cracks
				9.68E+03 , 7 Hz	~0.00242	1000k	Fatigue test. No cracks
				1.02E+04 , 7 Hz	~0.00255	1000k	Fatigue test. No cracks
				1.08E+04 , 7 Hz	~0.00269	1000k	Fatigue test. No cracks
				1.13E+04 , 7 Hz	~0.00282	1000k	Fatigue test. No cracks
				1.18E+04 , 7 Hz	~0.00296	1000k	Fatigue test. No cracks
				1.24E+04 , 7 Hz	~0.00309	200k	Fatigue test. No cracks
				9.68E+03 , 3 Hz	~0.00229	1000k	Fatigue test. Crack between 0 and 50k.
9b (10 Hz R=0.1) (Polished)	4.22	29.1	Load	9.68E+03	~0.00229	1000k	Fatigue test. No cracks
				1.02E+04	~0.00242	1000k	Fatigue test. No cracks
				1.08E+04	~0.00255	1000k	Fatigue test. No cracks
				1.13E+04	~0.00268	1000k	Fatigue test. No cracks
				1.18E+04	~0.00280	1000k	Fatigue test. No cracks
				1.24E+04	~0.00293	1000k	Fatigue test. No cracks
				1.29E+04	~0.00306	1000k	Fatigue test. Crack between 0 and 50k
10b (3Hz, R=0.5) (Polished)	4.15	28.6	Load	1.51E+04	~0.00363	200k	Fatigue test. No cracks
				1.61E+04	~0.00389	200k	Fatigue test. No cracks
				1.72E+04	~0.00415	200k	Fatigue test. No cracks
				1.83E+04	~0.00441	200k	Fatigue test. Crack observed near the lower grip between 0 and 50k.
				1.94E+04	~0.00466	200k	Fatigue test. No new crack
				2.04E+04	~0.00492	200k	Fatigue test. No new crack
				2.14E+04	~0.00517	200k	Fatigue test. No new crack
11b (3Hz, R = 0.1)	4.40	30.3	Load	7.53E+03	~0.00171	50k	Fatigue test. No cracks
				7.53E+03	~0.00171	200k	Fatigue test. No cracks
				8.60E+03	~0.00196	200k	Fatigue test. No cracks
				9.68E+03	~0.00220	200k	Fatigue test. No cracks
				1.02E+04	~0.00232	200k	Fatigue test. No cracks

				1.08E+04	~0.00244	200k	Fatigue test. No cracks
				1.13E+04	~0.00257	200k	Fatigue test. No cracks
				1.18E+04	~0.00269	200k	Fatigue test. No cracks
				1.29E+04	~0.00293	200k	Fatigue test. No cracks
				1.40E+04	~0.00318	200k	Fatigue test. No cracks
				1.51E+04	~0.00342	200k	Fatigue test. Crack between 50k and 100k.
12b (3Hz, R=0.5)	4.00	27.6	Load	6.45E+03	~0.00161	1000k	Fatigue test. No cracks
				7.53E+03	~0.00188	1000k	Fatigue test. No cracks
				8.60E+03	~0.00215	1000k	Fatigue test. No cracks
				9.68E+03	~0.00242	1000k	Fatigue test. No cracks
				1.08E+04	~0.00269	900k?	Fatigue test. No cracks...
				1.18E+04	~0.00296	1000k	Fatigue test. No cracks
				1.29E+04	~0.00323	1000k	Fatigue test. No cracks
				1.40E+04	~0.00349	1000k	Fatigue test. No cracks
				1.51E+04	~0.00376	200k	Fatigue test. No cracks
				1.61E+04	~0.00403	200k	Fatigue test. Crack between 50k and 100k
13b (10Hz, z, R=0.5)	4.10	28.3	Load	8.60E+03	~0.00184	1k	Tuning
				9.68E+03	~0.00236	200k	Fatigue test. No cracks
				1.02E+04	~0.00249	200k	Fatigue test. No cracks
				1.08E+04	~0.00262	200k	Fatigue test. No cracks
				1.13E+04	~0.00275	200k	Fatigue test. No cracks
				1.18E+04	~0.00288	200k	Fatigue test. No cracks
				1.29E+04	~0.00315	200k	Fatigue test. No cracks
				1.40E+04	~0.00341	200k	Fatigue test. Crack between 100 & 200k
14b (30Hz, z, R=0.5)	4.39	30.3	Load	5.38E+03	~0.00122	200k	Fatigue test. No cracks
				6.45E+03	~0.00147	200k	Fatigue test. No cracks
				7.53E+03	~0.00171	200k	Fatigue test. No cracks
				8.60E+03	~0.00196	200k	Fatigue test. No cracks
				9.68E+03	~0.00220	200k	Fatigue test. No cracks
				1.08E+04	~0.00245	200k	Fatigue test. No cracks
				1.13E+04	~0.00257	200k	Fatigue test. No cracks
				1.18E+04	~0.00269	200k	Fatigue test. No cracks
				1.24E+04	~0.00282	200k	Fatigue test. No cracks
				1.29E+04	~0.00294	200k	Fatigue test. No cracks
				1.40E+04	~0.00318	200k	Fatigue test. No cracks
				1.51E+04	~0.00343	200k	Fatigue test. No cracks
				1.61E+04	~0.00367	200k	Fatigue test. No cracks
1.72E+04	~0.00392		Fatigue test. No cracks				

					~0.00392	200k	Fatigue test. 1600 lbs performed again because I buckled the specimen in the grips (-500 lbs!). No cracks appeared for 200 k cycles @ 1600 lbs after this event. Next morning, specimen crushed due to improper control of machine.
15b (30Hz, R=0.5) (Polished)	4.24	29.2	Load	1.72E+04	~0.00406	200k	Fatigue test. No cracks
				1.83E+04	~0.00431	200k	Fatigue test. No cracks
				1.94E+04	~0.00456	200k	Fatigue test. No cracks
				2.04E+04	~0.00482	200k	Fatigue test. No cracks
				2.15E+04	~0.00507	200k	Fatigue test. No cracks
				2.26E+04	~0.00533	200k	Fatigue test. No cracks
				2.37E+04	~0.00558	200k	Fatigue test. No cracks
				2.47E+04	~0.00583	200k	Fatigue test. No cracks
				2.58E+04	~0.00609	200k	Fatigue test. Crack between 0 and 200k.
16b (30Hz, R=0.5)	4.11	28.3	Load	1.72E+04	~0.00419	200k	Fatigue test. No cracks
				1.83E+04	~0.00445	200k	Fatigue test. Crack between 100k and 200k
17b (30Hz, R=0.1)	4.20	29.0	Load	9.68E+03	~0.00230	200k	Fatigue test. No cracks
				1.08E+04	~0.00256	200k	Fatigue test. No cracks
				1.18E+04	~0.00282	200k	Fatigue test. No cracks
				1.29E+04	~0.00307	200k	Fatigue test. No cracks
				1.40E+04	~0.00333	200k	Fatigue test. No cracks
				1.51E+04	~0.00358	200k	Fatigue test. No cracks
				1.61E+04	~0.00384	200k	Fatigue test. No cracks
				1.72E+04	~0.00410	200k	Fatigue test. No cracks
1.83E+04	~0.00435	200k	Fatigue test. Cracked in 3 spots between 0 and 200k.				
18b (7Hz, 3Hz R=0.1)	4.46	30.7	Load	9.68E+03	~0.00217	200k	Fatigue test. No cracks
				1.02E+04	~0.00229	200k	Fatigue test. No cracks
				1.08E+04	~0.00241	200k	Fatigue test. No cracks
				1.13E+04	~0.00253	200k	Fatigue test. No cracks
				1.18E+04	~0.00265	200k	Fatigue test. No cracks
				1.24E+04	~0.00277	200k	Fatigue test. No cracks
				7.53E+03	~0.00169	200k	Fatigue test. No cracks
				8.60E+03	~0.00193	200k	Fatigue test. No cracks
				9.68E+03	~0.00217	200k	Fatigue test. No cracks
				1.08E+04	~0.00241	200k	Fatigue test. No cracks
				1.18E+04	~0.00265	200k	Fatigue test. No cracks
				1.29E+04	~0.00289	200k	Fatigue test. No cracks
				1.40E+04	~0.00313	200k	Fatigue test. No cracks
				1.51E+04	~0.00338	200k	Fatigue test. No cracks
1.61E+04	~0.00362	200k	Fatigue test. Cracked between 0 and 200k.				

19b	4.21	29.0		9.68E+03	N.A.	1	Static test. Got the modulus to complete modulus record for all 20 specimens in Batch B--no fatigue test performed on this specimen.
20b (Static Ult)	4.05	27.9	Displ.	6.77E+04	~0.0188		Static test. Ruptured at 6300 lbs, 0.0188 strain. First audible snap at 2200 lbs, and next observation at 2400 lbs had cracks.

APPENDIX F: EDGE REPLICATE ARCHIVE

Following images display the development of cracking in the 90° plies of cross-ply laminates from Batch A. Width of edge replicate is 1.0", and the number of cycles at which the replicate was taken are listed to the right of the replicate.

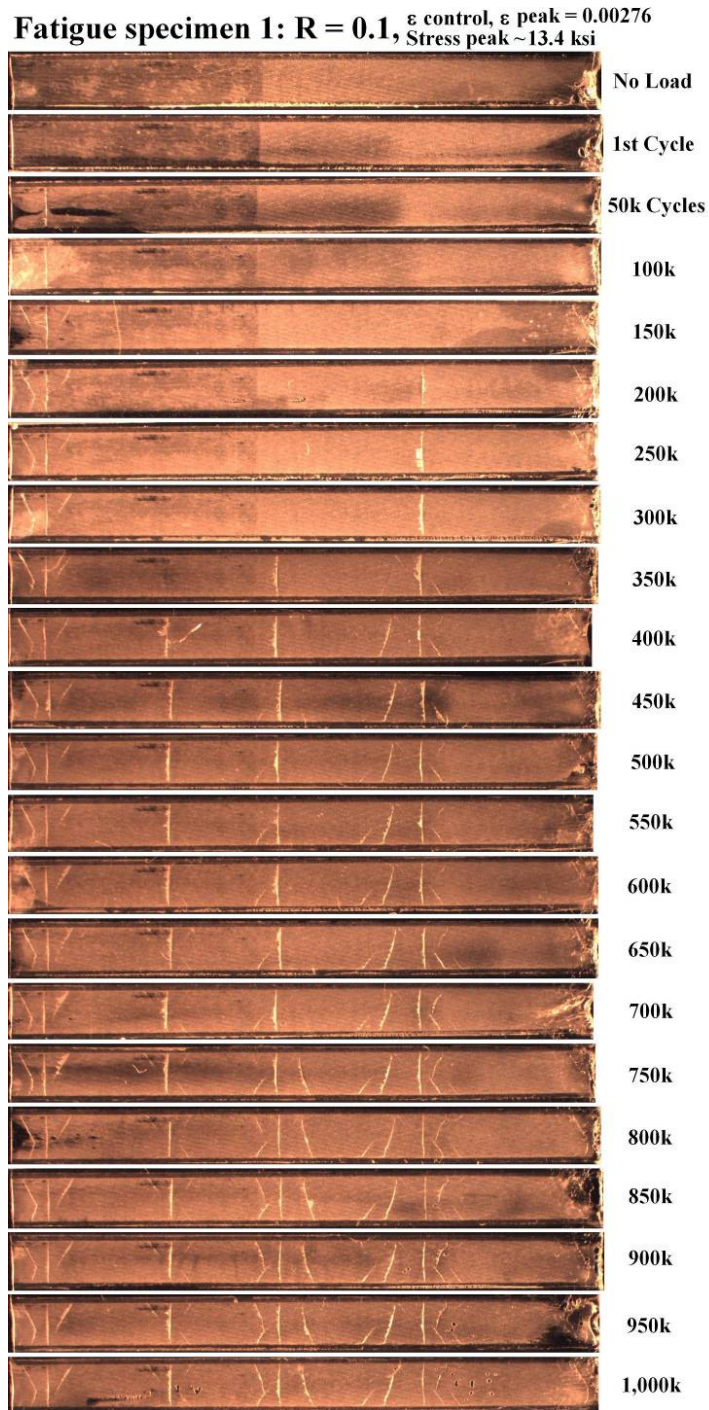


Figure 108. Specimen 1a edge replicate crack development.

Fatigue specimen 2: $R = 0.1$, equiv $\varepsilon = 0.004$,
Load control, peak stress = 17.4 ksi

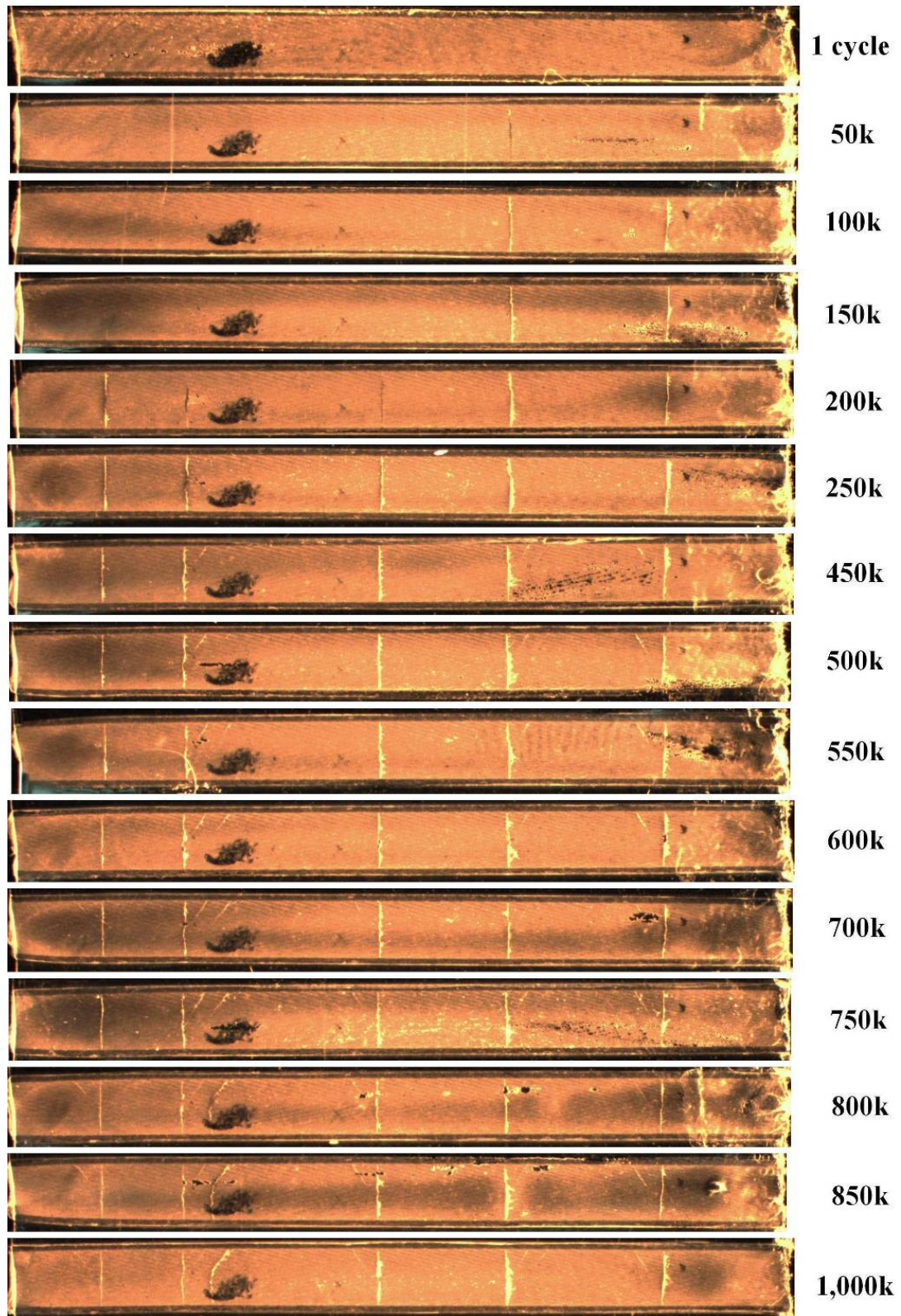


Figure 109. Specimen 2a edge replicate crack development.

Fatigue specimen 7 : $R = 0.1$, equiv $\varepsilon = 0.00276$,
Load control, peak stress = 12.7 ksi

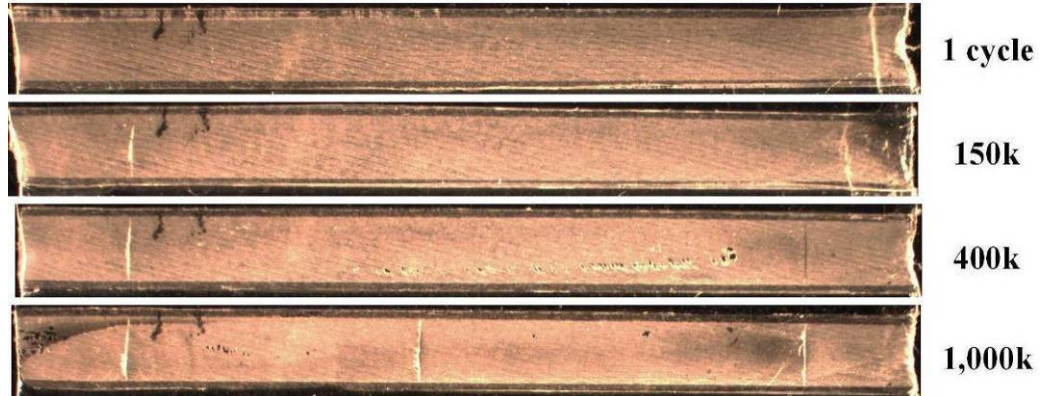


Figure 110. Specimen 7a edge replicate crack development.

Fatigue specimen 8 : $R = 0.1$, equiv $\varepsilon = 0.0035$,
Load control, peak stress = 15.2 ksi

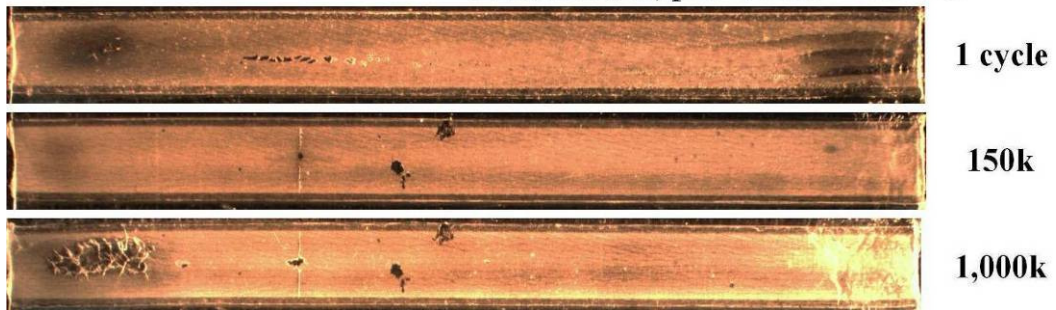


Figure 111. Specimen 8a edge replicate crack development.

Fatigue specimen 9 : $R = 0.1$, equiv $\varepsilon = 0.00276$,
Load control, peak stress = 12.5 ksi



FIGURE 99 (repeated from earlier), Specimen 9a edge replicate crack development.

Fatigue specimen 11: $R = 0.1$, equiv $\varepsilon = 0.004$,
Load control, peak stress = 17.9 ksi

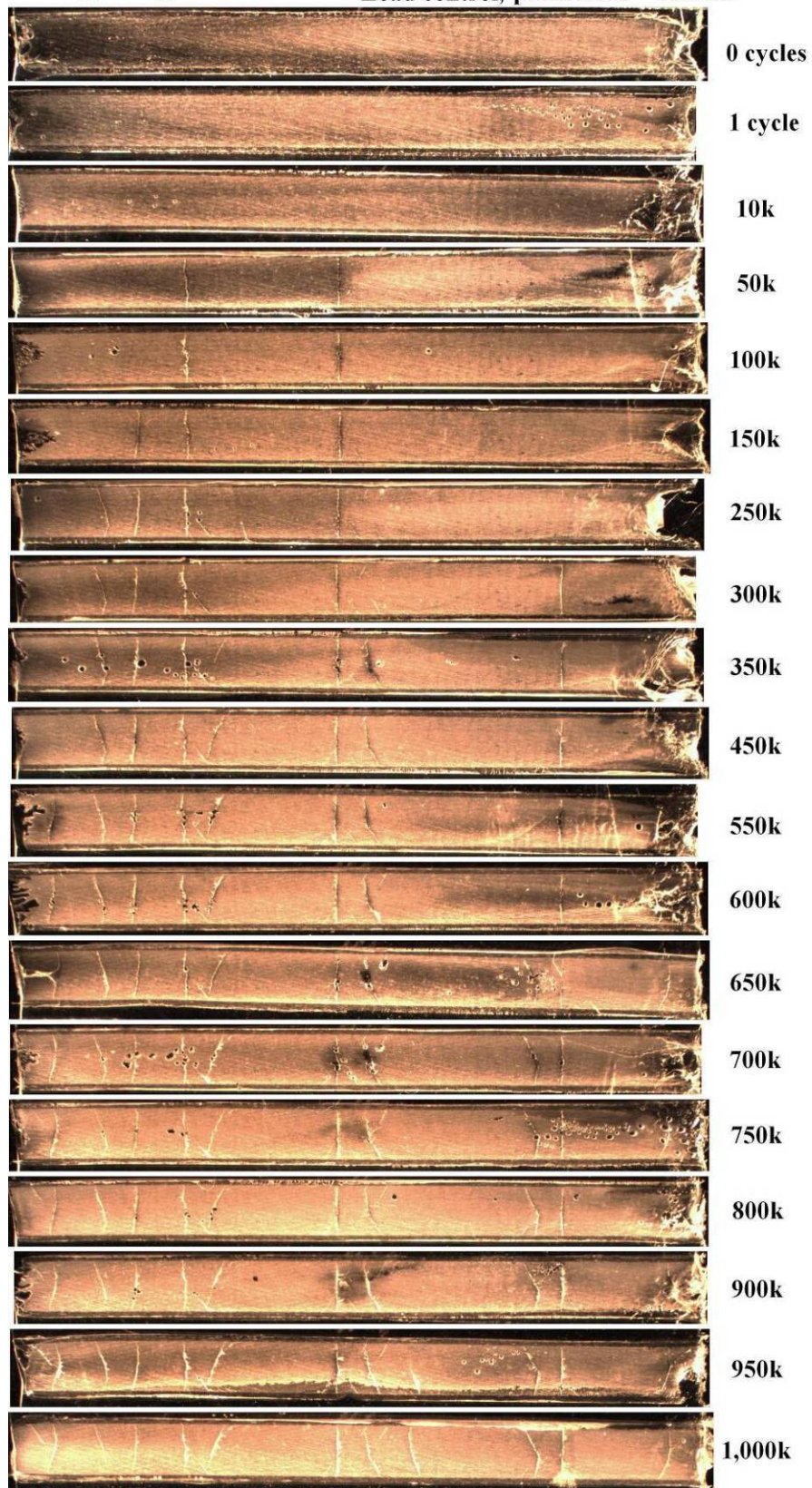


Figure 112. Specimen 11a edge replicate crack development.

Fatigue specimen 12: $R = 0.1$, equiv $\varepsilon = 0.004$,
Load control, peak stress = 18.3 ksi

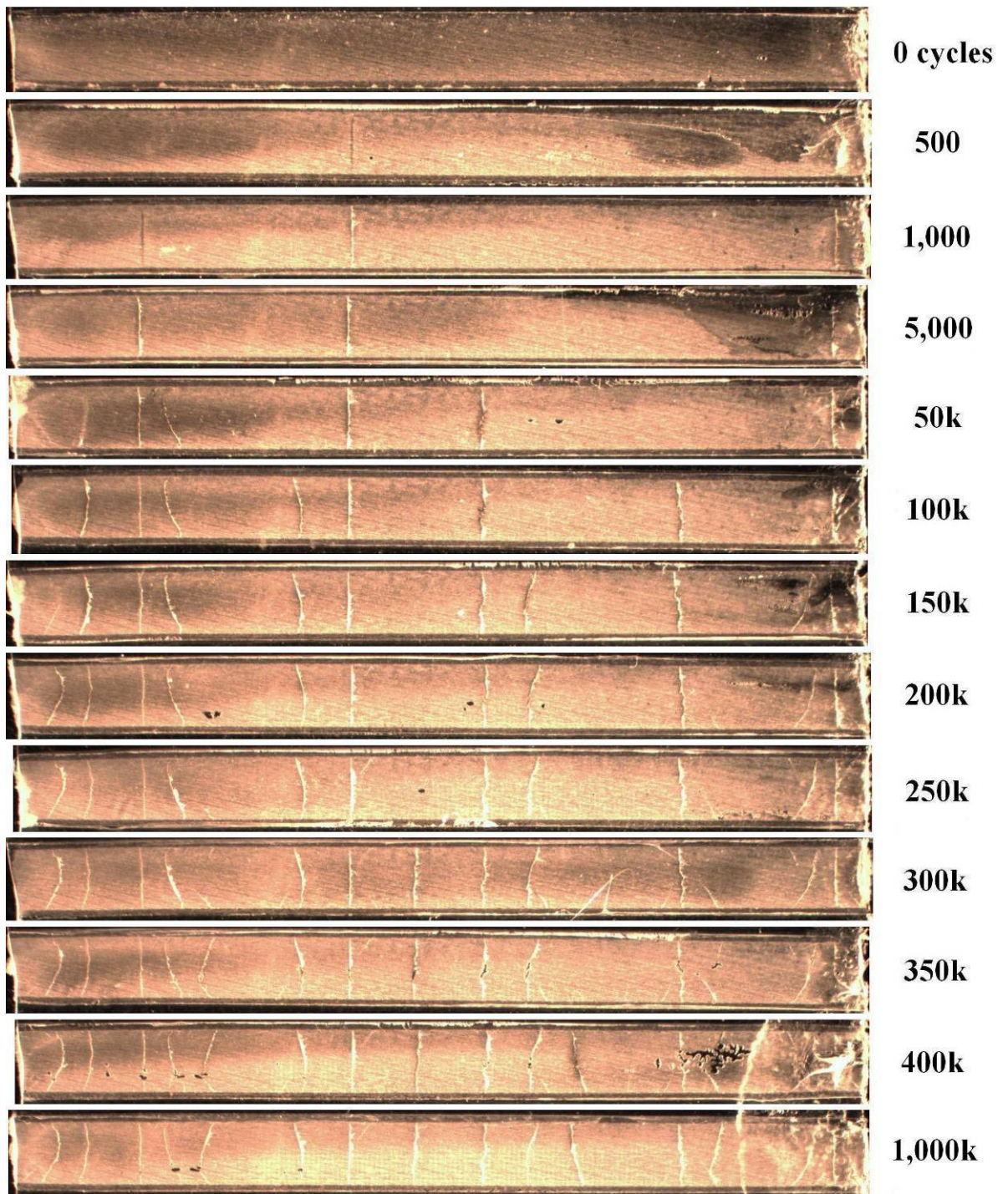


Figure 113. Specimen 12a edge replicate crack development.

Fatigue specimen 13: $R = 0.1$, equiv $\varepsilon = 0.0035$,
Load control, peak stress = 16.0 ksi

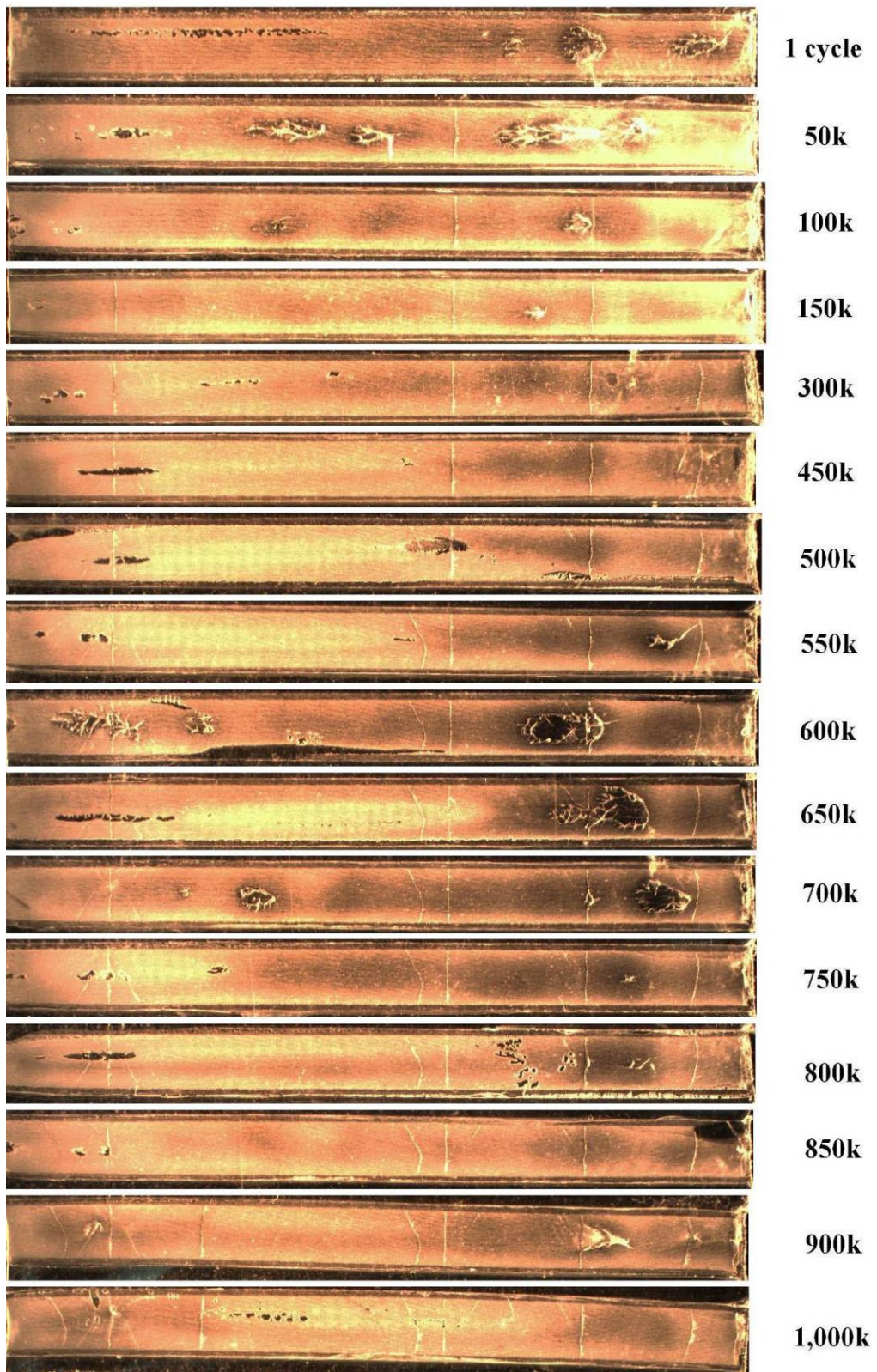


Figure 114. Specimen 13a edge replicate crack development.

REFERENCES

- ¹ T.E. Tay, S.H.N. Tan, V.B.C. Tan, J.H. Gosse, "Damage Progression by the Element-Failure Method (EFM) and Strain Invariant Failure Theory (SIFT)," *Composites Science and Technology*, 65 (2005), 935-944.
- ² R.W. Hertzberg and J.A. Manson, "Fatigue of Engineering Plastics," © 1980, Academic Press, 295 pages.
- ³ K.L. Reifsnider, Zhanjun Gao, "A Micromechanics Model for Composites Under Fatigue Loading," *International Journal of Fatigue*, 13, No. 2, (1991), pp. 149-156.
- ⁴ Reifsnider, K.L. "Some Fundamental Aspects of the Fatigue and Fracture Response of Composite Materials," 'Proceedings of the 14th Annual Meeting of Soc. Eng. Sci.,' Bethlehem, USA, 1977, pp. 373-384.
- ⁵ J.M. Berthelot, P. Leblond, A. El Mahi and J.F. Le Corre, "Transverse Cracking of Cross-Ply Laminates: Part 1. Analysis," *Composites Part A* 27A, 1996, pp. 989-1001.
- ⁶ P.K. Mallick, "Fiber-Reinforced Composites: Materials, Manufacturing, and Design," 2nd Ed., © 1993 by Marcel Dekker.
- ⁷ F.R. Eirich, *Appl. Polym Symp.* 1, 271 (1965), © 1965 by John Wiley and Sons, Inc.
- ⁸ A. Kumar, R.K. Gupta, "Fundamentals of Polymers," © 1998, McGraw-Hill Companies, Inc., 544 pages.
- ⁹ Gunther Hartwig, "Polymer Properties at Room and Cryogenic Temperatures," © 1994. Plenum Press, New York, 273 pages.
- ¹⁰ R.W. Hertzberg, "Deformation and Fracture Mechanics of Engineering Materials," © 1976 by John Wiley and Sons, Inc.
- ¹¹ E.H. Andrews, in "The Physics of Glassy Polymers" (R.N. Haward, ed.), p. 394. Wiley, New York, 1973.
- ¹² R. W. Hertzberg, "Fracture Surface Morphology in Engineering Solids," *Fractography of Modern Engineering Materials: Composites and Metals*, ASTM STP 948, J.E. Masters and J.J. Au, Eds., 1987, pp. 5-36.

-
- ¹³ Farrar, N.R., and E.J. Kramer: "Microstructure and Mechanics of Crazes in Oriented Polystyrene," *Polymer*, vol. 22, pp. 691-698. 1981.
- ¹⁴ Kramer, E.J.: *Craze Fibril Formation and Breakdown*, Cornell Materials Science Center Report 5038, 1983.
- ¹⁵ M.N. Riddell, G.P. Koo, and J.L. O'Toole, *Polym. Eng. Sci.* **6**, 363 (1966).
- ¹⁶ Schultz, J.M.: "Fatigue Behavior of Engineering Polymers," *Treatise on Materials Science and Technology*, vol. 10B, pp. 599-636, 1977.
- ¹⁷ R.J. Crawford and P.P. Benham, *Polymer*, 1975, 16, 908, IPC Business Press Ltd. ©.
- ¹⁸ P. Beardmore and S. Rabinowitz, "Treatise on Materials Science and Technology, Vol. 6," R.J. Arsenault, ed., Academic Press, New York, 1975, p. 267.
- ¹⁹ Bannantine, J.A., Comer, J.J., Handrock, J.L., "Fundamentals of Metal Fatigue Analysis," Prentice Hall, Upper Saddle River, NJ, 1989, 273 pages.
- ²⁰ R.W. Hertzberg, J.A. Manson, and M.D. Skibo, *Polym. Eng. Sci.* **15**, 252 (1975).
- ²¹ J.A. Manson and R.W. Hertzberg, *CRC Crit. Rev. Macromol. Sci.* **1**(4), p. 433 (1973).
- ²² M.D. Skibo, Ph.D. Dissertation, Lehigh University (1977).
- ²³ J.A. Manson, R.W. Hertzberg, S.L. Kim, and W.C. Wu, "Toughness and Brittleness of Plastics," (R.D. Deanin and A.M. Crugnola, eds.), p. 146. American Chemical Society, New York, 1976.
- ²⁴ J.S. Harris and I.M. Ward, *J. Mater. Sci.* **8**, 1655 (1973).
- ²⁵ R.W. Hertzberg, J.A. Manson, and M.D. Skibo, *Polymer*, 1978, 19, 359, IPC Business Press Ltd.
- ²⁶ M.D. Skibo, R.W. Hertzberg, and J.A. Manson, "Deformation, Yield and Fracture of Polymers," p. 4.1. Plastics and Rubber Institute, Cambridge, 1979.
- ²⁷ "Evolution of Aircraft Composites Panel," ASC2007 22nd Annual Technical Conference, Sep. 17-19, U. of Washington Campus, Seattle, Washington

-
- ²⁸ J.L. Rebiere, M.N. Maatallah, D. Gamby, "Analysis of Damage Mode Transition in a Cross-Ply Laminate Under Uniaxial Loading," *Composite Structures* 55 (2002) , pp.115-126.
- ²⁹ Alain Charewicz and Isaac M. Daniel, "Damage Mechanisms and Accumulation in Graphite/Epoxy Laminates," *Composite Materials: Fatigue and Fracture*, ASTM STP 907, H.T. Hahn, Ed., American Society for Testing and Materials, Philadelphia, 1986, pp. 274-297
- ³⁰ Jones, Robert M. "Mechanics of Composite Materials, 2nd Ed.," © 1999, Taylor & Francis, 519 pages.
- ³¹ Jonathan H. Gosse, Stephen Christensen, Qifeng Yu, "A Physics-Based Failure Theory for Composite Materials: The Strain Invariant Failure Theory (SIFT)," *Composites Science and Technology* (Submitted)
- ³² Lorenzo, L., and Hahn, H.T., "Fatigue Failure Mechanisms in Unidirectional Composites," *Composite Materials: Fatigue and Fracture*, ASTM STP 907, H.T. Hahn, Ed., 1986, pp. 210-232.
- ³³ Lagace, P.A., and Nolet, S.C., "Effect of Ply Thickness on Longitudinal Splitting and Delamination in Graphite/Epoxy Under Compressive Load," *Composite Materials: Fatigue and Fracture*, ASTM STP 907, H.T. Hahn, Ed., 1986, pp. 335-360.
- ³⁴ Carlsson, L., Eidefeldt, C., and Mohlin, T., "Influence of Sublaminar Cracks on the Tension Fatigue Behavior of a Graphite/Epoxy Laminate," *Composite Materials: Fatigue and Fracture*, ASTM STP 907, H.T. Hahn, Ed., 1986, pp. 361-382.
- ³⁵ Jamison, R.D., "On the Interrelationship Between Fiber Fracture and Ply Cracking in Graphite/Epoxy Laminates," *Composite Materials: Fatigue and Fracture*, ASTM STP 907, H.T. Hahn, Ed., 1986, pp. 252-273.
- ³⁶ A. Plumtree, L. Shi, "Fatigue Damage Evolution in Off-Axis Unidirectional CFRP," *International Journal of Fatigue*, 24 (2002), pp. 155-159.
- ³⁷ J.C. Halpin and J.L. Kardos, "The Halpin-Tsai Equations: A Review," *Polymer Eng. Sci.*, 16:344 (1976).
- ³⁸ K.L. Reifsnider, R. Jamison, "Fracture of Fatigue-Loaded Composite Laminates," *International Journal of Fatigue*, Oct. 1982, pp. 187-197.
- ³⁹ D.F. Adams and D.R. Doner, "Transverse Normal Loading of a Unidirectional Composite," *Journal of Composite Materials*, 1:152 (1967).

-
- ⁴⁰ L.B. Greszczuk, "Theoretical and Experimental Studies on Properties and Behavior of Filamentary Composites," Proc. 21st Annual Technical Conference, Society of the Plastics Industry (1966).
- ⁴¹ Cox, H.L., "The Elasticity and Strength of Paper and Other Fibrous Materials," British Journal of Applied Physics, 3, pp 72-79 (1952).
- ⁴² Johnson, W.S., "Micromechanics of Composites," 'Mechanical Behavior of Composites' Class Lecture Handout, Georgia Tech, Fall 2007.
- ⁴³ Fukunaga, H., Chou, T.-W., Peters, P.W.M., and Schulte, K., "Probabilistic Failure Strength Analyses of Graphite/Epoxy Cross-Ply Laminates," Journal of Composite Materials, 1984, 18, pp. 339-356.
- ⁴⁴ Lee, J.-W. and Daniel, I.M., "Progressive Transverse Cracking of Cross-Ply Composite Laminates," Comp. Sci. Technol., 1990, 24, pp 1225-1243.
- ⁴⁵ Massimo Caslini, Carlo Zanotti, T. Kevin O'Brien, "Study of Matrix Cracking and Delamination in Glass/Epoxy Laminates," Journal of Composites Technology & Research, Vol. 9, No. 4, Winter 1987, pp. 121-130.
- ⁴⁶ Wang ASD, Crossman FW, "Initiation and Growth of Transverse Cracks and Edge Delamination in Composite Laminates. Part I: An Energy Method," Journal of Composite Materials 1980; 14(Suppl): 71-87.
- ⁴⁷ Xu LY, "Interaction Between Matrix Cracking and Edge Delamination in Composite Laminates," Composite Science Technology, 1994; 50: pp. 469-478.
- ⁴⁸ Highsmith, A.L. and Reifsnider, K.L., "Internal Load Distribution Effects During Fatigue Loading of Composite Laminates," Composite Materials: Fatigue and Fracture, ASTM STP 907, H.T. Hahn, Ed.
- ⁴⁹ Arcan, L., Arcan, M., and Daniel, I.M., "SEM Fractography of Pure and Mixed-Mode Interlaminar Fractures in Graphite/Epoxy Composites," Fractography of Modern Engineering Materials: Composites and Metals, ASTM STP 948, J.E. Masters and J.J. Au, Eds., 1987, pp. 41-67.
- ⁵⁰ Hibbs, M.F., and Bradley, W.L., "Correlations Between Micromechanical Failure Processes and the Delamination Toughness of Graphite/Epoxy Systems," Fractography of Modern Engineering Materials: Composites and Metals, ASTM STP 948, J.E. Masters and J.J. Au, Eds., 1987, pp. 68-97.
- ⁵¹ Hashin, Z., and Rotem, A., "A Fatigue Criterion for Fiber Reinforced Materials," Journal of Composites, 7, pp 246-256.

-
- ⁵² Ansel C. Ugural, Saul K. Fenster, “Advanced Strength and Applied Elasticity, 4th ed.,” © 2003, Prentice Hall, Upper Saddle River, NJ, 544 pages.
- ⁵³ Aboudi, J., “Micromechanics Prediction of Fatigue Failure of Composite Materials,” *Journal of Reinforced Plastics and Composites*, 8, (1989), pp. 150-166.
- ⁵⁴ N.J. Pagano and R. Byron Pipes, “The Influence of Stacking Sequence on Laminate Strength,” *Journal of Composite Materials*, Jan. 1971, pp. 50-57.
- ⁵⁵ Gosse, J.H., Christensen, S., Yu, Qifeng, “A Physics-Based Failure Theory for Composite Materials: The Strain Invariant Failure Theory (SIFT),” *Composite Science and Technology* (Submitted)
- ⁵⁶ Hexcel IM7 Carbon Fiber manufacturer’s technical data sheet. Available at company website: http://www.hexcel.com/NR/rdonlyres/BD219725-D46D-4884-A3B3-AFC86020EFDA/0/HexTow_IM7_5000.pdf
- ⁵⁷ Cytec 977-3 Toughened Epoxy manufacturer’s technical data sheet. Available at company website: <http://www.cytec.com/engineered-materials/products/Datasheets/CYCOM%20977-3.pdf>
- ⁵⁸ Alton L. Highsmith, "Edge Replication for Laminated Composites," *Manual on Experimental Methods for Mechanical Testing of Composites*, Richard L. Pendleton & Mark E. Tuttle, eds., Society for Experimental Mechanics Inc., 1989, p. 165-169
- ⁵⁹ J. Bartley-Cho, S.G. Lim, H.T. Hahn, & P. Shyprykevich, “Damage Accumulation in Quasi-Isotropic Graphite/Epoxy Laminates Under Constant-Amplitude Fatigue and Block Loading,” *Composites Science and Technology*, 58, (1998), pp. 1535-1547.
- ⁶⁰ Skibo, M.D., Hertzberg, R.W., and Manson, J.A., *Journal of Materials Science*, Vol. 11, 1976, p. 479.